

Synchronized Trajectory Tracking Control for Parallel Robotic Manipulators

by

Lu Ren

A thesis submitted in conformity with the requirements
for the degree of Doctor of Philosophy
Department of Mechanical and Industrial Engineering
University of Toronto

© Copyright by Lu Ren, 2006



Library and
Archives Canada

Bibliothèque et
Archives Canada

Published Heritage
Branch

Direction du
Patrimoine de l'édition

395 Wellington Street
Ottawa ON K1A 0N4
Canada

395, rue Wellington
Ottawa ON K1A 0N4
Canada

Your file *Votre référence*
ISBN: 978-0-494-15863-0
Our file *Notre référence*
ISBN: 978-0-494-15863-0

NOTICE:

The author has granted a non-exclusive license allowing Library and Archives Canada to reproduce, publish, archive, preserve, conserve, communicate to the public by telecommunication or on the Internet, loan, distribute and sell theses worldwide, for commercial or non-commercial purposes, in microform, paper, electronic and/or any other formats.

The author retains copyright ownership and moral rights in this thesis. Neither the thesis nor substantial extracts from it may be printed or otherwise reproduced without the author's permission.

AVIS:

L'auteur a accordé une licence non exclusive permettant à la Bibliothèque et Archives Canada de reproduire, publier, archiver, sauvegarder, conserver, transmettre au public par télécommunication ou par l'Internet, prêter, distribuer et vendre des thèses partout dans le monde, à des fins commerciales ou autres, sur support microforme, papier, électronique et/ou autres formats.

L'auteur conserve la propriété du droit d'auteur et des droits moraux qui protègent cette thèse. Ni la thèse ni des extraits substantiels de celle-ci ne doivent être imprimés ou autrement reproduits sans son autorisation.

In compliance with the Canadian Privacy Act some supporting forms may have been removed from this thesis.

Conformément à la loi canadienne sur la protection de la vie privée, quelques formulaires secondaires ont été enlevés de cette thèse.

While these forms may be included in the document page count, their removal does not represent any loss of content from the thesis.

Bien que ces formulaires aient inclus dans la pagination, il n'y aura aucun contenu manquant.


Canada

Synchronized Trajectory Tracking Control for Parallel Robotic Manipulators

Ph.D. Thesis, 2006

Lu Ren

Department of Mechanical and Industrial Engineering

University of Toronto

Abstract

In this thesis, in order to solve the trajectory tracking control problem of parallel robotic manipulators, we propose a new control approach, termed synchronized control. In this control scheme, considering the closed-loop kinematic chain mechanism of parallel robotic manipulators, an additional feedback signal, termed the synchronization error, is employed. Different from the traditional tracking errors, i.e., position errors and velocity errors, the synchronization error represents the coordination degree of the active joints in a parallel robotic manipulator. Therefore, compared with traditional control approaches, e.g., PD control and PID control, the employment of the synchronization error in a synchronized controller improves the tracking performance of a parallel robotic manipulator. Experimental results also demonstrate this claim.

With respect to different operation conditions and tracking performance requirements, based on the synchronized control, we propose two new control approaches, termed adaptive synchronized (A-S) control and convex synchronized (C-S) control. The former is proposed to address unknown parameters in the dynamic model of a parallel robotic manipulator during practical operations. Through estimating unknown parameters during tracking control process by an estimator, the influence of the unknown parameters is eliminated. The latter is proposed to address the multiple simultaneous specification (MSS) problem during trajectory tracking. By using the convex combination method, the C-S controller is designed through combining multiple synchronized controllers. This control approach substantially lessens the burden of tuning control gains.

In principle, the proposed synchronized control, A-S control and C-S control are all suitable for parallel robotic manipulators with various structures. Experiments conducted on a 3-DOF P-R-R planar parallel robotic manipulator demonstrate the validity and effectiveness of these three control approaches.

Acknowledgements

I would like to sincerely thank Professor J.K. Mills for his guidance with the work presented in this thesis. Thanks for the opportunity that he gave to me to explore the exciting robot control field. His religious research attitude impressed me a lot. I would also like to thank him for his inspiration and encouragement throughout my study at the University of Toronto.

I would like to thank Professor B. Benhabib, Professor J.W. Zu, and Professor W.L. Cleghorn, who have been very helpful to me with their suggestions on my research work.

I would also like to thank Professor D. Sun in Department of Manufacturing Engineering and Engineering Management, City University of Hong Kong, Hong Kong, who provided me much help on the theoretical work of the synchronized control.

I wish to thank all the past and present members of the Laboratory for Nonlinear Systems Control: Ke Fu, Xiaoyun Wang, Shichun Zhu, Nick Dechev, Edward Park, Joon Kim, and others. They make me richer both in academic research and practical life.

Deep down in my heart, I wish to thank my parents, who indoctrinate me, encourage me and love me always. Without them, it is impossible for me to have a chance to study my Ph.D. program at the University of Toronto.

Finally, I wish to express my deep gratitude to my dear wife. Thanks for what she did for me in the past three years. Her love, mildness, and understanding are the most precious treasure for me. Thanks also for our lovely son. His everything makes my life more enjoyable.

Table of Contents

Abstract	ii
Acknowledgements	iii
Tables of Contents	iv
List of Figures	viii
List of Tables	xii
Nomenclatures	xiii
1 Introduction	1
1.1 Thesis Scope	1
1.1.1 Serial Robotic Manipulators versus Parallel Robotic Manipulators.....	2
1.1.2 Unconstrained Motion versus Constrained Motion	4
1.2 Literature Review	4
1.2.1 Model-Free Approaches	5
1.2.2 Model-Based Approaches	7
1.2.3 Synchronized Control Approaches	10
1.3 Thesis Objectives	12
1.4 Thesis Contributions	13
1.5 Thesis Overview	14
2 Dynamic Model of Parallel Robotic Manipulators, Spatial and Planar	15
2.1 Introduction	15

2.2	The Natural Orthogonal Complement Method	15
2.3	Dynamic Model of Parallel Robotic Manipulators	17
2.3.1	Dynamic Model of a Spatial Parallel Robotic Manipulator	18
2.3.2	Dynamic Model of a Planar Parallel Robotic Manipulator	20
2.4	Summary	22
3	Synchronized Control for Parallel Robotic Manipulators	24
3.1	Introduction	24
3.2	The Study of Synchronized Control	24
3.3	Synchronized Control Design	27
3.3.1	The Model-Based Synchronization Error	28
3.3.2	The Synchronized Controller	31
3.3.3	Stability Analysis of Synchronized Control	34
3.4	Summary	37
4	Experimental System and Experimentation	38
4.1	Introduction	38
4.2	Modeling of a P-R-R Type Manipulator	39
4.3	Experimental System and Software	44
4.4	Experimental Results Using PID Control and Synchronized Control	49
4.4.1	Trajectory Tracking with a Straight Line Path	49
4.4.2	Trajectory Tracking with a Quadrangle Path	55
4.5	Summary	60
5	Adaptive Synchronized Control	61

5.1	Introduction	61
5.2	A-S Control Design	62
5.3	Stability Analysis of A-S Control	66
5.4	Experimental Results Using Different Control Methods	70
5.4.1	Trajectory Tracking with a Straight Line Path without a Payload	71
5.4.2	Trajectory Tracking with a Quadrangle Path without a Payload	77
5.4.3	Trajectory Tracking with a Straight Line Path with a Payload	82
5.4.4	Trajectory Tracking with a Quadrangle Path with a Payload	86
5.5	Summary	89
6	Convex Synchronized Control	90
6.1	Introduction	90
6.2	C-S Control Design	91
6.2.1	The Convex Combination Method	91
6.2.2	The Model-Free Synchronization Error	95
6.2.3	C-S Control	98
6.3	Robustness Specification of C-S Control	103
6.3.1	Robustness Specification	103
6.3.2	Closed-loop Convex Robustness Specifications	109
6.4	Experiments	111
6.5	Summary	116
7	Conclusions and Discussions	123
7.1	Thesis Summary	123
7.2	Recommendations for Future Work	126

Bibliopoly	127
Appendix A: The Inverse Jacobian Matrix	137
Appendix B: The Expression of the Closed-loop Transfer Matrix	139

List of Figures

1.1(a)	Planar parallel robotic manipulator	3
1.1(b)	Spatial parallel robotic manipulator	3
2.1	Schematic diagram of a Stewart-type manipulator	18
2.2	Schematic diagram of a P-R-R type manipulator	21
3.1	Synchronization in a parallel robotic manipulator (4 active joints case)	26
3.2	The structure of the synchronized controller	33
4.1	Schematic diagram of a P-R-R manipulator	39
4.2	Generalized coordinate system of the P-R-R manipulator	40
4.3	Schematic diagram of the close-loop equation	41
4.4	A prototype of the P-R-R manipulator	44
4.5	Experimental system set-up	46
4.6	Interface of P-R-R manipulator control	47
4.7	Trajectory tracking control interface	48
4.8	Actual and desired trajectories of the platform using PID control	51
4.9	Actual and desired trajectories of the platform using synchronized control	51
4.10	Actual and desired poses of the platform using PID control	52
4.11	Actual and desired poses of the platform using synchronized control	52

4.12	Actual and desired positions of the three prismatic joint using PID control	53
4.13	Actual and desired positions of the three prismatic joint using synchronized control	53
4.14	Pose errors of the platform using PID and synchronized control	54
4.15	Position errors of the three prismatic joints using PID and synchronized control	54
4.16	Desired path of the platform	57
4.17	Desired position and orientation trajectories of the platform	57
4.18	Desired position trajectories of the three prismatic joints	58
4.19	Pose errors of the platform using PID and synchronized control	58
4.20	Position errors of the three prismatic joints using PID and synchronized control	59
5.1	The structure of the A-S controller	65
5.2	Desired path of the platform (tracking a straight line without a payload)	73
5.3	Desired position and orientation of the platform (tracking a straight line without a payload)	73
5.4	Desired positions of the three prismatic joints (tracking a straight line without a payload)	74
5.5	Pose errors of the platform (tracking a straight line without a payload)	74
5.6	Position errors of the three prismatic joints (tracking a straight line without a payload)	75

5.7	The synchronization error of the three prismatic joints using A-S control	75
5.8	Estimated parameters (tracking a straight line without a payload)	76
5.9	Desired path of the platform (tracking a quadrangle path without a payload)	79
5.10	Desired position and orientation of the platform (tracking a quadrangle path without a payload)	79
5.11	Desired positions of the three prismatic joints (tracking a quadrangle path without a payload)	80
5.12	Pose errors of the platform (tracking a quadrangle path without a payload)	80
5.13	Position errors of the three prismatic joints (tracking a quadrangle path without a payload)	81
5.14	Estimated parameters (tracking a quadrangle path without a payload)	81
5.15	Pose errors of the platform (tracking a straight line with a payload)	84
5.16	Position errors of the three prismatic joints (tracking a straight line with a payload)	84
5.17	Estimated parameters (tracking a straight line with a payload)	85
5.18	Pose errors of the platform (tracking a quadrangle path with a payload)	87
5.19	Position errors of the three prismatic joints (tracking a quadrangle path with a payload)	87
5.20	Estimated parameters (tracking a quadrangle path with a payload)	88
6.1	Linear system framework	92

6.2	Feedback linearization of the nonlinear robotic system	99
6.3	Closed-loop perturbation feedback form	105
6.4	Closed-loop system block diagram with perturbation feedback	107
6.5	Two systems connected in feedback loop	109
6.6	Desired path of the platform in Y axis	113
6.7	Actual path of the platform in Y axis of \bar{H}_1	117
6.8	Position error of the platform in Y axis of \bar{H}_1	117
6.9	Frequency response of \bar{H}_1	118
6.10	Actual path of the platform in Y axis of \bar{H}_2	118
6.11	Position error of the platform in Y axis of \bar{H}_2	119
6.12	Frequency response of \bar{H}_2	119
6.13	Actual path of the platform in Y axis of \bar{H}_3	120
6.14	Position error of the platform in Y axis of \bar{H}_3	120
6.15	Frequency response of \bar{H}_3	121
6.16	Actual path of the platform in Y axis of \bar{H}^*	121
6.17	Position error of the platform in Y axis of \bar{H}^*	122
6.18	Frequency response of \bar{H}^*	122

List of Tables

4.1	Kinematic Parameters of the P-R-R manipulator	45
4.2	Error comparison (tracking a straight line path)	55
4.3	Error comparison (tracking a quadrangle path)	59
5.1	Control gains of the employed controllers (tracking a straight line)	72
5.2	Error comparison (tracking a straight line without a payload)	76
5.3	Control gains of the employed controllers (tracking a quadrangle path)	78
5.4	Error comparison (tracking a quadrangle path without a payload)	82
5.5	Error comparison (tracking a straight line path with a payload)	85
5.6	Error comparison (tracking a quadrangle path with a payloads)	88
6.1	Control gains and specifications of the three sample controllers	115

Nomenclatures

General Symbols

a_{\max}	maximum acceleration during trajectory tracking
\bar{a}_{ix}	X directional component of the normalized positional vector from A_i to B_i
\bar{a}_{iy}	Y directional component of the normalized positional vector from A_i to B_i
\bar{b}_{ix}	X directional component of the normalized positional vector from B_i to C_i
\bar{b}_{iy}	Y directional component of the normalized positional vector from B_i to C_i
d_i	the bounded coupling parameters regarding the first-order errors e_i
\bar{e}_{ix}	X directional component of the normalized positional vector from P to C_i
\bar{e}_{iy}	Y directional component of the normalized positional vector from P to C_i
e_i	the i^{th} term of \mathbf{e}
k_0	pre-specified bound for the magnitude of $\bar{\mathbf{P}}$
l	length of the intermediate link of the P-R-R manipulator
n	the number of DOF of a parallel robotic manipulator
m	the number of the required closed-loop performance specifications
m_i	the mass of the i^{th} rigid body
r	the number of rigid body components in a parallel robotic manipulator

v_{\max}	maximum velocity during trajectory tracking
x_{ai}	Position of the origin of the i^{th} linear guide with respect to the fixed frame in X axis
x_{ci}	Position of the revolute joint of the platform facing the i^{th} intermediate link with respect to the fixed frame in X axis
x_p	position of the platform at its mass center in X axis
y_{ai}	Position of the origin of the i^{th} linear guide with respect to the fixed frame in Y axis
y_{ci}	Position of the revolute joint of the platform facing the i^{th} intermediate link with respect to the fixed frame in Y axis
y_p	position of the platform at its mass center in Y axis
A_i	home position of the i^{th} prismatic joint or bracket
B_i	moving position of the i^{th} prismatic joint or bracket
C_i	position of the revolute joint of the platform facing the i^{th} intermediate link
\hat{I}_i	scalar moment of inertia of the i^{th} rigid body
L	the lower bound of the system parameters
M^*	the maximum gain of the possible feedback perturbations
P	position of the platform at its mass center
T_p	the positive constant used to demonstrate persistently exciting
U	the upper bound of the system parameters
V	Lyapunov function

$\dot{c}_i \in \mathcal{R}^{3 \times 1}$	linear velocity vector of C_i
e, \dot{e}, \ddot{e}	errors of the generalized coordinates, velocities and accelerations of the active joints in a parallel robotic manipulator, respectively
e^*	coupling error in the form of (3.6)
\bar{e}^*	coupling error in the form of (6.19)
\dot{e}_{x_p}	derivative of the pose error of the platform
q, \dot{q}, \ddot{q}	generalized coordinates, velocities, and accelerations in a parallel robotic system, respectively
$q^d, \dot{q}^d, \ddot{q}^d$	desired values of q, \dot{q} and \ddot{q} , respectively
\bar{r}	reference value in the synchronized and A-S control
$t_i \in \mathcal{R}^{6 \times 1}$	twist of the i^{th} rigid body
t	manipulator twist
$u \in \mathcal{R}^{n_u}$	the vector of controlled input (actuator input) in the control system frame (Figure 6.1), which is also the output of the controller \bar{K}
$u^* \in \mathcal{R}^{n_u}$	the vector of controlled input (actuator input) in the control system frame (Figure 6.3), which includes the output of the feedback perturbation
$w \in \mathcal{R}^{n_w}$	the vector of exogenous inputs in the control system frame (Figure 6.1), which includes all the exogenous inputs to the controlled manipulator
$\tilde{w} \in \mathcal{R}^{n_w}$	the vector of exogenous inputs in the control system frame (Figure 6.3), which does not include the output of feedback perturbation
$y \in \mathcal{R}^{n_y}$	the vector of sensed output in the control system frame (Figure 6.1), which includes all the outputs that can be directly measured and is the input to \bar{K}

$\mathbf{z} \in \mathfrak{R}^{n_z}$	the vector of regulated output in the control system frame (Figure 6.1)
$\tilde{\mathbf{z}} \in \mathfrak{R}^{n_z}$	the vector of regulated output in the control system frame (Figure 6.3) which does not include the input to feedback perturbation
$\mathbf{0}_n$	$n \times n$ zero matrix
\mathbf{A}, \mathbf{B}	The state-space expression of the closed-loop robotic system $\bar{\mathbf{H}}^*(s)$
\mathbf{C}	coefficient matrix of Coriolis and centrifugal forces in the dynamic model
$\hat{\mathbf{C}}$	estimate of $\mathbf{C}(\mathbf{q}, \dot{\mathbf{q}})$
\mathbf{E}	second term of ϵ
\mathbf{G}	gravity force vector in the dynamic model
$\hat{\mathbf{G}}$	estimate of \mathbf{G}
\mathbf{H}	inertia matrix in the dynamic model
$\bar{\mathbf{H}}_i(s)$	closed-loop transfer matrix of the i^{th} sample system
$\bar{\mathbf{H}}^*(s)$	the closed-loop robotic system which satisfies all required specifications
$\bar{\mathbf{H}}^{\text{pert}}(\Delta)$	The closed-loop transfer matrix of the robotic system, which considers the feedback perturbation in the control system form (Figure 6.3)
$\bar{\mathbf{H}}_{\tilde{\mathbf{z}}\tilde{\mathbf{w}}}$	open-loop transfer matrix from $\tilde{\mathbf{w}}$ to $\tilde{\mathbf{z}}$, when feedback perturbation is considered
$\bar{\mathbf{H}}_{\tilde{\mathbf{z}}\zeta}$	open-loop transfer matrix from ζ to $\tilde{\mathbf{z}}$, when feedback perturbation is considered
$\bar{\mathbf{H}}_{\delta\tilde{\mathbf{w}}}$	open-loop transfer matrix from $\tilde{\mathbf{w}}$ to δ , when feedback perturbation is considered

$\bar{\mathbf{H}}_{\delta\zeta}$	open-loop transfer matrix from ζ to δ , when feedback perturbation is considered
$\hat{\mathbf{H}}$	estimate of \mathbf{H}
$\hat{\mathbf{I}}_i$	inertia matrix of the i^{th} rigid body
\mathbf{I}_n	$n \times n$ identity matrix
\mathbf{J}_p	Jacobian matrix representing the velocity relationship between the active joints and the platform
\mathbf{J}_p^d	desired Jacobian matrix
$\Delta\mathbf{J}_p$	determinant of the Jacobian matrix
\mathbf{K}	coefficient matrix of kinematic constraints
\mathbf{K}_e	control gain matrix in the synchronized controller and A-S controller before $\bar{\mathbf{r}}$
\mathbf{K}_r	control gain matrix in the synchronized controller and A-S controller before \mathbf{e}^*
\mathbf{K}_p	proportional control gain matrix in PID controller
\mathbf{K}_i	integral control gain matrix in PID controller
\mathbf{K}_d	derivative control gain matrix in PID controller
$\bar{\mathbf{K}} \in \mathfrak{R}^{n_u \times n_y}$	The transfer matrix controller from sensed output \mathbf{y} to \mathbf{u} in the control system frame (Figure 6.1)
$\bar{\mathbf{K}}_i(s)$	the transfer matrix of the i^{th} sample controller
$\bar{\mathbf{K}}^*(s)$	The controller derived from the closed-loop transfer matrix $\bar{\mathbf{H}}^*$

\mathbf{M}_i	the inertia dyad of the i^{th} rigid body
\mathbf{M}	manipulator mass matrix
$\mathbf{P}(s)$	the open-loop transfer matrix of the robotic system, which is the augmented open-loop transfer matrix in the control system frame (Figure 6.1)
$\mathbf{P}_{zw} \in \mathfrak{R}^{n_z \times n_w}$	open-loop transfer matrix from \mathbf{w} to \mathbf{z}
$\mathbf{P}_{zu} \in \mathfrak{R}^{n_z \times n_u}$	open-loop transfer matrix from \mathbf{u} to \mathbf{z}
$\mathbf{P}_{yu} \in \mathfrak{R}^{n_y \times n_u}$	open-loop transfer matrix from \mathbf{u} to \mathbf{y}
$\mathbf{P}_{yu} \in \mathfrak{R}^{n_y \times n_u}$	open-loop transfer matrix from \mathbf{u} to \mathbf{y}
$\mathbf{P}^{pert}(s)$	the open-loop transfer matrix of the robotic system with unknown parameters
$\bar{\mathbf{P}}$	diagonal gain matrix of the BGF estimator
\mathbf{S}	constant gain matrix of $\bar{\epsilon}$
$\mathbf{S}^*(s)$	sensitivity transfer function of the closed-loop robotic system
\mathbf{T}	natural orthogonal complement
$\mathbf{T}^*(s)$	the complementary sensitivity function of the closed-loop robotic system
\mathbf{W}_i	the angular velocity dyad of the i^{th} rigid body
\mathbf{W}	manipulator angular-velocity matrix
\mathbf{X}_p	vector denoting the position and orientation of the platform at its mass center
\mathbf{X}_p^d	desired pose of the platform at its mass center
\mathbf{Y}	regression matrix

Greek Symbols

α_i	the i^{th} expected specification value of specification ϕ_i
$\bar{\alpha}_i$	angle between the X axis of the fixed frame and the i^{th} linear guide
α_p	the positive constant used to demonstrate persistently exciting
$\bar{\beta}_i$	angle between the fixed X axis and the i^{th} intermediate link
ϕ_i	the i^{th} specification value
ϕ_{ij}	the i^{th} specification value ϕ_i under the j^{th} sample system $\bar{\mathbf{H}}_j$
ϕ_{PPA}	the specification of percent of path accuracy
ϕ_{ST}	the specification of settling time
ϕ_R	The specification of robustness
ρ_i	the completed translation or rotation of the i^{th} active joint at the end of its desired trajectory
ε_i	The i^{th} term of ϵ , which is fed back to the i^{th} active joint
$\bar{\varepsilon}_i$	The i^{th} term of $\bar{\epsilon}$, which is fed back to the i^{th} active joint
φ	orientation of the platform with respect to the fixed frame
ζ	boundary condition of the synchronization error
λ_0	positive constant representing the maximum forgetting rate
σ	constant gain matrix, which denotes the weight of the synchronization error in the coupling error
ϵ	synchronization error in the form of (3.5)

$\bar{\epsilon}$	synchronization error in the form of (6.16)
τ_a	actuating force vector
$\omega_i \in \mathfrak{R}^{3 \times 1}$	angular velocity vector of Ω_i
v	output of a linear controller to be designed for a linearized robotic system
η	uncertainty during feedback linearization of the robotic system
ς	the output signal of the feedback perturbation in the robotic system
δ	the input signal to the perturbation feedback
ψ_{\max}	maximum value of $e^*(t) - \Gamma E(t)$
ψ_{\min}	minimum value of $e^*(t) - \Gamma E(t)$
$\theta \in \mathfrak{R}^{n \times 1}$	vector containing all unknown dynamic parameters in the dynamic model
$\hat{\theta}$	estimate of θ
θ_{true}	vector of the true values of the estimated parameters
Γ	coefficient matrix of the coupling error
Λ	coefficient matrix of \bar{u}
$\bar{\Lambda}$	combination vector, where $\lambda_i > 0$, $\sum_{i=1}^m \lambda_i = 1$
$\Phi = \{\phi_{ij}\}$	the $m \times m$ matrix whose entries are ϕ_{ij}
$\Omega_i \in \mathfrak{R}^{3 \times 3}$	the angular-velocity matrix of the i^{th} rigid body
Ψ	the vector of required specification values
Δ	transfer matrix of the feedback perturbation

Notations

\square	end of proof or definition
$\ \cdot\ $	norm
\triangleq	defined by
$(\cdot)^T$	transpose
$(\cdot)^{-1}$	inverse
$\max(\cdot)$	maximum
$\min(\cdot)$	minimum
$\sup(\cdot)$	supremum of a function or set

Acronyms

A-S	Adaptive Synchronized
BGF	Bounded-Gain-Forgetting
C-S	Convex Synchronized
DOF	Degree of Freedom
LNSC	Laboratory for Nonlinear Systems Control
MSS	Multiple Simultaneous Specification
NOC	Natural Orthogonal Complement
PD	Proportional-Derivative
PID	Proportional-Integral-Derivative

Chapter 1

Introduction

In this introductory chapter, the motivations for this work are given and the major topics addressed in this thesis are briefly discussed within the context of research on the subject of synchronized-based trajectory tracking control for parallel robotic manipulators. The main contributions and the outline of the thesis are presented.

1.1 Thesis Scope

Robotics is an interdisciplinary field of study, which involves many areas such as physics, mechanical design, motion analysis and planning, actuators and drivers, control design, sensors, computer algorithm and so on. During industrial applications of robotic manipulators, how to solve the control problem so that pre-specified performance can be achieved is indispensable. The control problem for a robotic system is the problem of determining the time history of joint inputs required to cause the end-effector to execute a commanded task (Spong, M.W., *et al.*, 1989 [70]).

In contrast to serial robotic manipulators, parallel robotic manipulators have the advantages of high stiffness, high payload, and high accuracy. As a consequence, since the 1990's, parallel robotic manipulators have received significant attention and been applied in various industrial areas, such as flight simulation (Stauffer, R.N., 1984 [71]),

precision machining (Chen, N.X., *et al.*, 1994 [12]), telescopes (Carretero, J.A., *et al.*, 1998 [9]) and high speed assembly operations (Clavel, R., 1998 [16]), and so on. In this thesis, the trajectory controller design for parallel robotic manipulators during unconstrained motion at high speed and high acceleration is of interest. The purpose of control law design is to improve, or in some cases enable the performance of a robotic system; and the objective of trajectory control of a robotic manipulator is to control the end-effector move along a path in space with a particular orientation. It is desired to cause close trajectory tracking for an arbitrary trajectory even when an unknown payload is held by the end-effector in the presence of manipulator dynamic parameter uncertainties.

1.1.1 Serial Robotic Manipulators versus Parallel Robotic Manipulators

Serial robotic manipulators have an open kinematic chain structure and usually have a long reach and a large workspace. Thus, they have experienced a sustained application growth surge for the past two decades. On the other hand, due to inherent lower rigidity and poor dynamic performance at high speed, acceleration and high dynamic loading operating conditions, serial robotic manipulators, however, have consequent limitations in their industrial applications. Since the 1990's, increasing needs for high speed, acceleration and accuracy in all fields of industry has increased the need for new kinds of robust, light and multi-use structures for robotic manipulators.

Parallel robotic manipulators, another major category of robotic manipulators, have a closed-loop chain structure, which consists of multiple branches acting in parallel on a common payload platform. As a result, parallel robotic manipulators are superior to serial

counterparts providing generally higher stiffness, higher load-carrying capacity. In particular, since the actuators of the branches act in parallel, sharing a common payload, errors due to inaccurate device manufacture or sensing, act in parallel rather than in serial, avoiding multiplication of the error and thereby improving accuracy of the end-effector. Furthermore, the majority of the parallel robotic manipulators studied are fully parallel robotic manipulators in which the number of chains is strictly equal to the number of degrees of freedom (DOF) of the end-effector. Fully parallel robotic manipulators¹ can be divided into two main categories: planar parallel robotic manipulators, which have three DOF in the plane, and spatial parallel robotic manipulators, which move out of the plane (Merlet, 2000 [43]) and have more than three DOF, as shown in Figure 1.1(a) and Figure 1.1(b), respectively.

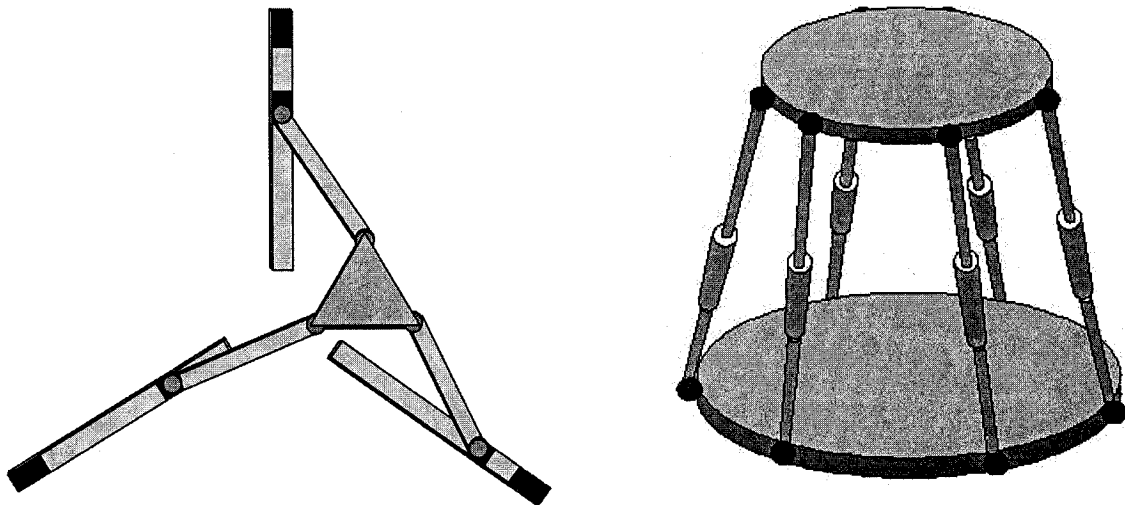


Figure 1.1: (a) Planar parallel robotic manipulator (b) Spatial parallel robotic manipulator

¹ In the rest of this thesis, unless otherwise specified, “fully parallel robotic manipulators” is abbreviated as “parallel robotic manipulators”.

1.1.2 Unconstrained motion versus Constrained motion

Unconstrained motion and constrained motion are two types of tasks for trajectory control. In unconstrained motion, the manipulator end-effector does not touch any surface during operations such as paint spraying, while in constrained motion, the manipulator end-effector is in contact with a rigid surface during an operation such as parts assembly. Although both of these tasks are important, considering the major practical applications of parallel robotic manipulators such as flight simulation, high speed pick-and-place operations, unconstrained motion is perceived as more important because robotic manipulator end-effector does not contact a rigid surface. Therefore, in this thesis, only the trajectory during unconstrained motion is studied².

1.2 Literature Review

Various control approaches have been proposed to improve performance of trajectory control area of parallel robotic manipulators. These approaches are loosely divided into two categories: model-free approaches and model-based approaches. To clarify that our use of the term “model-free” and “model-based” is to be taken literally, the definitions are given as follows:

*Model-free approach: the approach uses the system measurement to determine the control function **without** the need to estimate or assume a model for the system (Spall, J.C., 1998 [69]).*

² In the rest of this thesis, unless otherwise specified, “unconstrained trajectory tracking control” is abbreviated as “trajectory tracking control”.

Model-based approach: the approach uses the system measurement to determine the control function with the need to estimate or assume a model for the system (Spall, J.C., 1998 [69]).

1.2.1 Model-Free Approaches

In complex physical, socioeconomic, or biological systems, the forms of the system equations (typically nonlinear) are often unknown as well as the parameters, making it is problematic to determine the control law needed. This provides the motivation for developing a control procedure, the model-free approach, which does not require a model for the underlying system.

The commonly used model-free approaches include the well-known PD control and PID control (Homsup, W., *et al.*, 1987 [26]), which are widely employed in industrial areas. These controllers are simple and easy to implement, however, they also exhibit inherently low rejection to exogenous disturbances (Spong, M.W., *et al.*, 1989 [70]). Chiacchio, P., *et al.*, (1993 [13]) proposed a linear control scheme, in which an acceleration feedback term is used so that the control law is more robust to exogenous disturbances than a simple PID. Dawson, D.M., *et al.*, (1990 [18]) studied the stability of a PD controller for trajectory control problem of a robotic manipulator. It is shown that if the PD control gains are chosen greater than a specified bound, and if the initial tracking error is zero, the velocity and position tracking errors are uniformly bounded. Quyang, P.R., *et al.*, (2004 [49]) proposed a nonlinear PD control, whose control gains are time-varying determined by two functions. This approach enjoys advantages over fixed-gain

PD control in term of disturbance rejection and has less sensitive to delays than fixed-gain PD control.

Fuzzy control and neural network control are also categorized as a model-free control approach. Different from PD or PID control based on a mathematical model, i.e., using one or more differential equations that define the system response to its inputs, fuzzy control is based on empirical rules, which may be more effective in the case, in which mathematical model of the control process may not exist, or use of such a model may be too “expensive” in terms of computer processing power and memory. Furthermore, this approach is well suited to low-cost implementation based on cheap sensors and low-resolution analog-to-digital converters. Jin, S., *et al.*, (1993 [28]) proposed a learning fuzzy controller, in which several elemental fuzzy controllers are processed in parallel. Wu, H., *et al.*, (2004 [83]) proposed a hybrid fuzzy controller, which combines fuzzy self-tuning PD and fuzzy self-tuning PI through a simple design scheme, to achieve good transient response, small transient error and small steady-state error. The advantage of neural network control relies on its universal approximation capabilities of the multilayer perception. By adding feedback loops to a feedforward network and utilizing the dynamic network, Wan, Y., *et al.*, (2004 [82]) proposed a dynamic neural network controller to a hydraulic parallel robot, whose experimental results show that the controller design is independent on system model, and the proposed controller has self-adaptability to time-varying parameters and robustness to large load disturbance with the satisfactory static and dynamic performance.

Although the model-free approach is appropriate for many practical systems and sometimes easy to implement due to its simplicity (for example, PD or PID control), it is

generally inappropriate for systems where a reliable system model can be determined. One reason, of course, is that with a reliable model, the controller will generally achieve optimal control more quickly. Further, in some cases, a reliable model allows for theoretical analysis of such issues as stability and controllability and for the calculation of state estimates for use in system performance monitoring and feedback to the controller (Spall, J.C., 1998 [69]).

1.2.2 Model-Based Approaches

In a model-based control approach, the system dynamic model is explicitly considered and utilized; therefore, good control performance can be achieved when the model is reliable and accurate. A large number of approaches belong to this category, including computed-torque control, sliding mode control, impedance control, adaptive control and etc.

The computed-torque method is the pioneer design of this kind. This method is a PD control through the feedback linearization technique, which is initially proposed by Paul, R.P. (1972 [50]) and Bejczy, A.K. (1974 [4]) for serial robotic manipulators, and later Kokkinis, T., *et al.*, (1996 [32]) for parallel robotic manipulators. By application of feedback linearization technique, the nonlinear system is transformed in a system in Brunovsky canonical form. The resultant closed-loop system can then be stabilized using standard pole placement. Despite of its powerful theoretical value, the computed-torque control has limited implementation because of its poor robustness properties to parameter uncertainties due to modelling inaccuracies or unknown payload and viscous joint friction. To improve this shortcoming, some researchers focus on finding more inherent

characteristics of the computed-torque control. Qu, Z., *et al.*, (1996 [53]) showed that under bounded system model uncertainty, the computed-torque control can make the system robust if the proportional derivative gains are properly selected. Others follow the idea that low robustness to parameter uncertainties may be improved through combining another control technique with computer-torque control. Guo, L.S., *et al.*, (2001 [24]), Tarokh, M. (1992 [78]), proposed an adaptive computed-torque control method, using adaptive control technique to estimate model uncertainties and guarantee the accuracy of the system dynamic model. Chen, C., *et al.*, (1998 [11]) employed sliding mode control with computed-torque control to compensate unknown parameters and bounded disturbances.

The sliding mode control method was initially developed in the Soviet Union more than 40 years ago. The idea behind sliding mode control is to choose a suitable surface in state space, called the switching surface, and switch the control input on this surface. The control input is then chosen to guarantee that the trajectories near the sliding surface are directed toward the surface. Once the system is trapped on the surface, since the surface is defined by the designer, the closed-loop system dynamics will be independent of perturbations in the parameters of the system and thus, robustness is achieved, Spong, M.W., *et al.*, (1989 [70]). In practice, however, because of time delays, sampling and other imperfections of real systems, this approach results in an undesirable chattering phenomenon. To overcome this disadvantage, several techniques have been employed. Begon, P., *et al.*, (1995 [3]) proposed a so-called fuzzy sliding mode approach, in which fuzzy logic technique was used to define a new switching method to avoid chattering. Ertugrul, M., *et al.*, (1997 [19]) proposed a synergistic combination of neural networks

with sliding mode control. As a result, the chattering was eliminated and error performance was improved.

Various adaptive control schemes have been proposed in the literature to accommodate changing payload and unknown parameters during trajectory tracking motion of parallel robotic manipulators. These methods can be divided into two categories: model reference adaptive control and adaptive self-tuning control, in both of which, an adaptation law is constructed to learn explicitly unknown parameters (Slotine, J.-J.E., *et al.*, 1991 [68]). Oh, P.Y., *et al.*, (1997 [48]) used the Euler operator to design a model reference adaptive control for a Stewart platform. Nguyen, C., *et al.*, (1993 [46]) proposed a self-tuning adaptive control scheme to a Stewart platform-based manipulator to track a vertical and circular path under step changes in payload. In this scheme, the gains of PD controller are adjusted by an adaptation law. Huang, C., (2004 [27]) proposed an adaptive backstepping control approach for trajectory control of a Stewart platform, which can drive the tracking errors asymptotically converge to zero.

Generally, model-based approaches achieve better performance than model-free approaches when the system dynamic model is accurate. Even when the model is inaccurate, some of the model-based approaches may achieve good performance through the real time estimation of unknown parameters. But undoubtedly, in some cases, these approaches are problematic to implement, because of the large computational burden, for example.

Reviewing the literature related to model-free and model-based approaches applied to parallel robotic manipulators, note that few of these approaches consider the coupling effect amongst the active joints due to the closed-loop chain structure of a parallel

manipulator. This coupling effect, in some sense can be treated as a synchronization problem (Ren, L., *et al.*, 2004 [56]) (discussed in Chapter 3 in detail), which may be defined as the mutual time conformity of two or more processes, and this conformity can be characterized by the appearance of certain relations between some functions depending on the processes (Blekhman, I.I., *et al.*, 1995 [5]). This synchronization should be considered; otherwise, in some severe situations, for instance, when accelerations of active joints are high, damage of the manipulator mechanical structure may occur. Studying the literature addressing this synchronization control problem in dynamic systems, the so-called synchronized control approach (Nijmeijer, H., *et al.*, 2003 [47]) takes on increased significance.

1.2.3 Synchronized Control Approaches

First recognized in 1665 by Christiaan Huygens (Pikovsky, A., *et al.*, 2001 [52]), synchronization phenomena are abundant in science, nature, engineering and social life. The synchronized control approach, however, was first proposed by Koren Y. in 1980, (Koren, Y., 1980 [33]). This approach employs the cross-coupling control technique, which provides unique advantage and opportunity to solve the synchronized control problem of dynamic systems (Koren, Y., 1980 [33]). Since the 1990s, similar approaches using the cross-coupling technique have been applied mainly to machine tools (Kulkarni, P.K., *et al.*, 1990 [35], Tomizuha, M., *et al.*, 1992 [81], Koren, Y., *et al.*, 1992 [34]). Many of these researches dealt with velocity synchronization problem especially for two-axis motions. Recently, great progress has been made in utilizing cross-coupling concept to solve position synchronization of multiple motion axes (Chiu, T.C., *et al.*, 1998 [14],

Sun, D., 2003 [76]). Other synchronized control approaches, including fuzzy logic coupling control (Lee, H.C., *et al.*, 1998 [36]), neuro-controller for synchronization (McNab, R.J., *et al.*, 2000 [42]), etc., have been applied to this area as well.

In robotics, almost all of the proposed synchronized control approaches focus on two research fields: motion of mobile robots (Feng, L., *et al.*, 1993 [20], Borenstein, J., 1995 [7], Sun, D., *et al.*, 2005 [77]), and coordination of multi-robots (Sun, D., *et al.*, 2002 [74], Naumovic, M., 1991 [45], Rodriguez-Angeles, A. *et al.*, 2004 [64]). Noticeably, for trajectory tracking control of parallel robotic manipulator, only Chuang, H.-Y., *et al.*, (2000 [15]) proposed a synchronized approach to reduce the contour error of a 3-PRPS parallel robotic manipulator so far. However, in their experiments, the manipulator moved at relative low speed (7m/min) and acceleration was not considered.

Reviewing the proposed synchronized control approaches, since the use of an additional feedback error must be required in the control scheme, which is typically defined based on the system model, the majority of the proposed synchronized control approaches should be categorized as model-based (Ren, L. *et al.*, 2003 [55], 2004 [57], Sun, D., *et al.*, 2002 [74], etc.). In particular, Su (Su, Y., *et al.*, 2005 [72]) proposed a model-free synchronized approach for a 3-DOF planar parallel robotic manipulator, because in his control scheme, the additional feedback error was not defined according to the system model.

In conclusion, for a parallel robotic manipulator moving at high speed and acceleration (above 20 G), how to utilize and solve the coupling effects amongst its active joints and then design an appropriate controller to solve the trajectory tracking control problem is an open research topic. We note that: 1) The majority of the approaches

proposed for the trajectory control of parallel manipulators, whether model-free or model-based, do not explicitly consider the coupling effects amongst the active joints. 2) The proposed synchronized approaches are typically applied to multi-axis machine tools, mobile robots, and multi-robot systems.

1.3 Thesis Objectives

The objectives of this thesis are three fold:

1. Propose a synchronized approach to solve the trajectory tracking control problem of parallel robotic manipulators with various structures, in which high accuracy, i.e., small transient error and tiny steady-state error, should be achieved during high speed, high acceleration tracking motions. An additional feedback signal should be defined with respect to the mechanical structure of the manipulator so that the coupling effects amongst the active joints can be feedback to each active joint. In addition, the proposed approach should be proved stable. Furthermore, considering that uncertain parameters may exist due to unknown payloads in a practical industrial environment, the proposed approach can be combined with another control technique, i.e., adaptive control, to yield satisfactory tracking performance through estimation of uncertain parameters.
2. Propose a synchronized-based approach, which utilizes the convex properties of common performance criteria, to solve the multiple simultaneous specification (MSS) problem during trajectory tracking control of parallel robotic manipulators with various structures moving at high speed and high acceleration.

3. Verify the validity and effectiveness of the proposed theory and methodology in (1) and (2) through experimentation on a P-R-R type planar parallel robotic manipulator.

1.4 Thesis Contributions

By arriving at its objectives, the contributions of this thesis are as follows:

1. With analysis of the closed-loop kinematic chain structure of parallel robotic manipulators, two questions, whether there is a controlled synchronization problem during trajectory control of a parallel robotic manipulator and whether it is appropriate to propose a synchronized control approach to solve this trajectory control problem, are answered. Through analyzing manipulator kinematics, how to define a synchronized error is addressed. This provides a background to proposing the synchronized control approach to a parallel robotic manipulator.
2. A generic methodology, referred to as the synchronized control method, is developed to solve the trajectory tracking control problem of parallel robotic manipulators with high speed and acceleration motions. Specifically, with respect to different environments and system requirements, i.e., with and without unknown parameters in the system dynamic model, one and multiple performance specifications, different control methods based on the proposed synchronized control are developed.
3. The analysis of existence of solutions to the proposed methods and the stability analysis of the closed-loop system are undertaken. Experimental work proves its effectiveness.

4. Other synchronized control methods also have been tested on an experimental parallel robotic manipulator. Experimental work demonstrates the correctness and effectiveness of applying synchronized control to parallel robotic manipulators.

1.5 Thesis Overview

The outline of the remainder of the thesis is as follows. In Chapter 2, the dynamic model of a general parallel robotic manipulator developed using the natural orthogonal complement method is briefly introduced. Chapter 3 presents the feasibility of applying the synchronized control approach to a parallel robotic manipulator, and proposes a synchronization error definition based on the mechanical structure of the parallel manipulator. Stability analysis of the proposed synchronized control approach is then developed. In Chapter 4, the experimental system, a P-R-R type planar parallel robotic manipulator, is introduced. Experimental results applying PID control and synchronized control to the manipulator are given. Chapter 5 addresses a new approach, termed the adaptive synchronized (A-S) approach. The stability analysis of the closed-loop system is provided and experimental results using the P-R-R type parallel robotic manipulator are given. In Chapter 6, another new control approach, the convex synchronized (C-S) approach, is proposed. The conditions under which the proposed control is stable are given and proved. The stability analysis of the closed-loop system derived with the C-S approach is undertaken and experimental results on the P-R-R manipulator are given as well. Finally, Chapter 7 offers conclusions and discussions.

Chapter 2

Dynamic Model of Parallel Robotic Manipulators, Spatial and Planar

2.1 Introduction

In this chapter, we briefly introduce the natural orthogonal complement method and then present the derivation of the dynamic model of parallel robotic manipulators. The rest of this chapter is organized as follows. In section 2, we briefly introduce the natural orthogonal complement method, which is employed to derive the dynamic model of parallel robotic manipulators. Then in section 3, we address the dynamic models of both spatial and planar parallel robotic manipulators. Finally, a summary is given in section 4.

2.2 The Natural Orthogonal Complement Method

The study of the robotic dynamics is classical. A number of methods have been proposed and utilized to derive the dynamic model of parallel robotic systems, such as the Newton-Euler method (Merlet, J.-P., 2000 [43]), the Lagrange formulation (Tsai, L.W., 1999 [79]), the principle of virtual work (Kang, B., *et al.*, 2001 [29], Tsai, L.W., 2000 [80]), screw theory (Gallardo, J. *et al.*, 2003 [23]), and etc. The Newton-Euler method typically

has a large computation burden, because it needs the exact calculation of all the internal reactions of constraints of the system, even if they are not employed in the control law of the manipulator. The Lagrangian and the principle of virtual work formulations are both based on the computation of the energy of the whole system with the adoption of a generalized coordinate framework. Such energy approaches to the parallel robotic manipulator may be further simplified (Rico, J.M., *et al.*, 1999 [61]). Here, we employ the so-called natural orthogonal complement (NOC) method proposed by Angeles (Angeles J., 2003 [1]) to derive the dynamic model of a parallel robotic manipulator, because two characteristics obtained during derivation are required in stability analysis for the proposed control methods, which are addressed in Chapter 3 and Chapter 5, respectively.

The NOC method is based on constraint wrenches and the feasible twist of a manipulator. The major procedure of NOC can be described as follows.

Considering a parallel robotic system composed of r rigid bodies and with n DOF,

- (i) Define $\mathbf{t} \in \mathfrak{R}^{6n \times 1}$ as the manipulator twist and express the kinematic constraints of the system in the form of $\mathbf{Kt} = \mathbf{0}$, where $\mathbf{K} \in \mathfrak{R}^{6n \times 6n}$ is obtained from the mechanical structure of the manipulator.
- (ii) According to the twist-shape relationship, $\mathbf{t} = \mathbf{T}\dot{\mathbf{q}}$, \mathbf{t} is represented as a linear transformation of the independent generalized speed, $\dot{\mathbf{q}} \in \mathfrak{R}^{6n \times 1}$. Where $\mathbf{T} \in \mathfrak{R}^{6n \times n}$ is defined as the twist-shaping matrix.
- (iii) Substitute the kinematic constraints into the twist-shape relationship, $\mathbf{KT} = \mathbf{0}$ is derived. Since \mathbf{K} is known, then \mathbf{T} referred as the natural orthogonal

complement of \mathbf{K} is solved. Subsequently, the dynamic equations of the robotic manipulator are obtained.

2.3 Dynamic Model of Parallel Robotic Manipulators

Parallel robotic manipulators are typically composed of a base platform, which is usually fixed on the ground, a moving platform³, and several branches, each of which comprises a certain number of joints, i.e., prismatic joints, revolute joints, and spherical joints. Spatial parallel robotic manipulators can be categorized as many types, in terms of the number of branches (typically from 3 to 6) and the sequence of the joints. Planar parallel robotic manipulators, relatively simple, typically have three branches and consequently have three DOF. According to the sequence of the joints in each branch, planar parallel robotic manipulators can be categorized as $\underline{\text{P}}\text{-R-R}^4$, $\underline{\text{R}}\text{-R-R}$, $\text{R-}\underline{\text{P}}\text{-R}$ type, etc. R, P here means revolute and prismatic joints, respectively; the joint denoted by an underline is active; otherwise, it is passive.

In this section, we employ the NOC method to derive the dynamic model of a parallel robotic manipulator. A Stewart-type manipulator is selected as an example of spatial parallel robotic manipulators and a P-R-R type manipulator is selected as an example of planar parallel robotic manipulators.

³ In the rest of this thesis, unless otherwise specified, “moving platform” is abbreviated as “platform”.

⁴ In the rest of this thesis, unless otherwise specified, “ $\underline{\text{P}}\text{-R-R}$ ” is represented by “P-R-R”.

2.3.1 Dynamic Model of a Spatial Parallel Robotic Manipulator

Since spatial parallel robotic manipulators have many different mechanical structures, it is hard to derive their dynamic models one by one. Therefore, in this sub-section, we choose a Stewart-type manipulator as an example to derive the dynamic model of all spatial parallel robotic manipulators within a common form.

We consider here a Stewart-type manipulator composed of r rigid bodies and with n DOF, as shown in Figure 2.1. Fix an inertia frame (X, Y, Z) at the center of the base platform with the Z axis pointing vertically upward.

Let $\mathbf{M}_i \in \mathfrak{R}^{6 \times 6}$ denote the inertia dyad of the i^{th} rigid body and $\mathbf{W}_i \in \mathfrak{R}^{6 \times 6}$ denote the angular velocity dyad of the same body, given as:

$$\mathbf{M}_i = \begin{bmatrix} \hat{\mathbf{I}}_i & \mathbf{0}_3 \\ \mathbf{0}_3 & m_i \mathbf{I}_3 \end{bmatrix}, \quad \mathbf{W}_i = \begin{bmatrix} \boldsymbol{\Omega}_i & \mathbf{0}_3 \\ \mathbf{0}_3 & \mathbf{0}_3 \end{bmatrix}, \quad i = 1, 2, \dots, r \quad (2.1)$$

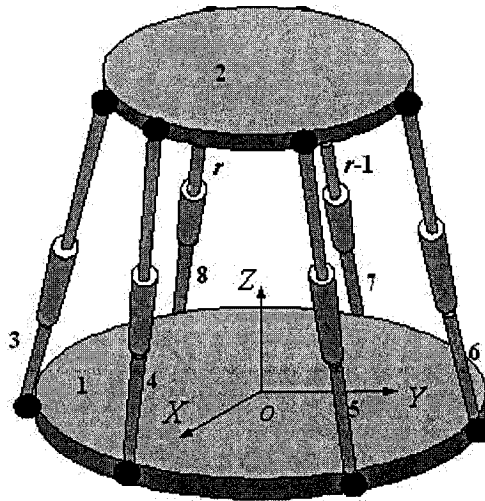


Figure 2.1: Schematic diagram of a Stewart-type manipulator

where: $\mathbf{0}_3 \in \mathfrak{R}^{3 \times 3}$, $\mathbf{I}_3 \in \mathfrak{R}^{3 \times 3}$ denote the zero and identity matrices, respectively; $\hat{\mathbf{I}}_i \in \mathfrak{R}^{3 \times 3}$, $\mathbf{\Omega}_i \in \mathfrak{R}^{3 \times 3}$ denotes the inertia and angular-velocity matrices of the i^{th} rigid body, with respect to its mass center C_i , respectively; m_i denotes the mass of the i^{th} rigid body. Then the manipulator mass matrix $\mathbf{M} \in \mathfrak{R}^{6r \times 6r}$ and manipulator angular-velocity matrix $\mathbf{W} \in \mathfrak{R}^{6r \times 6r}$, which are both block symmetric, are as follows:

$$\mathbf{M} = \text{diag}(\mathbf{M}_1, \mathbf{M}_2, \dots, \mathbf{M}_r) \quad (2.2)$$

$$\mathbf{W} = \text{diag}(\mathbf{W}_1, \mathbf{W}_2, \dots, \mathbf{W}_r) \quad (2.3)$$

Let $\mathbf{t}_i \in \mathfrak{R}^{6 \times 1}$ denote the twist of the i^{th} rigid body, in terms of the angular velocity vector $\boldsymbol{\omega}_i \in \mathfrak{R}^{3 \times 1}$ of $\mathbf{\Omega}_i$ and the linear velocity vector $\dot{\mathbf{c}}_i \in \mathfrak{R}^{3 \times 1}$ of C_i . Then the generalized twists can be expressed as $\mathbf{t} \in \mathfrak{R}^{6r \times 1}$:

$$\mathbf{t}_i = [\boldsymbol{\omega}_i \quad \dot{\mathbf{c}}_i]^T, \quad i = 1, 2, \dots, r \quad (2.4)$$

$$\mathbf{t} = [\mathbf{t}_1 \quad \mathbf{t}_2 \quad \dots \quad \mathbf{t}_r]^T \quad (2.5)$$

Since all kinematic pairs allow one DOF motion between the coupled bodies, we can express the kinematic constraints of the system in linear homogeneous form, namely,

$$\mathbf{Kt} = \mathbf{0} \quad (2.6)$$

where: $\mathbf{K} \in \mathfrak{R}^{6r \times 6r}$ is a coefficient matrix.

In order to derive the dynamic model of the manipulator from the twist-shape relationship, $\mathbf{t} = \mathbf{T}\dot{\mathbf{q}}$, $\mathbf{T} \in \mathfrak{R}^{6r \times n}$ should be solved. Since $\mathbf{KT} = \mathbf{0}$, and \mathbf{K} is available through the analysis of the mechanical structure of the manipulator, \mathbf{T} is obtained. The

detailed expressions of \mathbf{K} and \mathbf{T} are given in (Angeles J., 2003 [1]). Defining $\mathbf{q} \in \mathcal{R}^{n \times 1}$ as the generalized coordinates, in which q_h denotes the translation or rotation angle of the h^{th} , $h = 1, 2, \dots, n$, active joint, the dynamic model of the manipulator is derived:

$$\mathbf{H}(\mathbf{q})\ddot{\mathbf{q}} + \mathbf{C}(\mathbf{q}, \dot{\mathbf{q}})\dot{\mathbf{q}} + \mathbf{G}(\mathbf{q}) = \boldsymbol{\tau}_a \quad (2.7)$$

where: $\mathbf{H}(\mathbf{q}) \in \mathcal{R}^{n \times n}$ is the symmetric, positive-definite inertia matrix; $\mathbf{C}(\mathbf{q}, \dot{\mathbf{q}}) \in \mathcal{R}^{n \times n}$ is the coefficient matrix of Coriolis and centrifugal forces; $\mathbf{G}(\mathbf{q}) \in \mathcal{R}^{n \times 1}$ is the gravity force vector; $\boldsymbol{\tau}_a \in \mathcal{R}^{n \times 1}$ is the actuating force exerted on the active joints. The frictional effects are neglected here. The expressions for $\mathbf{H}(\mathbf{q})$ and $\mathbf{C}(\mathbf{q}, \dot{\mathbf{q}})$ are displayed below (Angeles J., 2003 [1]):

$$\mathbf{H}(\mathbf{q}) = \mathbf{T}^T \mathbf{M} \mathbf{T} \quad (2.8)$$

$$\mathbf{C}(\mathbf{q}, \dot{\mathbf{q}}) = \mathbf{T}^T \mathbf{M} \dot{\mathbf{T}} + \mathbf{T}^T \mathbf{W} \mathbf{M} \mathbf{T} \quad (2.9)$$

Although other types of spatial parallel robotic manipulators have different mechanical structures, following the above procedure, the same compact dynamic equations as (2.7) can be derived.

2.3.2 Dynamic Model of a Planar Parallel Robotic Manipulator

For reasons given in the previous sub-section, in this sub-section, we select a P-R-R type manipulator as an example to derive the dynamic model of all planar parallel robotic manipulators within a common form.

Considering a P-R-R type manipulator composed of r rigid bodies, as shown in Figure 2.2, the inertia frame (X, Y, Z) is fixed at the center of the base platform with the Z axis pointing vertically upward. Since the manipulator has three DOF, its end-effector, i.e., the platform moves in the horizontal plane. Using the NOC method, the dynamic equations of the manipulator are derived.

$$\mathbf{H}(\mathbf{q})\ddot{\mathbf{q}} + \mathbf{C}(\mathbf{q}, \dot{\mathbf{q}})\dot{\mathbf{q}} = \boldsymbol{\tau}_a \quad (2.10)$$

The derived dynamic equations are somewhat different from (2.7):

- (i) Compared with (2.4), $\mathbf{t}_i = [\omega_i \quad \dot{\mathbf{c}}_i]^T$ is a 3-dimensional vector, where ω_i is the scalar angular velocity of the i^{th} rigid body, and $\dot{\mathbf{c}}_i$ is the 2-dimensional velocity of its mass center. In addition, \mathbf{K} is $3r \times 3r$ and \mathbf{T} is $3r \times 3$.

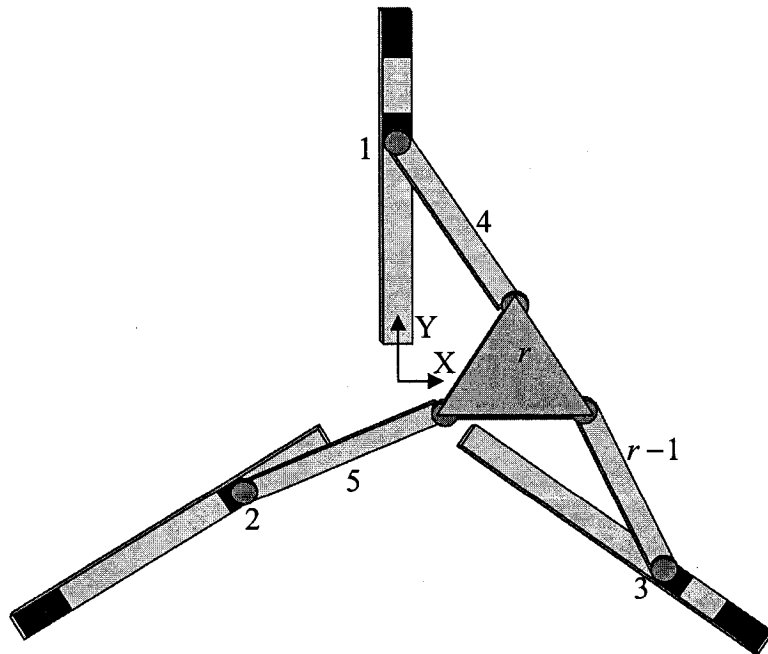


Figure 2.2: Schematic diagram of a P-R-R type manipulator

- (ii) Compared with (2.1), the inertia dyad \mathbf{M}_i and angular velocity dyad \mathbf{W}_i are both now a 3×3 matrix, i.e.,

$$\mathbf{M}_i = \begin{bmatrix} \hat{I}_i & \mathbf{0}_{2 \times 2} \\ \mathbf{0}_{2 \times 1} & m_i \mathbf{I}_3 \end{bmatrix}, \quad \mathbf{W}_i = \begin{bmatrix} \boldsymbol{\Omega}_i & \mathbf{0}_{1 \times 2} \\ \mathbf{0}_{2 \times 1} & \mathbf{0}_{2 \times 2} \end{bmatrix}, \quad i = 1, 2, \dots, r \quad (2.11)$$

Where $\hat{I}_i \in \mathfrak{R}^+$ denotes the scalar moment of inertia of the i^{th} rigid body through its center of mass, \mathbf{I}_2 is the 2×2 identity matrix; $\boldsymbol{\Omega}_i \in \mathfrak{R}$ denotes the angular velocity of the i^{th} rigid body around the Z axis.

- (iii) From (2.9), $\mathbf{W}_i \mathbf{M}_i = \mathbf{0}$ is derived, and as a consequence, $\mathbf{C}(\mathbf{q}, \dot{\mathbf{q}}) = \mathbf{T}^T \mathbf{M} \dot{\mathbf{T}}$ instead of (2.9). Furthermore, since all rigid bodies of the manipulator move horizontally, therefore, the gravity term, $\mathbf{G}(\mathbf{q})$, is vanished.

Although other types of planar parallel robotic manipulators have different mechanical structures, we can derive the same compact dynamic equations as (2.10) by the means of NOC.

2.4 Summary

Studying the derived dynamic equations (2.7) and (2.10), we find that the dynamic equations of any parallel robotic manipulator can be written in the same compact form, $\mathbf{H}(\mathbf{q})\ddot{\mathbf{q}} + \mathbf{C}(\mathbf{q}, \dot{\mathbf{q}})\dot{\mathbf{q}} + \mathbf{G}(\mathbf{q}) = \boldsymbol{\tau}_a$, assuming that frictional effects can be neglected. The only differences with respect to spatial and planar parallel robotic manipulators are the expression for $\mathbf{C}(\mathbf{q}, \dot{\mathbf{q}})$, the dimensions of $\mathbf{H}(\mathbf{q})$ and $\mathbf{C}(\mathbf{q}, \dot{\mathbf{q}})$, and the value of $\mathbf{G}(\mathbf{q})$.

Therefore, (2.7) is adopted as the dynamic model of parallel robotic manipulators. Based on (2.7), two important features have been proved: (i) $\dot{\mathbf{H}}(\mathbf{q}) - 2\mathbf{C}(\mathbf{q}, \dot{\mathbf{q}})$ is a skew-symmetric matrix; (ii) there are no constraints in the derived dynamic equations (2.7) (Angeles J., 2003 [1]). These two features are necessary to prove stability of the control methods addressed in Chapter 3 and Chapter 5.

Chapter 3

Synchronized Control for Parallel Robotic Manipulators

3.1 Introduction

In this chapter, we propose a synchronized control approach to solve the trajectory tracking control problem of parallel robotic manipulators, with the assumption that the dynamic model parameters of the manipulator are known. In section 2, two questions are raised and answered, which are important to synchronized control: Whether there exists a controlled synchronization problem during trajectory control of a parallel robotic manipulator? Whether it is appropriate to propose a synchronized control approach to solve this trajectory control problem? In section 3, guidelines for the definition of the synchronization error, and definition of the synchronization error, are presented. With the presentation of a new synchronization error, a model-based synchronized control approach is proposed for trajectory control of parallel robotic manipulators. Subsequently, stability analysis is addressed. Finally, a summary is presented in section 4.

3.2 The Study of Synchronized Control

As introduced in the literature review, synchronized control has been applied to many fields involving synchronization phenomenon, such as cooperation amongst multi-robotic

systems, machining of multi-axis machine tools, etc. Here, referred to (Nijmeijer, H., *et al.*, 2003 [47]), in terms of the formulation of the controlled synchronization problem, distinction is made between *internal synchronization* and *external synchronization*. The definitions of the two types of synchronizations are given as below.

Internal synchronization: all synchronized objects occur on equal terms in the unified multi-composed system. Thus the synchronous motion occurs as the result of interaction of all elements of the system, e.g., cooperative systems. The majority of synchronizations belong to this category.

External synchronization: one object in the multi-composed system is more powerful than the others and its motion can be considered as independent of the motion of the other objects. Therefore the resulting synchronous motion is predetermined by this dominant independent system, e.g. master-slave system.

(Nijmeijer, H., *et al.*, 2003 [47]),

For the trajectory control of parallel robotic manipulators, two questions are raised: *whether there exists a controlled synchronization problem? If the answer is positive, then whether it is appropriate to utilize the synchronized control technique to solve the trajectory control problem?*

Examining the structure of a parallel robotic manipulator, we note that the platform and each pair of branches consist of a closed-loop kinematic chain, and therefore the mechanical structure of the manipulator is closed-loop. Due to this characteristic, motion of each active joint is constrained by the motions of the other active joints through the

platform and rigid intermediate links, which shows the coupling effects amongst the active joints. During trajectory control, therefore, all active joints should move along their pre-calculated paths synchronously to control the platform to move along the desired trajectory. From another point of viewing, each branch, comprised of several rigid intermediate links, active and passive joints, may be treated as a serial robotic manipulator, hence termed a sub-manipulator, due to their open loop kinematic chain structure. Typically, there is only one active joint in a sub-manipulator. Therefore, the single parallel robotic system can be treated as a multi-robotic system, a cooperative system, in which the platform is the common payload grasped by the sub-manipulators. In other words, the trajectory control problem of a parallel robotic manipulator may be treated as the cooperation control problem of multiple sub-manipulators, i.e., all sub-manipulators should move synchronously to guarantee the common payload moving

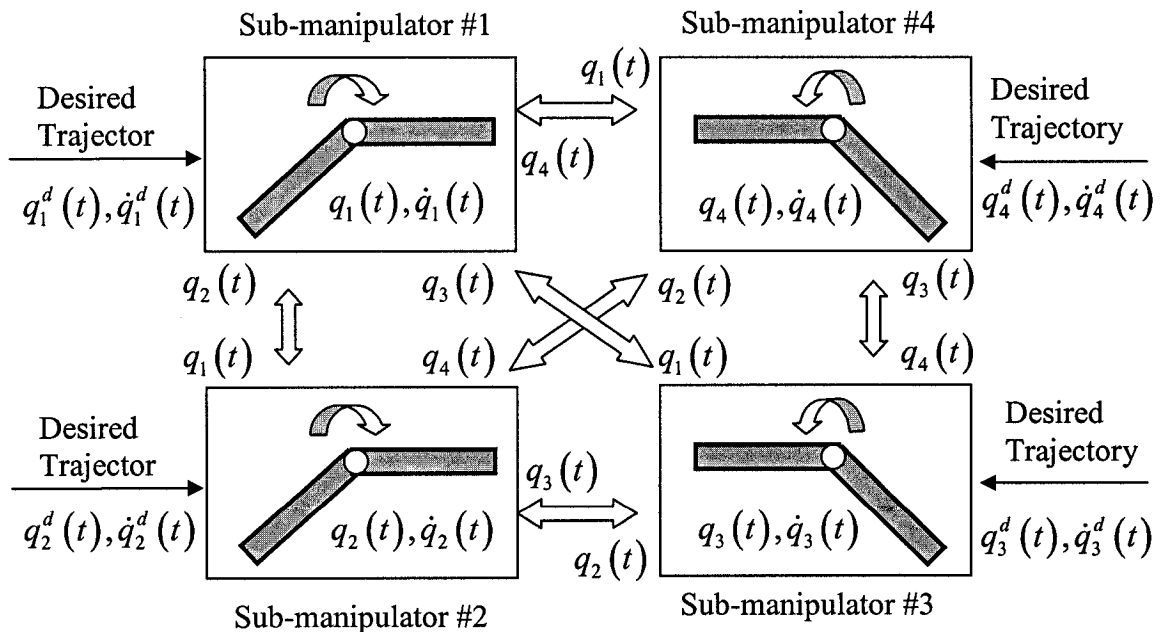


Figure 3.1: Synchronization in a parallel robotic manipulator (4 active joints case)

along the desired trajectory, as shown in Figure 3.1. As we introduced at the beginning of this section, the cooperation control problem is a synchronized control problem and is categorized as internal synchronization. Therefore, the answer to the first question is positive.

In terms of the literature review introduced in Chapter 1, few synchronized control approaches have been proposed for trajectory control of a parallel robotic manipulator, in particular moving at high speed and high acceleration. However, during trajectory tracking of a parallel robotic manipulator, the synchronization problem does exist, and in some cases, it significantly affects control performance. For instance, when accelerations of active joints are high and the mass of the platform including the payload is large, tracking accuracy will be low and damage of the manipulator mechanical structure may occur. Thus, it is necessary to consider the synchronization problem here and it is appropriate to employ the synchronization control technique to solve this problem.

3.3 Synchronized Control Design

While applying synchronized control to a mechanical system, how to utilize the system's physical features to define an additional feedback signal, termed synchronization error, is the most important, because this error represents the coordination degree of synchronized motions of all active joints. Obviously, the synchronization error is different from the traditional tracking errors, i.e., position errors, velocity errors, etc. Moreover, with the employment of the synchronization error, each active joint receives feedback signals both from itself and from the other active joints. As a result, tracking performance is improved.

In this section, we first introduce guidelines for the definition of the synchronization error and the definition of a synchronization error with respect to the mechanical structure of parallel robotic manipulators. Then, based on the defined synchronization error, a new synchronized control approach is proposed under the assumption that the dynamic model parameters are known. Finally, stability analysis of the proposed approach is offered.

3.3.1 The Model-Based Synchronization Error

Reviewing the synchronization errors defined in various synchronized control approaches, a guideline is concluded: the synchronization error is typically defined through combining the position or velocity errors of all axes (machine tools) or of all active joints (multi-robotic systems) via a coefficient matrix, termed synchronization coefficient matrix. Obviously, how to construct this synchronization coefficient matrix is crucial. The methods to construct the matrix can be loosely divided into two main approaches according to different application objectives.

- (i) For a multi-axis machine tool and a mobile robot: the matrix is typically constructed based on the contour error of its end-effector (Koren, Y., 1980 [33], Chen, B.-C., *et al.*, 1998 [10], Lo, C.-C., 1999 [41], Borenstein, J. *et al.*, 1987 [6], Sun, D. *et al.*, 2002 [75]). For a mobile robot, the end-effector is its geometric center.
- (ii) For multi-robot systems: the matrix may be constructed based on a function utilizing both the geometric shape of the common payload and using a Taylor

series expansion (Sun, D. *et al.*, 2002 [74]); or based on the trial-and-error method (Rodriguez-Angeles, A. *et al.*, 2003 [63]).

For a parallel robotic manipulator, however, these methods may not be the most appropriate, because the forward kinematics of the manipulator is somewhat more complicated than robots considered in the above literature. Specifically, in a parallel robotic manipulator, there are passive joints in addition to active joints, and employed sensors typically measure only the translations or rotations of the active joints. However, the positions of the sub-manipulators are required within the previous methods. Thus here, we develop a new method to define the synchronization error for parallel robotic manipulators based on the kinematic constraints of its sub-manipulators, i.e., active joints.

In order to define a suitable synchronization error reflecting the coupling effects amongst the active joints in a parallel robotic manipulator, it is reasonable to consider the manipulator kinematics, parts of which demonstrate the kinematic relationships amongst the active joints and the manipulator end-effector. For a parallel robotic manipulator with n DOF, based on the robotic kinematics, utilizing the time derivative of the generalized coordinates and that of the pose of the platform, we have:

$$\dot{\mathbf{X}}_p(t) = (\mathbf{J}_p(t))^{-1} \dot{\mathbf{q}}(t) \quad (3.1)$$

where: $\mathbf{X}_p(t) \in \mathfrak{R}^{n \times 1}$ vector denotes the position and orientation of the platform at its mass center; $\mathbf{J}_p(t) \in \mathfrak{R}^{n \times n}$ Jacobian matrix represents the velocity relationship between the active joints and the platform. Let $\mathbf{X}_p^d(t)$, $\mathbf{q}^d(t)$, $\mathbf{J}_p^d(t)$ denote the desired value of $\mathbf{X}_p(d)$, $\mathbf{q}(t)$ and $\mathbf{J}_p(t)$, respectively. Replacing terms in (3.1) with the desired values, we obtain:

$$\dot{\mathbf{X}}_p^d(t) = (\mathbf{J}_p^d(t))^{-1} \dot{\mathbf{q}}^d(t) \quad (3.2)$$

Since $\dot{\mathbf{X}}_p(d)$, $\dot{\mathbf{X}}_p^d(t)$ demonstrate the kinematic relationship between the derivative of the (desired) pose of the platform and the derivative of the (desired) positions of all sub-manipulators, subtracting (3.1) from (3.2), the function describing the kinematic constraints of the active joints in the parallel robotic manipulator is derived:

$$\dot{\mathbf{e}}_{x_p} = (\mathbf{J}_p(t))^{-1} \cdot \dot{\mathbf{e}}(t) + \left((\mathbf{J}_p(t))^{-1} - (\mathbf{J}_p^d(t))^{-1} \right) \cdot \dot{\mathbf{q}}^d(t) \quad (3.3)$$

where: $\mathbf{e}(t) = \mathbf{q}(t) - \mathbf{q}^d(t) \in \mathbb{R}^{n \times 1}$, $\dot{\mathbf{e}}(t) = \dot{\mathbf{q}}(t) - \dot{\mathbf{q}}^d(t) \in \mathbb{R}^{n \times 1}$ denote the errors of the generalized coordinates and the errors of the generalized speed, respectively. Note that $\dot{\mathbf{e}}_{x_p}(t) = (\dot{\mathbf{X}}_p(t) - \dot{\mathbf{X}}_p^d(t)) \in \mathbb{R}^{n \times 1}$ describes the kinematic constraints of the active joints with respect to the geometry of the platform and kinematic chains, rather than the derivative of the pose error of the platform in the task space. This derived function $\dot{\mathbf{e}}_{x_p}(t)$ is similar to the function defined for a multi-robot system (Sun, D., *et al.*, 2002), which describes the kinematic constraints amongst the multiple serial robots with respect to the geometry of the common payload.

In order to reflect these kinematic constraints onto each active joint, left multiplying $\mathbf{J}_p(t)$ on both sides of (3.3), we have:

$$\mathbf{J}_p(t) \dot{\mathbf{e}}_{x_p}(t) = \dot{\mathbf{e}}(t) + \left(\mathbf{I}_n - \mathbf{J}_p(t) (\mathbf{J}_p^d(t))^{-1} \right) \dot{\mathbf{q}}^d(t) \quad (3.4)$$

where: $\mathbf{I}_n \in \mathbb{R}^{n \times n}$ is the identity matrix. Furthermore, utilizing a similar boundary control construction as in (Corless, M.J. *et al.*, 1981) to guarantee the synchronization error be bounded when $\mathbf{e}(t), \dot{\mathbf{e}}(t)$ are bounded, the synchronization error is defined based on (3.4):

$$\epsilon(t) = \begin{cases} \dot{\epsilon}(t) + \frac{\mathbf{I}_n - \mathbf{J}_p(t)(\mathbf{J}_p^d(t))^{-1}}{\|\mathbf{I}_n - \mathbf{J}_p(t)(\mathbf{J}_p^d(t))^{-1}\|} \dot{\mathbf{q}}^d(t) & \text{if } \|\mathbf{I}_n - \mathbf{J}_p(t)(\mathbf{J}_p^d(t))^{-1}\| > \zeta \\ \dot{\epsilon}(t) + \frac{1}{\zeta} \cdot (\mathbf{I}_n - \mathbf{J}_p(t)(\mathbf{J}_p^d(t))^{-1}) \dot{\mathbf{q}}^d(t) & \text{if } \|\mathbf{I}_n - \mathbf{J}_p(t)(\mathbf{J}_p^d(t))^{-1}\| \leq \zeta \end{cases} \quad (3.5)$$

where: $\epsilon(t) \in \mathfrak{R}^{n \times 1}$ denotes the defined synchronization error; $\zeta \in \mathfrak{R}^+$ is a positive constant. Based on the maximum absolute row sum norm of $\mathbf{I}_n - \mathbf{J}_p(t)(\mathbf{J}_p^d(t))^{-1}$, $\epsilon(t)$ has two expressions, as given above.

Here, two points should be noted for the defined synchronization error. First, since this synchronization error is defined from the kinematic constraints of the sub-manipulators in a parallel robotic manipulator, it represents the coupling effects amongst all sub-manipulators, i.e., all kinematic chains; furthermore, it represents the coupling effects amongst all active joints. Therefore, $\epsilon(t)$ represents the coordination degree of synchronization amongst all active joints. Second, the coefficient matrix of $\epsilon(t)$ is time varying and is constructed from the Jacobian matrix of the parallel robotic manipulator, thus, the defined synchronization error is model-based and nonlinear with respect to the positions of active joints. The value of the Jacobian matrix at each sampling time can be obtained through iterative algebraic calculations.

3.3.2 The Synchronized Controller

After the synchronization error is defined, a new synchronized controller is then developed. In the proposed synchronized control scheme, two types of errors are

employed: tracking error $\mathbf{e}(t)$ and synchronization error $\boldsymbol{\epsilon}(t)$. Combining these two errors, we define a coupling error, $\mathbf{e}^*(t) \in \mathfrak{R}^{n \times 1}$:

$$\mathbf{e}^*(t) = \mathbf{e}(t) + \boldsymbol{\Gamma} \cdot \boldsymbol{\epsilon}(t) \quad (3.6)$$

where: $\boldsymbol{\Gamma} \in \mathfrak{R}^{n \times n}$ is a diagonal positive coefficient matrix. Based on the coupling error, define a command vector $\bar{\mathbf{u}}(t) \in \mathfrak{R}^{n \times 1}$ as follows:

$$\bar{\mathbf{u}}(t) \stackrel{\Delta}{=} \dot{\mathbf{q}}^d(t) - \boldsymbol{\Lambda} \mathbf{e}^*(t) \quad (3.7)$$

where: $\boldsymbol{\Lambda} \in \mathfrak{R}^{n \times n}$ is a positive diagonal coefficient matrix. Definition of $\bar{\mathbf{u}}(t)$ in (3.7) leads to the following coupled position and velocity errors:

$$\bar{\mathbf{r}}(t) \stackrel{\Delta}{=} \dot{\mathbf{q}}(t) - \bar{\mathbf{u}}(t) = \dot{\mathbf{e}}^*(t) + \boldsymbol{\Lambda} \mathbf{e}^*(t) \quad (3.8)$$

where: $\bar{\mathbf{r}}(t) \in \mathfrak{R}^{n \times 1}$ is referred to as a “reference value” (Slotine, J.-J.E., *et al.*, 1983 [67]), and $\bar{\mathbf{r}}(t)$ can be treated as a measure of trajectory tracking accuracy. Our objective is to design a control law such that the coupling error, i.e., the position, velocity, and synchronization errors, converges to zero. In other words, the control law should be able to restrict $\bar{\mathbf{r}}(t)$ to lie on the sliding surface:

$$\bar{\mathbf{r}}(t) = \dot{\mathbf{e}}^*(t) + \boldsymbol{\Lambda} \mathbf{e}^*(t) = \mathbf{0} \quad (3.9)$$

The proposed control law is defined as follows:

$$\boldsymbol{\tau}_a = \mathbf{H}(\mathbf{q}) \ddot{\bar{\mathbf{u}}}(t) + \mathbf{C}(\mathbf{q}, \dot{\mathbf{q}}) \bar{\mathbf{u}}(t) + \mathbf{G}(\mathbf{q}) - \mathbf{K}_r \bar{\mathbf{r}}(t) - \mathbf{K}_e \dot{\mathbf{e}}^*(t) \quad (3.10)$$

where: $\mathbf{K}_r \in \mathfrak{R}^{n \times n}$, $\mathbf{K}_e \in \mathfrak{R}^{n \times n}$ are both positive diagonal gain matrices.

The structure of the synchronized controller is shown in Figure 3.2. The required set-point inputs to the controller are the desired positions, velocities, and accelerations of

the active joints. The required measurements are the actual positions and velocities of the active joints. In addition, the controller consists of two main parts. The first part is a form of full dynamic compensation, which attempts to provide the active joints necessary dynamic torques to produce the desired motions. The second part contains two terms representing a PD feedback, since:

$$-\mathbf{K}_r \bar{\mathbf{r}}(t) - \mathbf{K}_e \dot{\mathbf{e}}^*(t) = -(\mathbf{K}_r \Lambda + \mathbf{K}_e) \mathbf{e}^*(t) - \mathbf{K}_r \dot{\mathbf{e}}^*(t) \quad (3.11)$$

This part regulates the actual trajectories of both active joints and the platform to their desired trajectories. Studying the two parts, we find that the proposed control law (3.10) has generality for all parallel robotic manipulators, because the dynamic compensation is based on the dynamic model derived in Chapter 2, which is suitable for both spatial and planar parallel robotic manipulators, and the feedback errors, $\mathbf{e}^*(t)$ and its first derivative, in the PD feedback are also defined with respect to a general parallel robotic manipulator.

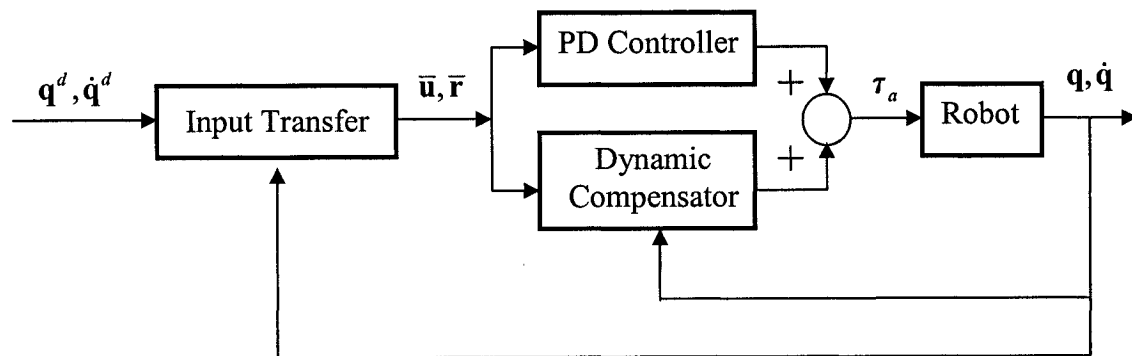


Figure 3.2: The structure of the synchronized controller

After the control law is proposed, it is necessary to prove whether the closed-loop controller is stable and specify under which conditions the controller is stable; otherwise, the controller developed is meaningless or cannot be implemented in practice.

3.3.3 Stability Analysis of Synchronized Control

Through construction of a Lyapunov function and use of Barbalat's Lemma (Slotine, J.-J.E. *et al.*, 1991 [68]) and with three assumptions, Theorem 1, which addresses the stability of the proposed control algorithm, is proved.

Three assumptions are:

Assumption 1: The desired trajectories are continuous and bounded and do not cross singular points in the workspace of the parallel robotic manipulator.

Assumption 2: $\mathbf{H}(\mathbf{q})$ and $\mathbf{C}(\mathbf{q}, \dot{\mathbf{q}})$ are bounded if their arguments are bounded.

Assumption 3: Frictional effects can be neglected.

Theorem 1: The proposed synchronized tracking controller (3.10) guarantees the asymptotic convergence of the position errors, synchronization error, and coupling errors, i.e., $\mathbf{e}(t) \rightarrow \mathbf{0}$, $\epsilon(t) \rightarrow \mathbf{0}$ and $\mathbf{e}^*(t) \rightarrow \mathbf{0}$ as $t \rightarrow \infty$.

Proof: Substituting the control law (3.10) into the dynamic equations (2.7), the closed-loop dynamics of a parallel robotic manipulator are:

$$\mathbf{H}(\mathbf{q})\dot{\bar{\mathbf{r}}}(t) + \mathbf{C}(\mathbf{q}, \dot{\mathbf{q}})\bar{\mathbf{r}}(t) + \mathbf{K}_r\bar{\mathbf{r}}(t) + \mathbf{K}_e\mathbf{e}^*(t) = \mathbf{0} \quad (3.12)$$

Define a positive definite function:

$$V(t) = \frac{1}{2} \left[\bar{\mathbf{r}}^T(t) \mathbf{H}(\mathbf{q}) \bar{\mathbf{r}}(t) + \mathbf{e}^*(t)^T \mathbf{K}_e \mathbf{e}^*(t) \right] \quad (3.13)$$

This function is based on the kinetic energy of the parallel robotic system with respect to

$\bar{\mathbf{r}}(t)$, and the coupling effect with respect to the coupling error $\mathbf{e}^*(t)$.

Differentiating $V(t)$ with respect to time yields:

$$\dot{V}(t) = \bar{\mathbf{r}}^T(t) \mathbf{H}(\mathbf{q}) \dot{\bar{\mathbf{r}}}(t) + \frac{1}{2} \bar{\mathbf{r}}^T(t) \dot{\mathbf{H}}(\mathbf{q}) \bar{\mathbf{r}}(t) + \mathbf{e}^*(t)^T \mathbf{K}_e \dot{\mathbf{e}}^*(t) \quad (3.14)$$

Left multiplying both sides of (3.12) by $\bar{\mathbf{r}}^T(t)$, then substituting into (3.14), we have:

$$\dot{V}(t) = \bar{\mathbf{r}}^T(t) \left(\frac{1}{2} \dot{\mathbf{H}}(\mathbf{q}) - \mathbf{C}(\mathbf{q}, \dot{\mathbf{q}}) \right) \bar{\mathbf{r}}(t) - \bar{\mathbf{r}}^T(t) \mathbf{K}_r \bar{\mathbf{r}}(t) - \bar{\mathbf{r}}^T(t) \mathbf{K}_e \mathbf{e}^*(t) + \mathbf{e}^*(t)^T \mathbf{K}_e \dot{\mathbf{e}}^*(t) \quad (3.15)$$

Since $\dot{\mathbf{H}}(\mathbf{q}) - 2\mathbf{C}(\mathbf{q}, \dot{\mathbf{q}})$ is a skew-symmetric matrix, the first term on the right side of (3.15) is eliminated. Substituting (3.9), we have:

$$\begin{aligned} \dot{V}(t) &= -\bar{\mathbf{r}}^T(t) \mathbf{K}_r \bar{\mathbf{r}}(t) - \left(\dot{\mathbf{e}}^*(t)^T + \mathbf{e}^*(t)^T \Lambda \right) \mathbf{K}_e \mathbf{e}^*(t) + \mathbf{e}^*(t)^T \mathbf{K}_e \dot{\mathbf{e}}^*(t) \\ &= -\bar{\mathbf{r}}^T(t) \mathbf{K}_r \bar{\mathbf{r}}(t) - \mathbf{e}^*(t)^T \Lambda \mathbf{K}_e \mathbf{e}^*(t) \leq 0 \end{aligned} \quad (3.16)$$

Since $V(t) \geq 0$ and $\dot{V}(t) \leq 0$, $V(t)$ remains bounded. Given the expression (3.13) of $V(t)$, this implies that $\bar{\mathbf{r}}(t)$, $\mathbf{e}^*(t)$ are bounded. From (3.9), $\dot{\mathbf{e}}^*(t)$ is bounded. As a consequence, $\mathbf{e}^*(t)$ is uniformly continuous. Using Barbalat's Lemma, it follows that $\mathbf{e}^*(t) \rightarrow \mathbf{0}$ as $t \rightarrow \infty$.

Since the desired trajectory is continuous and bounded, then $\mathbf{q}^d(t)$, $\dot{\mathbf{q}}^d(t)$ and $\ddot{\mathbf{q}}^d(t)$ are all continuous and bounded. Furthermore, since the desired trajectory does not cross singular points in the workspace, then $\mathbf{J}_p^d(t)$ is bounded.

Let $\mathbf{E}(t) \in \mathcal{R}^{n \times 1}$ denote the second term of $\epsilon(t)$. Substituting (3.5) into (3.6), we derive:

$$\mathbf{e}(t) + \Gamma \dot{\mathbf{e}}(t) = \mathbf{e}^*(t) - \Gamma \mathbf{E}(t) \quad (3.17)$$

Since the desired trajectory of the platform is continuous and bounded, then the trajectories of the active joints calculated from the inverse kinematics are continuous and bounded. Therefore, $\Gamma \mathbf{E}(t)$ is bounded and the right side of (3.17) is bounded. Moreover, since Γ is constant, hence, (3.17) is a first order ordinary differential equation. Solving (3.17), we obtain its analytical solution:

$$\mathbf{e}(t) = \mathbf{e}^{-\Gamma t} \left\{ \int_0^t \left[e^{s\Gamma} \left(\Gamma^{-1} \mathbf{e}^*(s) - \mathbf{E}(s) \right) \right] ds + \mathbf{e}(0) \right\} \quad (3.18)$$

Differentiating (3.18) with respect to time yields:

$$\dot{\mathbf{e}}(t) = \Gamma^{-1} \mathbf{e}^{-\Gamma t} \left\{ \int_0^t \left[e^{s\Gamma} \left(\Gamma^{-1} \mathbf{e}^*(s) - \mathbf{E}(s) \right) \right] ds + \mathbf{e}(0) \right\} + \Gamma^{-1} \mathbf{e}^*(t) - \mathbf{E}(t) \quad (3.19)$$

Let ψ_{\max} and ψ_{\min} demonstrate the maximum and minimum value of the right side of (3.17), respectively. Assuming $\mathbf{e}(0) = \mathbf{0}$, we can derive:

$$\psi_{\min} - e^{-\Gamma t} \psi_{\min} \leq \mathbf{e}(t) \leq \psi_{\max} - e^{-\Gamma t} \psi_{\max} \quad (3.20)$$

$$\Gamma^{-1} e^{-\Gamma t} \psi_{\min} \leq \dot{\mathbf{e}}(t) \leq \Gamma^{-1} e^{-\Gamma t} \psi_{\max} \quad (3.21)$$

Therefore, $\mathbf{e}(t)$ and $\dot{\mathbf{e}}(t)$ are continuous and bounded. Similarly, we can derive that $\ddot{\mathbf{e}}(t)$ is also bounded. Since $\dot{\mathbf{e}}(t)$ is bounded, then $\mathbf{e}(t)$ is uniformly continuous. From Barbalat's lemma, it follows that $\mathbf{e}(t) \rightarrow \mathbf{0}$ as $t \rightarrow \infty$. Since $\mathbf{e}(t) \rightarrow \mathbf{0}$ as $t \rightarrow \infty$, then $\mathbf{J}_p(t) (\mathbf{J}_p^d(t)) \rightarrow \mathbf{I}_n$ as $t \rightarrow \infty$. In addition, since $\dot{\mathbf{e}}(t)$ and $\dot{\mathbf{q}}^d(t)$ are both bounded, then $\dot{\mathbf{q}}(t)$ is bounded. Thus, from (3.5), $\boldsymbol{\epsilon}(t) \rightarrow \mathbf{0}$ as $t \rightarrow \infty$. Subsequently, from (3.6), $\mathbf{e}^*(t) \rightarrow \mathbf{0}$ as $t \rightarrow \infty$. \square

Theorem 1 demonstrates that with the three assumptions, the synchronization error, the coupling error and tracking errors of the system will asymptotically converge to zero

during trajectory tracking, and therefore, proves that the proposed control law (3.10) is stable. For the three assumptions, the first two are easy to satisfy, while the third one is somewhat difficult to meet during practical operations. If frictional effects cannot be neglected, an additional term representing frictional force should be added to the left side of dynamic equations (2.7). In this case, if the frictional force is bounded, a synchronized control law similarly as (3.10), which has an additional term denoting the frictional force on the right side, can also be proved stable employing the above method.

3.4 Summary

In this chapter, we define a new synchronization error with respect to the mechanical structure of parallel robotic manipulators. Subsequently, based on this synchronization error, we propose a synchronized controller to solve the trajectory tracking control problem of parallel robotic manipulators. Under the assumption that the dynamic model of the manipulator is exactly known and frictional effects can be neglected, the proposed controller is proved stable through construction of a Lyapunov function and using Barbalat's Lemma. Experimental results will be shown in the following chapter.

Chapter 4

Experimental System and Experimentation

4.1 Introduction

In order to demonstrate the validity and effectiveness of the developed synchronized control approach, we conduct experiments on a P-R-R type planar parallel robotic manipulator⁵. As a comparison, experiments employing only PID control are also conducted. In this chapter, we present the experimental system set-up of a P-R-R manipulator, which was designed and assembled by the Laboratory for Nonlinear Systems Control (LNSC) at the University of Toronto (Kang, B. *et al.*, 2001 [29]). In addition, experimental results using PID control and the proposed synchronized control are shown.

The rest of this chapter is organized as follows. Section 2 briefly introduces the kinematic and dynamic model of the P-R-R type manipulator. Section 3 addresses the experimental system that was designed and assembled at LNSC and briefly introduces the experimental software developed by Zhu, S. and Ren, L. Section 4 presents experimental results using synchronized control and PID control to follow different desired trajectories. Subsequently, analysis of experimental results is provided. Finally, section 5 offers a summary of this chapter.

⁵ In the rest of this thesis, unless otherwise specified, “P-R-R type planar parallel robotic manipulator” is abbreviated as “P-R-R manipulator”.

4.2 Modeling of a P-R-R Type Manipulator

As introduced in Chapter 2, the P-R-R manipulator is a type of planar parallel manipulators with three DOF. This manipulator has three branches, in each of which there is an active prismatic joint and two consecutive passive revolute joints, as illustrated in Figure 4.1.

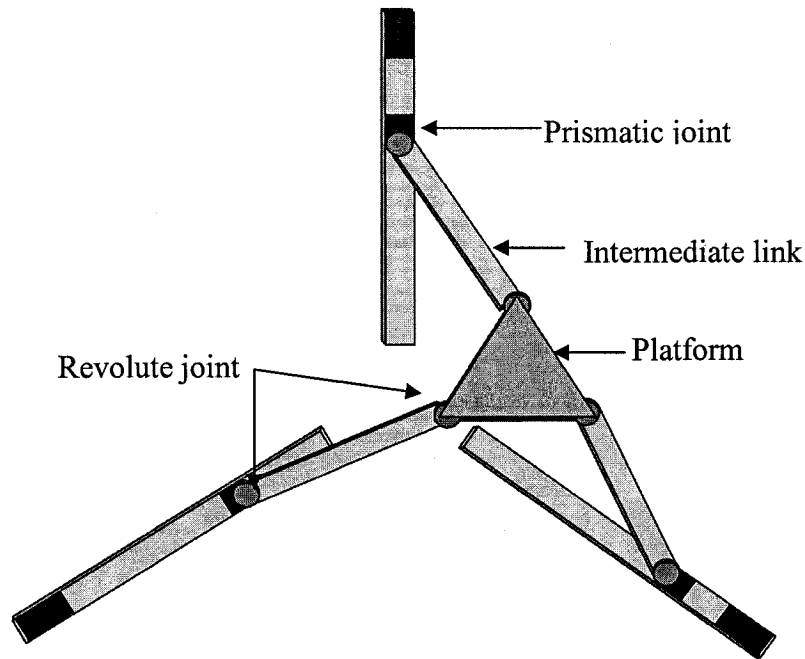


Figure 4.1: Schematic diagram of a P-R-R manipulator

In order to facilitate modeling analysis, a generalized coordinate frame is defined, as shown in Figure 4.2. In Figure 4.2, the inertia frame is fixed at the mass center of the base platform; $P = (x_p, y_p)$ is the position of the platform at its mass center; φ is the orientation of the platform with respect to the fixed frame; A_i, B_i are the home and moving position of the i^{th} prismatic joint or bracket, respectively; C_i is the position of

the revolute joint of the platform facing the i^{th} intermediate link; q_i is the translation distance from the home position of the i^{th} prismatic joint to its current position; $\bar{\alpha}_i$ is the angle between the X axis of the fixed frame and the i^{th} linear guide; $\bar{\beta}_i$ is the angle between the fixed X axis and the i^{th} intermediate link; $i=1,2,3$. During trajectory tracking, $\bar{\alpha}_i$ ($\bar{\alpha}_1=120\text{deg}$, $\bar{\alpha}_2=270\text{deg}$, $\bar{\alpha}_3=30\text{deg}$) is fixed because of the fixed linear guides and $\bar{\beta}_i$ is varied with the motion of the platform.

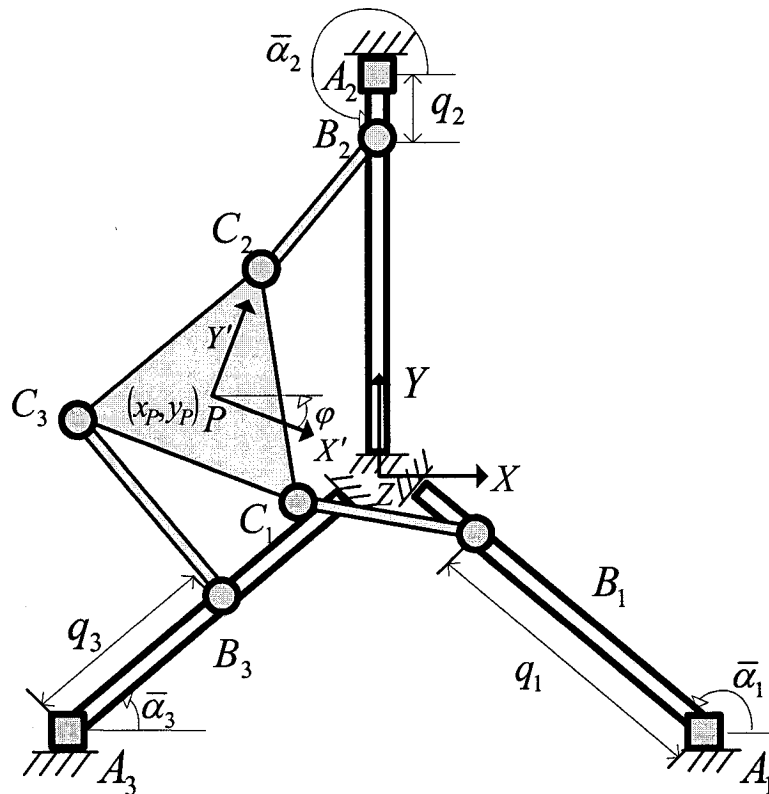


Figure 4.2: Generalized coordinate system of the P-R-R manipulator

Kinematics deals with the geometry of robot link motion with respect to a fixed reference coordinate system frame as a function of time without regarding the forces,

which cause such motions. For parallel robotic manipulators, inverse kinematics formulations are relatively simple while forward kinematics tends to be very complex, which is contrary to the serial robotic manipulator case.

In a P-R-R manipulator, for each branch, a close-loop equation can be written using vectors defined as follows:

$$\overline{A_i P} + \overline{P C_i} = \overline{A_i B_i} + \overline{B_i C_i} \quad (4.1)$$

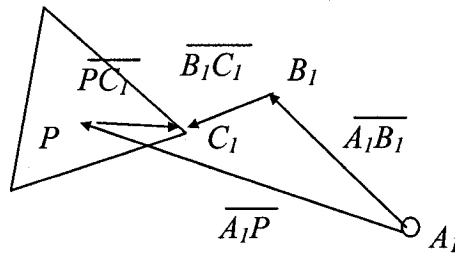


Figure 4.3: Schematic diagram of the close-loop equation

Figure 4.3 shows the diagram of equation (4.1) when the first branch is considered. On the right-hand side of equation (4.1), the coordinates of C_i , with respect to the fixed frame, are written as

$$x_{ci} = x_{ai} + q_i \cos \bar{\alpha}_i + l \cos \bar{\beta}_i \quad (4.2)$$

$$y_{ci} = y_{ai} + q_i \sin \bar{\alpha}_i + l \sin \bar{\beta}_i \quad (4.3)$$

where x_{ai} and y_{ai} are coordinates of point A_i and l is length of the intermediate link.

Based on (4.2) and (4.3), the solution of manipulator inverse kinematics is calculated as:

$$q_i = M_i \pm \sqrt{l^2 - S_i^2} \quad i = 1, 2, 3 \quad (4.4)$$

where:

$$M_i = (x_{ci} - x_{ai}) \cos \bar{\alpha}_i + (y_{ci} - y_{ai}) \sin \bar{\alpha}_i \quad (4.5)$$

$$S_i = (x_{ci} - x_{ai}) \sin \bar{\alpha}_i - (y_{ci} - y_{ai}) \cos \bar{\alpha}_i \quad (4.6)$$

where: x_{ci} , y_{ci} denote the coordinates of the revolute joint of the platform, facing the i^{th} intermediate link, with respect to the fixed frame; x_{ai} , y_{ai} are the coordinates of the origin of the i^{th} linear guide with respect to the fixed frame. Detailed derivations of (4.4) are addressed in (Kang, B., 2001, [30]). Since there are two possible solutions for each branch, this manipulator can take on a maximum of eight configurations for a set of given coordinates of the platform. However, during experiments, only one solution represents a reasonable solution in terms of the prismatic joint positions at the previous sampling time. Note, only if the argument of the square root in equation (4.4) becomes zero, does equation (4.4) have a unique solution. If the argument is negative, there is no solution.

In the experiments conducted, we also must calculate the Jacobian and the inverse Jacobian matrix, because they are indispensable for forward kinematics, dynamic equations and the synchronization error. Based on (4.1), the Jacobian matrix \mathbf{J}_p is derived as follows:

$$\mathbf{J}_p = \begin{bmatrix} \frac{\bar{b}_{1x}}{\bar{a}_{1x}\bar{b}_{1x} + \bar{a}_{1y}\bar{b}_{1y}} & \frac{\bar{b}_{1y}}{\bar{a}_{1x}\bar{b}_{1x} + \bar{a}_{1y}\bar{b}_{1y}} & \frac{\bar{e}_{1x}\bar{b}_{1y} - \bar{e}_{1y}\bar{b}_{1x}}{\bar{a}_{1x}\bar{b}_{1x} + \bar{a}_{1y}\bar{b}_{1y}} \\ \frac{\bar{b}_{2x}}{\bar{a}_{2x}\bar{b}_{2x} + \bar{a}_{2y}\bar{b}_{2y}} & \frac{\bar{b}_{2y}}{\bar{a}_{2x}\bar{b}_{2x} + \bar{a}_{2y}\bar{b}_{2y}} & \frac{\bar{e}_{2x}\bar{b}_{2y} - \bar{e}_{2y}\bar{b}_{2x}}{\bar{a}_{2x}\bar{b}_{2x} + \bar{a}_{2y}\bar{b}_{2y}} \\ \frac{\bar{b}_{3x}}{\bar{a}_{3x}\bar{b}_{3x} + \bar{a}_{3y}\bar{b}_{3y}} & \frac{\bar{b}_{3y}}{\bar{a}_{3x}\bar{b}_{3x} + \bar{a}_{3y}\bar{b}_{3y}} & \frac{\bar{e}_{3x}\bar{b}_{3y} - \bar{e}_{3y}\bar{b}_{3x}}{\bar{a}_{3x}\bar{b}_{3x} + \bar{a}_{3y}\bar{b}_{3y}} \end{bmatrix} \quad (4.7)$$

where: \bar{a}_{ix} , \bar{a}_{iy} are the X and Y directional component of the normalized positional vector from A_i toward B_i ; \bar{b}_{ix} , \bar{b}_{iy} are the X and Y directional component of the normalized positional vector from B_i toward C_i ; \bar{e}_{ix} , \bar{e}_{iy} are the X and Y directional component of the normalized positional vector from P toward C_i ; $i=1,2,3$. The detail derivations of (4.7) are also given in (Kang, B. 2001, [30]).

The inverse Jacobian becomes

$$\mathbf{J}_P^{-1} = \frac{1}{\Delta \mathbf{J}_P} \begin{bmatrix} \mathbf{J}_{11}^* & \mathbf{J}_{12}^* & \mathbf{J}_{13}^* \\ \mathbf{J}_{21}^* & \mathbf{J}_{22}^* & \mathbf{J}_{23}^* \\ \mathbf{J}_{31}^* & \mathbf{J}_{32}^* & \mathbf{J}_{33}^* \end{bmatrix} \quad (4.8)$$

The detailed expression of (4.8) is given in Appendix A.

Compared with inverse kinematics, forward kinematics of the manipulator is much more complicated. This problem can be theoretically solved by constructing and solving a high-order polynomial equation (Kassner D.J., 1990 [30], Pennock G.R., *et al.*, 1990 [51], Merlet, J.P., 2000 [31]). During implementation, however, this problem is typically solved through iteratively calculating the Jacobian matrix and platform pose at each sampling time (Ren, L., *et al.*, 1998 [54]). Here, this detail of the manipulator forward kinematics will not be addressed since the emphasis of the thesis is control design.

The dynamic behaviour of the platform and intermediate links of the manipulator are described in terms of the time rate of change of the manipulator configuration in relation to the joint torques exerted by the actuators. This relationship is expressed by a set of differential equations, termed equations of motion. The details of the equations of motion of a P-R-R manipulator have been addressed in [1], we will not address any more here.

4.3 Experimental System and Software

The Laboratory of Nonlinear Systems Control at the University of Toronto is equipped with a P-R-R manipulator, with three DOF. This manipulator is designed to perform high speed ($v_{\max} \geq 0.1m/s$) and high acceleration ($a_{\max} \geq 50m/s^2$) motions while maintaining high tracking accuracy. Figure 4.4 illustrates the mechanical structure of the P-R-R manipulator.

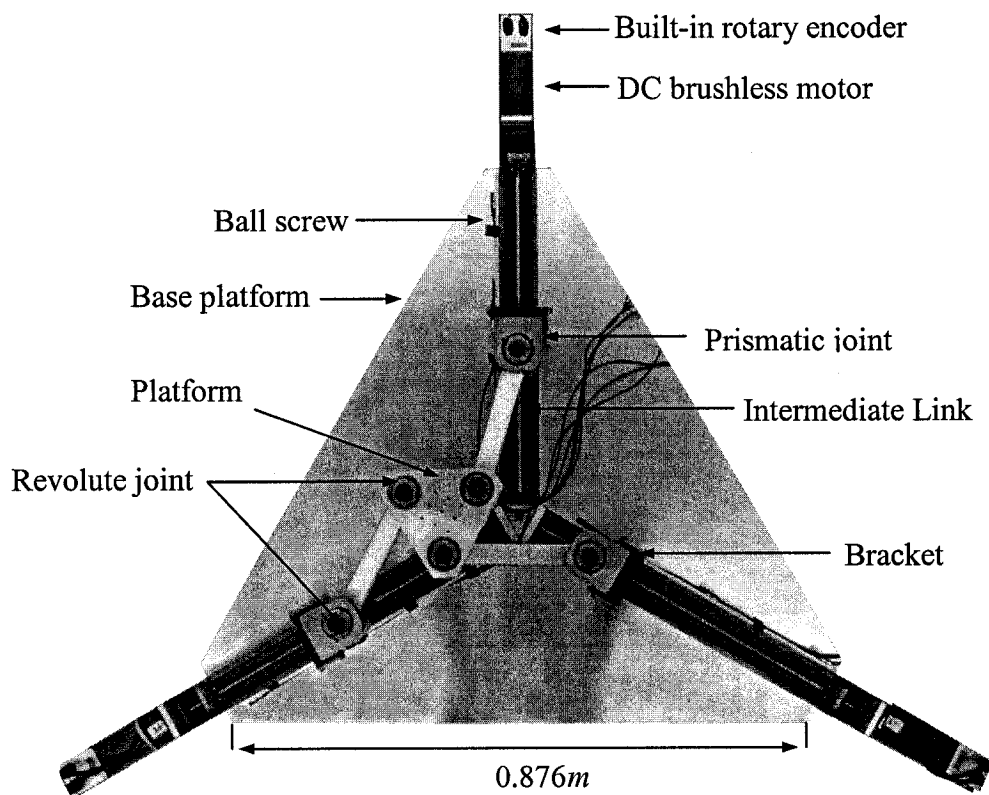


Figure 4.4: A prototype of the P-R-R manipulator

This assembled P-R-R manipulator is of aluminum and steel construction. The material of the platform and intermediate links is AA7075T6 (SAE215) with the density of $2.425 \times 10^{-6} kg/mm^3$. The material of the brackets, which connects a prismatic joint

and a revolute joint, is AS4140 with the density of $7.689 \times 10^{-6} \text{ kg/mm}^3$. The other parts of the manipulator are made of steel. Therefore, it is reasonable to treat the manipulator components as rigid bodies. Each bracket moves along a linear guide actuated by an Aerotech BM200 DC brushless motor via a THK KR3306 ball screw mechanism. The DC motors with their built-in rotary encoders and linear guides are fixed to the base platform, which is fixed on the ground. The other kinematic parameters of the manipulator are listed in Table 4.1.

Table 4.1: Kinematic Parameters of the P-R-R manipulator

Items	Values
Size of the platform (<i>mm</i>)	150.0×30.0×4.0
Size of the base platform (<i>mm</i>)	876.3×101.6×10.0
Size of the intermediate link(<i>mm</i>)	170.0×30.0×30.0
Prismatic joint stroke (<i>mm</i>)	400.0
Lead of the ball screw (<i>mm</i>)	6.0
Mass of the moving platform (<i>kg</i>)	4.045
Mass of the intermediate link (<i>kg</i>)	0.363
Mass of the bracket (<i>kg</i>)	3.512
Motor inertia (<i>kg·m²</i>)	1.3×10^{-5}
Viscous damping (<i>kg·m²</i>)	7.559×10^{-6}

The experimental system, as shown in Figure 4.5, consists of a P-R-R manipulator, a 400MHz Pentium II PC; a MCX-DSP-ISA 120Mflop/sec DSP controller with a sampling period of 1 ms, and three Aerotech BA20 SineDrive amplifiers. Built-in rotary encoders on the DC motors feed back their angular positions; hence the position of each prismatic joint is measured. Different payloads can be attached to the platform so that the P-R-R manipulator can operate different tasks, such as wire bonding and electronic component placement.

The experimental software was initially developed by Zhu, S. (Zhu, S., 2004 [84]) and then was improved by Ren, L. For trajectory tracking control of the P-R-R manipulator, this WindowsTM based software, as shown in Figure 4.6, offers user-friendly interfaces. Through changing parameters on the tracking control interface, as shown in Figure 4.7, the manipulator can exert tracking motions following different trajectories repetitively, such as straight lines, triangles and quadrangles. For details refer to (Zhu, S., 2004 [84], Ren, L., 2005 [60]).

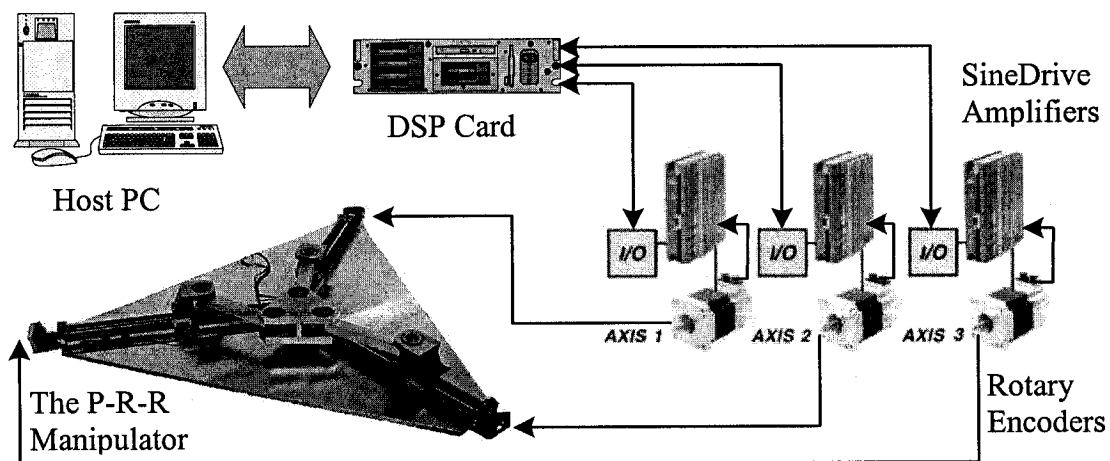
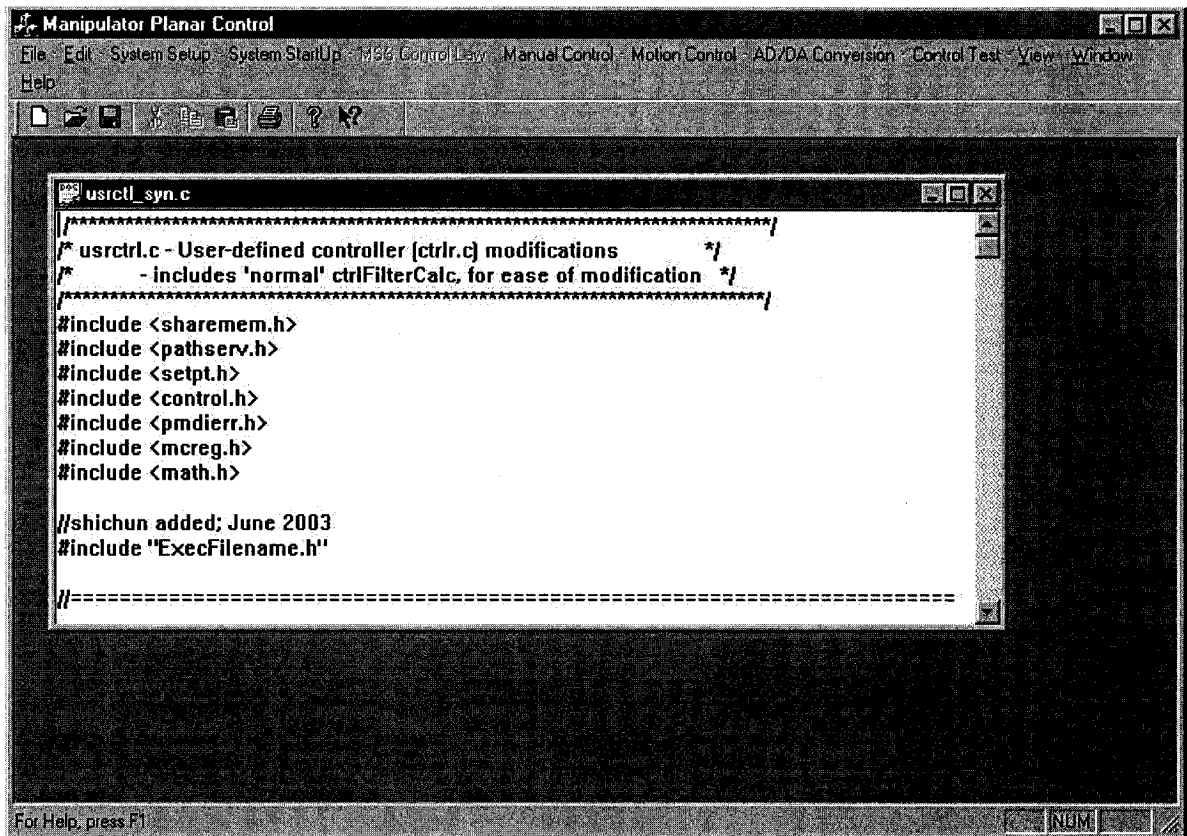


Figure 4.5: Experimental system set-up



The screenshot displays the 'Manipulator Planar Control' software interface. The main window has a menu bar with 'File', 'Edit', 'System Setup', 'System StartUp', '186 Control Law', 'Manual Control', 'Motion Control', 'AD/DA Conversion', 'Control Test', 'View', and 'Window'. Below the menu bar is a toolbar with various icons. The central area contains a code editor window titled 'usrctl_syn.c' with the following content:

```
usrctl_syn.c
/*****
 * usrctl.c - User-defined controller (ctrl.c) modifications
 * - includes 'normal' ctrlFilterCalc, for ease of modification
 *****/
#include <sharemem.h>
#include <pathsrv.h>
#include <setpt.h>
#include <control.h>
#include <pmdierr.h>
#include <mcreg.h>
#include <math.h>

//shichun added; June 2003
#include "ExecFilename.h"

//=====
```

At the bottom of the main window, there is a status bar with the text 'For Help, press F1' and a 'NUM' button.

Figure 4.6: Interface of P-R-R manipulator control

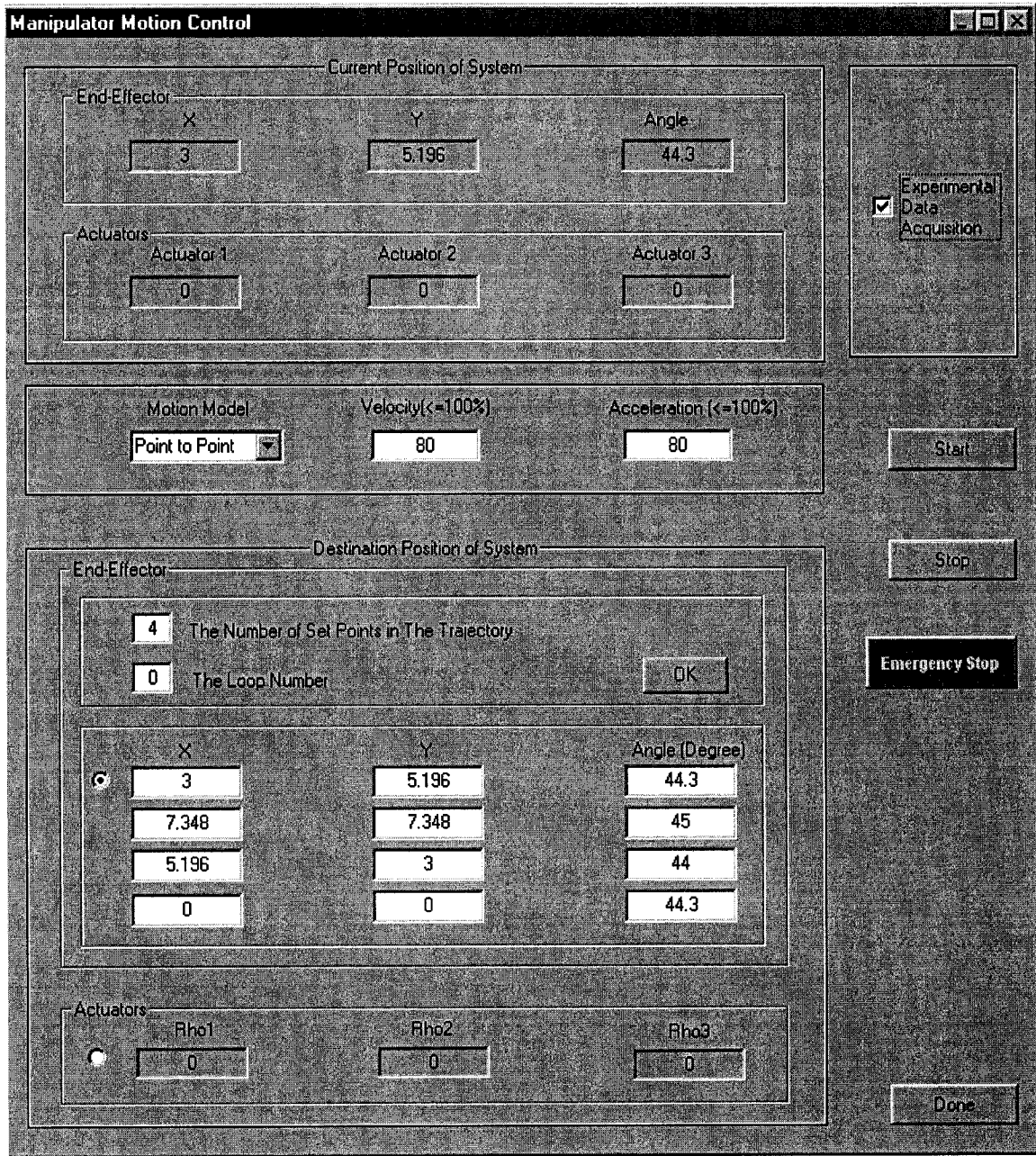


Figure 4.7: Trajectory tracking control interface

4.4 Experimental Results Using PID Control and Synchronized Control

In this section, to demonstrate the validity of the proposed synchronized control approach, experiments have been conducted on the P-R-R manipulator. To address the effectiveness of the proposed method, PID control, a typical control approach utilized in industry, has also been employed. Moreover, different trajectories, a straight line and a quadrangle, have been followed during experiments.

4.4.1 Trajectory Tracking with a Straight Line Path

During this set of experimentations, the platform is required to move along a straight line as follows: $P_0(5mm, 0mm, 45 \text{ deg}) \rightarrow P_1(40mm, 10mm, 45.04 \text{ deg})$, over a time interval of 1.5 seconds. The maximum velocity and acceleration are set as $0.16m/s$ and $80m/s^2$, respectively. Using a trial-and-error method, good tracking performance for the synchronized controller is achieved by selecting the following control gains: $\mathbf{K}_r = \text{diag}\{15.0\} (N \cdot s)$, $\mathbf{\Gamma} = \text{diag}\{1.0\} (s)$, $\mathbf{K}_e = \text{diag}\{30.4\} (N)$, and $\mathbf{\Lambda} = \text{diag}\{0.06\} (s^{-1})$.

In addition, in order to demonstrate the effectiveness of the developed synchronized control, standard PID control is also utilized to control the manipulator to complete the same task, because this control method is commonly used in industry. Although it is impossible to test all possibilities of the control gains of PID control, through the trial-and-error method, the control gains: $\mathbf{K}_p = \text{diag}\{1.8\} (N)$, $\mathbf{K}_i = \text{diag}\{1.0\} (N/s)$ and $\mathbf{K}_d = \text{diag}\{0.015\} (N \cdot s)$ are determined, by which the best performance for the PID controller is achieved, amongst all tested PID control gains.

Figures 4.8~4.9 illustrate the actual and desired trajectories of the platform with the two control methods; Figures 4.10~4.11 illustrate the actual and desired pose trajectories of the platform with the two control methods; Figures 4.12~4.13 illustrate the actual and desired position trajectories of the three prismatic joints with the two control methods, while Figures 4.14~4.15 illustrate errors, better illustrating the improved performance of synchronized control superior to PID control. Comparing each of the first three pairs of figures, it can be seen that the actual path (denoted by solid lines) better match the desired path (denoted by dotted lines) in the former than in the latter, which indicates that the proposed synchronized controller exhibits improved motion performance compared to the standard PID controller. To clearly show such performance improvement with the proposed synchronized control, Figure 4.14 and Figure 4.15 illustrates a comparison between the two methods, giving the pose errors of the platform, and position errors of the three prismatic joints, respectively, where solid lines denote the results obtained by the synchronized controller and dotted lines denote the results obtained by the standard PID controller. Obviously, the synchronized control exhibits much smaller errors and fewer vibrations. Table 4.2 gives a summary of the maximum absolute errors with these two methods. It can be seen from these experimental results that the proposed synchronized control improves tracking performance in controlling the parallel manipulator system, over PID control.

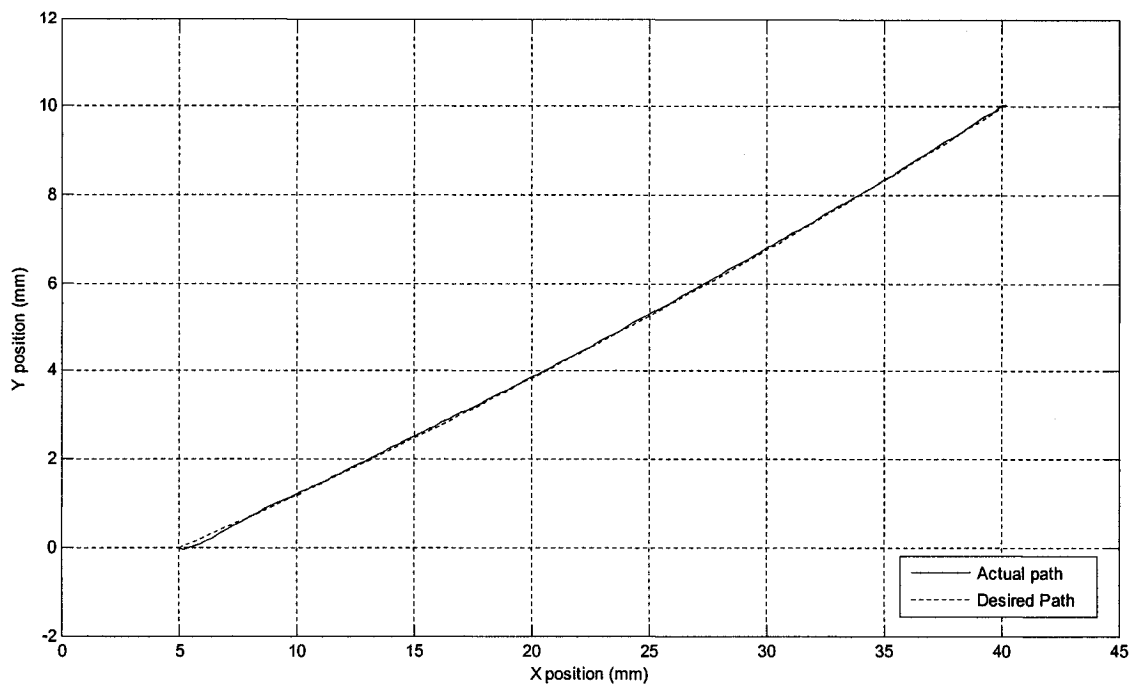


Figure 4.8: Actual and desired trajectories of the platform using PID control

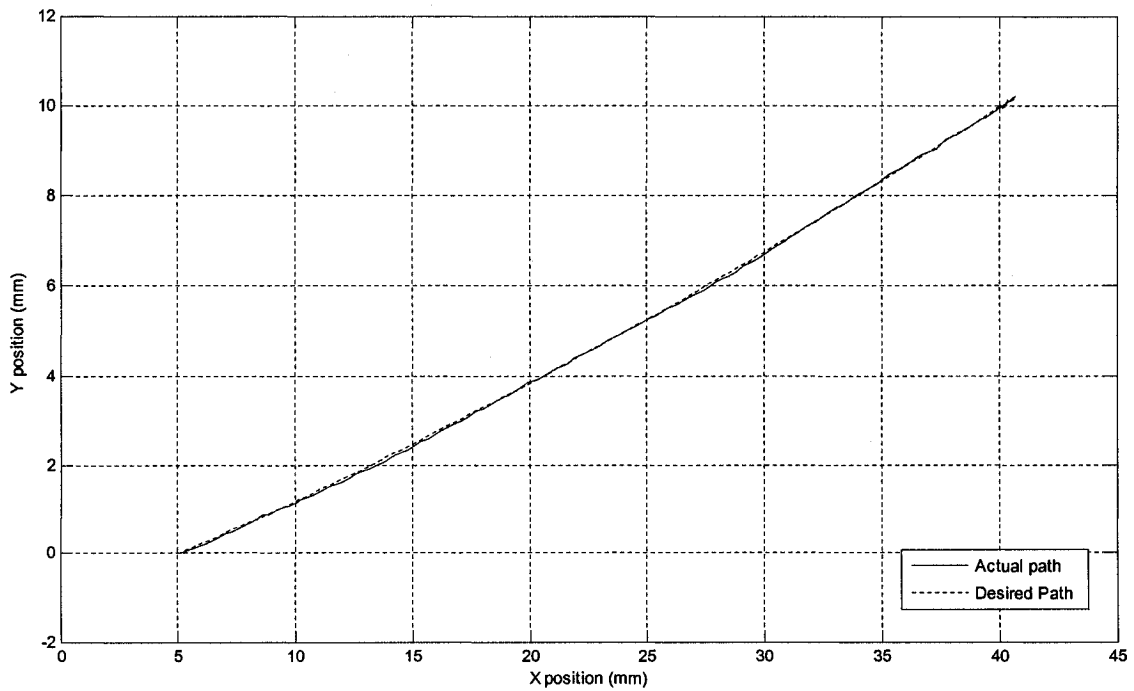


Figure 4.9: Actual and desired trajectories of the platform using synchronized control

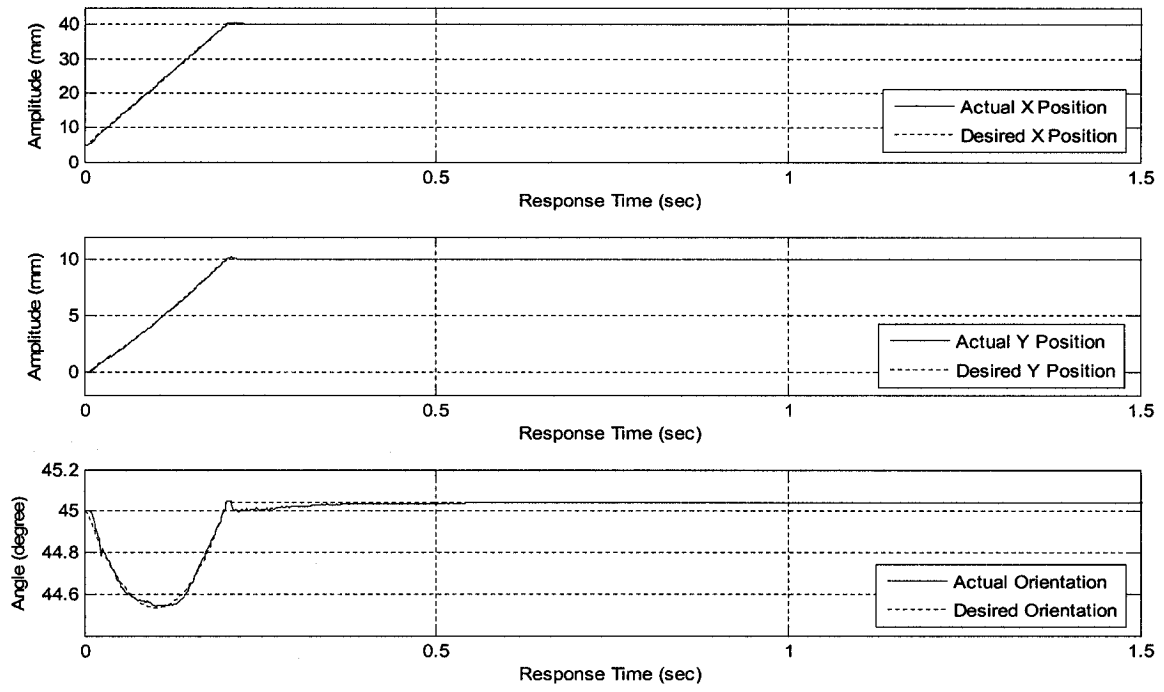


Figure 4.10: Actual and desired poses of the platform using PID control

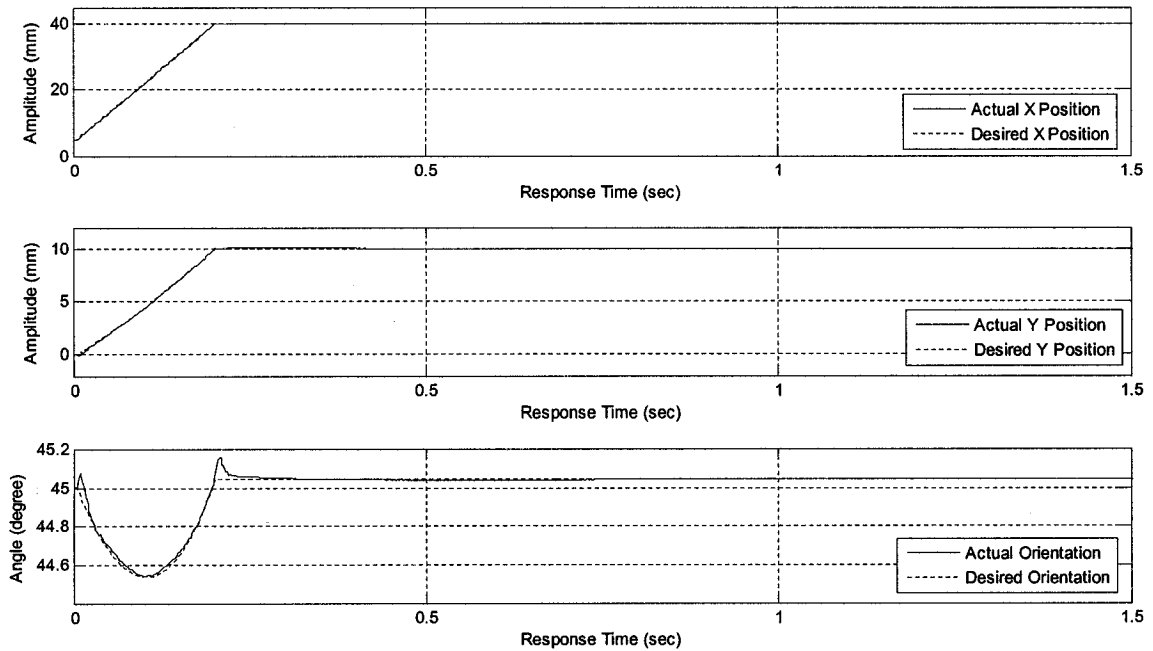


Figure 4.11: Actual and desired poses of the platform using synchronized control

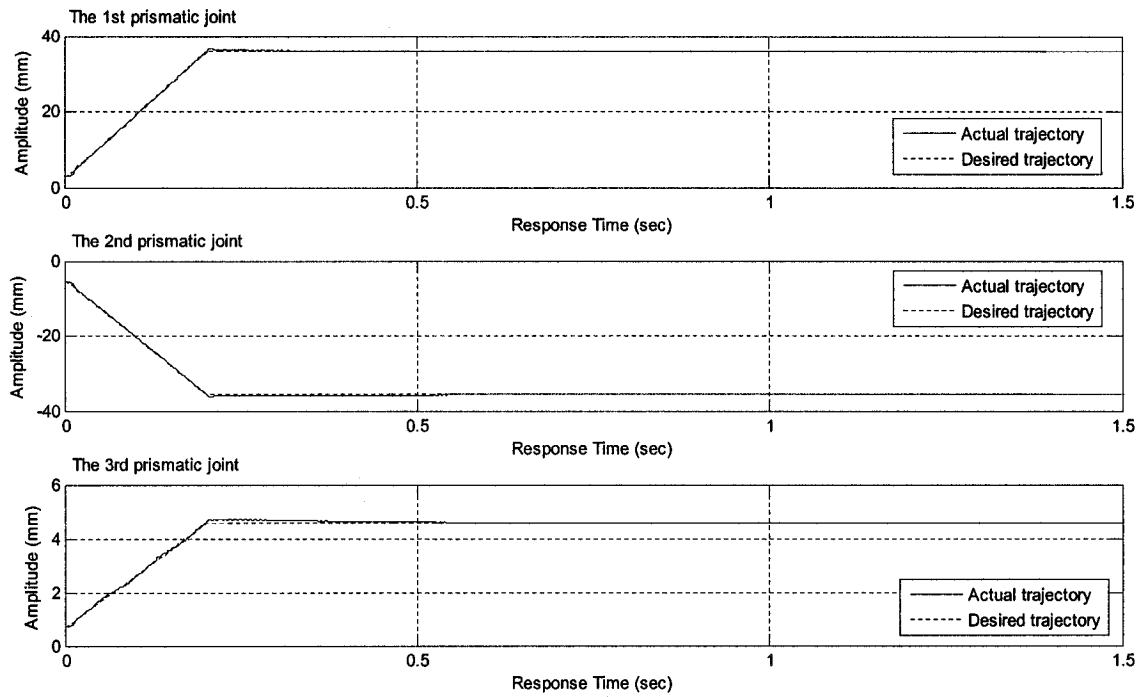


Figure 4.12: Actual and desired positions of the three prismatic joint using PID control

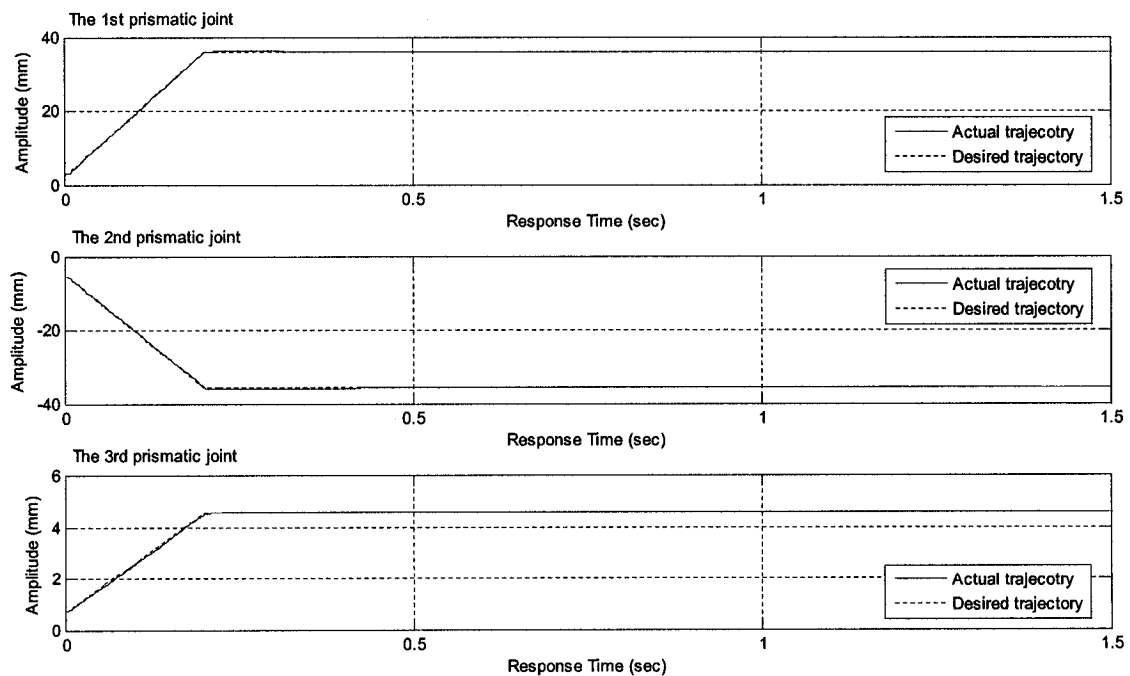


Figure 4.13: Actual and desired positions of the three prismatic joint using synchronized control

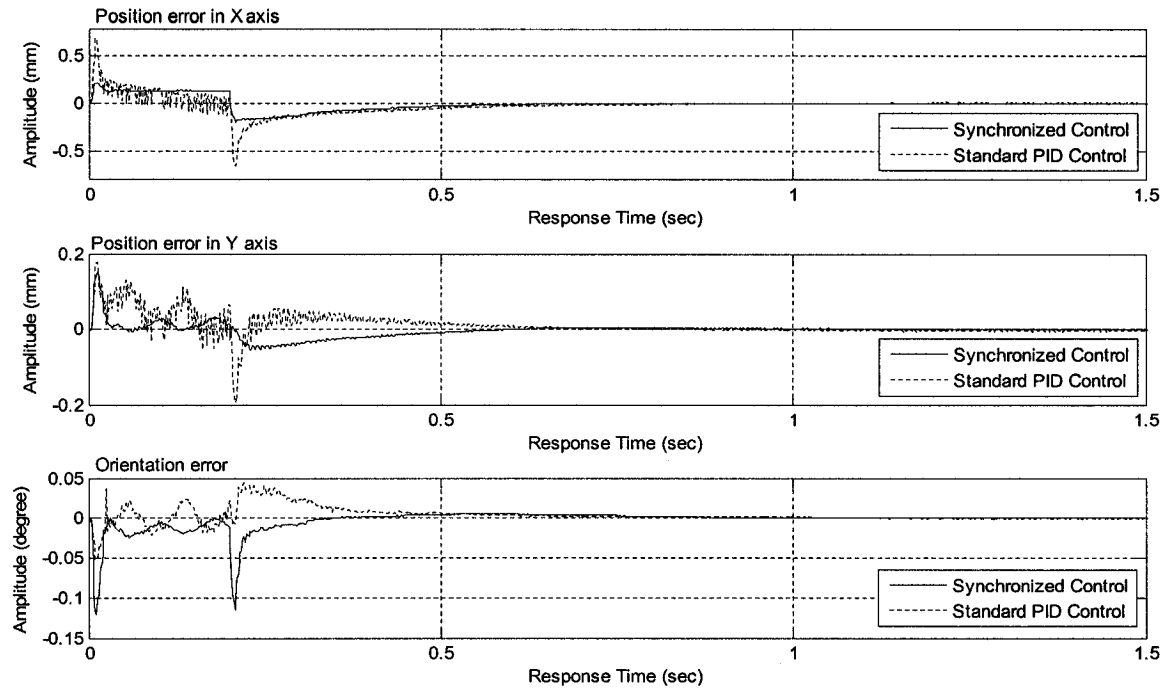


Figure 4.14: Pose errors of the platform using PID and synchronized control

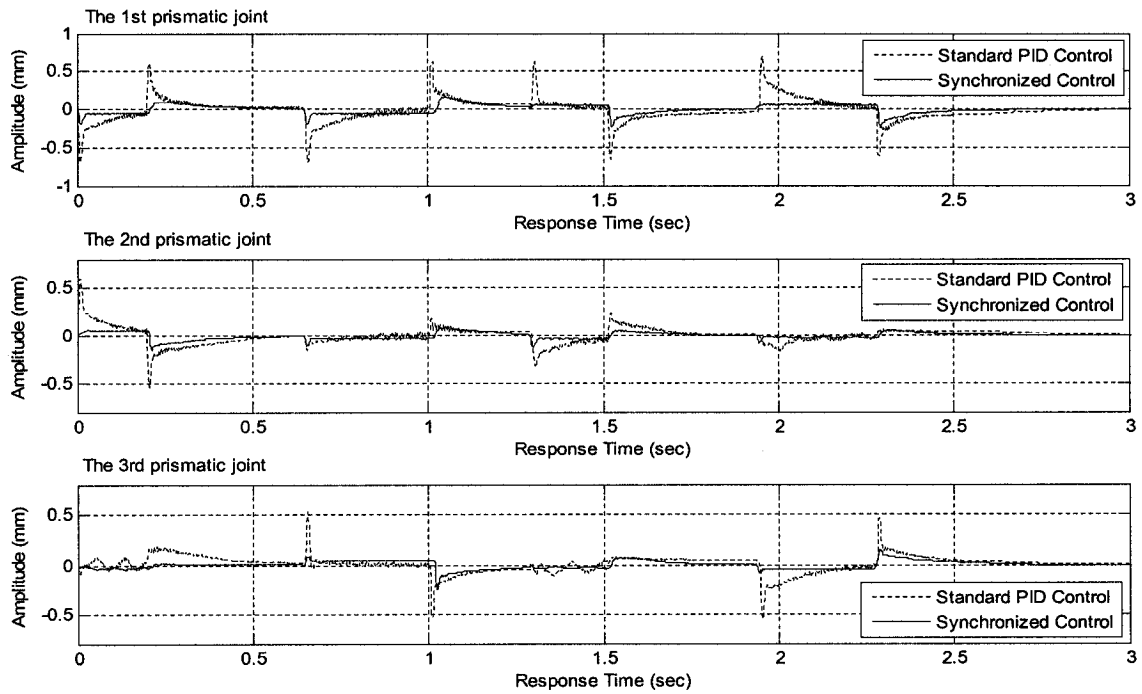


Figure 4.15: Position errors of the three prismatic joints using PID and synchronized control

Table 4.2: Error comparison (tracking a straight line path)

Max. Absolute Error	Synchronized Control	PID Control
Max. Absolute X Position Error(mm)	0.2126	0.6930
Max. Absolute Y Position Error(mm)	0.1519	0.1928
Max. Absolute Orientation Error(deg)	0.1210	0.0519
Max. 1 st Prismatic Joint Position Error(mm)	0.3790	0.6873
Max. 2 nd Prismatic Joint Position Error(mm)	0.2793	0.5833
Max. 3 rd Prismatic Joint Position Error(mm)	0.0825	0.1853

4.4.2 Trajectory Tracking with a Quadrangle Path

During this set of experimentations, the platform is required to move along a quadrangle trajectory, whose vertexes are selected as follows: $P_0(5mm, 0mm, 44.3 \text{ deg}) \rightarrow P_1(40mm, 10mm, 44.3 \text{ deg}) \rightarrow P_2(60mm, 70mm, 44.3 \text{ deg}) \rightarrow P_3(30mm, 50mm, 44.3 \text{ deg}) \rightarrow P_4(5mm, 0mm, 44.3 \text{ deg})$, stopping at each vertex for 0.5 seconds. The maximum velocity and acceleration are set as 0.16 m/s and 80 m/s^2 , respectively. In order to yield good performance, using a trial-and-error method, the control gains of the synchronized controller are chosen as $\mathbf{K}_r = \text{diag}\{15.0\} (N \cdot s)$, $\mathbf{\Gamma} = \text{diag}\{1.0\} (s)$, $\mathbf{K}_e = \text{diag}\{30.4\} (N)$, and $\mathbf{\Lambda} = \text{diag}\{0.06\} (s^{-1})$. Similarly as in the previous sub-section, for the comparison purpose, a standard PID controller is also utilized. Through the trial-and-error method as

well, the control gains: $\mathbf{K}_p = \text{diag}\{1.8\}$, $\mathbf{K}_i = \text{diag}\{1.0\}$ and $\mathbf{K}_d = \text{diag}\{0.015\}$, are selected, by which the best tracking performance for the PID controller is achieved, amongst all tested PID control gains.

Figure 4.16~4.18 illustrates the desired trajectory of the platform, the desired position and orientation trajectories of the platform, and the desired position trajectories of the three prismatic joints, respectively. Figure 4.19 and Figure 4.20 shows a comparison between synchronized control and PID control in the pose errors of the platform, and position errors of the three prismatic joints, respectively. In these two figures, solid lines denote the results obtained by the synchronized control and dotted lines denote the results obtained by standard PID control. Obviously, the proposed synchronized control yields smaller tracking errors and faster convergence speed than PID control. Table 4.3 lists the maximum absolute errors with these two methods. Comparing these experimental results, we can conclude that the proposed synchronized control may achieve good tracking performance superior to PID control.

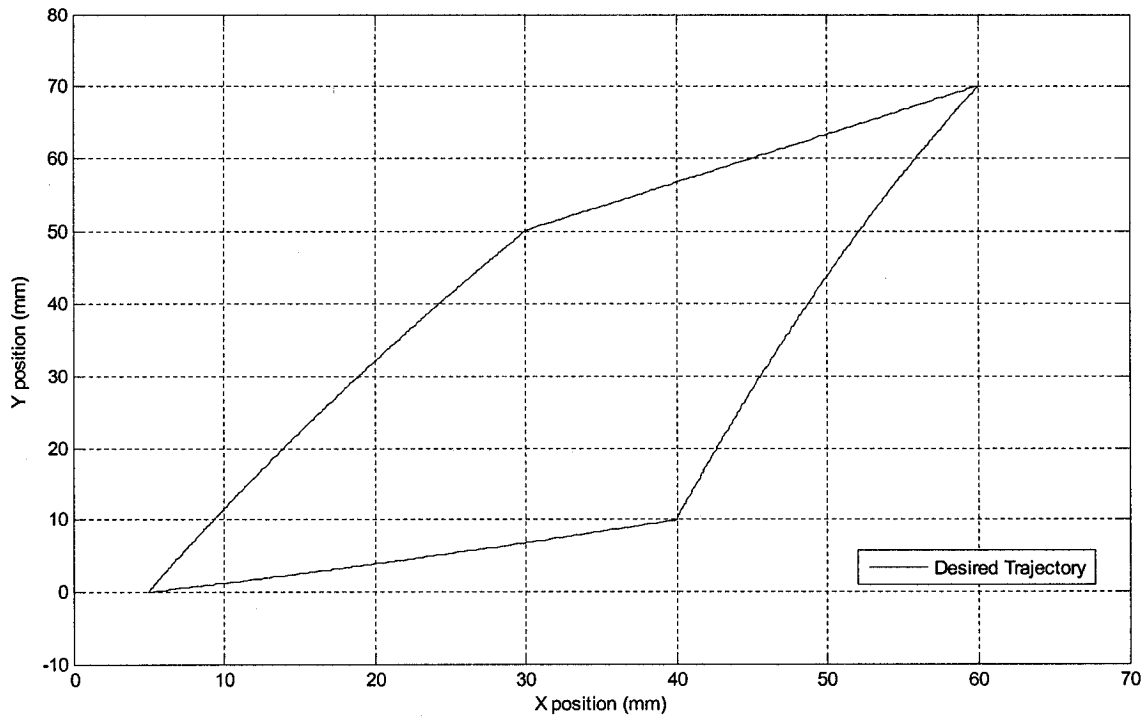


Figure 4.16: Desired path of the platform

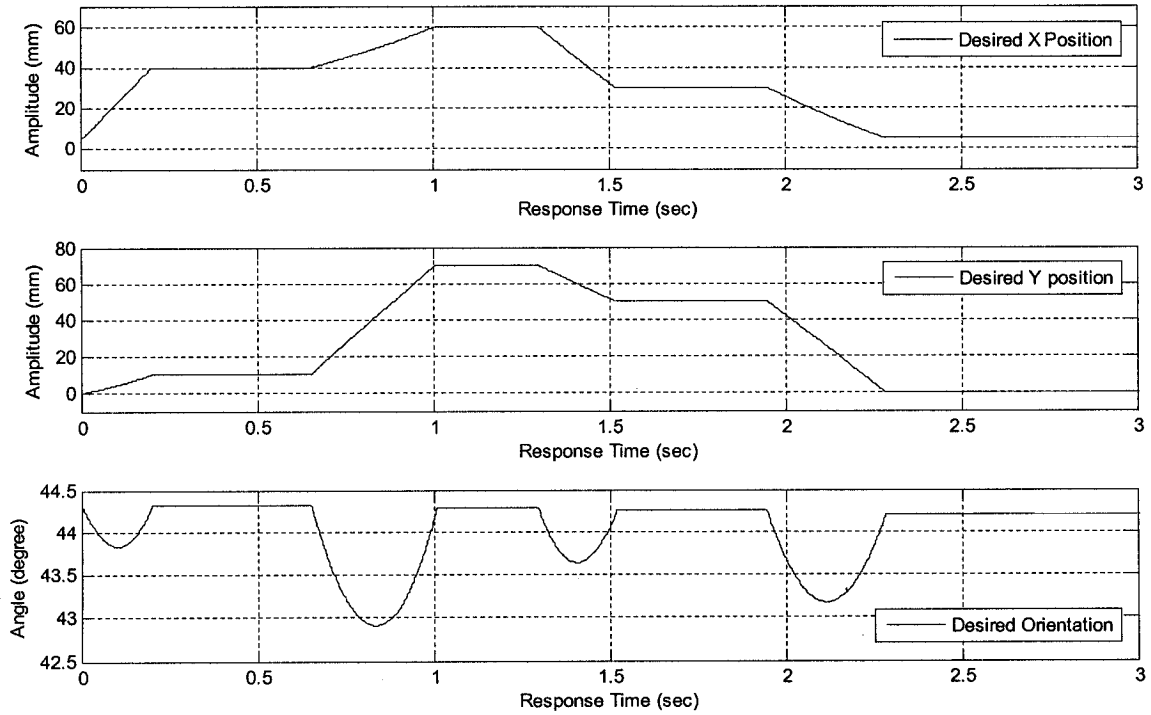


Figure 4.17: Desired position and orientation trajectories of the platform

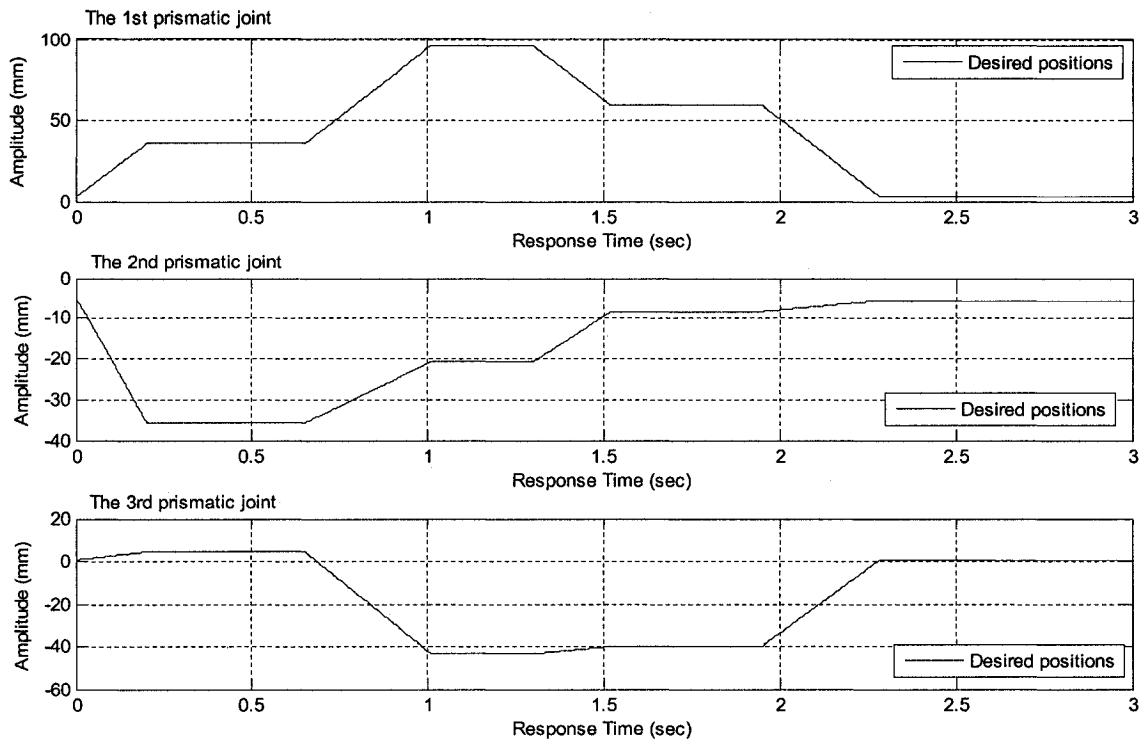


Figure 4.18: Desired position trajectories of the three prismatic joints

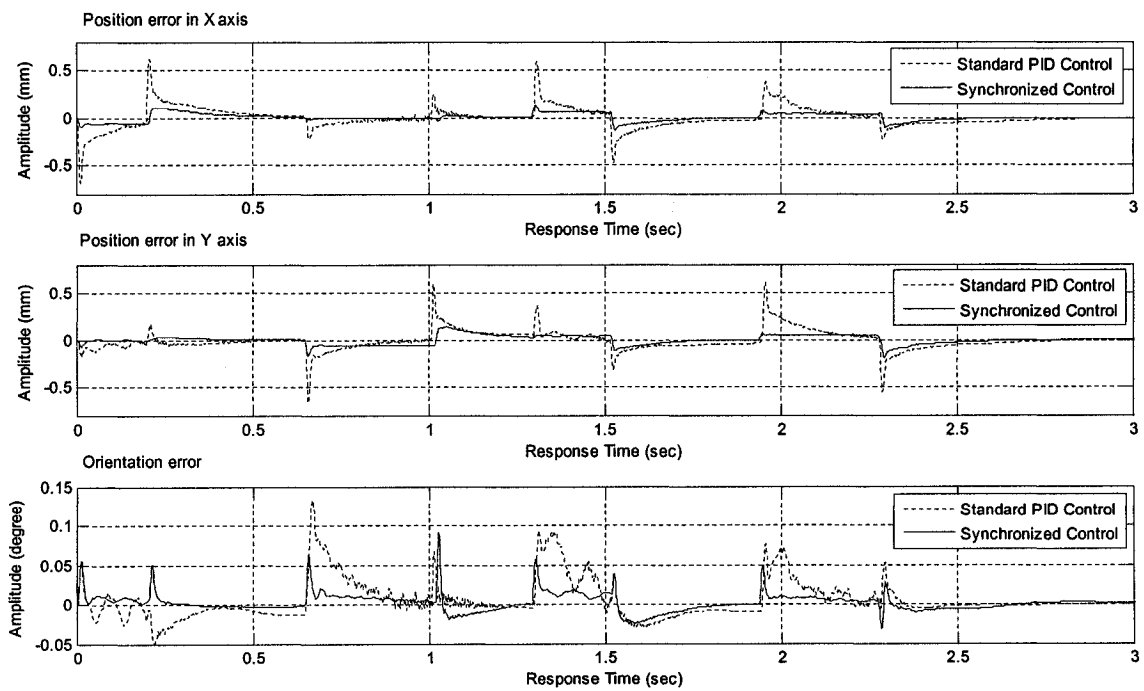


Figure 4.19: Pose errors of the platform using PID and synchronized control

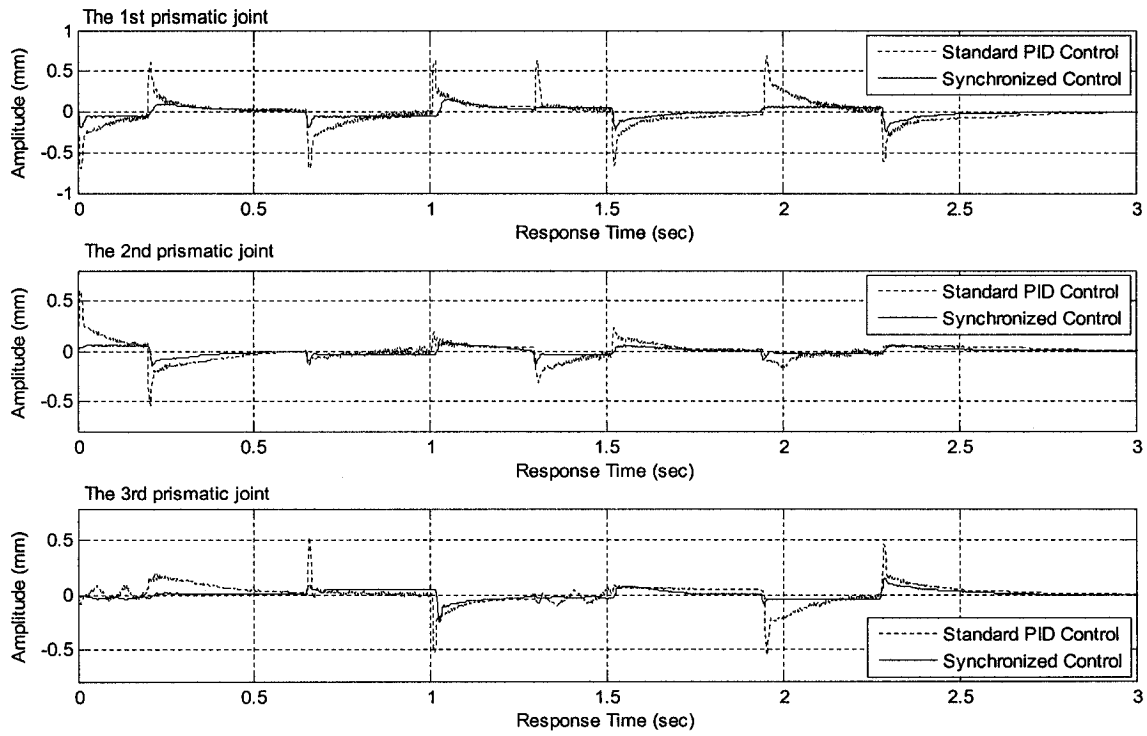


Figure 4.20: Position errors of the three prismatic joints using PID and synchronized control

Table 4.3: Error comparison (tracking a quadrangle path)

Max. Absolute Errors	Synchronized Control	PID Control
Max. Absolute X Position Error(mm)	0.1392	0.6873
Max. Absolute Y Position Error(mm)	0.1871	0.6614
Max. Absolute Orientation Error(deg)	0.0899	0.1321
Max. 1 st Prismatic Joint Position Error(mm)	0.2455	0.7043
Max. 2 nd Prismatic Joint Position Error(mm)	0.1463	0.5998
Max. 3 rd Prismatic Joint Position Error(mm)	0.2618	0.5601

4.5 Summary

In this chapter, we conducted experiments on an assembled P-R-R manipulator. During experiments, different trajectories have been followed and PID control has been also conducted as a comparison. Through analyzing experimental results with two control methods, we make the following conclusion: the synchronized control approach can improve trajectory tracking performance of a P-R-R manipulator. Here, two points should be noted. First, although we only conduct experiments on a P-R-R manipulator due to the limitation of experimental environment, it is reasonable to conclude that the proposed method can also yield good performance for other parallel robotic manipulators, whether spatial or planar, because of the theoretical generality of the proposed control approach with respect to parallel robotic manipulator. Second, during experiments, parameters of the kinematic model and dynamic model of the P-R-R manipulator are assumed to be known exactly. However, in practice, such an assumption is hard to satisfy due to varying payloads, etc. Therefore, it is necessary to propose a new control method based on the developed synchronized control approach to estimate unknown parameters during the control process, which is the research objective in the next chapter.

Chapter 5

Adaptive Synchronized Control

5.1 Introduction

During practical trajectory tracking processes with robotic manipulators, unknown parameters may exist due to varying payloads, frictional forces, etc. In some cases, unknown parameters deteriorate control performance (Slotine, J.-J.E., *et al.*, 1991 [67]). Therefore, the synchronized control approach proposed in Chapter 3, which is based on the assumption that the parameters of the robotic system are exactly known, is not appropriate to address the problem of unknown parameters. Considering adaptive control, capable of estimating unknown parameters during the control process and thus improving control performance, we propose a new control approach, termed adaptive synchronized (A-S) control, in this chapter. Since A-S control is the combination of adaptive control and synchronized control, it may overcome unknown parameters and improve tracking performance during trajectory tracking.

The rest of this chapter is organized as follows. Section 2 introduces the controller design of the A-S control. Section 3 provides the stability analysis of the proposed A-S control. Section 4 shows the experimental results using A-S control, conventional adaptive control, and standard PID control, and presents an experimental analysis. Finally, Section 5 offers a summary of this chapter.

5.2 A-S Control Design

In order to overcome the effects of unknown parameters in the system dynamic model and utilize the advantage of the proposed synchronized control, here, we develop a new control approach, termed A-S control. A-S control is the combination of adaptive control and synchronized control, as introduced in chapter 3. The reason to select adaptive control here is because of its inherent advantages: adaptive control permits changes in the values of the control gains or other parameters in the control law according to an on-line algorithm so that an appropriate set of parameters can be estimated during the control process, and control performance can be improved.

In the proposed A-S control scheme for a parallel robotic manipulator with n DOF, two types of errors are employed: the position errors of the active joints, $\mathbf{e}(t) \in \mathfrak{R}^{n \times 1}$, and synchronization error, $\boldsymbol{\epsilon}(t) \in \mathfrak{R}^{n \times 1}$,

$$\boldsymbol{\epsilon}(t) = \begin{cases} \dot{\mathbf{e}}(t) + \frac{\mathbf{I}_n - \mathbf{J}_p(t)(\mathbf{J}_p^d(t))^{-1}}{\|\mathbf{I}_n - \mathbf{J}_p(t)(\mathbf{J}_p^d(t))^{-1}\|} \dot{\mathbf{q}}^d(t) & \text{if } \|\mathbf{I}_n - \mathbf{J}_p(t)(\mathbf{J}_p^d(t))^{-1}\| > \zeta \\ \dot{\mathbf{e}}(t) + \frac{1}{\zeta} \cdot (\mathbf{I}_n - \mathbf{J}_p(t)(\mathbf{J}_p^d(t))^{-1}) \dot{\mathbf{q}}^d(t) & \text{if } \|\mathbf{I}_n - \mathbf{J}_p(t)(\mathbf{J}_p^d(t))^{-1}\| \leq \zeta \end{cases} \quad (5.1)$$

where: $\zeta \in \mathfrak{R}^+$ is a positive constant; $\mathbf{I}_n \in \mathfrak{R}^{n \times n}$ is the identity matrix; $\mathbf{J}_p(t) \in \mathfrak{R}^{n \times n}$ is the Jacobian matrix; $\dot{\mathbf{q}}(t) \in \mathfrak{R}^{n \times 1}$ is the vector denoting velocities or angular velocities of the active joints; $\dot{\mathbf{e}}(t) \in \mathfrak{R}^{n \times 1}$ are the velocity errors of the active joints; $\mathbf{J}_p^d(t)$, $\dot{\mathbf{q}}^d(t)$ are the desired value of $\mathbf{J}_p(t)$ and $\dot{\mathbf{q}}(t)$, respectively.

Combining $\mathbf{e}(t)$ and $\boldsymbol{\epsilon}(t)$, we define a coupling error, $\mathbf{e}^*(t) \in \mathfrak{R}^{n \times 1}$:

$$\mathbf{e}^*(t) = \mathbf{e}(t) + \boldsymbol{\Gamma} \cdot \boldsymbol{\epsilon}(t) \quad (5.2)$$

where: $\Gamma \in \mathfrak{R}^{n \times n}$ is a positive definite diagonal matrix, which denotes the relative weight of the synchronization error in the feedback signals. Each diagonal element of Γ should satisfy $0 \leq \Gamma_{ii} \leq 1$. Similarly as presented in chapter 3, two vectors, $\bar{\mathbf{u}}(t) \in \mathfrak{R}^{n \times 1}$ and $\bar{\mathbf{r}}(t) \in \mathfrak{R}^{n \times 1}$, are defined as follows:

$$\bar{\mathbf{u}}(t) \stackrel{\Delta}{=} \dot{\mathbf{q}}^d(t) - \Lambda \mathbf{e}^*(t) \quad (5.3)$$

$$\bar{\mathbf{r}}(t) \stackrel{\Delta}{=} \dot{\mathbf{q}}(t) - \bar{\mathbf{u}}(t) = \dot{\mathbf{e}}^*(t) + \Lambda \mathbf{e}^*(t) \quad (5.4)$$

where: $\Lambda \in \mathfrak{R}^{n \times n}$ is a positive definite diagonal matrix. The control objective is defined to design control torques so that both the coupling error $\mathbf{e}^*(t)$ and its derivative $\dot{\mathbf{e}}^*(t)$ tend to zero.

On the other hand, for a parallel robotic manipulator with n DOF, in practice, the matrices, $\mathbf{H}(\mathbf{q})$, $\mathbf{C}(\mathbf{q}, \dot{\mathbf{q}})$ and $\mathbf{G}(\mathbf{q})$ in (2.7) contain some unknown parameters, mainly due to varying payloads. To address these uncertain parameters, the technique of linear parameterization is used (Slotine, J.-J.E., *et al.*, 1991 [67]) and (2.7) can be expressed as in (Sirouspour, M.R., *et al.*, 2001 [66]).

$$\mathbf{H}(\mathbf{q})\ddot{\mathbf{q}}(t) + \mathbf{C}(\mathbf{q}, \dot{\mathbf{q}})\dot{\mathbf{q}}(t) + \mathbf{G}(\mathbf{q}) = \mathbf{Y}(\mathbf{q}, \dot{\mathbf{q}}, \ddot{\mathbf{q}})\boldsymbol{\theta}(t) \quad (5.5)$$

where: $\mathbf{Y}(\ddot{\mathbf{q}}, \dot{\mathbf{q}}, \mathbf{q}) \in \mathfrak{R}^{n \times \gamma}$ is a regression matrix; $\boldsymbol{\theta} \in \mathfrak{R}^{\gamma \times 1}$ is a vector containing all unknown dynamic parameters in $\mathbf{H}(\mathbf{q})$, $\mathbf{C}(\mathbf{q}, \dot{\mathbf{q}})$ and $\mathbf{G}(\mathbf{q})$. Using $\hat{\boldsymbol{\theta}}$ to represent the estimate of $\boldsymbol{\theta}$, an estimated dynamic model is given by:

$$\hat{\mathbf{H}}(\mathbf{q})\ddot{\mathbf{q}}(t) + \hat{\mathbf{C}}(\mathbf{q}, \dot{\mathbf{q}})\dot{\mathbf{q}}(t) + \hat{\mathbf{G}}(\mathbf{q}) = \mathbf{Y}(\mathbf{q}, \dot{\mathbf{q}}, \ddot{\mathbf{q}})\hat{\boldsymbol{\theta}}(t) \quad (5.6)$$

where: $\hat{\mathbf{H}}(\mathbf{q})$, $\hat{\mathbf{C}}(\mathbf{q}, \dot{\mathbf{q}})$, $\hat{\mathbf{G}}(\mathbf{q})$ denote the estimates of $\mathbf{H}(\mathbf{q})$, $\mathbf{C}(\mathbf{q}, \dot{\mathbf{q}})$ and $\mathbf{G}(\mathbf{q})$,

respectively.

It is important to stress that the derived dynamic equations, both (2.7) and (5.6), neglect the effects of joint elasticity and friction, intermediate link elasticity, and, in general, any unmodeled dynamics.

In terms of the dynamic equations derived in (5.6), the control law and adaptation law of the A-S control are defined as follows:

Control law:

$$\begin{aligned}\tau_a &= \hat{\mathbf{H}}(\mathbf{q})\dot{\bar{\mathbf{u}}}(t) + \hat{\mathbf{C}}(\mathbf{q}, \dot{\mathbf{q}})\bar{\mathbf{u}}(t) + \hat{\mathbf{G}}(\mathbf{q}) - \mathbf{K}_r \bar{\mathbf{r}}(t) - \mathbf{K}_e \mathbf{e}^*(t) \\ &= \mathbf{Y}(\mathbf{q}, \dot{\mathbf{q}}, \ddot{\mathbf{q}})\hat{\boldsymbol{\theta}}(t) - \mathbf{K}_r \bar{\mathbf{r}}(t) - \mathbf{K}_e \mathbf{e}^*(t)\end{aligned}\quad (5.7)$$

where: $\mathbf{K}_r \in \mathfrak{R}^{n \times n}$, $\mathbf{K}_e \in \mathfrak{R}^{n \times n}$ are both positive diagonal gain matrices.

Adaptation law:

$$\dot{\hat{\boldsymbol{\theta}}}(t) = -\bar{\mathbf{P}}(t)\mathbf{Y}(\mathbf{q}, \dot{\mathbf{q}}, \ddot{\mathbf{q}})^T (\bar{\mathbf{r}}(t) + \mathbf{Y}(\mathbf{q}, \dot{\mathbf{q}}, \ddot{\mathbf{q}})\tilde{\boldsymbol{\theta}}(t)) \quad (5.8)$$

$$d(\bar{\mathbf{P}}^{-1})/dt = -\lambda(t)\bar{\mathbf{P}}^{-1}(t) + \mathbf{Y}(\mathbf{q}, \dot{\mathbf{q}}, \ddot{\mathbf{q}})^T \mathbf{Y}(\mathbf{q}, \dot{\mathbf{q}}, \ddot{\mathbf{q}}) \quad (5.9)$$

$$\lambda(t) = \lambda_0 (1 - \|\bar{\mathbf{P}}\|/k_0) \quad (5.10)$$

where: $\bar{\mathbf{P}}(t) \in \mathfrak{R}^{n \times n}$ is the diagonal gain matrix of the estimator, which should be always positive definite; $\tilde{\boldsymbol{\theta}}(t) = \hat{\boldsymbol{\theta}}(t) - \boldsymbol{\theta}(t)$; $\lambda_0 (0 < \lambda_0 < 1)$, k_0 are positive constants representing the maximum forgetting rate and the pre-specified bound for the magnitude of $\bar{\mathbf{P}}(t)$, respectively. Equations (5.8) ~ (5.10) represent a bounded-gain-forgetting (BGF) estimator, which can filter noise and small disturbances, and avoid oscillation of the estimated parameters (Slotine, J.-J.E., *et al.*, 1991 [67]). In order to guarantee that $\bar{\mathbf{P}}(t)$ is positive definite and to yield accurate estimation of unknown parameters, it is

appropriate to set the initial value of $\bar{\mathbf{P}}(t)$ as $\bar{\mathbf{P}}(0) = c\mathbf{I}_n$, where c is a large positive constant. In order to maintain the estimation accuracy of unknown parameters, λ_0 should not be too small. It is appropriate to select λ_0 in the range 0.95~0.997 (Han, C.Z., *et al.*, 1987 [25]). In addition, in order to guarantee $\lambda(t)$ being positive, it is necessary to set k_0 as a suitable large constant so that $\|\bar{\mathbf{P}}\|/k_0$ is less than 1.

The structure of the A-S controller is shown in Figure 5.1. The required inputs to the A-S controller are the desired positions, velocities, and accelerations of the active joints. The required measurements are the actual positions and velocities of the active joints. Moreover, the controller consists of two main parts. The first is a form of full dynamic compensation, which attempts to provide the active joints necessary dynamic torques to produce the desired motions. The second regulates the actual trajectories to their desired trajectories and thus actually represents a PD feedback. Note that when $\Gamma = \mathbf{0}$, the A-S controller is equivalent to a conventional self-tuning adaptive controller.

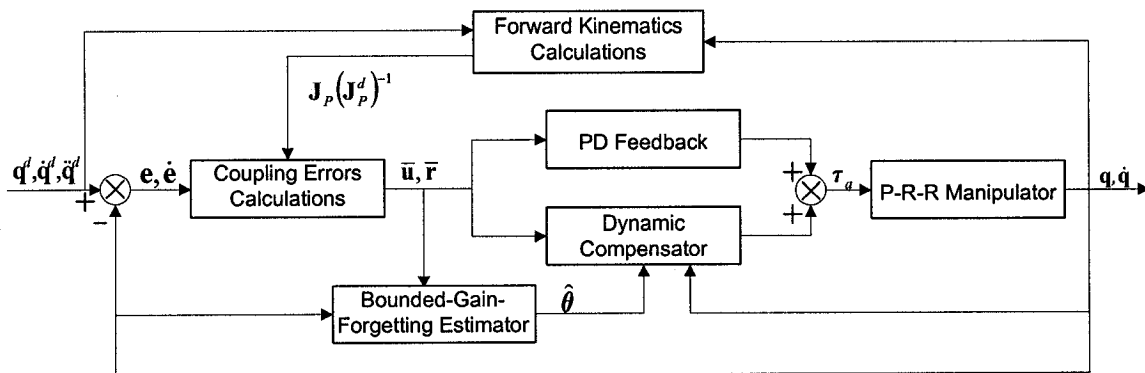


Figure 5.1: The structure of the A-S controller

Studying the two parts in the A-S control scheme, we find that the proposed A-S control (5.7) ~ (5.10) has generality for various parallel robotic manipulator configurations, because the dynamic compensation based on the dynamic model (5.6) is suitable for both spatial and planar parallel robotic manipulators, and the employed errors, $\mathbf{e}^*(t)$ and $\dot{\mathbf{e}}^*(t)$, in the PD feedback are also defined with respect to a general parallel robotic manipulator. After the control law and adaptation law are proposed, subsequently, it is necessary to prove that they are stable.

5.3 Stability Analysis of A-S Control

Through construction of a Lyapunov function and use of Barbalat's lemma, the proposed Theorem 1 and Theorem 2, which address the stability of the proposed A-S control algorithm, are proved with the following assumptions:

Assumption 1: The desired trajectories are continuous and bounded and do not cross singular points in the workspace of the parallel robotic manipulator.

Assumption 2: $\mathbf{H}(\mathbf{q})$ and $\mathbf{C}(\mathbf{q}, \dot{\mathbf{q}})$ are bounded if their arguments are bounded.

Assumption 3: Frictional effects can be neglected.

Theorem 1: For a parallel robotic manipulator whose dynamic equations can be expressed in (2.7), during trajectory tracking operations, its position errors $\mathbf{e}(t)$ and velocity errors $\dot{\mathbf{e}}(t)$ are both bounded by employing the proposed A-S control algorithm, (5.7)~(5.10).

Proof: Substituting the control law (5.7) into the dynamic equations (2.7), the closed-loop dynamics of the parallel robotic manipulator with n DOF are derived as:

$$\begin{aligned}
& \mathbf{H}(\mathbf{q})\dot{\bar{\mathbf{r}}}(t) + \mathbf{C}(\mathbf{q}, \dot{\mathbf{q}})\bar{\mathbf{r}}(t) + \mathbf{K}_r\bar{\mathbf{r}}(t) + \mathbf{K}_e\mathbf{e}^*(t) \\
& = (\hat{\mathbf{H}}(\mathbf{q}) - \mathbf{H}(\mathbf{q}))\dot{\bar{\mathbf{u}}}(t) + (\hat{\mathbf{C}}(\mathbf{q}, \dot{\mathbf{q}}) - \mathbf{C}(\mathbf{q}, \dot{\mathbf{q}}))\bar{\mathbf{u}}(t) + (\hat{\mathbf{G}}(\mathbf{q}) - \mathbf{G}(\mathbf{q})) \\
& = \mathbf{Y}(\mathbf{q}, \dot{\mathbf{q}}, \ddot{\mathbf{q}})\tilde{\boldsymbol{\theta}}(t)
\end{aligned} \tag{5.11}$$

Define a positive definite function as:

$$V(t) = \frac{1}{2} \left[\bar{\mathbf{r}}^T(t) \mathbf{H}(\mathbf{q}) \bar{\mathbf{r}}(t) + \tilde{\boldsymbol{\theta}}^T(t) \bar{\mathbf{P}}(t)^{-1} \tilde{\boldsymbol{\theta}}(t) + \mathbf{e}^{*T}(t) \mathbf{K}_e \mathbf{e}^*(t) \right] \tag{5.12}$$

Differentiating $V(t)$ with respect to time yields:

$$\begin{aligned}
\dot{V}(t) & = \bar{\mathbf{r}}^T(t) \mathbf{H}(\mathbf{q}) \dot{\bar{\mathbf{r}}}(t) + \frac{1}{2} \bar{\mathbf{r}}^T(t) \dot{\mathbf{H}}(\mathbf{q}) \bar{\mathbf{r}}(t) + \tilde{\boldsymbol{\theta}}^T(t) \dot{\bar{\mathbf{P}}}(t)^{-1} \tilde{\boldsymbol{\theta}}(t) \\
& \quad + \frac{1}{2} \tilde{\boldsymbol{\theta}}^T(t) \frac{d}{dt} (\bar{\mathbf{P}}(t)^{-1}) \tilde{\boldsymbol{\theta}}(t) + \mathbf{e}^{*T}(t) \mathbf{K}_e \dot{\mathbf{e}}^*(t)
\end{aligned} \tag{5.13}$$

Left multiplying both sides of (5.11) by $\bar{\mathbf{r}}^T(t)$, then substituting into (5.13), we have:

$$\begin{aligned}
\dot{V}(t) & = \bar{\mathbf{r}}^T(t) \left(\frac{1}{2} \dot{\mathbf{H}}(\mathbf{q}) - \mathbf{C}(\mathbf{q}, \dot{\mathbf{q}}) \right) \bar{\mathbf{r}}(t) - \bar{\mathbf{r}}^T(t) \mathbf{K}_r \bar{\mathbf{r}}(t) - \bar{\mathbf{r}}^T(t) \mathbf{K}_e \mathbf{e}^*(t) + \mathbf{Y}(\mathbf{q}, \dot{\mathbf{q}}, \ddot{\mathbf{q}}) \tilde{\boldsymbol{\theta}}(t) \\
& \quad + \tilde{\boldsymbol{\theta}}^T(t) \bar{\mathbf{P}}(t)^{-1} \dot{\tilde{\boldsymbol{\theta}}}(t) + \frac{1}{2} \tilde{\boldsymbol{\theta}}^T(t) \frac{d}{dt} (\bar{\mathbf{P}}(t)^{-1}) \tilde{\boldsymbol{\theta}}(t) + \mathbf{e}^{*T}(t) \mathbf{K}_e \dot{\mathbf{e}}^*(t)
\end{aligned} \tag{5.14}$$

Since $\dot{\mathbf{H}}(\mathbf{q}) - 2\mathbf{C}(\mathbf{q}, \dot{\mathbf{q}})$ is a skew-symmetric matrix (Angeles J., *et al.*, 1989 [2]), the first term on the right side of (5.14) is eliminated. Substituting (5.4), and the adaptation law (5.8) and (5.9) into (5.14), note that $\dot{\tilde{\boldsymbol{\theta}}}(t) = \dot{\hat{\boldsymbol{\theta}}}(t) - \dot{\boldsymbol{\theta}} = \dot{\hat{\boldsymbol{\theta}}}(t)$, we have:

$$\begin{aligned}
\dot{V}(t) & = -\bar{\mathbf{r}}^T(t) \mathbf{K}_r \bar{\mathbf{r}}(t) - (\dot{\mathbf{e}}^{*T}(t) + \mathbf{e}^{*T}(t) \boldsymbol{\Lambda}) \mathbf{K}_e \mathbf{e}^*(t) - \frac{1}{2} \tilde{\boldsymbol{\theta}}^T(t) \mathbf{Y}^T \mathbf{Y} \tilde{\boldsymbol{\theta}}(t) \\
& \quad - \frac{\lambda(t)}{2} \tilde{\boldsymbol{\theta}}^T(t) \bar{\mathbf{P}}(t)^{-1} \tilde{\boldsymbol{\theta}}(t) + \mathbf{e}^{*T}(t) \mathbf{K}_e \dot{\mathbf{e}}^*(t) \\
& = -\bar{\mathbf{r}}^T(t) \mathbf{K}_r \bar{\mathbf{r}}(t) - \mathbf{e}^{*T}(t) \boldsymbol{\Lambda} \mathbf{K}_e \mathbf{e}^*(t) - \frac{1}{2} \tilde{\boldsymbol{\theta}}^T(t) \mathbf{Y}^T \mathbf{Y} \tilde{\boldsymbol{\theta}}(t) \\
& \quad - \frac{\lambda(t)}{2} \tilde{\boldsymbol{\theta}}^T(t) \bar{\mathbf{P}}(t)^{-1} \tilde{\boldsymbol{\theta}}(t) \\
& \leq 0
\end{aligned} \tag{5.15}$$

Since $\dot{V}(t) \leq 0$, hence $\bar{\mathbf{r}}(t)$, $\mathbf{e}^*(t)$ and $\tilde{\boldsymbol{\theta}}(t)$ are all bounded. From (5.4), $\dot{\mathbf{e}}^*(t)$ is

bounded. Since the desired trajectory is continuous and bounded, then $\mathbf{q}^d(t)$, $\dot{\mathbf{q}}^d(t)$ and $\ddot{\mathbf{q}}^d(t)$ are all continuous and bounded. Furthermore, since the desired trajectory does not cross singular points in the workspace, then $(\mathbf{J}_p^d(t))^{-1}$ is bounded. .

Let $\mathbf{E}(t) \in \mathfrak{R}^{n \times 1}$ denote the second term of $\epsilon(t)$. Substituting (5.1) into (5.2), we derive:

$$\mathbf{e}(t) + \Gamma \dot{\mathbf{e}}(t) = \mathbf{e}^*(t) - \Gamma \mathbf{E}(t) \quad (5.16)$$

Since the desired trajectory of the platform is continuous and bounded, then the trajectories of the active joints calculated from the inverse kinematics are continuous and bounded. Therefore, $\Gamma \mathbf{E}(t)$ is bounded and the right side of (5.16) is bounded. Moreover, since Γ is constant, hence, (5.16) is a first order ordinary differential equation. Solving (5.16), we obtain its analytical solution:

$$\mathbf{e}(t) = \mathbf{e}^{-t\Gamma^{-1}} \left\{ \int_0^t \left[e^{s\Gamma^{-1}} (\Gamma^{-1} \mathbf{e}^*(s) - \mathbf{E}(s)) \right] ds + \mathbf{e}(0) \right\} \quad (5.17)$$

Differentiating (5.17) with respect to time yields:

$$\dot{\mathbf{e}}(t) = \Gamma^{-1} \mathbf{e}^{-t\Gamma^{-1}} \left\{ \int_0^t \left[e^{s\Gamma^{-1}} (\Gamma^{-1} \mathbf{e}^*(s) - \mathbf{E}(s)) \right] ds + \mathbf{e}(0) \right\} + \Gamma^{-1} \mathbf{e}^*(t) - \mathbf{E}(t) \quad (5.18)$$

Let $\psi_{\max} \in \mathfrak{R}^{n \times 1}$ and $\psi_{\min} \in \mathfrak{R}^{n \times 1}$ be the maximum and minimum value of the right side of (5.16), respectively. Assuming $\mathbf{e}(0) = \mathbf{0}$, we can derive:

$$\left\| \psi_{\min} - e^{-t\Gamma^{-1}} \psi_{\min} \right\|_2 \leq \left\| \mathbf{e}(t) \right\|_2 \leq \left\| \psi_{\max} - e^{-t\Gamma^{-1}} \psi_{\max} \right\|_2 \quad (5.19)$$

$$\left\| e^{-t\Gamma^{-1}} \Gamma^{-1} \psi_{\min} \right\|_2 \leq \left\| \dot{\mathbf{e}}(t) \right\|_2 \leq \left\| e^{-t\Gamma^{-1}} \Gamma^{-1} \psi_{\max} \right\|_2 \quad (5.20)$$

where: $\|\cdot\|_2$ denotes the $L2$ -norm of a vector. Therefore, $\mathbf{e}(t)$ and $\dot{\mathbf{e}}(t)$ are continuous

and bounded. Similarly, we can derive that $\ddot{e}(t)$ is also bounded. \square

Theorem 2: If $\mathbf{Y}(\mathbf{q}, \dot{\mathbf{q}}, \ddot{\mathbf{q}})$ is persistently exciting, then the proposed controller gives rise to asymptotic convergence of tracking error, synchronization error, coupling error and uncertainty estimated errors, i.e., $\mathbf{e}(t) \rightarrow \mathbf{0}$, $\boldsymbol{\epsilon}(t) \rightarrow \mathbf{0}$, $\mathbf{e}^*(t) \rightarrow \mathbf{0}$ and $\tilde{\boldsymbol{\theta}}(t) \rightarrow \mathbf{0}$ as $t \rightarrow \infty$.

Proof: Since the desired trajectory of the moving platform is bounded and continuous, and $\mathbf{e}(t)$, $\dot{\mathbf{e}}(t)$, $\ddot{\mathbf{e}}(t)$ are bounded, then $\mathbf{q}(t)$, $\dot{\mathbf{q}}(t)$ and $\ddot{\mathbf{q}}(t)$ are bounded and continuous. Consequently, $\mathbf{H}(\mathbf{q})$ and $\mathbf{C}(\mathbf{q}, \dot{\mathbf{q}})$ are both bounded. Since $\bar{\mathbf{r}}(t)$, $\mathbf{e}^*(t)$ are bounded, \mathbf{K}_r , \mathbf{K}_e are constant, from (5.11), $\dot{\bar{\mathbf{r}}}(t)$ is bounded. As a function of $\mathbf{q}(t)$, $\dot{\mathbf{q}}(t)$ and $\ddot{\mathbf{q}}(t)$, $\mathbf{Y}(\mathbf{q}, \dot{\mathbf{q}}, \ddot{\mathbf{q}})$ is bounded and continuous; subsequently, $\dot{\mathbf{Y}}(\mathbf{q}, \dot{\mathbf{q}}, \ddot{\mathbf{q}})$ is bounded. It is assumed that $\mathbf{Y}(\mathbf{q}, \dot{\mathbf{q}}, \ddot{\mathbf{q}})$ is persistently exciting, i.e., there exists positive constants α_p and T_p such that for any $t > 0$,

$$\int_t^{t+T_p} \mathbf{Y}(\mathbf{q}(s), \dot{\mathbf{q}}(s), \ddot{\mathbf{q}}(s)) \mathbf{Y}^T(\mathbf{q}(s), \dot{\mathbf{q}}(s), \ddot{\mathbf{q}}(s)) ds \geq \alpha_p \mathbf{I} \quad (5.21)$$

Where $\mathbf{I} \in \mathcal{R}^{r \times r}$ is an identity matrix. Hence, $\bar{\mathbf{P}}(t)^{-1}$ and $\lambda(t)$ are both bounded (Slotine, J.-J.E., *et al.*, 1991). Differentiating $\dot{V}(t)$ and analyzing each term of $\ddot{V}(t)$, we show that $\ddot{V}(t)$ is bounded.

$$\begin{aligned} \ddot{V}(t) = & -2\bar{\mathbf{r}}^T(t) \mathbf{K}_r \dot{\bar{\mathbf{r}}}(t) - 2\mathbf{e}^*(t)^T \boldsymbol{\Lambda} \mathbf{K}_e \dot{\mathbf{e}}^*(t) - \tilde{\boldsymbol{\theta}}^T(t) \mathbf{Y}^T \dot{\mathbf{Y}} \tilde{\boldsymbol{\theta}}(t) - \tilde{\boldsymbol{\theta}}^T(t) \mathbf{Y}^T \dot{\mathbf{Y}} \tilde{\boldsymbol{\theta}}(t) \\ & - \frac{\dot{\lambda}(t)}{2} \tilde{\boldsymbol{\theta}}^T(t) \bar{\mathbf{P}}(t)^{-1} \tilde{\boldsymbol{\theta}}(t) - \frac{3\lambda(t)}{2} \tilde{\boldsymbol{\theta}}^T(t) \mathbf{Y}^T \mathbf{Y} \tilde{\boldsymbol{\theta}}(t) + \frac{\lambda(t)^2}{2} \tilde{\boldsymbol{\theta}}^T(t) \bar{\mathbf{P}}(t)^{-1} \tilde{\boldsymbol{\theta}}(t) \end{aligned} \quad (5.22)$$

Since the differentiable function $V(t)$ is bounded and $\dot{V}(t)$ is bounded, from Barbalat's lemma, it follows that $\dot{V}(t) \rightarrow 0$ as time $t \rightarrow \infty$. From (5.16), it is obvious

that $\bar{\mathbf{r}}(t) \rightarrow \mathbf{0}$, $\mathbf{e}^*(t) \rightarrow \mathbf{0}$, and $\tilde{\boldsymbol{\theta}}(t) \rightarrow \mathbf{0}$ as $t \rightarrow \infty$. Since $\ddot{\mathbf{e}}(t)$ is bounded as derived in Theorem 1, similarly, from Barbalat's lemma, we can derive that $\dot{\mathbf{e}}(t) \rightarrow \mathbf{0}$ as $t \rightarrow \infty$. Finally, since $\dot{\mathbf{e}}(t) \rightarrow \mathbf{0}$ and $\mathbf{e}^*(t) \rightarrow \mathbf{0}$ as $t \rightarrow \infty$, from (5.1) and (5.2), we can derive that $\mathbf{e}(t) \rightarrow \mathbf{0}$, $\boldsymbol{\epsilon}(t) \rightarrow \mathbf{0}$ as $t \rightarrow \infty$. \square

Theorem 1 and Theorem 2 demonstrate that during trajectory tracking, the position errors, velocity errors of the active joints and the synchronization error will asymptotically converge to zero while the estimated parameters will converge to their true values. As a result, the proposed A-S control is stable. On the other hand, the first two assumptions are easy to satisfy while the third assumption, in some cases, may be hard to meet. While the frictional force cannot be neglected, its frictional coefficients are typically unknown and should be estimated. Correspondingly, the expression of the regression matrix $\mathbf{Y}(\mathbf{q}, \dot{\mathbf{q}}, \ddot{\mathbf{q}})$ becomes very complicated. How to deal with frictional forces is a major task in our future research. In particular, in Theorem 2, there is an additional assumption that $\mathbf{Y}(\mathbf{q}, \dot{\mathbf{q}}, \ddot{\mathbf{q}})$ should be persistently exciting. Proof of this assumption is a major task for future research because for a parallel robotic manipulator, the expression for $\mathbf{Y}(\mathbf{q}, \dot{\mathbf{q}}, \ddot{\mathbf{q}})$ is very complicated. However, from the experimentation view, this assumption can be met by selecting an appropriate desired trajectory in the workspace.

5.4 Experimental Results Using Different Control Methods

In this section, to demonstrate the validity of the proposed A-S control approach, experiments have been conducted on a P-R-R manipulator test bed, which was introduced

in chapter 4. In addition, to address the effectiveness of the proposed method, a conventional self-tuning adaptive controller and a PID controller have also been employed. Moreover, different trajectories, a straight line and a quadrangle path, have been followed, and different payloads have been attached during experiments.

5.4.1 Trajectory Tracking with a Straight Line Path without a Payload

During this set of experiments, the platform is required to move along a straight line as follows: $P_0(0mm, 0mm, 44.33 \text{ deg}) \rightarrow P_1(5mm, 3mm, 45.03 \text{ deg})$, over a time interval of 0.2 seconds. The maximum velocity and acceleration are set as $0.261m/s$ and $124m/s^2$, respectively. In the experiments conducted, we set $\theta = [3.90kg \ 0.32kg \ 3.3kg]^T$ as the initial values of the mass of the platform without a payload, the mass of the intermediate link and the mass of the bracket (see Figure 4.4), which are the parameter estimated. The other parameters, such as geometry of every manipulator components, are assumed to be known exactly. Using a trial-and-error method, good tracking performance for the A-S controller is achieved by selecting the control gains as listed in Table 5.1. The estimated parameters converge to $\theta = [4.045kg \ 0.362kg \ 3.512kg]^T$, as shown in Figure 5.8, while their true values are $\theta_{true} = [4.046kg \ 0.362kg \ 3.511kg]^T$. In addition, in order to demonstrate the effectiveness of the developed A-S controller, a conventional adaptive controller without synchronization, with the control law (5.7) but $\Gamma = \mathbf{0}$, and a standard PID controller are also utilized to control the manipulator to complete the same task. Since it is impossible to test all possible control gains of the adaptive controller and those of the PID controller, through a large number of experiments, the control gains of these two controllers are

determined, listed in Table 5.1, by which the best performance for the adaptive controller and the PID controller are achieved, amongst all tested control gains.

Figure 5.2~5.4 illustrates the desired trajectory of the platform, the desired position and orientation trajectories of the platform, and the desired position trajectories of the three prismatic joints, respectively. Figure 5.5 and Figure 5.6 shows a comparison among A-S control, adaptive control without synchronization and PID control in the pose errors of the platform, and position errors of the three prismatic joints, respectively. In these two figures, solid lines denote the results obtained by A-S control, dotted lines denote the results obtained by adaptive control without synchronization, and dashed lines denote the results obtained by standard PID control. Obviously, the proposed A-S controller yields the smallest tracking errors and fastest convergence speed. Figure 5.7 shows the synchronization errors of the A-S controller, which are fed back to the three prismatic joints. Table 5.2 lists the maximum absolute errors with these three control methods. Comparing these experimental results, we can conclude that the proposed A-S controller may achieve good tracking performance over adaptive control and PID control.

Table 5.1: Control gains of the employed controllers
(tracking a straight line without a payload)

Control Gains	A-S Control	Adaptive Control	Control Gains	PID Control
$\Lambda (1/s)$	$diag\{1.04\}$	$diag\{1.05\}$	$\mathbf{K}_p (N)$	$diag\{1.8\}$
$\Gamma (s)$	$diag\{0.06\}$	$diag\{0.0\}$	$\mathbf{K}_i (N/s)$	$diag\{1.0\}$
$\mathbf{K}_r (N \cdot s)$	$diag\{15.0\}$	$diag\{16.0\}$	$\mathbf{K}_d (N \cdot s)$	$diag\{0.015\}$
$\mathbf{K}_e (N)$	$diag\{2.2\}$	$diag\{2.2\}$		

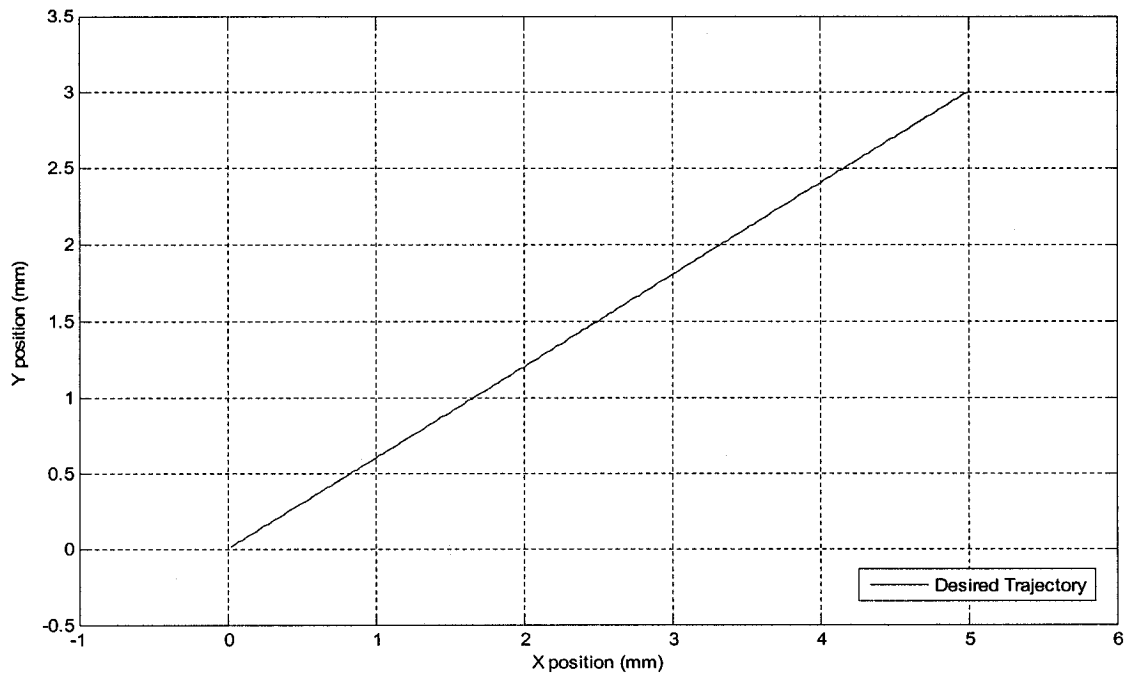


Figure 5.2: Desired path of the platform (tracking a straight line without a payload)

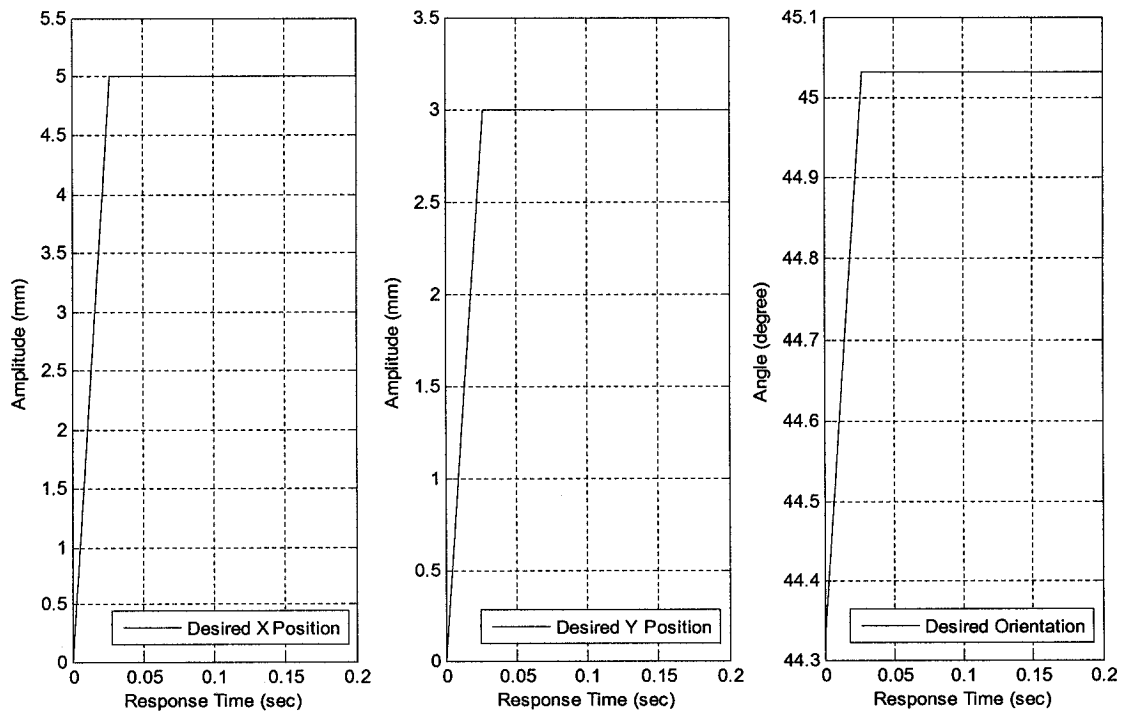


Figure 5.3: Desired position and orientation of the platform
(tracking a straight line without a payload)

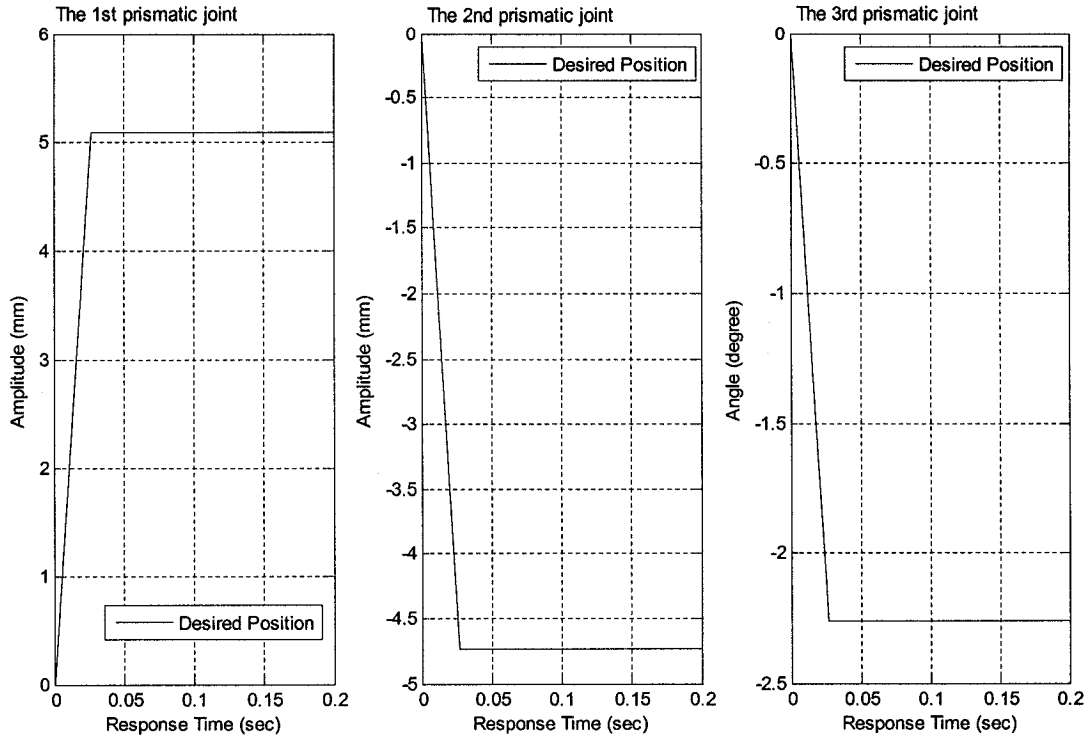


Figure 5.4: Desired positions of the three prismatic joints (tracking a straight line)

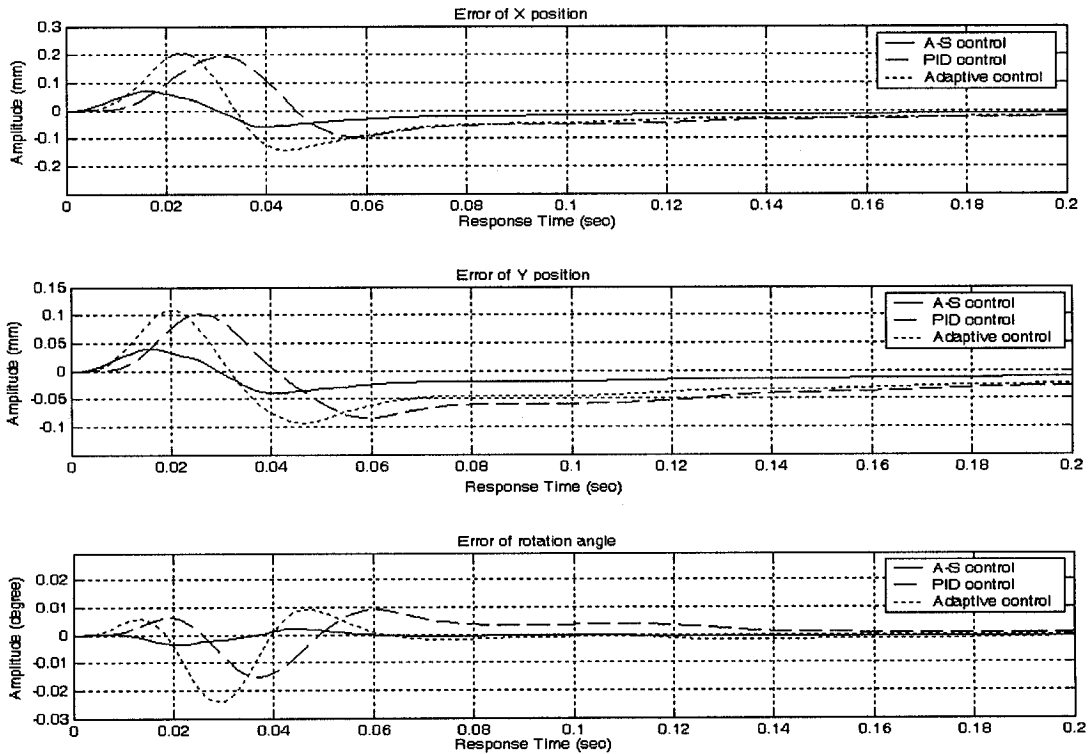


Figure 5.5: Pose errors of the platform (tracking a straight line without a payload)

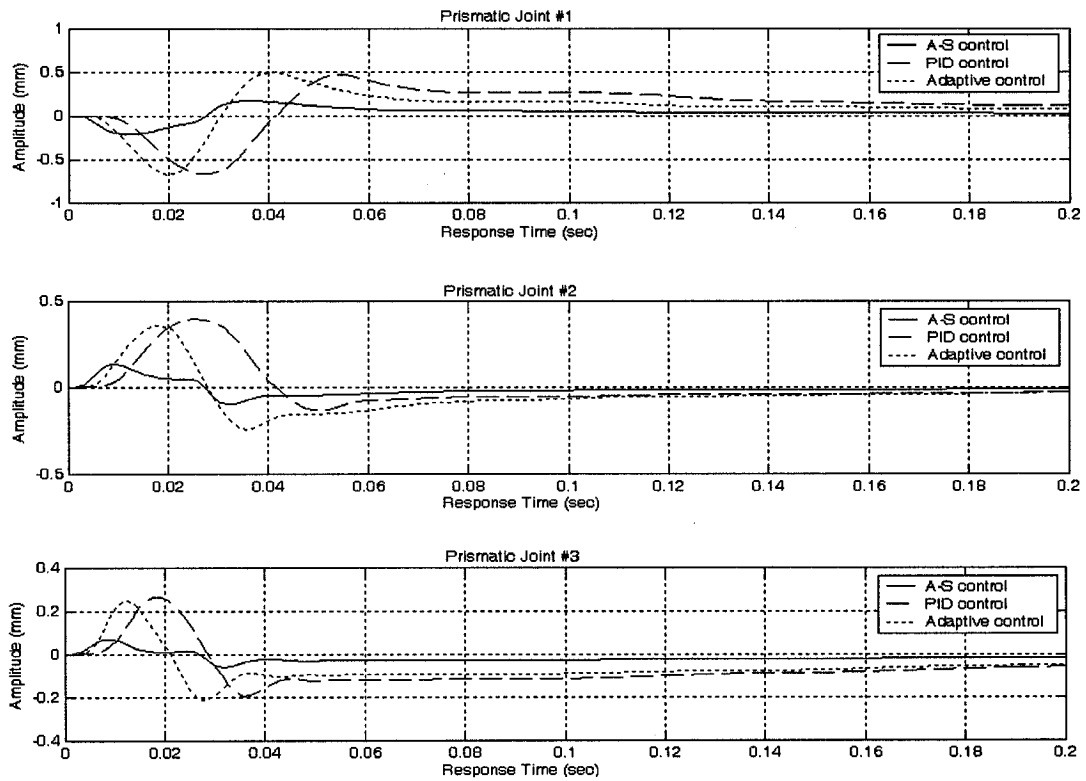


Figure 5.6: Position errors of the three prismatic joints
(tracking a straight line without a payload)

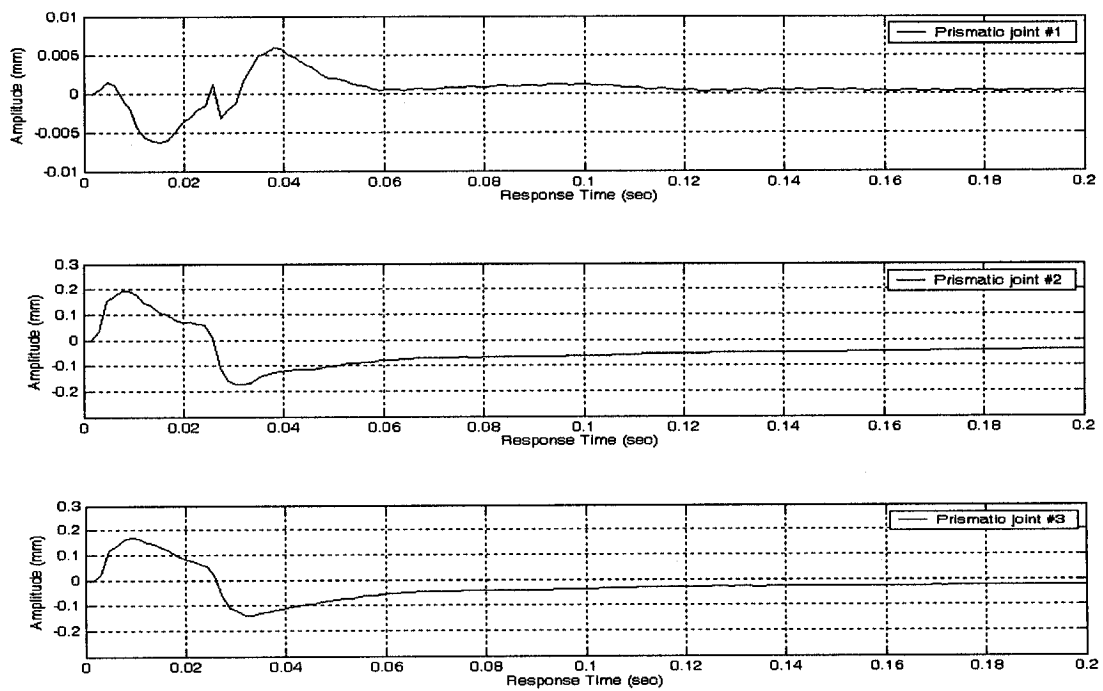


Figure 5.7: The synchronization error of the three prismatic joints using A-S control

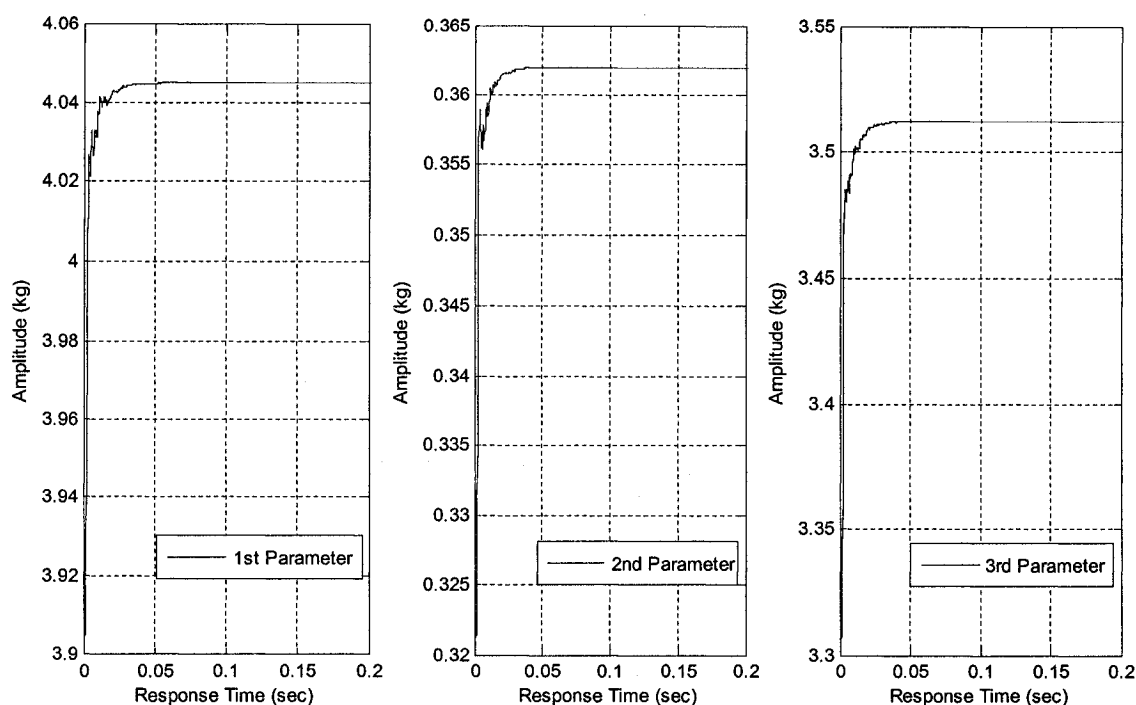


Figure 5.8: Estimated parameters (tracking a straight line without a payload)

Table 5.2: Error comparison (tracking a straight line without a payload)

Maximum Absolute Values	A-S Control	Adaptive Control	PID Control
Max. X Position Error(mm)	0.0701	0.2053	0.1946
Max. Y Position Error(mm)	0.0402	0.1094	0.1015
Max. Rotation Angle Error(deg)	0.0021	0.0231	0.0158
Max. 1 st Prismatic Joint Position Error(mm)	0.2120	0.6720	0.6763
Max. 2 nd Prismatic Joint Position Error(mm)	0.1313	0.3584	0.3933
Max. 3 rd Prismatic Joint Position Error(mm)	0.0671	0.2463	0.2642

5.4.2 Trajectory Tracking with a Quadrangle Path without a Payload

During this set of experimentations, the platform is required to move along a quadrangle trajectory, whose vertexes are selected as follows: $P_0(5mm, 0mm, 44.3 \text{ deg}) \rightarrow P_1(40mm, 10mm, 44.3 \text{ deg}) \rightarrow P_2(60mm, 70mm, 44.3 \text{ deg}) \rightarrow P_3(30mm, 50mm, 44.3 \text{ deg}) \rightarrow P_4(5mm, 0mm, 44.3 \text{ deg})$, stopping at each vertex for 0.2 seconds. This trajectory is shown in Figure 5.8. The maximum velocity and acceleration are set as 0.2 m/s and 100 m/s^2 , respectively. During the experiments conducted, the mass of the platform without a payload, the mass of the intermediate link and the mass of the bracket are assumed to be not exactly known, with initial values set as $\theta = [3.90 \text{ kg} \quad 0.32 \text{ kg} \quad 3.3 \text{ kg}]^T$. These estimated parameters converge to $\theta = [4.047 \text{ kg} \quad 0.362 \text{ kg} \quad 3.511 \text{ kg}]^T$, as shown in Figure 5.14. In order to achieve good performance, using the trial-and-error method, the control gains of the A-S controller are chosen as listed in Table 5.3. Similarly as in the previous sub-section, for comparison purposes, an adaptive controller with the same control law of the A-S controller except with $\Gamma = \mathbf{0}$, and a PID controller are also employed. By conducting a large number of experiments, the control gains are selected, as listed in Table 5.3, by which the best tracking performance for the adaptive controller and the PID controller are achieved, amongst all tested control gains.

Figure 5.9 ~5.11 illustrates the desired trajectory of the platform, the desired position and orientation trajectories of the platform, and the desired position trajectories of the three prismatic joints, respectively. Figure 5.12 and Figure 5.13 shows a comparison among A-S control, adaptive control without synchronization and PID control in the pose errors of the platform, and position errors of the three prismatic joints, respectively. In

these two figures, solid lines denote the results obtained by A-S control, dashed lines denote the results obtained by adaptive control without synchronization, and dotted lines denote the results obtained by PID control. Obviously, the proposed A-S controller yields the smallest tracking errors and fastest convergence speed. Table 5.4 lists the maximum errors with these three methods. Comparing these experimental results, we can conclude that the proposed A-S control approach may achieve good tracking performance superior to the adaptive control without the synchronization and PID control.

Table 5.3: Control gains of the employed controllers
(tracking a quadrangle path without a payload)

Control Gains	A-S Control	Adaptive Control	Control Gains	PID Control
$\Lambda (1/s)$	$diag\{1.04\}$	$diag\{1.04\}$	$\mathbf{K}_p (N)$	$diag\{2.0\}$
$\Gamma (s)$	$diag\{0.05\}$	$diag\{0.0\}$	$\mathbf{K}_i (N/s)$	$diag\{1.0\}$
$\mathbf{K}_r (N \cdot s)$	$diag\{15.0\}$	$diag\{16.0\}$	$\mathbf{K}_d (N \cdot s)$	$diag\{0.017\}$
$\mathbf{K}_e (N)$	$diag\{2.2\}$	$diag\{2.0\}$		

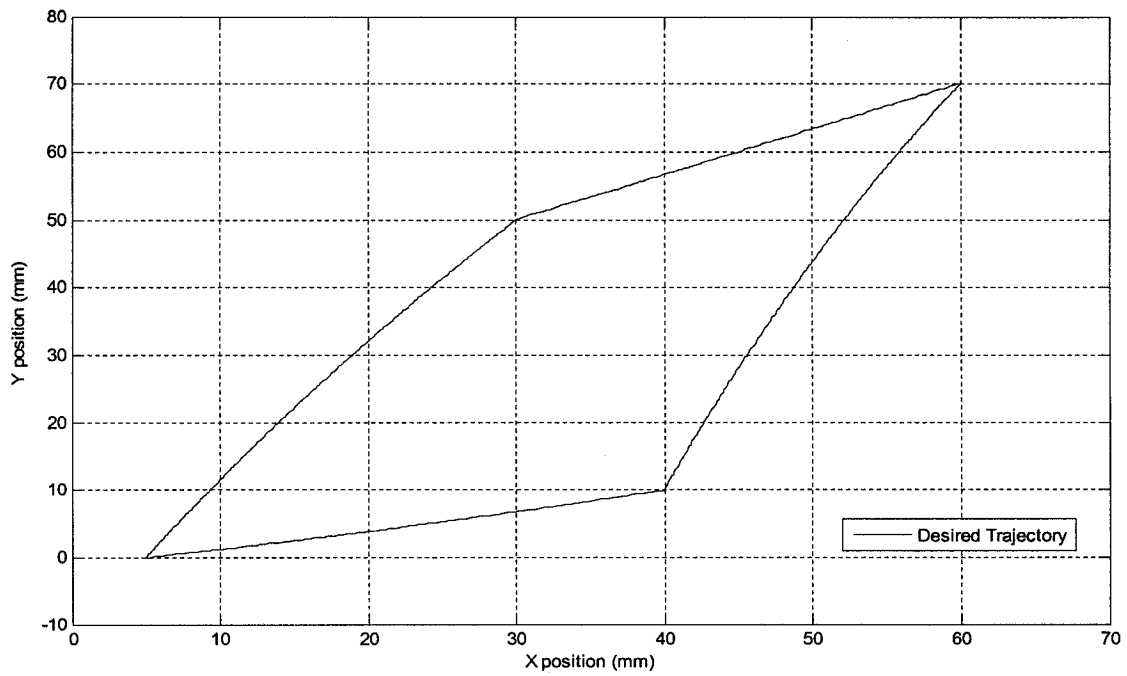


Figure 5.9: Desired path of the platform (tracking a quadrangle path without a payload)

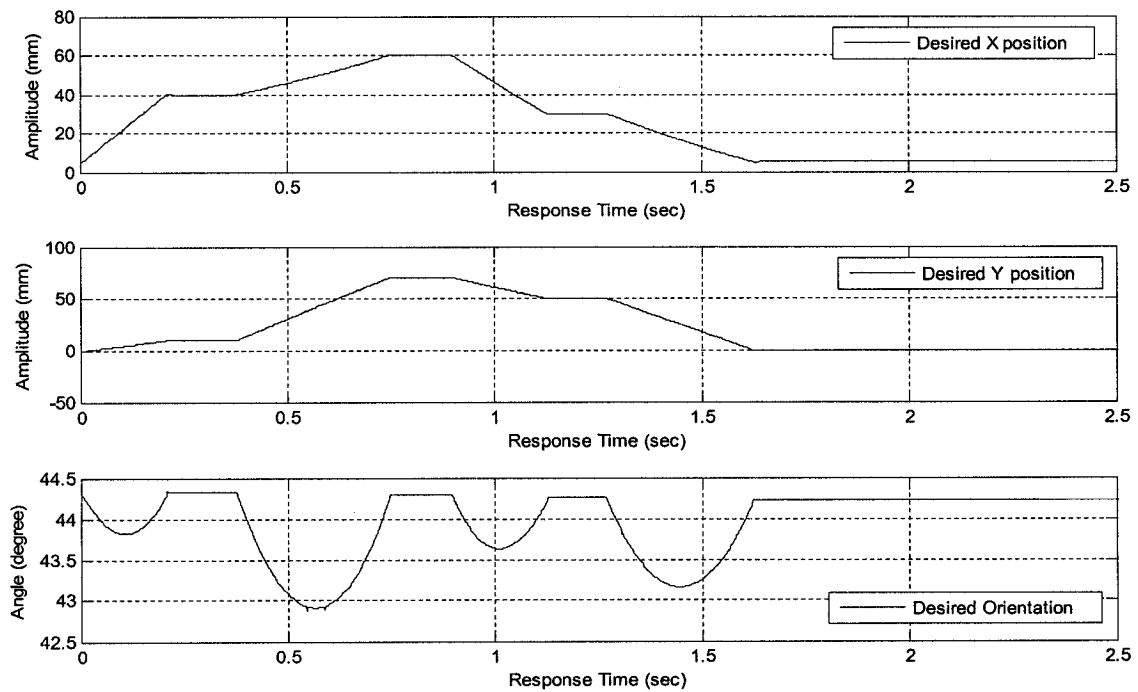


Figure 5.10: Desired position and orientation of the platform (tracking a quadrangle path without a payload)

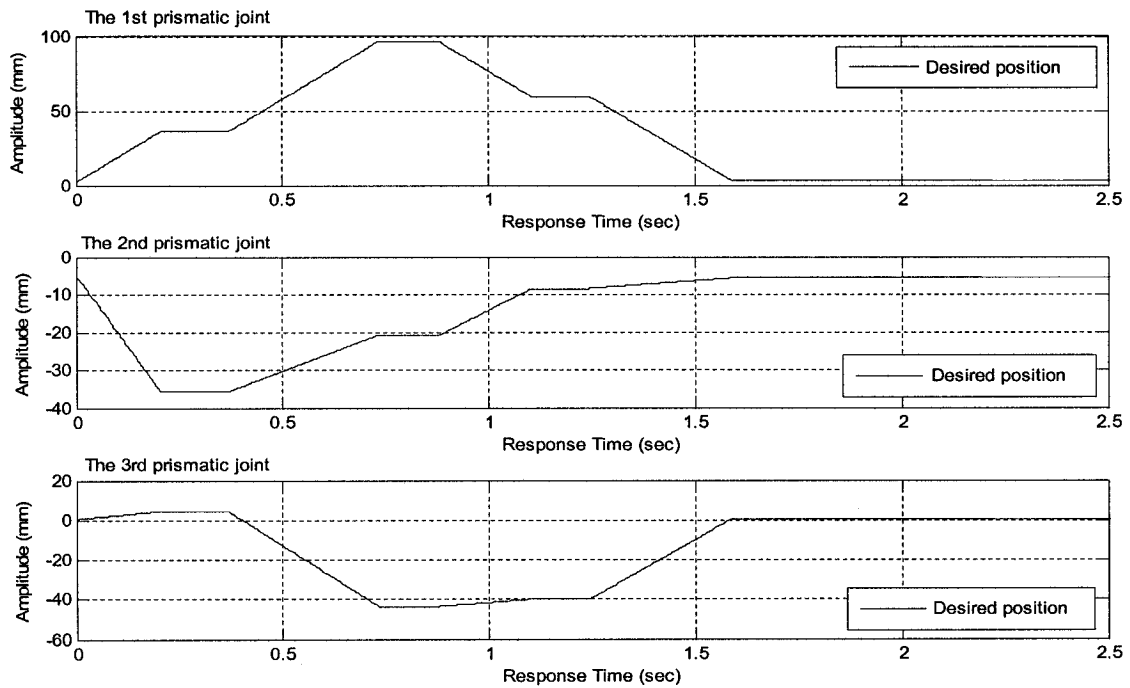


Figure 5.11: Desired positions of the three prismatic joints
(tracking a quadrangle path without a payload)

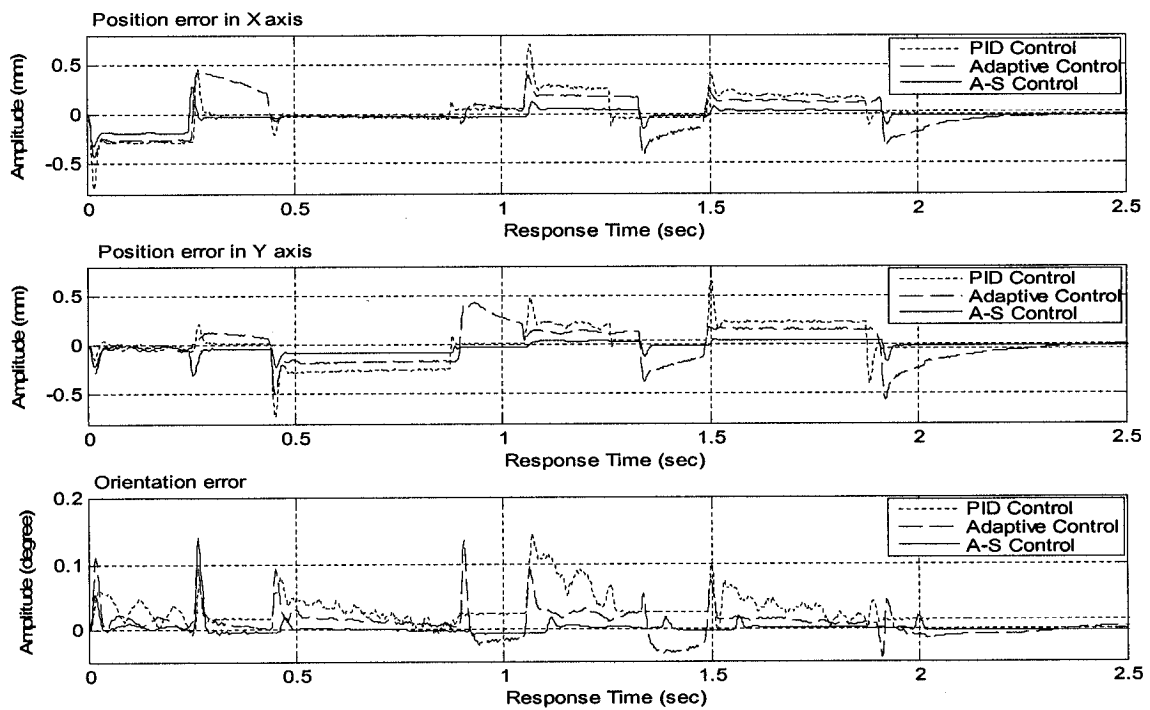


Figure 5.12: Pose errors of the platform (tracking a quadrangle path without a payload)

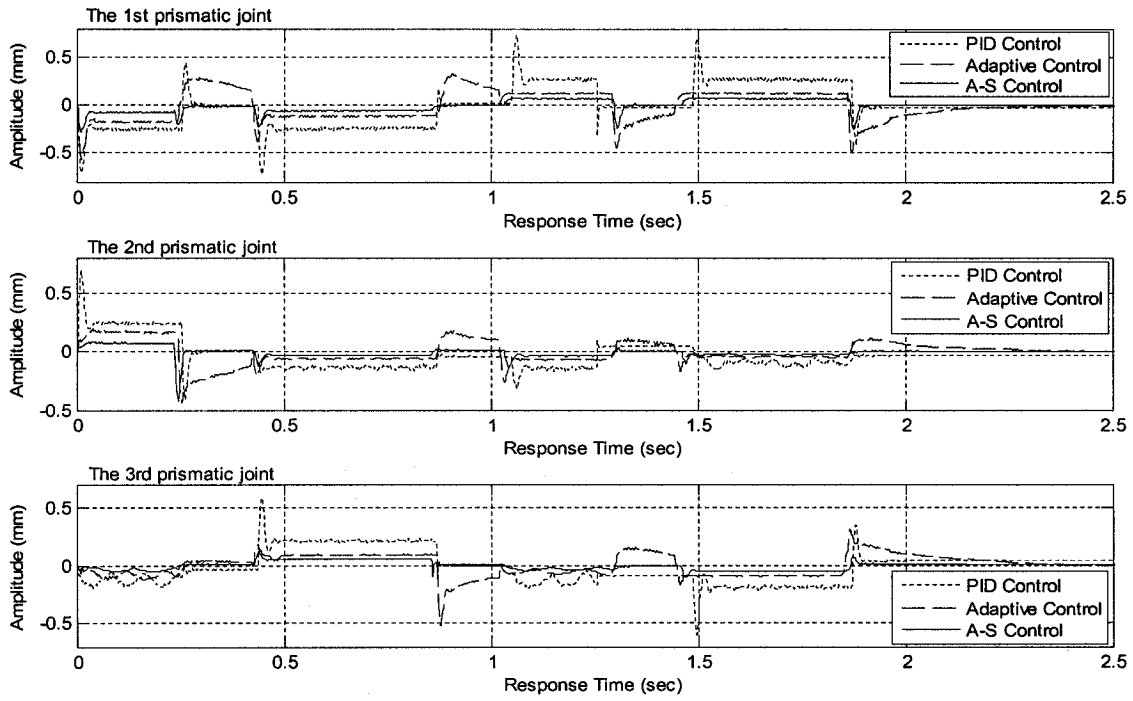


Figure 5.13: Position errors of the three prismatic joints (tracking a quadrangle path without a payload)

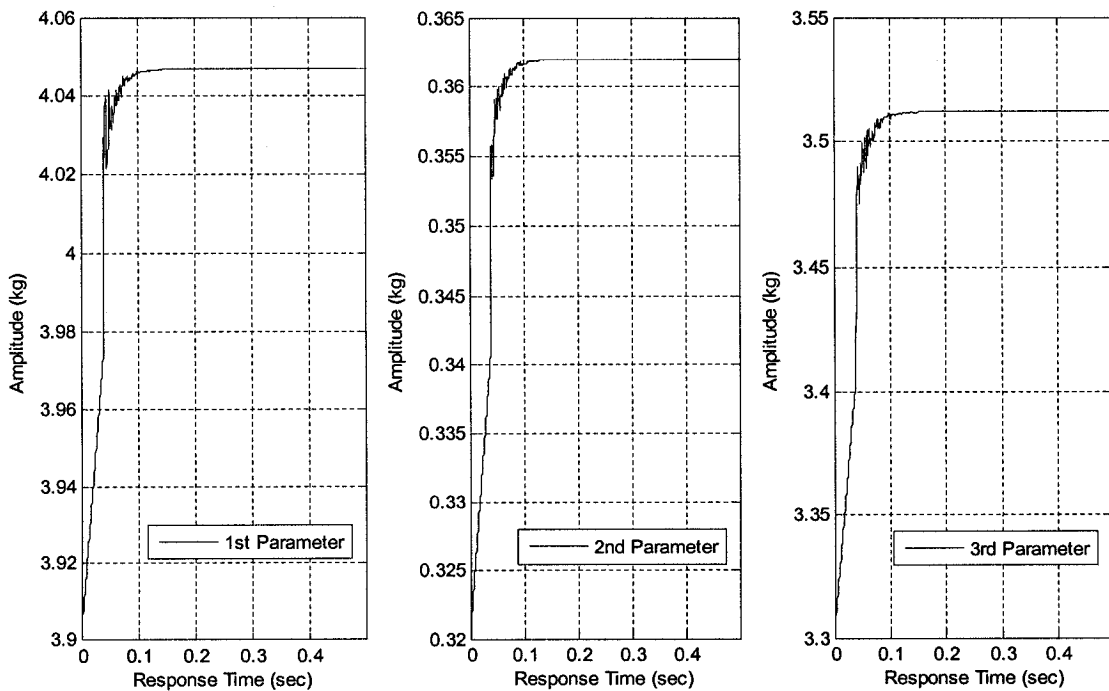


Figure 5.14: Estimated parameters (tracking a quadrangle path without a payload)

Table 5.4: Error comparison (tracking a quadrangle path without a payload)

Maximum Absolute Values	A-S Control	Adaptive Control	PID Control
Max. X Position Error(mm)	0.3207	0.4249	0.7523
Max. Y Position Error(mm)	0.3107	0.5696	0.7352
Max. Rotation Angle Error(deg)	0.1403	0.1356	0.1454
Max. 1 st Prismatic Joint Position Error(mm)	0.2785	0.4910	0.7261
Max. 2 nd Prismatic Joint Position Error(mm)	0.3220	0.2959	0.6851
Max. 3 rd Prismatic Joint Position Error(mm)	0.1213	0.5237	0.6043

5.4.3 Trajectory Tracking with a Straight Line Path with a Payload

During this set of experimentations, a payload is fixed on the platform at its geometry center. In order to evaluate the differences of control performance between the cases without payload and with payload, the same straight line trajectory of the platform, as presented in sub-section 5.4.1, is followed. On the other hand, in order to demonstrate the effectiveness of A-S control, adaptive control and PID control are also employed. Moreover, to evaluate the effects of unknown parameters with large uncertainty on these three control approaches, identical control gains have been selected to those chosen in sub-section 5.4.1 (see Table 5.2). At the initial time, the mass of the platform (with a payload), the mass of the intermediate link and the mass of the bracket are assumed to be unknown, but with some uncertainty, while the other parameters are assumed to be

known exactly. In the experiments conducted, we set $\theta = [3.90\text{kg} \ 0.32\text{kg} \ 3.3\text{kg}]^T$ as the initial values of the parameter estimated, i.e., the mass of the platform with the payload, the mass of the intermediate link, and the mass of the bracket. The estimated parameters converge to $\theta = [4.89\text{kg} \ 0.36\text{kg} \ 3.51\text{kg}]^T$, as shown in Figure 5.17, while the true values are $\theta_{me} = [4.89\text{kg} \ 0.36\text{kg} \ 3.51\text{kg}]^T$. The maximum speed and acceleration are set as 0.261m/s and 124m/s^2 , respectively.

Figure 5.15 and Figure 5.16 shows a comparison amongst A-S control, adaptive control without synchronization and PID control for pose errors of the platform, and position errors of the three prismatic joints, respectively. In these two figures, solid lines denote the results obtained by A-S control, dashed lines denote the results obtained by adaptive control without synchronization, and dotted lines denote the results obtained by the PID control. Table 5.5 lists the maximum absolute errors with these three methods. Comparing experimental results obtained in both this sub-section and sub-section 5.4.1, we conclude the following three points: (i) The proposed A-S control yields the smallest tracking errors and fastest convergence speed because its adaptation law estimates unknown parameters and thus improve tracking performance while its synchronized control law considers the coupling effects amongst the active joints and improve the performance, further; (ii) Adaptive control yields better tracking performance than PID control, i.e., smaller tracking errors and faster convergence speed, because of its capability of estimating unknown parameters; (iii) As a result, the proposed A-S control may achieve good tracking performance over the adaptive control without the synchronization and PID control.

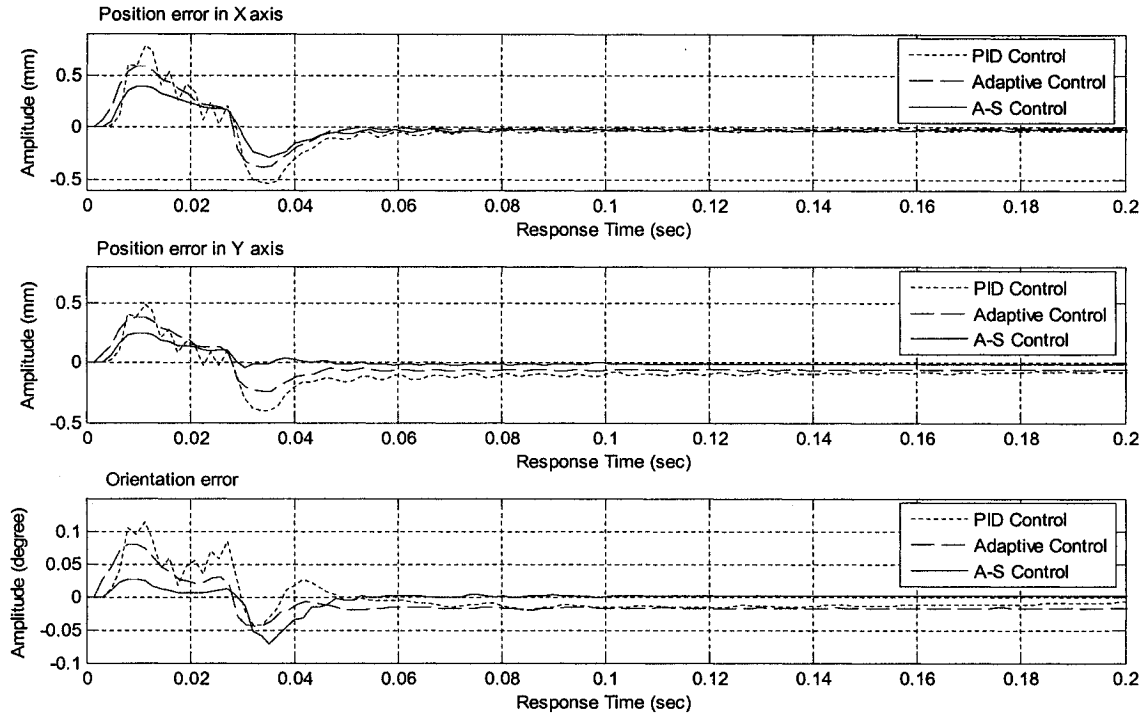


Figure 5.15: Pose errors of the platform (tracking a straight line with a payload)

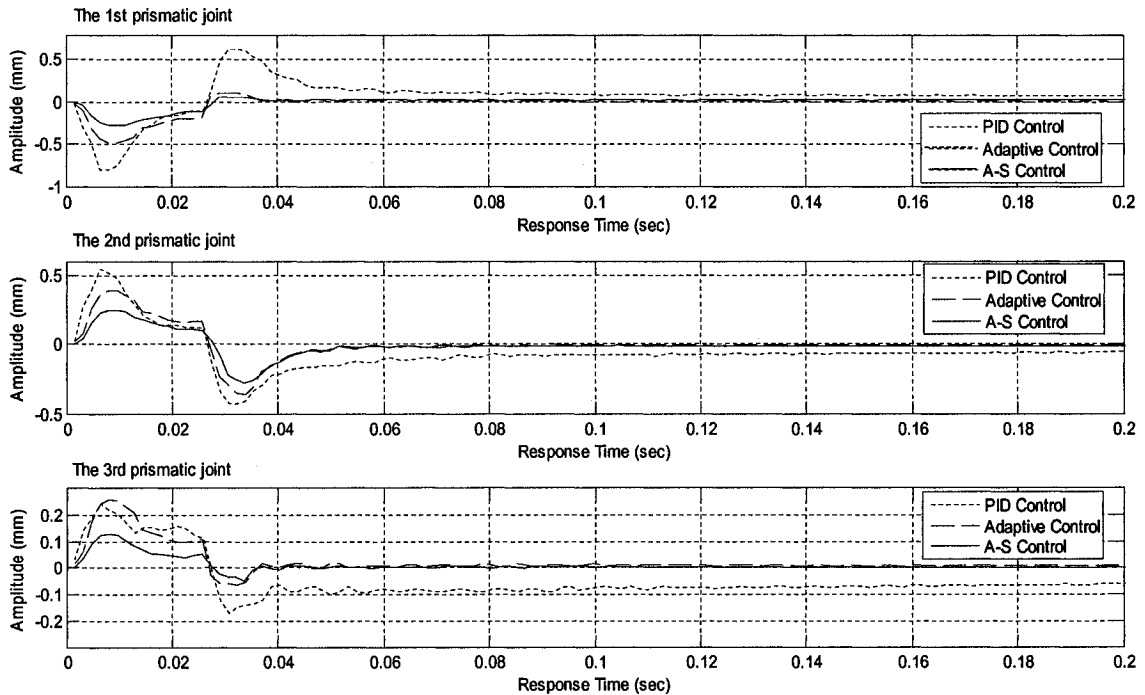


Figure 5.16: Position errors of the three prismatic joints
(tracking a straight line with a payload)

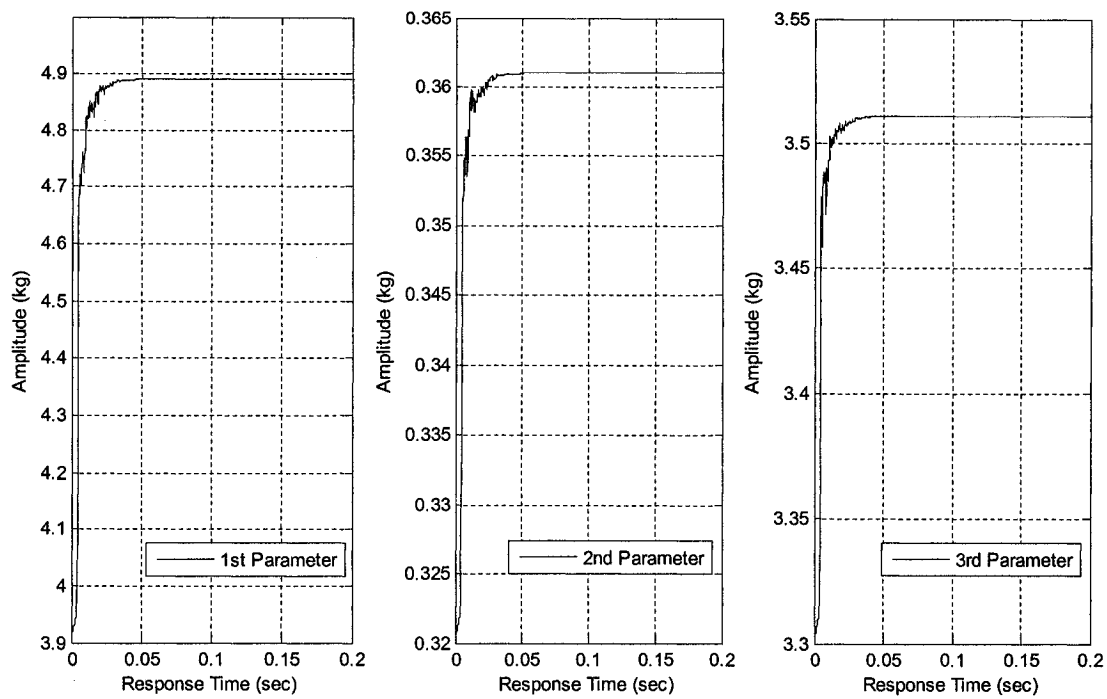


Figure 5.17: Estimated parameters (tracking a straight line with a payload)

Table 5.5: Error comparison (tracking a straight line path with a payload)

Maximum Absolute Values	A-S Control	Adaptive Control	PID Control
Max. X Position Error(mm)	0.3929	0.5855	0.7862
Max. Y Position Error(mm)	0.2429	0.3813	0.4874
Max. Rotation Angle Error(deg)	0.0717	0.0903	0.1139
Max. 1 st Prismatic Joint Position Error(mm)	0.2774	0.4757	0.7993
Max. 2 nd Prismatic Joint Position Error(mm)	0.2808	0.4313	0.5487
Max. 3 rd Prismatic Joint Position Error(mm)	0.1269	0.2504	0.2422

5.4.4 Trajectory Tracking with a Quadrangle Path with a Payload

During this set of experiments, a payload is fixed on the platform at its geometry center. The same quadrangle trajectory of the platform, as presented in sub-section 5.4.2, is followed to evaluate the performance differences between the cases without a payload and with a payload. On the other hand, in order to demonstrate the effectiveness of A-S control, adaptive control and PID control are also employed. Moreover, to evaluate the effects of unknown parameters with large uncertainty on these three control approaches, same control gains have been selected as those in sub-section 5.4.2 (see Table 5.4). During the experiments conducted, we set $\theta = [3.90\text{kg} \quad 0.32\text{kg} \quad 3.3\text{kg}]^T$ as the initial values of the parameters estimated, i.e., the mass of the platform with a payload, the mass of the intermediate link and the mass of the bracket. The other system parameters are assumed to be known exactly. The estimated parameters converge to $\theta = [4.891\text{kg} \quad 0.362\text{kg} \quad 3.511\text{kg}]^T$, which are identical to their true values, $\theta_{me} = [4.891\text{kg} \quad 0.362\text{kg} \quad 3.511\text{kg}]^T$, as shown in Figure 5.20. The maximum speed and acceleration are set as 0.2m/s and 100m/s^2 , respectively.

Figure 5.18 and Figure 5.19 shows a comparison among A-S control, adaptive control without synchronization and PID control in the pose errors of the platform, and position errors of the three prismatic joints, respectively. In these two figures, solid lines denote the results obtained by A-S control, dashed lines denote the results obtained by adaptive control without synchronization, and dotted lines denote the results obtained by PID control. Table 5.6 lists the maximum absolute errors with these three methods. Comparing experimental results obtained in both this sub-section and sub-section 5.4.2, similar conclusions are made as those presented in the previous sub-section.

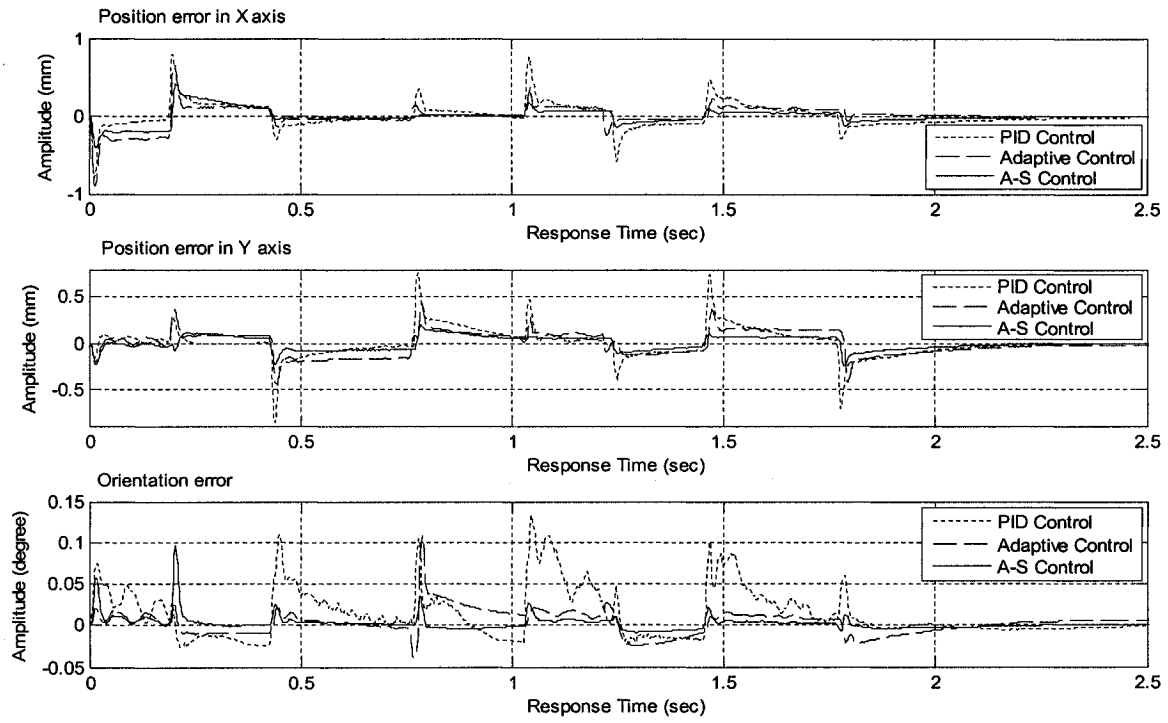


Figure 5.18: Pose errors of the platform (tracking a quadrangle path with a payload)

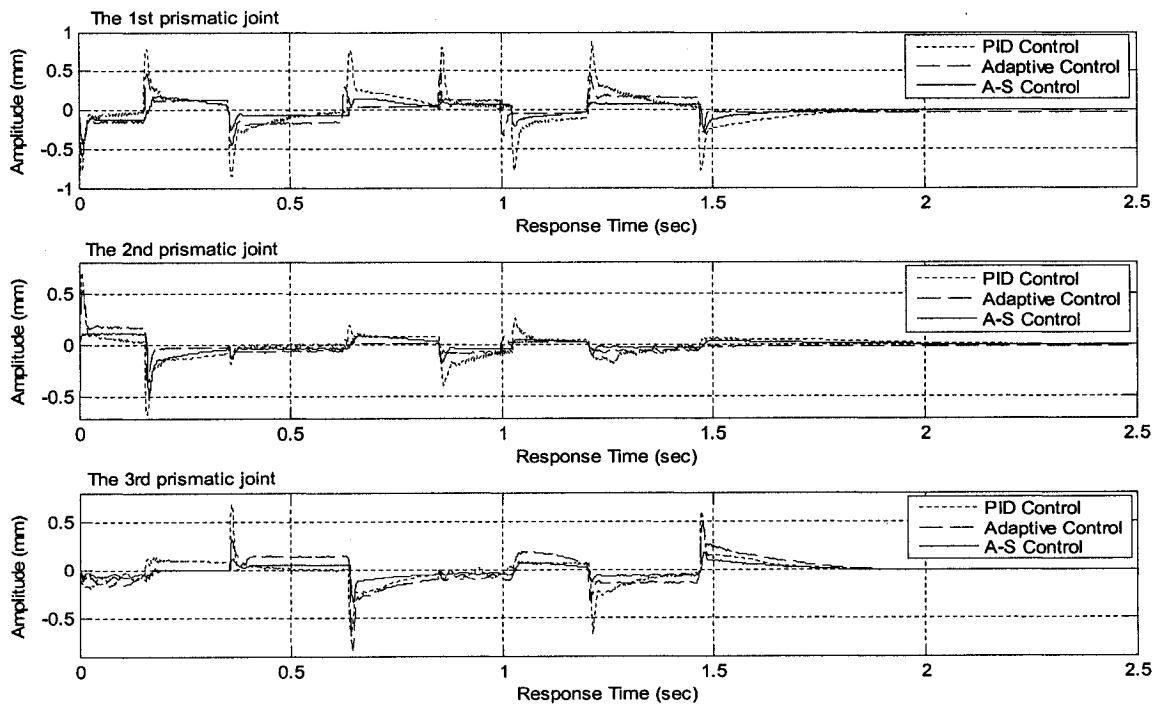


Figure 5.19: Position errors of the three prismatic joints (tracking a quadrangle path with a payload)

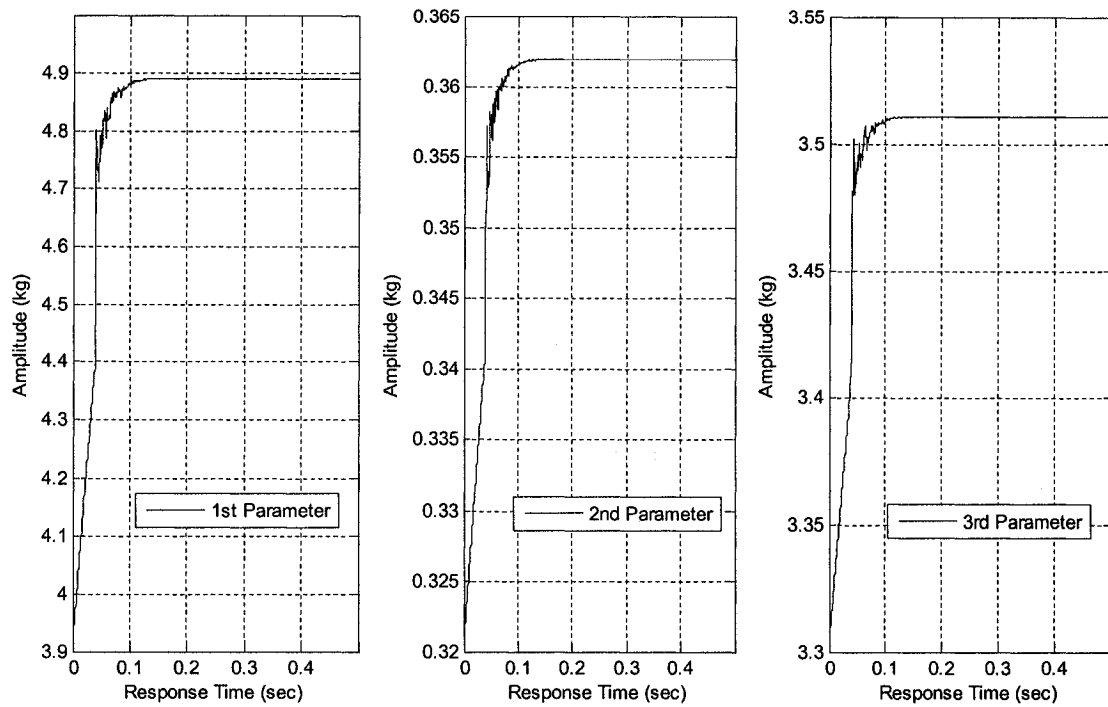


Figure 5.20: Estimated parameters (tracking a quadrangle path with a payload)

Table 5.6: Error comparison (tracking a quadrangle path with a payloads)

Maximum Absolute Values	A-S Control	Adaptive Control	PID Control
Max. X Position Error(mm)	0.4223	0.9073	0.8016
Max. Y Position Error(mm)	0.2430	0.4391	0.8549
Max. Rotation Angle Error(deg)	0.0963	0.1077	0.1325
Max. 1 st Prismatic Joint Position Error(mm)	0.4408	0.5997	0.8663
Max. 2 nd Prismatic Joint Position Error(mm)	0.4833	0.5439	0.6954
Max. 3 rd Prismatic Joint Position Error(mm)	0.3366	0.8414	0.6878

5.5 Summary

In this chapter, we proposed a new control approach, termed A-S control, with respect to trajectory tracking control of a parallel robotic manipulator with unknown parameters. Through experimentation, in detail, applying A-S control, adaptive control without synchronization and PID control on a P-R-R manipulator to follow different trajectories with and without payloads, we conclude that the proposed A-S control may achieve good tracking performance superior to the adaptive control without the synchronization and PID control.

Chapter 6

Convex Synchronized Control

6.1 Introduction

In this chapter, in order to satisfy multiple performance specifications simultaneously during trajectory tracking of parallel robotic manipulators, we propose a new control approach, termed convex synchronized (C-S) control, which is based on the so-called *convex combination method* proposed by Liu, H. (Liu, H., *et al.*, 1996 [37]). This method was proposed for solving the multiple simultaneous specification (MSS) problem, where the multiple specifications are convex with respect to the closed-loop transfer function, and conflicting with each other, i.e., when one specification is improved, another one will be deteriorated. By combining multiple linear controllers, so-called sample controllers, via a combination vector, a final controller is derived, which satisfies all closed-loop performance specifications simultaneously. Each sample controller is required to satisfy at least one specification. The task of determining these sample controllers is thus very simple, and consequently this method is far less complex compared with the task of finding a single closed-loop controller that satisfies multiple simultaneous specifications. Hence, compared with the traditional trial-and-error method, the convex combination method is more efficient and straightforward. On the other hand, in the C-S control scheme, each sample controller can achieve good performance on a parallel robotic manipulator because of the use of the synchronization error. As a result, a C-S controller

derived from sample controllers can satisfy multiple specifications simultaneously and achieve good tracking performance during trajectory tracking of a parallel manipulator.

The rest of this chapter is organized as follows. Section 2 introduces the controller design of the C-S control, in which the framework of the convex combination method is briefly introduced and a new synchronization error is defined. Section 3 provides the robustness analysis of the proposed C-S control and presents some convex robustness specifications. Section 4 shows the experimental results using the C-S controller. Finally, Section 5 offers a summary of this chapter.

6.2 C-S Control Design

In this section, we first briefly introduce the framework of the convex combination method. Then, through defining a new synchronization error, which is based on the one proposed by Su, Y. (Su, Y., *et al.*, 2005 [73]), the C-S control approach is presented.

6.2.1 The Convex Combination Method

The convex combination method was developed based on the convex optimization theory, which was proposed by Boyd, S.P., *et al.*, (Boyd, S.P., *et al.*, 1991 [8]). This theory shows that many design specifications have a simple geometric convex property (Definition 6.1). Under this condition, a linear controller can be analytically derived using the convex theories (Rockafellar, R.T., 1970 [62]).

Definition 6.1 (Convexity) A closed-loop performance specification is *convex* if the functional ϕ on the closed-loop transfer matrix $\bar{\mathbf{H}}$ has the property that for any $\bar{\mathbf{H}}, \tilde{\mathbf{H}} \in \mathbf{H}$, and any constant $\lambda \in [0, 1]$:

$$\phi(\lambda\bar{\mathbf{H}} + (1-\lambda)\tilde{\mathbf{H}}) \leq \lambda\phi\bar{\mathbf{H}} + (1-\lambda)\phi\tilde{\mathbf{H}} \quad (6.1)$$

□

Moreover, the convex combination method was proposed for linear time-invariant (LTI) systems, which can be formulated in a uniform framework as shown in Figure 6.1. In the figure, vector $\mathbf{u} \in \mathfrak{R}^{n_u}$ denotes the actuator inputs, which are generated by the controller; vector $\mathbf{w} \in \mathfrak{R}^{n_w}$ denotes the exogenous inputs; vector $\mathbf{y} \in \mathfrak{R}^{n_y}$ denotes the measured signals, which consists of the output signals that are accessible to the controller; and vector $\mathbf{z} \in \mathfrak{R}^{n_z}$ denotes the regulated output signals that are interest to the designer.

In the frequency domain, the system framework is represented by the following transfer matrices:

$$\text{Open-loop} \quad \begin{bmatrix} \mathbf{z}(s) \\ \mathbf{y}(s) \end{bmatrix} = \begin{bmatrix} \mathbf{P}_{zw}(s) & \mathbf{P}_{zu}(s) \\ \mathbf{P}_{yw}(s) & \mathbf{P}_{yu}(s) \end{bmatrix} \cdot \begin{bmatrix} \mathbf{w}(s) \\ \mathbf{u}(s) \end{bmatrix} \quad (6.2)$$

$$\text{Controller} \quad \mathbf{u}(s) = \bar{\mathbf{K}}(s) \cdot \mathbf{y}(s) \quad (6.3)$$

$$\text{Closed-loop} \quad \mathbf{z}(s) = \bar{\mathbf{H}}(s) \cdot \mathbf{w}(s) \quad (6.4)$$

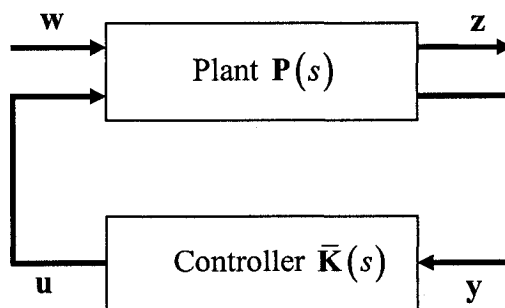


Figure 6.1: Linear system framework

where $\mathbf{P}_{zw} \in \mathfrak{R}^{n_z \times n_w}$ is the transfer matrix from \mathbf{w} to \mathbf{z} ; $\mathbf{P}_{zu} \in \mathfrak{R}^{n_z \times n_u}$ is the transfer matrix from \mathbf{u} to \mathbf{z} ; $\mathbf{P}_{yw} \in \mathfrak{R}^{n_y \times n_w}$ is the transfer matrix from \mathbf{w} to \mathbf{y} ; $\mathbf{P}_{yu} \in \mathfrak{R}^{n_y \times n_u}$ is the transfer matrix from \mathbf{u} to \mathbf{y} ; $\bar{\mathbf{K}} \in \mathfrak{R}^{n_u \times n_y}$ is the controller transfer matrix from \mathbf{y} to \mathbf{u} ; and $\bar{\mathbf{H}} \in \mathfrak{R}^{n_z \times n_w}$ is the closed-loop transfer matrix from \mathbf{w} to \mathbf{z} .

Assume m convex specifications are to be satisfied simultaneously

$$\begin{cases} \phi_1(\bar{\mathbf{H}}) \leq \alpha_1 \\ \phi_2(\bar{\mathbf{H}}) \leq \alpha_2 \\ \vdots \\ \phi_m(\bar{\mathbf{H}}) \leq \alpha_m \end{cases} \quad (6.5)$$

where α_i ($i=1,2,\dots,m$) denotes the expected specification value, then the convex combination method can be applied through the following two-stage strategy (Liu, H., *et al.*, 1997):

I. Sample controller: Select m linear controllers: $\bar{\mathbf{K}}_1(s), \bar{\mathbf{K}}_2(s), \dots, \bar{\mathbf{K}}_m(s)$, called sample controllers, such that each controller $\bar{\mathbf{K}}_i(s)$ satisfies at least one specification ϕ_i , ($i=1,2,\dots,m$). Such sample controllers can be selected by using any linear control approach (e.g., PID or PD control) for one specification each time. Consequently, it lessens much burden on the control gain selections, which is the most important advantage of the convex combination method. When the sample controllers are determined, calculate the m specification values under every sample controller: $\phi_{ij} = \phi_i(\bar{\mathbf{H}}_j(s))$ is the specification ϕ_i value under the sample control structure $\bar{\mathbf{H}}_j(s)$, where $\bar{\mathbf{H}}_j(s)$ is the closed-loop transfer matrix with the sample controller $\bar{\mathbf{K}}_j(s)$.

II. Combination: Find the combination vector $\bar{\Lambda}$ through solving a linear programming problem

$$\Phi \cdot \bar{\Lambda} \leq \Psi \quad (6.6)$$

where $\Phi = \{\phi_{ij}\}$, $\bar{\Lambda} = [\lambda_1 \ \lambda_2 \ \dots \ \lambda_m]^T$, $\left(\lambda_i \geq 0, \sum_{i=1}^m \lambda_i = 1\right)$, $\Psi = [\alpha_1 \ \alpha_2 \ \dots \ \alpha_m]^T$,

$(1 \leq i, j \leq m)$. Furthermore, if the following conditions are satisfied, then there exists a solution to the above inequality (6.6). The detailed proof has been given in (Fu, K., *et al.*, 2003 [22]).

$$\left\{ \begin{array}{l} F(\psi) = F \left(\begin{bmatrix} \alpha_1 \\ \alpha_2 \\ \vdots \\ \alpha_m \end{bmatrix} \right) = (-1)^{m+1} \begin{vmatrix} \alpha_1 & \dots & \alpha_m & 1 \\ \phi_{11} & \dots & \phi_{m1} & 1 \\ \vdots & \ddots & \vdots & 1 \\ \phi_{1m} & \dots & \phi_{mm} & 1 \end{vmatrix} \begin{vmatrix} \phi_{11} & \dots & \phi_{1m} \\ \vdots & \ddots & \vdots \\ \phi_{m1} & \dots & \phi_{mm} \end{vmatrix}^{-1} \geq 0 \\ \alpha_i \geq \min(\phi_i(\bar{\mathbf{H}}_1), \phi_i(\bar{\mathbf{H}}_2), \dots, \phi_i(\bar{\mathbf{H}}_m)) = \min(\phi_{i1}, \phi_{i2}, \dots, \phi_{im}), \quad i = 1, 2, \dots, m \end{array} \right. \quad (6.7)$$

Assume $\bar{\Lambda}^* = [\lambda_1^* \ \lambda_2^* \ \dots \ \lambda_m^*]^T$ is one solution of (6.6), a controller $\bar{\mathbf{K}}^*$ satisfying all closed-loop performance specifications simultaneously is derived through the convex combination of m closed-loop transfer matrices with the combination vector $\bar{\Lambda}^*$.

$$\bar{\mathbf{K}}^*(s) = [\mathbf{I} + \mathbf{R}^*(s) \mathbf{P}_{yu}(s)]^{-1} \mathbf{R}^*(s) \quad (6.8)$$

where

$$\mathbf{R}^*(s) = \mathbf{P}_{zu}^{-1}(s) (\bar{\mathbf{H}}^*(s) - \mathbf{P}_{zw}(s)) \mathbf{P}_{yw}^{-1} \quad (6.9)$$

$$\bar{\mathbf{H}}^*(s) = \lambda_1 \bar{\mathbf{H}}_1(s) + \lambda_2 \bar{\mathbf{H}}_2(s) + \dots + \lambda_m \bar{\mathbf{H}}_m(s) \quad (6.10)$$

See details in (Liu, H., *et al.*, 1998).

6.2.2 A Model-Free Synchronization Error

Studying the synchronization error $\epsilon(t)$ defined in Chapter 3 with the expression of (3.5), we find that it is nonlinear with respect to the system outputs $\mathbf{q}(t)$. As a result, a controller employing this synchronization error may also be nonlinear with respect to $\mathbf{q}(t)$. It is contradictory to the requirements of the convex combination method that sample controllers should be linear to the system outputs. In order to use the convex combination method, here we define a new synchronization error based on (Su, Y., *et al.*, 2005). This synchronization error is linear with respect to the system outputs $\mathbf{q}(t)$, and is defined as follows.

For a parallel robotic manipulator with n active joints, i.e., n DOF, the synchronization goal is motivated by the following fact:

When the ratio of the actual position or rotation of each active joint at each sampling time to its final desired translation or rotation is equal to those of all other active joints, all active joints move in a synchronous manner and the desired pose of the platform is maintained.

Thus the synchronization goal can be defined as:

$$\frac{q_1(t)}{\rho_1} = \frac{q_2(t)}{\rho_2} = \dots = \frac{q_n(t)}{\rho_n}, \quad (i=1, \dots, n) \quad (6.11)$$

where $q_i(t)$ denotes the actual position or rotation of the i^{th} active joint at each sampling time; ρ_i denotes the completed translation or rotation of the i^{th} active joint at the end of its desired trajectory. Note that ρ_i is time-invariant.

In order to be implemented easily, the synchronization goal (6.11) is rewritten as a set of sub-goals, namely $\frac{q_i(t)}{\rho_i} = \frac{q_{i+1}(t)}{\rho_{i+1}} = \frac{q_{i-1}(t)}{\rho_{i-1}}$, subject to the boundary conditions: when $i=1$, $q_{i-1} = q_n$, $\rho_{i-1} = \rho_n$; when $i=n$, $q_{i+1} = q_1$, $\rho_{i+1} = \rho_1$. Thus, the synchronization strategy for a parallel robotic manipulator is described as follows:

The control torque applied to each active joint is designed to stabilize the position tracking of this active joint, while synchronizing motions between this active joint and the other two active joints with the adjacent sequence number. Specifically, the control torque τ_{a_i} for the i th sub-manipulator is to control $e_i(t) \rightarrow 0$ and at the same time, to synchronize the motion of the $(i-1)$ th active joint, the i th active joint, and the $(i+1)$ th active joint so that synchronization error $\bar{e}_i(t) \rightarrow 0$.

Accordingly, a series of synchronization functions corresponding to these sub-goals are derived as:

$$f(q_i(t), q_{i+1}(t), q_{i-1}(t)) = 2 \frac{q_i(t)}{\rho_i} - \frac{q_{i+1}(t)}{\rho_{i+1}} - \frac{q_{i-1}(t)}{\rho_{i-1}} = 0 \quad (6.12)$$

As defined in Chapter 3, the vector $\mathbf{e}(t) = \mathbf{q}(t) - \mathbf{q}^d(t) \in \mathfrak{R}^{n \times 1}$ denotes the position or rotation errors of the active joints. Using a Taylor series expansion, the following equations can be derived from (6.12), in a similar manner to (Sun, D., *et al.*, 2002)

$$d_i(t)e_i(t) + d_{i+1}(t)e_{i+1}(t) + d_{i-1}(t)e_{i-1}(t) = 0 \quad (6.13)$$

where $e_i(t)$ denotes the i^{th} term of $\mathbf{e}(t)$; $d_i(t)$ denotes the bounded coupling parameters regarding the first-order errors $e_i(t)$, expressed by

$$d_i(t) = \left. \frac{\partial f(q_i(t), q_{i+1}(t), q_{i-1}(t))}{\partial q_i} \right|_{q_i^d(t)} \quad (6.14)$$

Based on (6.11) ~ (6.14), the goal of synchronization is defined as deriving the synchronization error, defined below, to zero

$$\begin{aligned} \bar{e}_1(t) &= \frac{2}{\rho_1} e_1(t) - \frac{1}{\rho_2} e_2(t) - \frac{1}{\rho_n} e_n(t) \\ \bar{e}_2(t) &= \frac{2}{\rho_2} e_2(t) - \frac{1}{\rho_3} e_3(t) - \frac{1}{\rho_1} e_1(t) \\ &\vdots \\ \bar{e}_n(t) &= \frac{2}{\rho_n} e_n(t) - \frac{1}{\rho_1} e_1(t) - \frac{1}{\rho_{n-1}} e_{n-1}(t) \end{aligned} \quad (6.15)$$

Rewrite the above synchronization errors in a compact form as follows

$$\bar{\epsilon}(t) = \mathbf{S} \cdot \mathbf{e}(t) \quad (6.16)$$

where vector $\bar{\epsilon}(t) = [\bar{e}_1(t) \ \bar{e}_2(t) \ \dots \ \bar{e}_n(t)]^T \in \mathfrak{R}^{n \times 1}$ is the defined synchronization error,

and $\mathbf{S} \in \mathfrak{R}^{n \times n}$ is a constant gain matrix, expressed by

$$\mathbf{S} = \begin{bmatrix} 2s_1 & -s_2 & 0 & \dots & -s_n \\ -s_1 & 2s_2 & -s_3 & \dots & 0 \\ \vdots & & \ddots & & \vdots \\ 0 & \dots & -s_{n-2} & 2s_{n-1} & -s_n \\ -s_1 & 0 & \dots & -s_{n-1} & 2s_n \end{bmatrix} \quad (6.17)$$

Note that the matrix \mathbf{S} is of full rank because $s_i = \frac{1}{\rho_i}$, $i = 1, 2, \dots, n$, are not zero, and

this synchronization error is model-free. Now the control objective is to design the active joint inputs to cause $\mathbf{e}(t) \rightarrow \mathbf{0}$, $\bar{\epsilon}(t) \rightarrow \mathbf{0}$ as $t \rightarrow \infty$.

Through combining the synchronization error $\bar{\epsilon}(t)$ and the position error $\mathbf{e}(t)$, a coupling error $\bar{\mathbf{e}}^*(t)$ is defined by

$$\bar{\mathbf{e}}^*(t) = \mathbf{e}(t) + \sigma \mathbf{S} \bar{\mathbf{e}}(t) \quad (6.18)$$

where σ is a constant gain matrix that is diagonal and positive definite.

Substitute (6.16) into (6.18) yields

$$\bar{\mathbf{e}}^*(t) = (\mathbf{I}_n + \sigma \mathbf{S}) \cdot \mathbf{e}(t) \quad (6.19)$$

where $\mathbf{I}_n \in \mathfrak{R}^{n \times n}$ is an identity matrix. Studying the expression of the coupling error $\bar{\mathbf{e}}^*(t)$, we find that σ is related to the effect of the synchronization. The higher the gain σ , the more enhanced the synchronization control. However, each term in σ has a maximum value, which should be less than 1, typically. Obviously, from (6.18), the coupling error $\bar{\mathbf{e}}^*(t)$ is linear with respect to both the synchronization error $\bar{\mathbf{e}}(t)$ and the position errors $\mathbf{e}(t)$ of the active joints. In addition, since $\bar{\mathbf{e}}(t)$ is also linear with respect to $\mathbf{e}(t)$ from (6.16), convergence to zero of the coupling error leads to convergence to zero both of the position error and the synchronization error. Therefore, we may use the coupling error as the feedback signal for each sample controller during controller design.

6.2.3 C-S Control

Consider the dynamics of a n DOF parallel robotic manipulator

$$\mathbf{H}(\mathbf{q})\ddot{\mathbf{q}} + \mathbf{C}(\mathbf{q}, \dot{\mathbf{q}})\dot{\mathbf{q}} + \mathbf{G}(\mathbf{q}) = \boldsymbol{\tau}_a \quad (6.20)$$

where: $\mathbf{H}(\mathbf{q}) \in \mathfrak{R}^{n \times n}$ is the symmetric, positive-definite inertia matrix; $\mathbf{C}(\mathbf{q}, \dot{\mathbf{q}}) \in \mathfrak{R}^{n \times n}$ is the coefficient matrix of Coriolis and centrifugal forces; $\mathbf{G}(\mathbf{q}) \in \mathfrak{R}^{n \times 1}$ is the gravity force vector; $\boldsymbol{\tau}_a \in \mathfrak{R}^{n \times 1}$ is the actuating force exerted on the active joints. For details refer to Chapter 2.

In order to employ the convex combination method, this dynamic model is simplified through application of feedback linearization technique (Spong, M.W., *et al.*, 1989 [70]), by assuming that perfect linearization is obtained⁶,

$$\tau_a = \mathbf{H}(\mathbf{q})(\ddot{\mathbf{q}}^d + \mathbf{v}) + \mathbf{C}(\mathbf{q}, \dot{\mathbf{q}})\dot{\mathbf{q}} + \mathbf{G}(\mathbf{q}) \quad (6.21)$$

where $\ddot{\mathbf{q}}^d$ is the vector of desired accelerations or angular accelerations; \mathbf{v} denotes the outputs of a linear controller to be designed. The complex highly coupled nonlinear dynamics of the parallel robotic manipulator is now replaced by a simple set of second-order linear differential equations:

$$\ddot{\mathbf{q}}(t) = \ddot{\mathbf{q}}^d(t) + \mathbf{v}(t) \quad (6.22)$$

Therefore, it is highly advantageous from a control viewpoint to consider the linearized system and to quantify the performance. Figure 6.2 shows the block diagram of the linearized robotic system through feedback linearization.

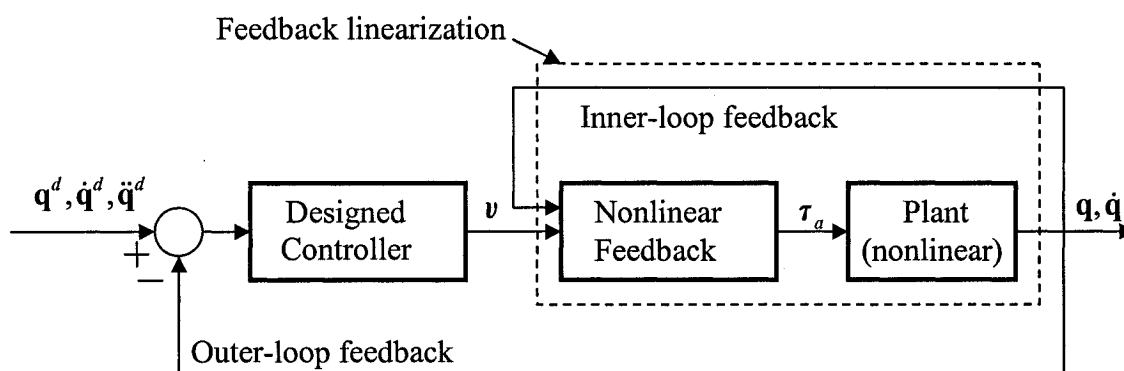


Figure 6.2: Feedback linearization of the nonlinear robotic system

⁶ As a matter of fact, perfect linearization is hard to achieve. There always exist system uncertainties. To validate the proposed linear method, robustness is an important issue. We will address it in section 6.3.

Let $\mathbf{p}(t) = [\mathbf{q}(t) \quad \dot{\mathbf{q}}(t)]^T$, $\mathbf{r}(t) = \ddot{\mathbf{q}}^d(t)$, $\mathbf{g}(t) = [\mathbf{q}^d(t) \quad \dot{\mathbf{q}}^d(t)]^T$. Then the linearized system can be described by the state space equation

$$\dot{\mathbf{p}}(t) = \mathbf{A}\mathbf{p}(t) + \mathbf{B}\mathbf{r}(t) + \mathbf{B}\mathbf{v}(t) \quad (6.23)$$

$$\dot{\mathbf{g}}(t) = \mathbf{A}\mathbf{g}(t) + \mathbf{B}\mathbf{r}(t) \quad (6.24)$$

where

$$\mathbf{A} = \begin{bmatrix} \mathbf{0}_n & \mathbf{I}_n \\ \mathbf{0}_n & \mathbf{0}_n \end{bmatrix} \quad \mathbf{B} = \begin{bmatrix} \mathbf{0}_n \\ \mathbf{I}_n \end{bmatrix} \quad (6.25)$$

where $\mathbf{0}_n \in \mathfrak{R}^{n \times n}$ is a zero matrix⁷.

Describe this linear system in the frequency domain, we have:

$$\mathbf{p}(s) = \mathbf{N}(s)\mathbf{r}(s) + \mathbf{N}(s)\mathbf{v}(s) \quad (6.26)$$

$$\mathbf{g}(s) = \mathbf{N}(s)\mathbf{r}(s) \quad (6.27)$$

where

$$\mathbf{N}(s) = (s\mathbf{I}_n - \mathbf{A})^{-1} \mathbf{B} = \begin{bmatrix} \frac{1}{s^2} \mathbf{I}_n \\ \frac{1}{s} \mathbf{I}_n \end{bmatrix} \quad (6.28)$$

When the linear control law utilizes linear feedback of the coupling error, which consists of the synchronization error and the position error, it has the following form:

$$\mathbf{v}(s) = \mathbf{L}(s) \cdot \bar{\mathbf{e}}^*(s) \quad (6.29)$$

where $\mathbf{L}(s) \in \mathfrak{R}^{n \times n}$ is the transfer matrix of the controller. For simplicity, here we select a

PD type controller, thus $\mathbf{L}(s)$ has the following form:

⁷ In the rest of this thesis, unless otherwise specified, $\mathbf{0}_n$ represents a $n \times n$ zero matrix.

$$\mathbf{L}(s) = \mathbf{K}_p + \mathbf{K}_d s \quad (6.30)$$

where $\mathbf{K}_p \in \mathfrak{R}^{n \times n}$ is the proportional control gain; $\mathbf{K}_d \in \mathfrak{R}^{n \times n}$ is the derivative control gain. \mathbf{K}_p and \mathbf{K}_d are both positive definite diagonal.

From (6.19), we have

$$\begin{bmatrix} \bar{\mathbf{e}}^*(s) \\ s\bar{\mathbf{e}}^*(s) \end{bmatrix} = \begin{bmatrix} (\mathbf{I}_n + \sigma\mathbf{S})\mathbf{e}(s) \\ s(\mathbf{I}_n + \sigma\mathbf{S})\mathbf{e}(s) \end{bmatrix} = \begin{bmatrix} (\mathbf{I}_n + \sigma\mathbf{S}) & \mathbf{0}_n \\ \mathbf{0}_n & (\mathbf{I}_n + \sigma\mathbf{S}) \end{bmatrix} \cdot (\mathbf{p}(s) - \mathbf{g}(s)) \quad (6.31)$$

Substitute (6.31) into (6.29), then $\mathbf{v}(s)$ has the following form,

$$\mathbf{v}(s) = \begin{bmatrix} \mathbf{K}_p & \mathbf{K}_d \end{bmatrix} \cdot \begin{bmatrix} (\mathbf{I}_n + \sigma\mathbf{S}) & \mathbf{0}_n \\ \mathbf{0}_n & (\mathbf{I}_n + \sigma\mathbf{S}) \end{bmatrix} \cdot (\mathbf{p}(s) - \mathbf{g}(s)) \quad (6.32)$$

Define

$$\hat{\mathbf{K}}(s) = \begin{bmatrix} \mathbf{K}_p & \mathbf{K}_d \end{bmatrix} \cdot \begin{bmatrix} (\mathbf{I}_n + \sigma\mathbf{S}) & \mathbf{0}_n \\ \mathbf{0}_n & (\mathbf{I}_n + \sigma\mathbf{S}) \end{bmatrix} \quad (6.33)$$

Then we have:

$$\mathbf{v}(s) = \hat{\mathbf{K}}(s) \cdot (\mathbf{p}(s) - \mathbf{g}(s)) \quad (6.34)$$

Describing this linearized control system in the uniform framework (6.2) through the definition of

$$\mathbf{z}(s) = \mathbf{p}(s), \mathbf{y}(s) = \mathbf{p}(s) - \mathbf{g}(s), \mathbf{u}(s) = \mathbf{v}(s), \mathbf{w}(s) = \begin{bmatrix} \mathbf{g}(s) & \mathbf{r}(s) \end{bmatrix}^T \quad (6.35)$$

we have

$$\begin{bmatrix} \mathbf{p}(s) \\ \dots \\ \mathbf{p}(s) - \mathbf{g}(s) \end{bmatrix} = \begin{bmatrix} \mathbf{0}_{2n \times 2n} & \mathbf{N}(s) & \vdots & \mathbf{N}(s) \\ \dots & \dots & \vdots & \dots \\ -\mathbf{I}_{2n \times 2n} & \mathbf{N}(s) & \vdots & \mathbf{N}(s) \end{bmatrix} \begin{bmatrix} \mathbf{g}(s) \\ \mathbf{r}(s) \\ \dots \\ \mathbf{v}(s) \end{bmatrix} \quad (6.36)$$

Therefore

$$\mathbf{P}_{zw}(s) = \begin{bmatrix} \mathbf{0}_{2n \times 2n} & \mathbf{N}(s) \end{bmatrix} \quad (6.37)$$

$$\mathbf{P}_{zu}(s) = \mathbf{N}(s) \quad (6.38)$$

$$\mathbf{P}_{yw}(s) = \begin{bmatrix} -\mathbf{I}_{2n \times 2n} & \mathbf{N}(s) \end{bmatrix} \quad (6.39)$$

$$\mathbf{P}_{yu}(s) = \mathbf{N}(s) \quad (6.40)$$

In terms of (6.36) and (6.3), we derive the transfer matrix of the C-S controller:

$$\bar{\mathbf{K}}(s) = \hat{\mathbf{K}}(s) \quad (6.41)$$

In addition, from section 6.2.1, we also have to derive the closed-loop transfer matrix, $\bar{\mathbf{H}}(s)$. In terms of (6.2) ~ (6.4), we derive:

$$\bar{\mathbf{H}}(s) = \mathbf{P}_{zw}(s) + \mathbf{P}_{zu}(s) \mathbf{K}(s) (\mathbf{I} - \mathbf{P}_{yu}(s) \mathbf{K}(s))^{-1} \mathbf{P}_{yw}(s) \quad (6.42)$$

Substitute (6.37) ~ (6.40) into (6.42), we have the closed-loop transfer matrix of the manipulator system using the C-S control:

$$\bar{\mathbf{H}}(s) = \begin{bmatrix} -\mathbf{N}(s) \cdot \bar{\mathbf{K}}(s) \cdot (\mathbf{I}_{2n \times 2n} - \mathbf{N}(s) \cdot \bar{\mathbf{K}}(s))^{-1} & (\mathbf{I}_{2n \times 2n} - \mathbf{N}(s) \cdot \bar{\mathbf{K}}(s))^{-1} \cdot \mathbf{N}(s) \end{bmatrix} \quad (6.43)$$

Note the scale of each matrix in the above derivations: $\mathbf{p}(s) \in \mathcal{R}^{2n \times 1}$, $\mathbf{g}(s) \in \mathcal{R}^{2n \times 1}$, $\mathbf{v}(s) \in \mathcal{R}^{n \times 1}$, $\mathbf{r}(s) \in \mathcal{R}^{n \times 1}$, $\hat{\mathbf{K}}(s) \in \mathcal{R}^{n \times 2n}$, $\bar{\mathbf{K}}(s) \in \mathcal{R}^{n \times 2n}$ and $\bar{\mathbf{H}}(s) \in \mathcal{R}^{2n \times 3n}$.

In this section, we propose the C-S control law under the assumption that perfect linearization of the dynamic model of parallel robotic manipulators can be achieved. However, in practice, such an assumption is hard to satisfy because the dynamic model and dynamic parameters of the robotic system may not be known exactly. In order to guarantee control performance of the C-S controller under the influence of unknown dynamic parameters and unmodeled dynamics, we need to find a way to improve the robustness of the C-S control to those uncertainties.

6.3 Robustness Specification of C-S Control

In section 6.2, we discussed how to use the proposed C-S control to satisfy multiple simultaneous specifications during trajectory tracking of a parallel robotic manipulator. This control method requires that the nonlinear system be linearized, through a feedback linearization technique. This linearization depends on knowledge of the robotic manipulator dynamics. Unfortunately, there are always uncertainties, e.g., unknown payload, friction, unmodeled dynamics, etc., in manipulator dynamics. In order to guarantee control performance of the manipulator using the C-S control, in other words, to improve the robustness of the C-S control to uncertainties in the dynamic model, we investigate how to define a convex robustness specification. Through employing this robustness specification as one of the multiple closed-loop performance specifications to be satisfied, the derived C-S controller has strong robustness to uncertainties while satisfying multiple performance specifications simultaneously; and therefore the proposed C-S control has practical application value.

6.3.1 Robustness Specification

For the dynamic model of a parallel robotic manipulator with n DOF, (6.20), we assumed that perfect linearization can be achieved through (6.21) in the previous section. However, due to uncertainties in the dynamic model, it is hard to obtain the exact values of $\mathbf{H}(\mathbf{q})$, $\mathbf{C}(\mathbf{q}, \dot{\mathbf{q}})$, $\mathbf{G}(\mathbf{q})$ at each sampling time. Therefore, in practice, (6.21) should be written as:

$$\tau_a = \hat{\mathbf{H}}(\mathbf{q})(\ddot{\mathbf{q}}^d + \mathbf{v}) + \hat{\mathbf{C}}(\mathbf{q}, \dot{\mathbf{q}})\dot{\mathbf{q}} + \hat{\mathbf{G}}(\mathbf{q}) \quad (6.44)$$

where $\hat{\mathbf{H}}(\mathbf{q})$, $\hat{\mathbf{C}}(\mathbf{q}, \dot{\mathbf{q}})$, $\hat{\mathbf{G}}(\mathbf{q})$ are the estimates of $\mathbf{H}(\mathbf{q})$, $\mathbf{C}(\mathbf{q}, \dot{\mathbf{q}})$ and $\mathbf{G}(\mathbf{q})$, respectively.

Substitute (6.41) into (6.17), the closed-loop dynamic model of the parallel robotic manipulator is derived

$$\mathbf{H}(\mathbf{q})\ddot{\mathbf{q}} + \boldsymbol{\eta} = \hat{\mathbf{H}}(\mathbf{q})(\ddot{\mathbf{q}}^d + \mathbf{v}) \quad (6.45)$$

where

$$\boldsymbol{\eta} = \mathbf{C}(\mathbf{q}, \dot{\mathbf{q}})\dot{\mathbf{q}} + \mathbf{G}(\mathbf{q}) - \hat{\mathbf{C}}(\mathbf{q}, \dot{\mathbf{q}})\dot{\mathbf{q}} - \hat{\mathbf{G}}(\mathbf{q}) \quad (6.46)$$

Rearrange terms in (6.46), we have

$$\ddot{\mathbf{q}}(t) - \ddot{\mathbf{q}}^d(t) = \mathbf{v}(t) - \hat{\mathbf{H}}^{-1}(\mathbf{q}(t))\boldsymbol{\eta}(t) + (\mathbf{I}_n - \mathbf{H}(\mathbf{q}(t))\hat{\mathbf{H}}^{-1}(\mathbf{q}(t)))\ddot{\mathbf{q}}(t) \quad (6.47)$$

Define

$$\boldsymbol{\varsigma}(t) = (\mathbf{I}_n - \mathbf{H}(\mathbf{q}(t))\hat{\mathbf{H}}^{-1}(\mathbf{q}(t)))\ddot{\mathbf{q}}(t) - \hat{\mathbf{H}}^{-1}(\mathbf{q}(t))\boldsymbol{\eta}(t) \quad (6.48)$$

Then (6.47) can be rewritten as

$$\ddot{\mathbf{q}}(t) = \ddot{\mathbf{q}}^d(t) + \mathbf{v}(t) + \boldsymbol{\varsigma}(t) \quad (6.49)$$

Compared with (6.22), (6.49) has an additional term $\boldsymbol{\varsigma}(t) \in \mathcal{R}^{n \times 1}$, which may be treated as a feedback perturbation in the robotic system. Because of the existence of this perturbation, it is necessary for us to develop a convex robustness specification for the convex synchronized controller so that the bounds on the performance deterioration can be guaranteed.

Based on (Boyd, S.P., *et al.*, 1991 [8]), the closed-loop transfer matrix of a parallel robotic manipulator with perturbation can be derived from the following analysis. Let $\mathbf{P}(t)$ denote the nominal plant, which represents the true dynamic model of the robotic system and let $\mathbf{P}^{pert}(t)$ denote the real plant with unknown parameters. Define $\boldsymbol{\Delta} \in \Delta$ as the transfer matrix of the feedback perturbation, where Δ is a set of transfer matrices of

the appropriate size; define $\delta(t)$ as the input signal to the perturbation feedback, which can be considered an output signal of the plant $P(t)$; define $\varsigma(t)$ as the output signal of the perturbation feedback, which can be considered an input signal to the plant $P(t)$. Then the exogenous input signal w and the regulated output signal z are assumed to be augmented to contain ς and δ , respectively :

$$w = \begin{bmatrix} \tilde{w} \\ \varsigma \end{bmatrix}, \quad z = \begin{bmatrix} \tilde{z} \\ \delta \end{bmatrix} \quad (6.50)$$

where \tilde{w} and \tilde{z} denote the original signals from Figure 6.1. This is shown in Figure 6.3.

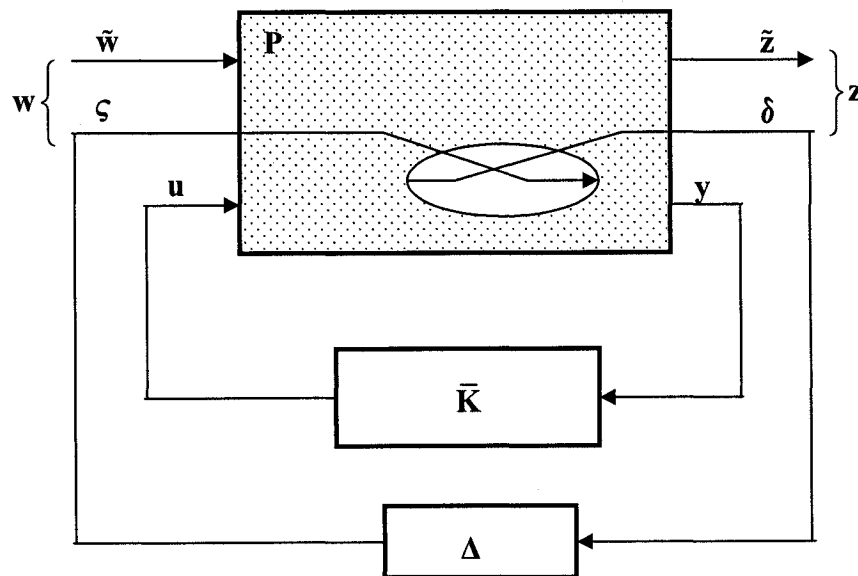


Figure 6.3: Closed-loop perturbation feedback form (Boyd, S.P., *et al.*, 1991 [8])

Similar to (6.2), the augmented plant open-loop transfer matrix can be expressed as

$$\mathbf{P}(s) = \begin{bmatrix} \mathbf{P}_{\bar{z}\bar{w}}(s) & \mathbf{P}_{\bar{z}\zeta}(s) & \mathbf{P}_{\bar{z}u}(s) \\ \mathbf{P}_{\delta\bar{w}}(s) & \mathbf{P}_{\delta\zeta}(s) & \mathbf{P}_{\delta u}(s) \\ \mathbf{P}_{y\bar{w}}(s) & \mathbf{P}_{y\zeta}(s) & \mathbf{P}_{yu}(s) \end{bmatrix} \quad (6.51)$$

Then the perturbed plant can be expressed as

$$\mathbf{P}^{pert}(\Delta) = \begin{bmatrix} \mathbf{P}_{\bar{z}\bar{w}}(s) & \mathbf{P}_{\bar{z}u}(s) \\ \mathbf{P}_{y\bar{w}}(s) & \mathbf{P}_{yu}(s) \end{bmatrix} + \begin{bmatrix} \mathbf{P}_{\bar{z}\zeta}(s) \\ \mathbf{P}_{y\zeta}(s) \end{bmatrix} \cdot \Delta(s) \cdot (\mathbf{I}_n - \mathbf{P}_{\delta\zeta}(s) \cdot \Delta(s))^{-1} \cdot \begin{bmatrix} \mathbf{P}_{\delta\bar{w}}(s) & \mathbf{P}_{\delta u}(s) \end{bmatrix} \quad (6.52)$$

By substituting (6.52) into (6.4), we find that the transfer matrix of the perturbed closed-loop system is

$$\bar{\mathbf{H}}^{pert}(\Delta) = \bar{\mathbf{H}}_{\bar{z}\bar{w}} + \bar{\mathbf{H}}_{\bar{z}\zeta} \Delta (\mathbf{I}_n - \bar{\mathbf{H}}_{\delta\zeta} \Delta)^{-1} \bar{\mathbf{H}}_{\delta\bar{w}} \quad (6.53)$$

where

$$\bar{\mathbf{H}}_{\bar{z}\bar{w}} = \mathbf{P}_{\bar{z}\bar{w}} + \mathbf{P}_{\bar{z}u} \bar{\mathbf{K}} (\mathbf{I}_n - \mathbf{P}_{yu} \bar{\mathbf{K}})^{-1} \mathbf{P}_{y\bar{w}} \quad (6.54)$$

$$\bar{\mathbf{H}}_{\bar{z}\zeta} = \mathbf{P}_{\bar{z}\zeta} + \mathbf{P}_{\bar{z}u} \bar{\mathbf{K}} (\mathbf{I}_n - \mathbf{P}_{yu} \bar{\mathbf{K}})^{-1} \mathbf{P}_{y\zeta} \quad (6.55)$$

$$\bar{\mathbf{H}}_{\delta\bar{w}} = \mathbf{P}_{\delta\bar{w}} + \mathbf{P}_{\delta u} \bar{\mathbf{K}} (\mathbf{I}_n - \mathbf{P}_{yu} \bar{\mathbf{K}})^{-1} \mathbf{P}_{y\bar{w}} \quad (6.56)$$

$$\bar{\mathbf{H}}_{\delta\zeta} = \mathbf{P}_{\delta\zeta} + \mathbf{P}_{\delta u} \bar{\mathbf{K}} (\mathbf{I}_n - \mathbf{P}_{yu} \bar{\mathbf{K}})^{-1} \mathbf{P}_{y\zeta} \quad (6.57)$$

From (6.53), we may interpret

$$\bar{\mathbf{H}}^{pert}(\Delta) - \bar{\mathbf{H}}_{\bar{z}\bar{w}} = \bar{\mathbf{H}}_{\bar{z}\zeta} \Delta (\mathbf{I}_n - \bar{\mathbf{H}}_{\delta\zeta} \Delta)^{-1} \bar{\mathbf{H}}_{\delta\bar{w}} \quad (6.58)$$

as the change of the closed-loop transfer matrix that is caused by the feedback perturbation Δ . We have the following interpretations: Since $\bar{\mathbf{H}}_{\bar{z}\bar{w}}$ is the closed-loop transfer matrix of the nominal system, before its exogenous input and regulated output

were augmented with the signals ζ and δ , then if the three closed-loop transfer matrices $\bar{\mathbf{H}}_{z\zeta}$, $\bar{\mathbf{H}}_{\delta\tilde{w}}$, and $\bar{\mathbf{H}}_{\delta\zeta}$ are all small, our design will be robust to the perturbations, i.e., the change in the closed-loop transfer matrix, given in (6.58), will also be small (Boyd, S.P., *et al.*, 1991 [8]).

In our case, in terms of (6.49), the perturbation feedback form of the closed-loop system can be represented in the Figure 6.

From Figure 6.3, the real input signal

$$\mathbf{u}^* = \mathbf{u} + \zeta \quad (6.59)$$

where

$$\zeta = \Delta\delta = \Delta\mathbf{u} \quad (6.60)$$

Here, for simplicity, Δ can be assumed as a constant gain. Then consider ζ and δ , in terms of (6.49), (6.23) is changed to be

$$\dot{\mathbf{p}}(t) = \mathbf{A}\mathbf{p}(t) + \mathbf{B}\mathbf{r}(t) + \mathbf{B}\mathbf{v}(t) + \mathbf{B}\zeta(t) \quad (6.61)$$

Correspondingly, (6.36) changed to be

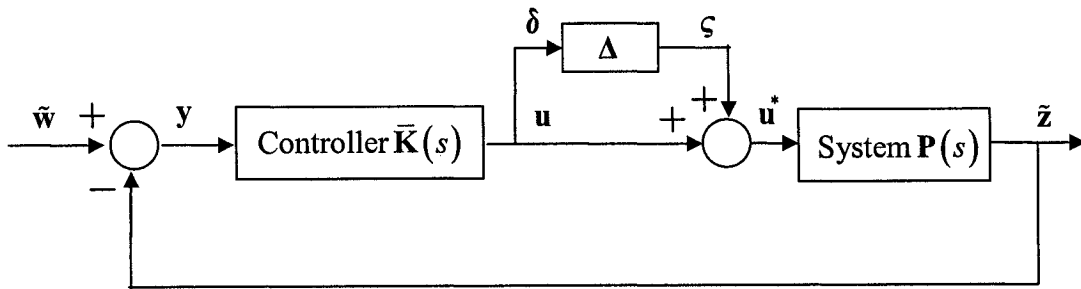


Figure 6.4: Closed-loop system block diagram with perturbation feedback

$$\begin{bmatrix} \mathbf{p}(s) \\ \dots \\ \delta(s) \\ \dots \\ \mathbf{p}(s) - \mathbf{g}(s) \end{bmatrix} = \begin{bmatrix} \mathbf{0}_{2n \times 2n} & \mathbf{N}(s) & \vdots & \mathbf{N}(s) & \vdots & \mathbf{N}(s) \\ \dots & \dots & \vdots & \dots & \vdots & \dots \\ \mathbf{0}_{n \times 2n} & \mathbf{0}_{n \times n} & \vdots & \mathbf{0}_{n \times n} & \vdots & \mathbf{I}_n \\ \dots & \dots & \vdots & \dots & \vdots & \dots \\ -\mathbf{I}_{2n \times 2n} & \mathbf{N}(s) & \vdots & \mathbf{N}(s) & \vdots & \mathbf{N}(s) \end{bmatrix} \begin{bmatrix} \mathbf{g}(s) \\ \mathbf{r}(s) \\ \dots \\ \boldsymbol{\zeta}(s) \\ \dots \\ \mathbf{v}(s) \end{bmatrix} \quad (6.62)$$

Then in terms of (6.54) ~ (6.57), we can derive

$$\bar{\mathbf{H}}_{\bar{\mathbf{z}}\bar{\mathbf{w}}}(s) = \begin{bmatrix} -\mathbf{N}(s) \cdot \bar{\mathbf{K}}(s) \cdot (\mathbf{I}_{2n \times 2n} - \mathbf{N}(s) \cdot \bar{\mathbf{K}}(s))^{-1} & (\mathbf{I}_{2n \times 2n} - \mathbf{N}(s) \cdot \bar{\mathbf{K}}(s))^{-1} \cdot \mathbf{N}(s) \end{bmatrix} \quad (6.63)$$

$$\bar{\mathbf{H}}_{\bar{\mathbf{z}}\boldsymbol{\zeta}} = (\mathbf{I}_{2n \times 2n} - \mathbf{N}(s) \cdot \bar{\mathbf{K}}(s))^{-1} \cdot \mathbf{N}(s) \quad (6.64)$$

$$\bar{\mathbf{H}}_{\delta\bar{\mathbf{w}}} = \begin{bmatrix} -\bar{\mathbf{K}}(s) \cdot (\mathbf{I}_{2n \times 2n} - \mathbf{N}(s) \cdot \bar{\mathbf{K}}(s))^{-1} & \bar{\mathbf{K}}(s) \cdot (\mathbf{I}_{2n \times 2n} - \mathbf{N}(s) \cdot \bar{\mathbf{K}}(s))^{-1} \cdot \mathbf{N}(s) \end{bmatrix} \quad (6.65)$$

$$\bar{\mathbf{H}}_{\delta\boldsymbol{\zeta}} = \bar{\mathbf{K}}(s) \cdot (\mathbf{I}_{2n \times 2n} - \mathbf{N}(s) \cdot \bar{\mathbf{K}}(s))^{-1} \cdot \mathbf{N}(s) \quad (6.66)$$

Let

$$\mathbf{T}^*(s) = \bar{\mathbf{K}}(s) \cdot (\mathbf{I}_{2n \times 2n} - \mathbf{N}(s) \cdot \bar{\mathbf{K}}(s))^{-1} \cdot \mathbf{N}(s) \quad (6.67)$$

$$\mathbf{S}^*(s) = (\mathbf{I}_{2n \times 2n} - \mathbf{N}(s) \cdot \bar{\mathbf{K}}(s))^{-1} \quad (6.68)$$

where $\mathbf{T}^*(s) \in \mathfrak{R}^{n \times n}$ is the complementary sensitivity function of the closed-loop system and $\mathbf{S}^*(s) \in \mathfrak{R}^{2n \times 2n}$ is the sensitivity transfer function (Sanchez-Pena, R.S, *et al.*, 1998 [65]). Then

$$\bar{\mathbf{H}}_{\bar{\mathbf{z}}\bar{\mathbf{w}}}(s) = \begin{bmatrix} -\mathbf{N}(s) \cdot \bar{\mathbf{K}}(s) \cdot \mathbf{S}^*(s) & \bar{\mathbf{K}}(s) \cdot \mathbf{S}^*(s) \end{bmatrix} \quad (6.69)$$

$$\bar{\mathbf{H}}_{\bar{\mathbf{z}}\boldsymbol{\zeta}} = \mathbf{S}^*(s) \cdot \mathbf{N}(s) \quad (6.70)$$

$$\bar{\mathbf{H}}_{\delta\bar{\mathbf{w}}} = \begin{bmatrix} -\bar{\mathbf{K}}(s) \cdot \mathbf{S}^*(s) & \mathbf{T}^*(s) \end{bmatrix} \quad (6.71)$$

$$\bar{\mathbf{H}}_{\delta\boldsymbol{\zeta}} = \mathbf{T}^*(s) \quad (6.72)$$

6.3.2 Closed-loop Convex Robustness Specifications

In order to design a convex robustness specification, we use the small gain theorem (Boyd, S.P., *et al.*, 1991 [8]).

Small Gain Theorem: Consider the feedback connection shown in Figure 6.5.

Assuming that this feedback connection is well-posed, meaning that $\det(\mathbf{I} - \mathbf{H}_1\mathbf{H}_2) \neq 0$,

the transfer matrix from \mathbf{w} to \mathbf{z} is $\mathbf{G} = \mathbf{H}_1(\mathbf{I} - \mathbf{H}_2\mathbf{H}_1)^{-1}$.

If $\|\mathbf{H}_1\|_{gn} \cdot \|\mathbf{H}_2\|_{gn} < 1$ holds⁸, then the feedback connection is well-posed and we have

$$\|\mathbf{G}\|_{gn} \leq \frac{\|\mathbf{H}_1\|_{gn}}{1 - \|\mathbf{H}_1\|_{gn} \cdot \|\mathbf{H}_2\|_{gn}} \quad (6.73)$$

□

Following the similar way presented in (Boyd, S.P., *et al.*, 1991 [8]), a convex robustness specification is defined as follows.

For the parallel robotic system with a perturbation feedback, let M^* denote the maximum gain of the possible feedback perturbations, i.e.,

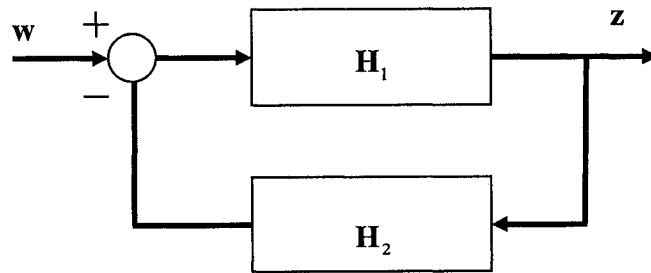


Figure 6.5: Two systems connected in feedback loop

⁸ $\|H\|_{gn} \stackrel{\Delta}{=} \sup_{\omega} \|H(j\omega)\|_{\infty}$, where $\|\cdot\|$ is used to measure the size of both input and output signals

$$M^* = \sup_{\Delta \in \Delta} \|\Delta\|_{gn} \quad (6.74)$$

Then apply the small gain theorem to the right side of the transfer matrix of the perturbed system (6.58), we know that if

$$\|\bar{\mathbf{H}}_{\delta\zeta}\|_{gn} M^* < 1 \quad (6.75)$$

Then we have for all $\Delta \in \Delta$,

$$\left\| \Delta (\mathbf{I}_n - \bar{\mathbf{H}}_{\delta\zeta} \Delta)^{-1} \right\|_{gn} \leq \frac{M^*}{1 - M^* \|\bar{\mathbf{H}}_{\delta\zeta}\|_{gn}} \quad (6.76)$$

From (6.58), we therefore have

$$\|\bar{\mathbf{H}}^{pert}(\Delta) - \bar{\mathbf{H}}_{z\bar{w}}\|_{gn} \leq \frac{M^* \|\bar{\mathbf{H}}_{z\zeta}\|_{gn} \|\bar{\mathbf{H}}_{\delta\bar{w}}\|_{gn}}{1 - M^* \|\bar{\mathbf{H}}_{\delta\zeta}\|_{gn}} \text{ for all } \Delta \in \Delta, \quad (6.77)$$

From (6.77), it is obvious that the closed-loop system will be robust if the three transfer matrices, $\bar{\mathbf{H}}_{z\zeta}$, $\bar{\mathbf{H}}_{\delta\bar{w}}$, and $\bar{\mathbf{H}}_{\delta\zeta}$ are all small enough. Therefore, the closed-loop convex specifications on $\bar{\mathbf{H}}(s)$ given by

$$\|\bar{\mathbf{H}}_{\delta\zeta}\|_{gn} < 1/M^* \quad (6.78)$$

$$\|\bar{\mathbf{H}}_{z\zeta}\|_{gn} < \infty \quad (6.79)$$

$$\|\bar{\mathbf{H}}_{\delta\bar{w}}\|_{gn} < \infty \quad (6.80)$$

$$\|\bar{\mathbf{H}}_{z\bar{w}}\|_{gn} < \infty \quad (6.81)$$

implies that

$$\|\bar{\mathbf{H}}^{pert}(\Delta)\|_{gn} \leq \infty \text{ for all } \Delta \in \Delta, \quad (6.82)$$

If inequalities (6.78) ~ (6.81) are true, which means $\bar{\mathbf{H}}_{z_c}$, $\bar{\mathbf{H}}_{\delta\bar{w}}$, $\bar{\mathbf{H}}_{\delta c}$, and $\bar{\mathbf{H}}_{z\bar{w}}$ are stable, then the $\bar{\mathbf{H}}^{pert}$ is stable. In this case, we may think of the specification (6.78) ~ (6.81) as a closed-loop specification that guarantee robust stability (Boyd, S.P., *et al.*, 1991 [8]). Moreover, since the small gain condition in (6.75) depends only on M^* , the inequality (6.77) holds if and only if

$$\|\Delta\|_{gn} \leq M^* \text{ for all } \Delta \in \Delta, \quad (6.83)$$

Based on the perturbation feedback shown in Figure 6.3, the maximum of gain of the perturbations is

$$M^* = \max \left\{ \|L-1\|_{gn}, \|U-1\|_{gn} \right\} = \max \{1-L, U-1\} \quad (6.84)$$

where L and U are the lower and upper bounds of the system parameters.

Since $\bar{\mathbf{H}}_{\delta c} = \mathbf{T}^*(s)$, then the small gain condition is (Boyd, S.P., *et al.*, 1991):

$$\|\mathbf{T}^*\|_{gn} < \frac{1}{M^*} = \min \left\{ \frac{1}{1-L}, \frac{1}{U-1} \right\} \quad (6.85)$$

The inequality (6.85) is also one of the closed-loop convex robustness specifications. In the following experiments, (6.85) is selected as one of the multiple performance specifications.

6.4 Experiments

In this section, we apply the proposed C-S controller on the P-R-R manipulator experimental system. During experiments, three convex specifications, including the robustness specification, are required to satisfy at the same time during trajectory tracking. Through selecting three PD type synchronized sample controller, each of which

satisfies at least one specification, a C-S controller is obtained. Analyzing experimental results, the designed C-S controller does satisfy the three specifications simultaneously.

Similar to the synchronized control and A-S control introduced in Chapter 3 and 5, respectively, experiments of the C-S control are also conducted on the 3 DOF P-R-R manipulator, which is introduced in Chapter 4 in detail. During experiments, three closed-loop performance specifications, percent of path accuracy (ϕ_{PPA}), settling time (ϕ_{ST}) and robustness (ϕ_R), are required to be satisfied simultaneously. Here ϕ_{PPA} is defined as the ratio of the path accuracy to the desired translation of the platform. Since the convexity of path accuracy and settling time have been proved in (Liu, H., 1998), ϕ_{PPA} is obvious convex, and therefore, all the three specifications are convex. In addition, with respect to the fixed inertial frame as shown in Figure 4.2, the platform of the P-R-R manipulator is expected to move from $(0mm, 0mm, 45deg)$ to $(0mm, 30mm, 45deg)$. The maximum speed and the maximum acceleration are set as $0.16m/s$ and $80m/s^2$, respectively. The desired trajectory of the platform is shown in Figure 6.6.

Now, following the two-stage design strategy introduced in section 6.2, the C-S controller is designed as follows.

I. Sample Controller. Each sample controller is selected to satisfy at least one specification. In experiments, we select the computed torque control employing the synchronization error as the sample controller. The control structure of the synchronized computed torque is

$$\tau_a = \mathbf{H}(\mathbf{q})(\ddot{\mathbf{q}}^d + \mathbf{K}_p \bar{\mathbf{e}}^* + \mathbf{K}_d \dot{\bar{\mathbf{e}}}^*) + \mathbf{C}(\mathbf{q}, \dot{\mathbf{q}})\dot{\mathbf{q}} \quad (6.86)$$

Substitute (6.18) into (6.86), then (6.86) is changed to be

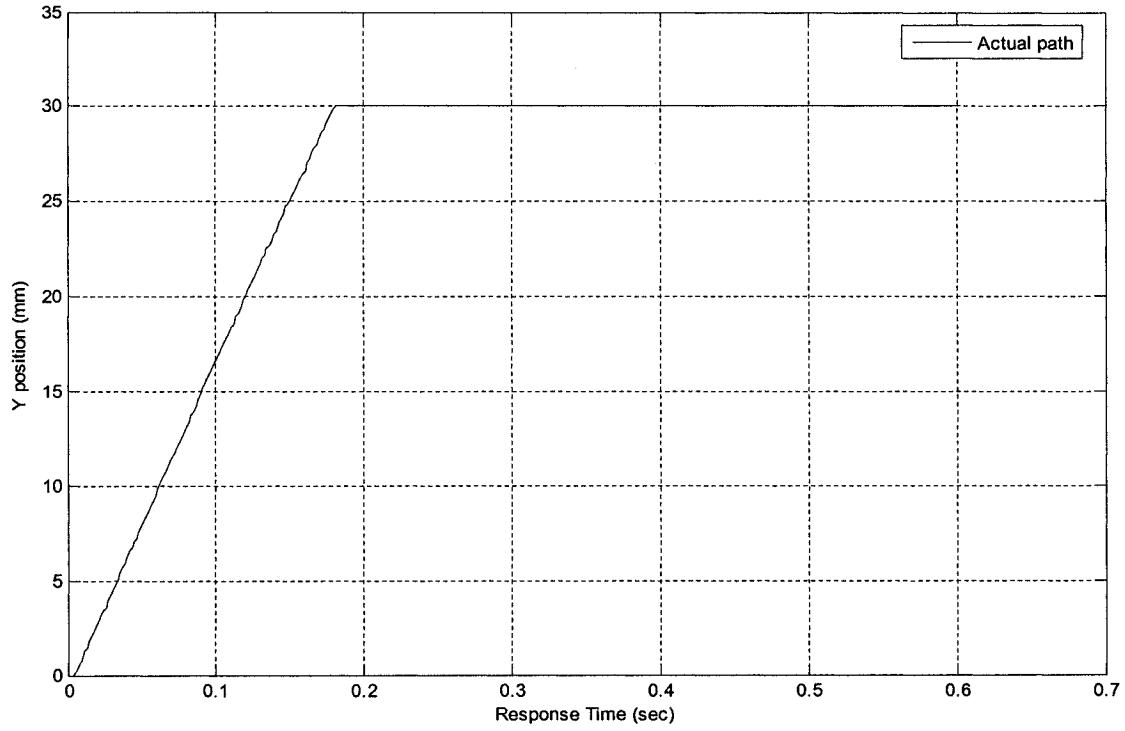


Figure 6.6: Desired path of the platform in Y axis

$$\tau_a = \mathbf{H}(\mathbf{q})(\ddot{\mathbf{q}}^d + \mathbf{K}_p(\mathbf{I}_n + \sigma\mathbf{S})\mathbf{e} + \mathbf{K}_d(\mathbf{I}_n + \sigma\mathbf{S})\dot{\mathbf{e}}) + \mathbf{C}(\mathbf{q}, \dot{\mathbf{q}})\dot{\mathbf{q}} \quad (6.87)$$

where $\mathbf{K}_p = \text{diag}\{K_p\} \in \mathcal{R}^{3 \times 3}$, $\mathbf{K}_d = \text{diag}\{K_d\} \in \mathcal{R}^{3 \times 3}$ are diagonal matrices whose elements are positive constants.

Since the platform of the P-R-R manipulator is required to move from $(0\text{mm}, 0\text{mm}, 45\text{deg})$ to $(0\text{mm}, 30\text{mm}, 45\text{deg})$, using inverse kinematics, the translations of the three prismatic joints (active joints) are calculated: $\rho_1 = 23.025\text{mm}$, $\rho_2 = 9.159\text{mm}$, $\rho_3 = -30.583\text{mm}$. Select $\sigma = \text{diag}\{0.2\}$ and consider the units of e_i and ρ_i , then we have

$$\mathbf{S} = \begin{bmatrix} \frac{2}{\rho_1} & \frac{-1}{\rho_2} & \frac{-1}{\rho_3} \\ \frac{-1}{\rho_1} & \frac{2}{\rho_2} & \frac{-1}{\rho_3} \\ \frac{-1}{\rho_1} & \frac{-1}{\rho_2} & \frac{2}{\rho_3} \end{bmatrix} = \begin{bmatrix} 0.086 & -0.109 & 0.033 \\ -0.043 & 0.218 & 0.033 \\ -0.043 & -0.109 & -0.066 \end{bmatrix} \quad (6.88)$$

$$\mathbf{I} + \sigma \mathbf{S} = \begin{bmatrix} 1.172 & -0.109 & 0.033 \\ -0.043 & 1.436 & 0.033 \\ -0.043 & -0.109 & 0.868 \end{bmatrix} \quad (6.89)$$

Compared with (6.21), the linear sample controller \mathbf{v} is the local PD control. The detailed expression of $\bar{\mathbf{H}}$ is presented in Appendix B. Select three sample controllers, as listed in Table 6.1, each of which satisfies at least one required specification. The actual path of the platform in Y axis, the position error of the platform in Y axis, and the frequency response of the three selected sample controllers are shown in Figure 6.7 ~ Figure 6.9, Figure 6.10 ~ Figure 6.12, Figure 6.13 ~ Figure 6.15, respectively. The three specifications of each sample controller obtained are listed in Table 6.1. Note that the units of the third specification ϕ_R is dB. From Table 6.1, it is obvious that no sample controller can satisfy all the three specifications at the same time. Although it is not hard to adjust the PD gains to satisfy one specification, it is difficult and time-consuming to tune the PD gains to trial and satisfy the simultaneous specifications. Here, we apply the convex combination method to design a C-S controller to satisfy these three specifications simultaneously.

II. Combination. Based on the specification values listed in Table 6.1, the following linear programming problem is formulated:

$$\begin{bmatrix} 1.13 & 1.52 & 3.28 \\ 0.193 & 0.014 & 0.204 \\ 0.604 & 2.01 & 0.424 \end{bmatrix} \begin{bmatrix} \lambda_1 \\ \lambda_2 \\ \lambda_3 \end{bmatrix} \leq \begin{bmatrix} 1.8 \\ 0.14 \\ 1 \end{bmatrix} \quad (6.90)$$

The combination vector is solved as:

$$\bar{\Lambda} = [\lambda_1 \quad \lambda_2 \quad \lambda_3]^T = [0.4597 \quad 0.3102 \quad 0.2300]^T \quad (6.91)$$

Through combining the three closed-loop transfer matrices ($\bar{\mathbf{H}}_i$, $i=1,2,3$) of the sample controllers via the combination vector, the closed-loop transfer matrix of the satisfactory controller is obtained:

$$\bar{\mathbf{H}}^*(s) = \lambda_1 \bar{\mathbf{H}}_1(s) + \lambda_2 \bar{\mathbf{H}}_2(s) + \lambda_3 \bar{\mathbf{H}}_3(s) \quad (6.92)$$

where $\lambda_1, \lambda_2, \lambda_3$ are determined in (6.88). The detailed expression of $\bar{\mathbf{H}}^*(s)$ is given in Appendix B. Based on the closed-loop system $\bar{\mathbf{H}}^*(s)$, from (6.8) ~ (6.10), the closed-loop C-S controller $\bar{\mathbf{K}}^*(s)$ is calculated, also given in Appendix B.

Table 6.1: Control gains and specifications of the three sample controllers

Sample Systems	$\bar{\mathbf{H}}_1$	$\bar{\mathbf{H}}_2$	$\bar{\mathbf{H}}_3$	Required specification values
\mathbf{K}_p	$diag\{2.0\}$	$diag\{1.8\}$	$diag\{3.2\}$	
\mathbf{K}_d	$diag\{0.016\}$	$diag\{0.012\}$	$diag\{0.012\}$	
ϕ_{PPA} ($\times 100\%$)	1.13	1.52	3.28	1.8
ϕ_{ST} (sec)	0.193	0.014	0.204	0.14
ϕ_R (dB)	0.604	2.010	0.424	1

Applying $\bar{\mathbf{K}}^*(s)$ on the experimental system, the path of the platform in Y axis, the position error of the platform in Y axis and the frequency response are obtained, as shown in Figure 6.16, Figure 6.17 and Figure 6.18, respectively. The specification values of the closed-loop system are calculated, as:

$$\begin{cases} \phi_{PPA}(\bar{\mathbf{H}}^*) = 1.08 < 1.8 \\ \phi_{ST}(\bar{\mathbf{H}}^*) = 0.016 < 0.14 \\ \phi_R(\bar{\mathbf{H}}^*) = 0.637 < 1 \end{cases} \quad (6.93)$$

Thus, the final designed C-S controller $\bar{\mathbf{K}}^*(s)$ satisfies all three closed-loop specifications at the same time.

6.5 Summary

In this chapter, with respect to the multiple simultaneous specification problem during trajectory tracking of parallel robotic manipulators, we propose the C-S control. The advantages of the C-S control may be shown in two aspects: (i) using the synchronization error to improve tracking performance for each sample controller, consequently, the control performance of the finally determined controller is improved further; (ii) through using the convex combination method, the time-consuming work of tuning control gains to satisfy all specifications is avoided, which shows great application value in industrial areas. In addition, regarding uncertainties in robotic systems, a convex robustness specification is proposed. With the employment of this specification, the robustness of the C-S controller to uncertainties is improved and tracking performance is guaranteed.

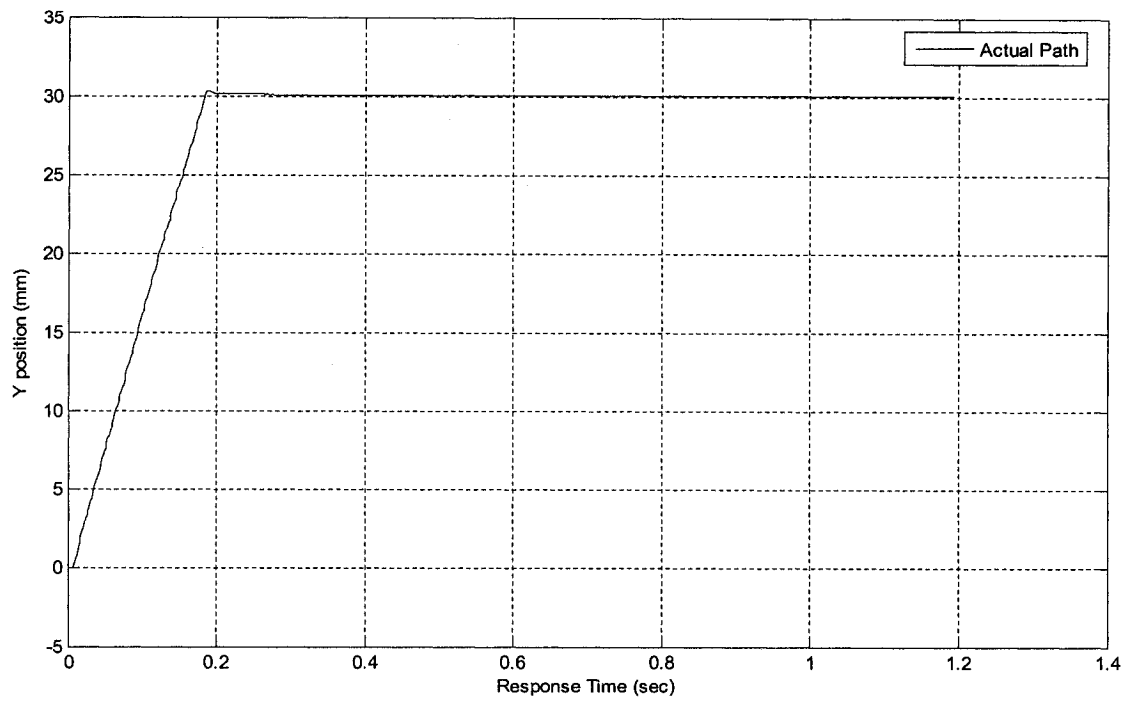


Figure 6.7: Actual path of the platform in Y axis of \bar{H}_1

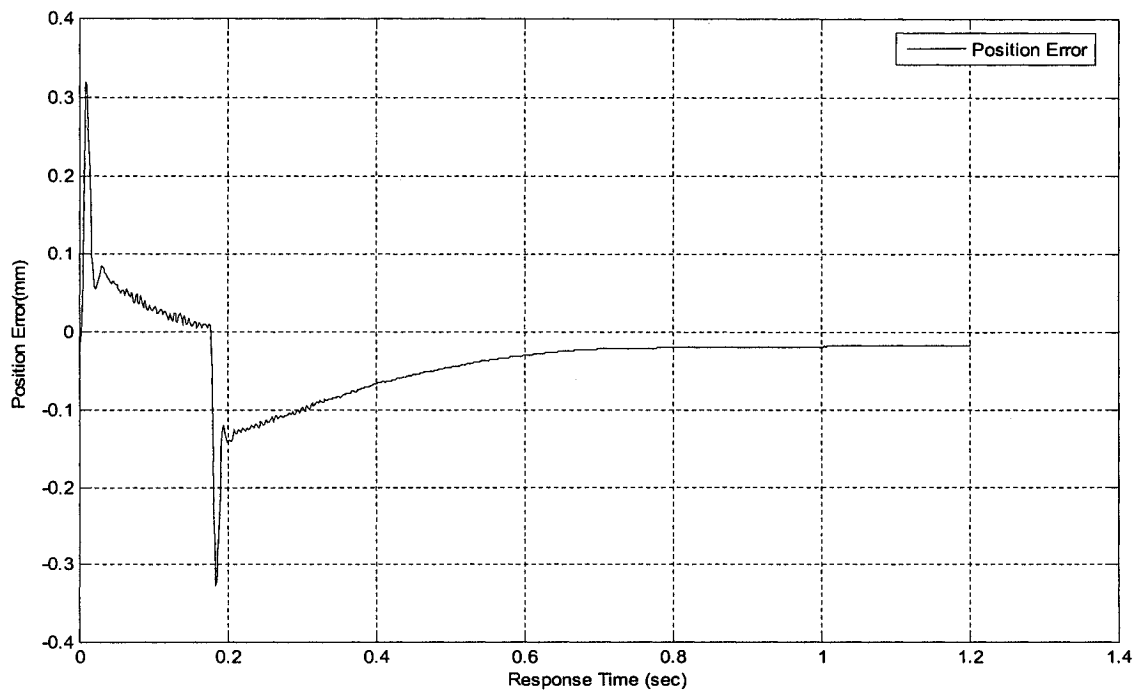
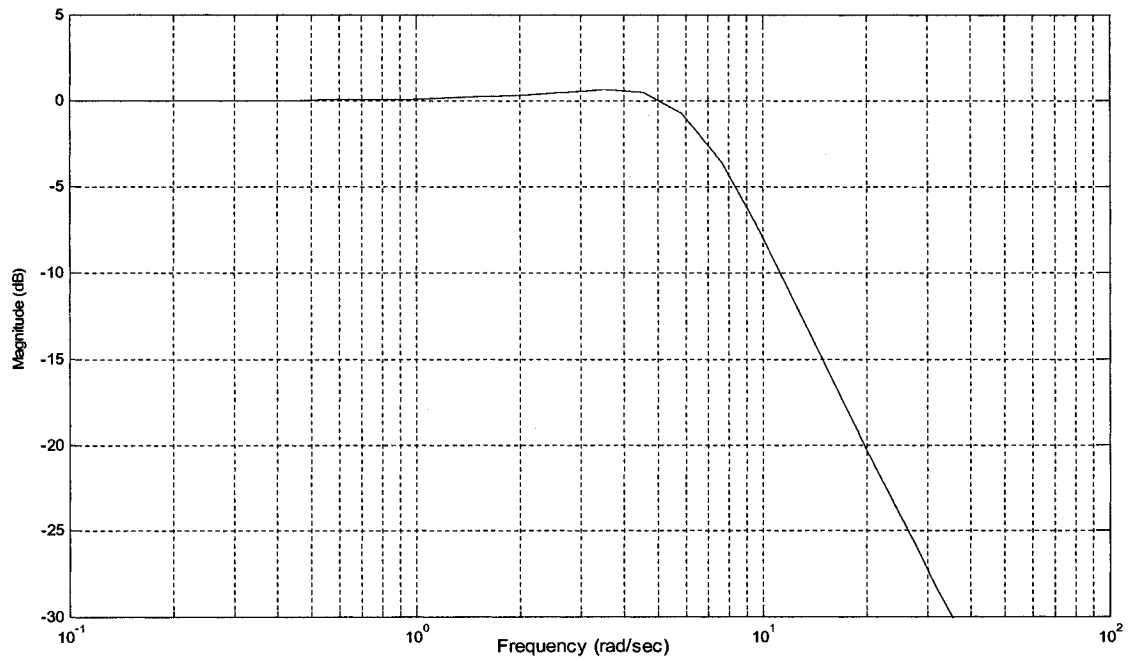
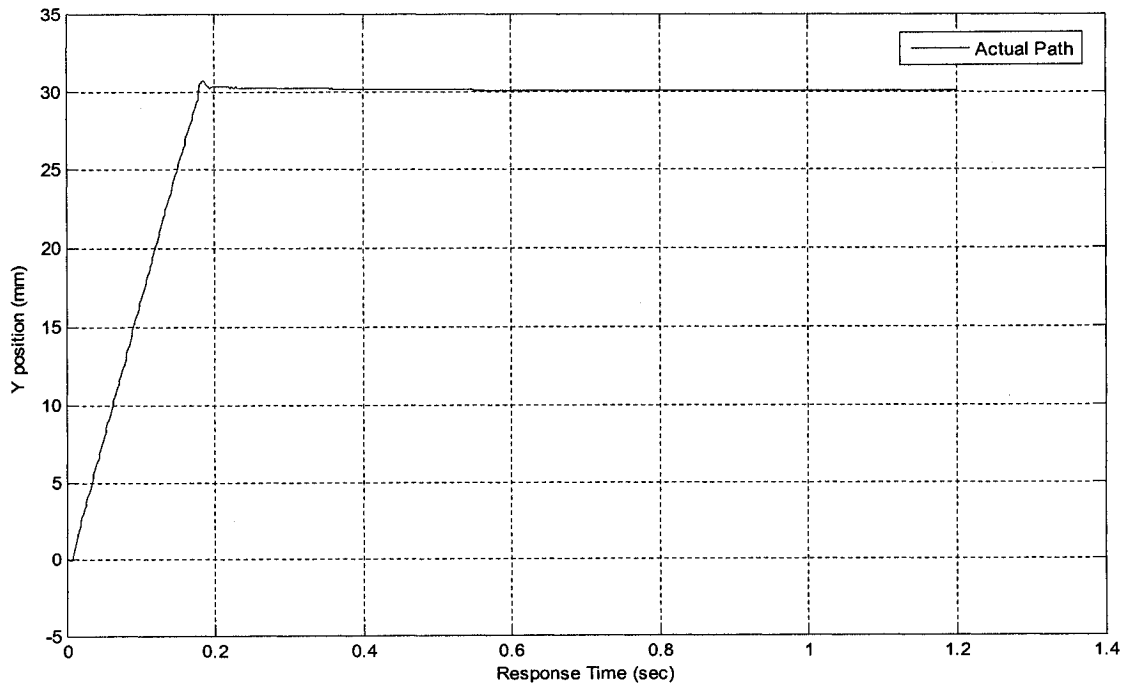
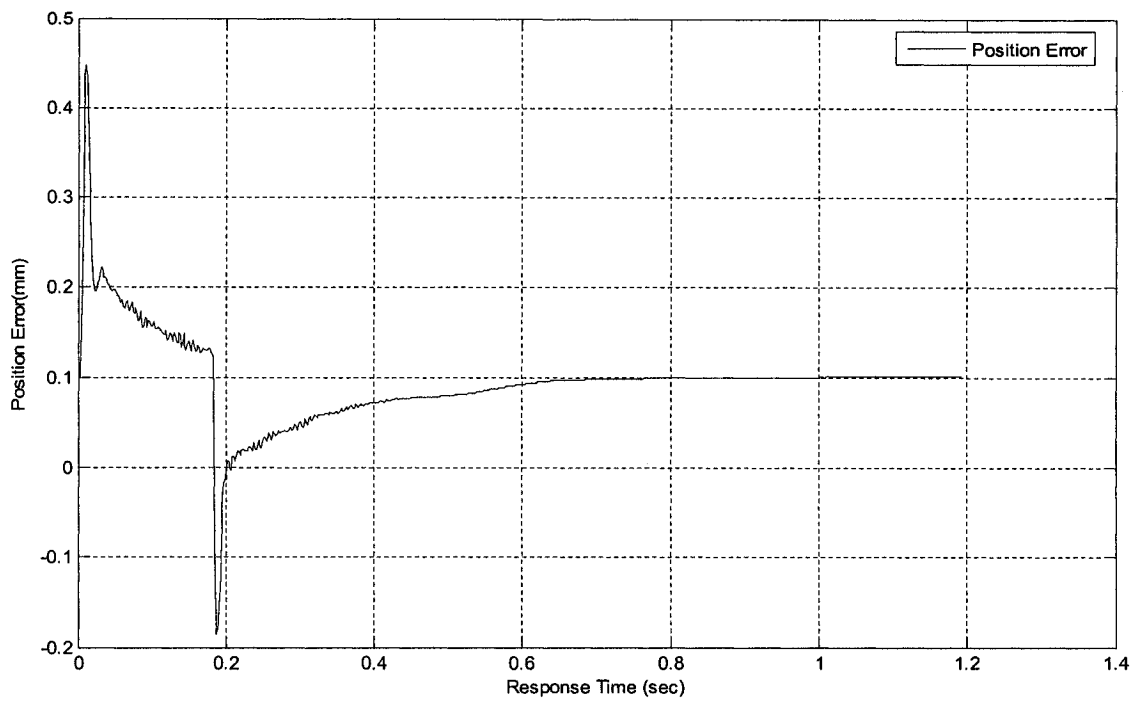
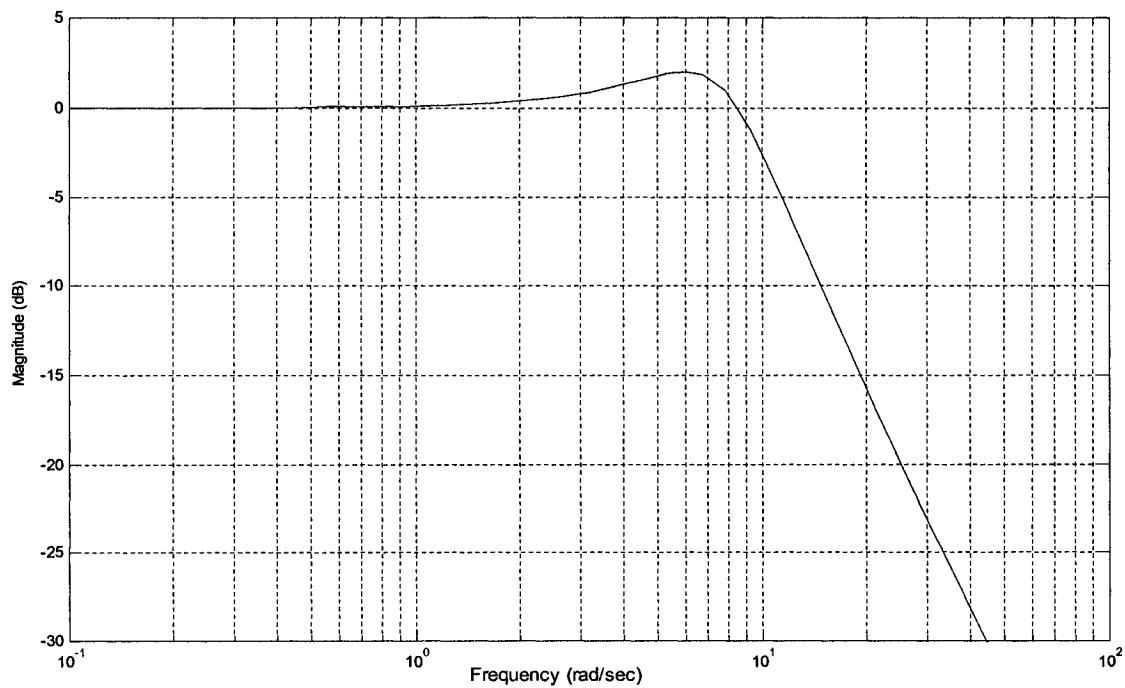


Figure 6.8: Position error of the platform in Y axis of \bar{H}_1

Figure 6.9: Frequency response of \bar{H}_1 Figure 6.10: Actual path of the platform in Y axis of \bar{H}_2

Figure 6.11: Position error of the platform in Y axis of \bar{H}_2 Figure 6.12: Frequency response of \bar{H}_2

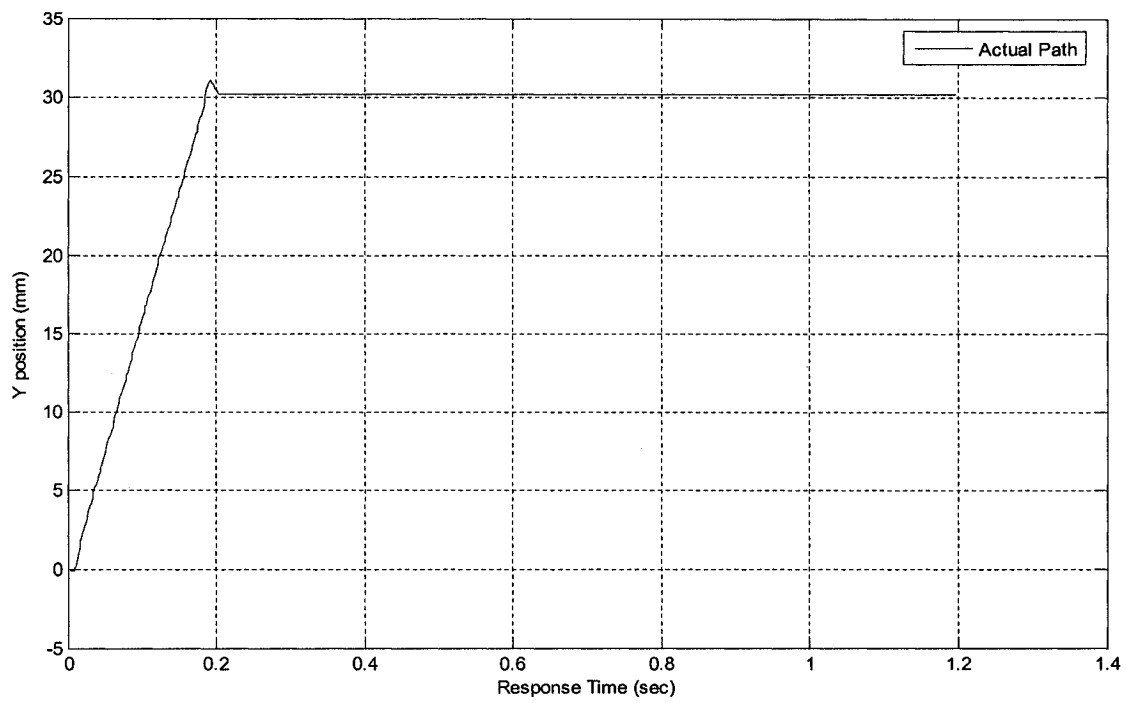


Figure 6.13: Actual path of the platform in Y axis of \bar{H}_3

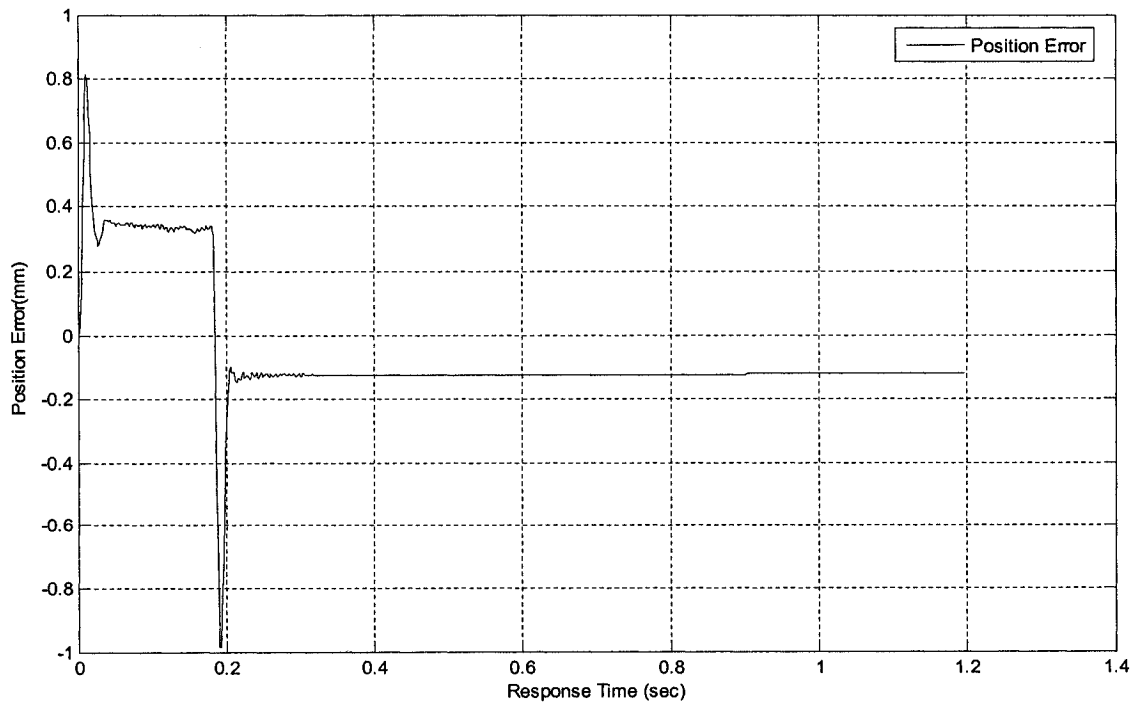


Figure 6.14: Position error of the platform in Y axis of \bar{H}_3

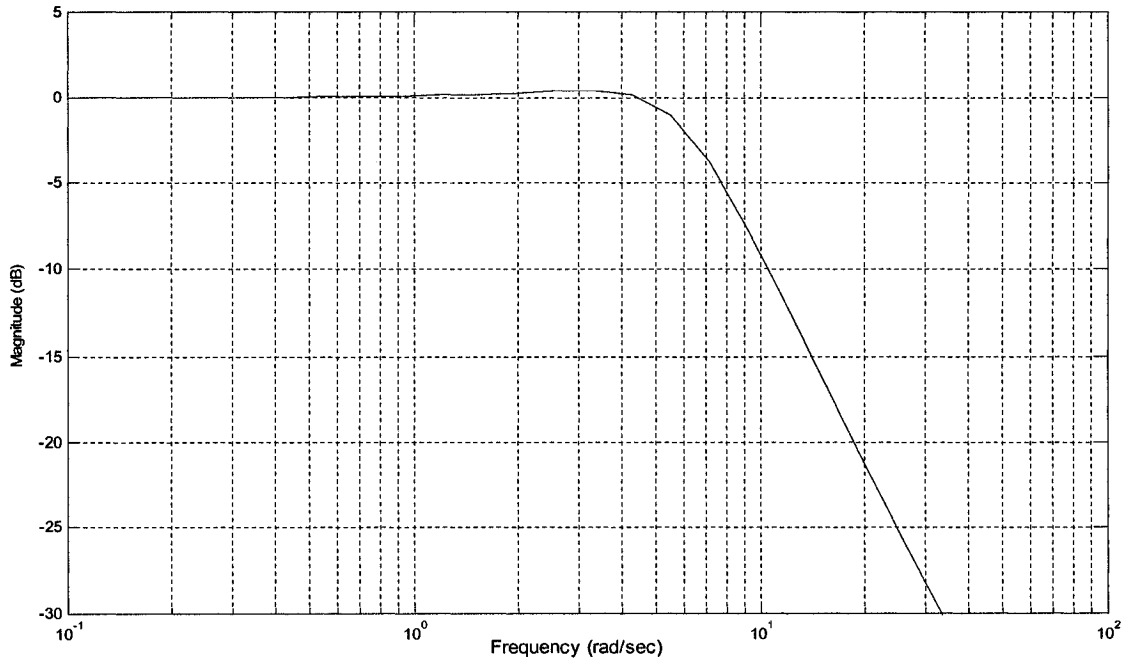


Figure 6.15: Frequency response of \bar{H}_3

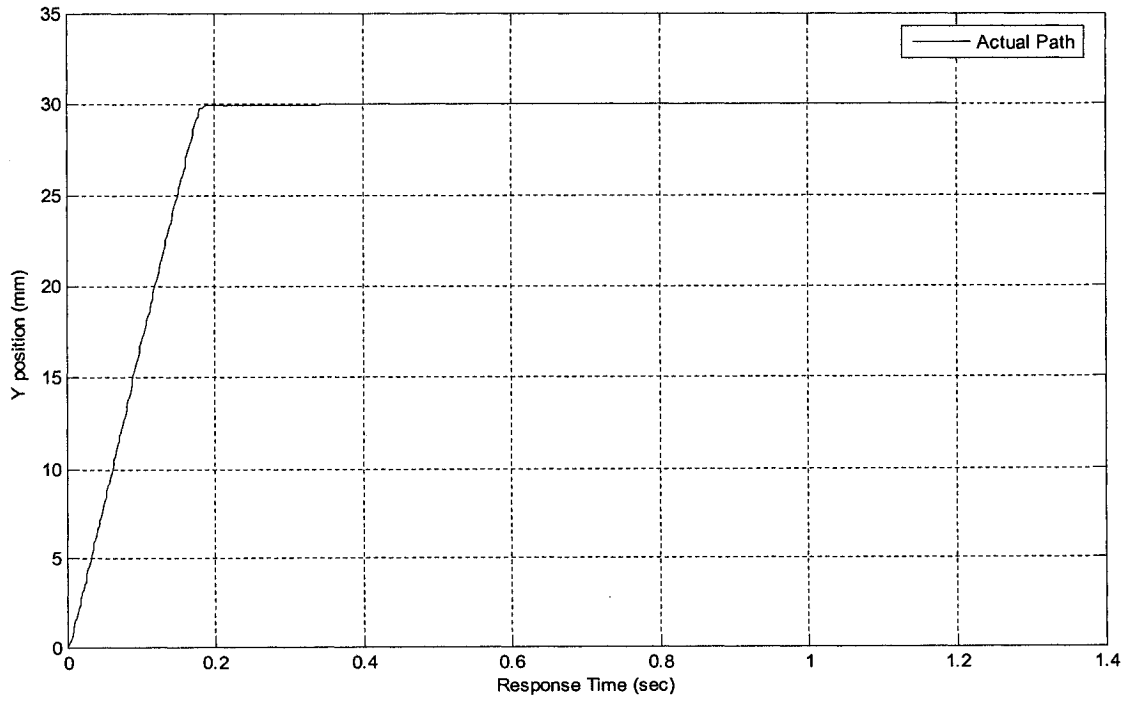


Figure 6.16: Actual path of the platform in Y axis of \bar{H}^*

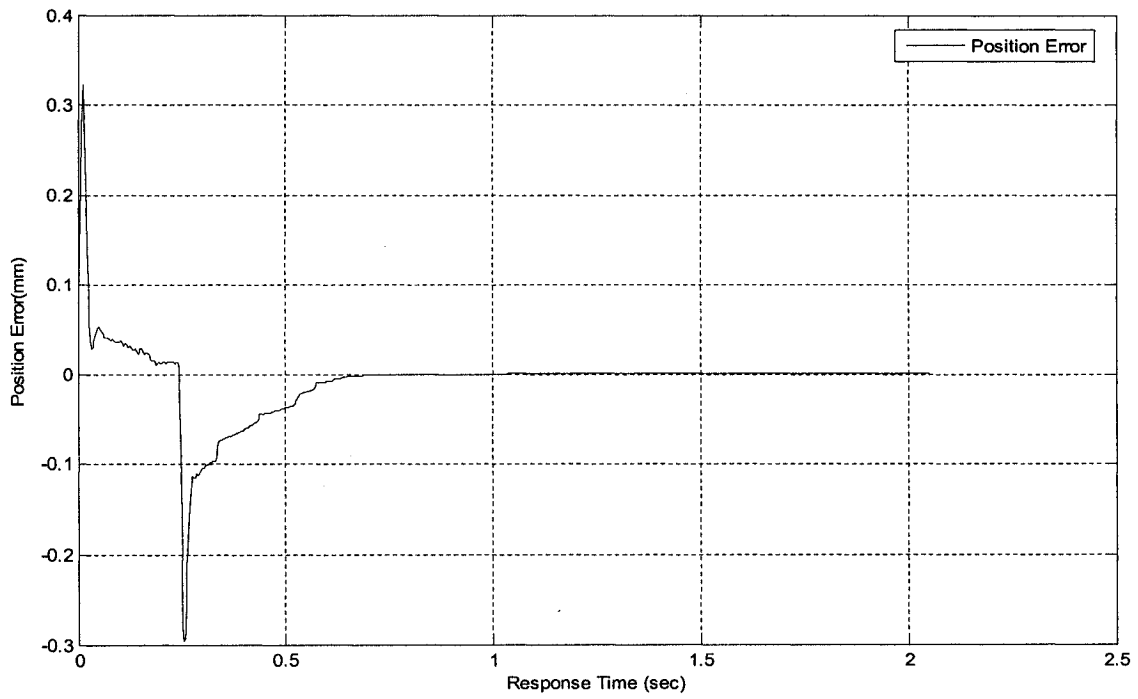


Figure 6.17: Position error of the platform in Y axis of \bar{H}^*

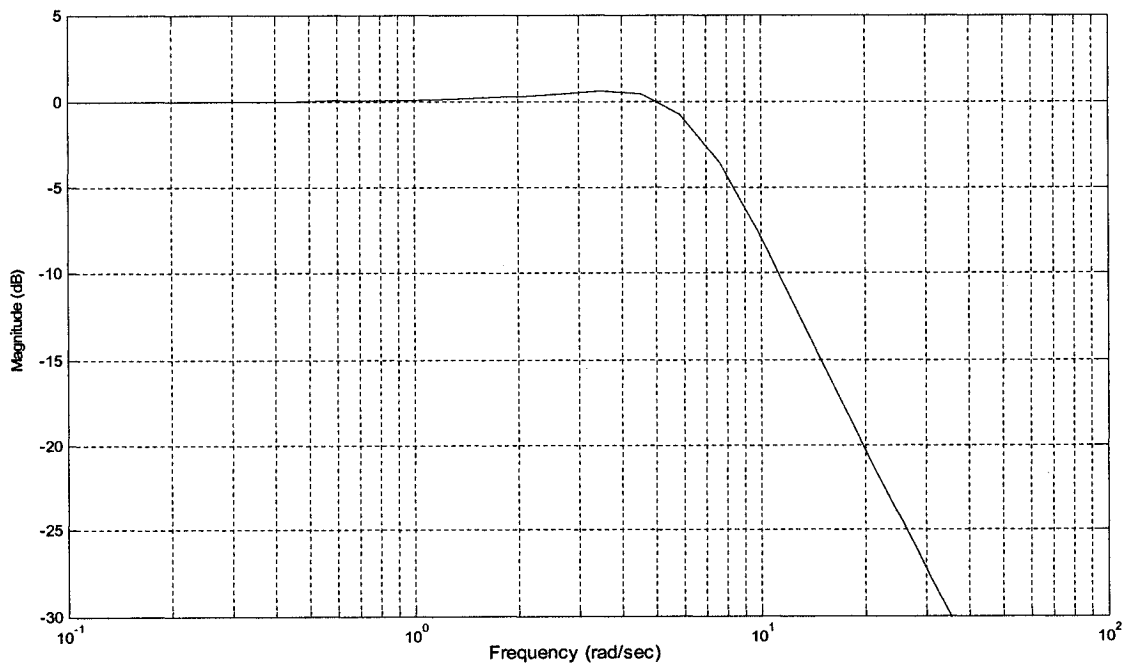


Figure 6.18: Frequency response of \bar{H}^*

Chapter 7

Conclusions and Discussions

7.1 Thesis Summary

This thesis is concerned with the trajectory tracking control problem of parallel robotic manipulators. Consider the coupling effects amongst the active joints in a parallel robotic manipulator, in this thesis, a new control approach, termed synchronized control, is proposed and experimentally verified on a 3 DOF P-R-R manipulator. In addition, with respect to different operation conditions and performance requirements, two new control approaches, termed adaptive synchronized (A-S) control and convex synchronized (C-S) control, are proposed. Experiments utilizing these two controllers have been conducted on the P-R-R manipulator as well. In the following, the thesis work is summarized, and some important contributions of this thesis work are restated:

- Because of the closed-loop chain structure, active joints in a parallel robotic manipulator are kinematic constrained. Therefore, it is necessary to consider the coupling effects amongst the active joints when solving the trajectory tracking control problem of parallel robotic manipulators. To reflect the degree of coordination amongst the active joints, we define two different synchronization errors in Chapter 3 and Chapter 6, respectively. The former is model-based and is nonlinear with respect to the generalized coordinates, while the latter is model-

- free and is linear with respect to the generalized coordinates. With the employment of a synchronization error, each active joint receives feedback information of both itself and the other active joints. As a result, the platform of the manipulator can be controlled to move along the desired trajectory accurately.
- By assuming that the dynamic model parameters of a parallel robotic manipulator are exactly known, the synchronized control approach is proposed for solving the trajectory tracking control problem of parallel robotic manipulators. Through feeding back the synchronization error to each active joint, the coupling effects amongst the active joints are considered during trajectory tracking control. As a result, the tracking control performance of the proposed synchronization control is improved. On the other hand, theoretically, the synchronized controller can be any type of controller with the employment of the synchronization error. Here, for simplicity, the synchronized controller is selected as the PD type. Furthermore, experiments of both the synchronized control and standard PID control without synchronization conducted on a 3 DOF planar parallel robotic manipulator demonstrate the effectiveness of the synchronization error in the control scheme.
 - Considering that unknown parameters always exist in the dynamic model of a parallel robotic manipulator due to unknown payload, friction, etc., we propose the so-called A-S control, which is a combination of adaptive control and the proposed synchronized control. The advantages of the A-S control are exhibited in the following two aspects: (i) the employed bounded-gain-forgetting estimator estimates unknown parameters, and thus eliminates the influence caused by unknown parameters; (ii) when the synchronization error is fed back to each

active joint in a parallel robotic manipulator, all active joints move in a synchronous manner so that the tracking performance is improved. By constructing a Lyapunov function and using Barbalat's lemma, the A-S control is proved stable in theoretical. Experiments of the A-S control, adaptive control without synchronization and traditional PID control conducted on the P-R-R manipulator demonstrate the claimed advantages of the proposed A-S control.

- During trajectory tracking of parallel robotic manipulators, sometimes, multiple closed-loop performance specifications are required to be satisfied simultaneously. Since these specifications may be conflicting with each other, it will be time-consuming and hard to tune control gains of a controller to satisfy them at the same time. In this case, we propose the C-S control approach, which utilizes the convex combination method and the synchronization error. In the C-S control scheme, since the controller is designed through combining multiple sample controllers, each of which only needs to satisfy one specification, it is relative easy to obtain a satisfactory C-S controller. In addition, regarding uncertainties in the dynamic model, a convex robustness specification is defined to guarantee the control performance of the C-S controller. Experiments conducted on the P-R-R manipulator demonstrate the above claims of the C-S control.
- In principle, the proposed synchronized control, A-S control and C-S control are suitable for parallel robotic manipulators with various structures. The validity of these three control approach has been demonstrated by the experiments conducted on the P-R-R manipulator.

7.2 Recommendations for Future Work

Reviewing this thesis, the following tasks should be considered in future work.

- In the proposed synchronized control and A-S control schemes, we define a model-based synchronization error. Although this synchronization error reflects the coupling effect amongst the active joints and improves tracking performance of parallel robotic manipulators, its construction is somewhat complicated to be implemented and is nonlinear with respect to the positions of active joints. Therefore, how to define a new model-based synchronization error with a relatively simple expression, while being linear with respect to the positions of all active joints, becomes an interesting research topic. Such a synchronization error may be defined following the idea of the contour error defined for tracking control of machine tools (Koren, Y., 1980), as long as a sensor, which can measure the pose of the platform directly, is available.
- Although the proposed synchronized control, A-S control and C-S control have been theoretically proved suitable for parallel robotic manipulators with various structures, and have been applied on a 3 DOF P-R-R manipulator, to demonstrate their generality, more experiments should be conducted on some parallel robotic manipulators with different structures, for example, a standard 6 DOF Stewart type robotic manipulator.

Bibliography

- [1] Angeles J., *Fundamentals of Robotic Mechanical Systems, Theory, Methods, and Algorithms*, 2nd Edition, Springer-Verlag New York, Inc. 2003, Chapter 6.
- [2] Angeles, J. and Lee, S.K., "The modeling of holonomic mechanical systems using a natural orthogonal complement", *Trans. CSME*, Vol. 13, No. 4, pp. 81-89, 1989.
- [3] Begon, P., Pierrot, F. and Dauchez, P., "Fuzzy sliding mode control of a fast parallel robot", *Proc. IEEE Int. Conf. on Robotics and Automation*, Vol. 1, pp. 1178-1183, 1995.
- [4] Bejczy, A.K., "Robot arm dynamics and control", *NASA-JPL Technical Memorandum*, TM 33-669, February, 1974.
- [5] Blekhman, I.I., Land, P.S. and Rosenblum, M.G., "Synchronization and chaotization in interacting dynamical systems", *ASME Applied Mechanical Review*, Vol. 48, pp. 733-752.
- [6] Borenstein, J. and Koren, Y., "Motion control analysis of a mobile robot", *J. Dynamic Systems, Measurement, and Control*, Vol. 109, 72-79, June, 1987.
- [7] Borenstein, J., "Control and kinematic design of multi-degree-of freedom mobile robots with compliant linkage", *IEEE Trans. on Robotics and Automation*, Vol. 11, pp. 21-35, February, 1995.
- [8] Boyd, S.P. and Barratt, C.H., *Linear Controller Design: Limits of Performance*, Prentice Hall, 1991.

-
- [9] Carretero, J.A., Nahon, M. and Podhorodeski, R.P., "Workspace analysis of a 3-DOF parallel mechanism", *Proc. IEEE Int. Conf. on Intelligent Robots and Systems*, Vol. 2, pp. 1021-1026, 1998.
- [10] Chen, B.-C., Tilbury, D.M. and Ulsoy, A.G., "Modular control for machine tools: cross-coupling control with friction compensation", *Proc. ASME Dynamic Systems and Control Division*, Vol. 64, pp. 455-462, 1998.
- [11] Chen, C. and Lin, C., "Tracking control of robots using computed torque based sliding mode controller", *Trans. of the Chinese Institute of Engineers*, Series C, Vol. 19, No. 2, pp. 177-185, April, 1998.
- [12] Chen, N.X. and Song, S., "Direct position analysis of 4-6 Stewart Platforms," *J. Mechanical Design*, Vol. 116, pp. 61-66, 1994.
- [13] Chiacchio, P., Pierrot, F., Sciavicco, L. and Siciliano, B., "Robust Design of independent joint controllers with experimentation on a high-speed parallel robot", *IEEE Trans. of Industrial Electronics*, Vol. 40, No. 4, pp. 393-403, 1993.
- [14] Chiu, T.C., and Tomizuka, M., "Coordinated position control of multi-axis mechanical systems." *ASME J. of Dynamic Systems, Measurement, and Control*, Vol. 120, No. 3, pp. 389-393, 1998.
- [15] Chuang, H.-Y. and Chang, Y.-C., "A novel contour error compensator for 3-PRPS platform", *J. Robotic Systems*, Vol. 17, No.5, pp. 273-289, 2000.
- [16] Clavel, R., "Delta, a fast robot with parallel geometry", *Proc. 18th Int. Symposium on Industrial Robots*, Lausanne, Switzerland, pp. 91-100, 1998.

-
- [17] Corless, M.J. and Leitmann, G., "Continuous state feedback guaranteeing uniform ultimate boundedness for uncertain dynamic systems", *IEEE Trans. on Automatic Control*, Vol. AC-26, No. 5, pp. 1139-1144, 1981.
- [18] Dawson, D.M., Qu, Z., Lewis, F.L. and Dorsey, J.F., "Robust control for the tracking of robot motion", *Proc. of the American Control Conf.*, pp. 722-726, May, 1990.
- [19] Ertugrul, M. and Kaynak, O., "Neuro sliding mode control of robotic manipulators", *Mechatronics*, Vol. 10, No. 1-2, pp. 239-263, February, 2000.
- [20] Feng, L., Koren, Y., and Borenstein, J., "Cross-coupling motion controller for mobile robots", *IEEE Control Systems and Magazine*, Vol. 13, No. 6, pp. 35-43, 1993.
- [21] Fu, K., *Convex Integrated Design of Controlled Mechanical Systems*, Ph.D. Thesis, University of Toronto, 2004.
- [22] Fu, K. and Mills, J.K., "Convex integrated design (CID): necessary and sufficient conditions for existence of solution", *Proc. IEEE Int. Conf. on Robotics, Intelligent Systems and Signal Processing*, Changsha, P.R. China, pp. 654-660, October, 2003.
- [23] Gallardo J., Rico, J.M., Frisoli, A., Checcacci, D. and Bergamsco, M., "Dynamics of parallel manipulators by means of screw theory", *Mechanism and Machine Theory*, Vol. 38, pp. 1113-1131, 2003.
- [24] Guo, L.S. and Zhang, Q., "Adaptive trajectory control of a two DOF closed-chain robot", *Proc. of the American Control Conf.*, Vol. 1, pp. 658-663, 2001.
- [25] Han, C.Z., Wang, Y.J., and Wan, B.W., *Theory of Stochastic Systems*, Xi'an Jiaotong University, Xi'an, P.R. China, 1987, Chapter 5.

-
- [26] Homsup, W. and Anderson, J.N., "PD control performance of robotic mechanisms", *Proc. of the American Control Conf.*, pp. 472-475, 1987.
- [27] Huang, C. and Fu, L., "Adaptive backstepping tracking control of the Stewart platform", *Proc. of the 43rd IEEE Conf. Decision and Control*, Vol. 5, pp. 5228-5233, 2004
- [28] Jin, S., Watanabe, K. and Nakamura, M., "Multiple fuzzy control of a robot manipulator", *Trans. of the Japan Society of Mechanical Engineers, Part C*, Vol. 59, No. 557, pp. 158-164, 1993.
- [29] Kang, B., Chu, J. and Mills, J.K. "Design of high speed planar parallel manipulator and multiple simultaneous specification control", *Proc. IEEE Conf. Robotics and Automation*, Vol. 3, pp. 2723-2728, 2001.
- [30] Kang, B., "Dynamic Equation of Planar Parallel Manipulator: Rigid Link and Flexible Link Cases", *Technique Report, Laboratory for Nonlinear Systems Control*, University of Toronto, 2001.
- [31] Kassner D.J., *Kinematic analysis of a planar three-degree-of-freedom platform-type robot manipulator*. Master thesis, Purdue University, Purdue, December, 1990.
- [32] Kokkinis, T. and Stoughton, R., "Dynamics and control of closed-chain robot arms with application to a new direct-drive robot arm", *Int. J. Robotics and Automation*, Vol. 6, No. 1, pp. 25-34, 1996.
- [33] Koren, Y., "Cross-coupled biaxial computer control for manufacturing systems", *ASME J. Dynamic Systems, Measurement, and Control*, Vol. 102, No. 4, pp. 265-272, 1980.

-
- [34] Koren, Y. and Lo, C.C., "Advanced controllers for feed drives." *Ann. CIRP*, pp. 689-698, 1992.
- [35] Kulkarni, P.K. and Srinivasan, K., "Cross-coupled control of biaxial feed drive servomechanisms", *ASME J. Dynamic Systems, Measurement, and Control*, Vol. 112, No. 2, pp. 225-232, 1990.
- [36] Lee, H.C. and Jeon, G.J., "A neuro-controller for synchronization of two motion axes", *Int. J. Intelligent Systems*, Vol. 13, No. 6, pp. 571-586, 1998.
- [37] Liu, H. and Mills J.K., "Robot control system design: Performance orientated method", *Proc. ASME: Symposium on Flexible Automation*, pp. 71-78, August, 1996.
- [38] Liu, H. and Mills J.K., "A new controller design methodology and its application to robot control systems", *Proc. CSME: 13th Symposium on Engineering Applications of Mechanics*, pp. 268-273, May, 1996.
- [39] Liu, H. and Mills J.K., "Controller design for multiple simultaneous specifications with application to robotic systems", *Proc. IEEE Int. Conf. Robotics and Automation*, pp. 2038-2043, April, 1997.
- [40] Liu, H., *Multiple Simultaneous Specification Control Problem and Its Application to Robot Trajectory Tracking System*, Ph.D. Thesis, University of Toronto, 1998.
- [41] Lo, C.-C., "An improved algorithm for cross-coupling control of multi-axis machine tools", *Trans. of the ASME*, Vol. 121, pp. 537-540, August, 1999.
- [42] McNab, R.J. and Tsao, T.C., "Receding horizon linear quadratic optimal control for multi-axis contour tracking." *ASME J. of Dynamic Systems, Measurement, and Control*, Vol. 122, No. 2, pp. 375-381, 2000.

-
- [43] Merlet, J.P., *Parallel Robots*, Kluwer Academic Publishers-Dordrecht/Boston/London, The Netherlands, 2000, pp. 9-10, Chapter 1.
- [44] Moore, P.R. and Chen, C.M., "Fuzzy logic coupling and synchronized control of multiple independent servo-drives", *Control Engineering Practice*, Vol. 3, No. 12, pp. 1697-1708, 1995.
- [45] Naumovic, M., "Cross-coupled motion controller for two cooperating robot arms", *Proc. IEEE Int. Symp. Industrial Electronics*, Vol. 2, pp. 909-913, 1991.
- [46] Nguyen, C., Antrazi, S.S., Zhou, Z., Campbell J. and Charles E., "Adaptive control of a Stewart platform-based manipulator" *J. of Robotic Systems*, Vol. 10, No. 5, pp. 657-687, July, 1993.
- [47] Nijmeijer, H. and Rodriguez-Angeles, A., *Synchronization of Mechanical Systems*, World Scientific Series on Nonlinear Science, Series A, Vol. 46, World Scientific Publishing Co. Pte. Ltd., 2003.
- [48] Oh, P.Y., "Improved model reference adaptive control using the Euler operator", *Proc. IEEE Int. Conf. Robotics and Automation*, Vol. 2, pp. 1626-1631, 1997.
- [49] Ouyang, P.R., Zhang, W.J., and Wu, F.X., "Nonlinear PD control for trajectory tracking with consideration of the design for control methodology", *Proc. IEEE Int. Conf. on Robotics and Automation*, Vol. 4, pp. 4126-4131, 2002.
- [50] Paul, R.P., "Modeling, trajectory calculation and servoing of a computer controlled arm", *Stanford Artificial Intelligence Laboratory, Stanford University*, AIM 177, 1972.

-
- [51] Pennock, G.R. and Kassner D.J. "Kinematic analysis of a planar eight-bar linkage: application to a platform-type robot", *ASME Proc. of the 21st Biennial Mechanisms Conf.*, Chicago, pp. 37-43, September, 1990.
- [52] Pikovsky, A., Rosenblum, M. and Kurths, J., *Synchronization*, The Press Syndicate of The University of Cambridge, 2001.
- [53] Qu, Z. and Dawson, D.M., *Robust Tracking Control of Robot Manipulators*. IEEE Press, 1996.
- [54] Ren, L., Song, B. and Feng, Z., "Weight iteration of displacement forward of a kind of parallel manipulators", *J. of Xi'an Jiaotong University*, Vol. 36, No. 2, pp. 186-189, 2001.
- [55] Ren, L., Mill, J.K. and Sun, D., "Adaptive synchronization control of a planar parallel manipulator", *Proc. of American Control Conf.*, Boston, USA, pp. 3980-3985, June, 2003.
- [56] Ren, L., Mills, J.K. and Sun, D., "Trajectory tracking control of a planar parallel manipulator: synchronization control", *Proc. CSME Forum*, London, Canada, pp. 326-333, June 1-4, 2004,
- [57] Ren, L. and Mills, J.K., "Different adaptive synchronization control strategies used for a parallel robotic manipulator", *Proc. 14th Int. Conf. on Flexible Automation and Intelligent Manufacturing (FAIM)*, Toronto, Canada, pp. 299-306, July 12-14, 2004.
- [58] Ren, L., Mills, J.K. and Sun, D., "Controller Design Applied to Planar Parallel Manipulators For Trajectory Tracking Control", *Proc. IEEE Conf. of Robotics Automation*, Barcelona, Spain, pp. 980-985, April, 2005.

-
- [59] Ren, L., Mill, J.K. and Sun, D., "Adaptive synchronized control of a planar parallel manipulator: theory and experiments", submitted to *ASME J. Dynamic Systems, Measurements, and Control*.
- [60] Ren, L. and Mills, J.K., "Trajectory tracking control for the P-R-R type manipulator", *Technical Report, Laboratory for Nonlinear Systems Control, University of Toronto*, 2005.
- [61] Rico, J.M., Gallardo, J. and Duffy, J., "Screw theory and higher order analysis of open serial and closed chains", *Mechanism and Machine Theory*, Vol. 34, No. 4, pp. 559-586, 1999.
- [62] Rockafellar, R.T., *Convex Analysis*, Princeton University Press, 1970.
- [63] Rodriguez-Angeles, A. and Nijmeijer, H., "Mutual synchronization of robots via estimated state feedback: A cooperative approach", *IEEE Trans. on Control Systems Technology*, Vol. 12, pp. 542-554, July, 2004.
- [64] Rodriguez-Angeles, A. and Nijmeijer, H., "Cooperative synchronization of robots via estimated state feedback", *Proc. 42nd IEEE Conf. Decision and Control*, Maui, Hawaii, USA, pp. 1514-1519, December, 2003.
- [65] Sanchez-Pena, R.S. and Sznajder, M., *Robust Systems: Theory and Application*, Toronto: John Wiley & Sons, Inc. 1998.
- [66] Sirouspour, M.R. and Salcudean, S.E., "Nonlinear control of hydraulic robots", *IEEE Trans. on Robotics and Automation*, Vol. 17, No. 2, pp. 173-182, 2001.
- [67] Slotine, J.-J.E. and Sastry, S.S., "Tracking control of nonlinear systems using sliding surfaces with application to robot manipulators", *Int. J. of Control*, Vol. 38, pp. 465-492, 1983.

-
- [68] Slotine, J.-J.E. and Li, W., *Applied Nonlinear Control*, Englewood Cliffs, N.J.: Prentice Hall, USA, 1991.
- [69] Spall, J.C. and Cristion, J.A., "Model-free control of nonlinear stochastic systems with discrete-time measurements", *IEEE Trans. on Automatic Control*, Vol. 43, No. 9, pp. 1198-1210, September, 1998.
- [70] Spong, M.W. and Vidyasagar, M., *Robot Dynamics and Control*, Jon Wiley & Sons, Inc., 1989.
- [71] Stauffer, R.N., "Flight simulation facility features robot position," *Robotics Today*, Vol. 6, No. 3, pp. 71-72, 1984.
- [72] Su, Y., Sun, D., Ren, L., Wang, X., and Mills, J.K., "Nonlinear PD synchronized control for parallel manipulators" *Proc. IEEE Conf. of Robotics Automation*, Barcelona, Spain, pp. 1386-1391, April, 2005.
- [73] Su, Y., Sun, D., Ren, L. and Mills, J.K., "Integration of saturated PI synchronous control and PD feedback for control of parallel manipulators", *accepted by Trans. of Robotics*.
- [74] Sun, D. and Mills, J.K., "Adaptive synchronized control for coordination of multirobot assembly tasks", *IEEE Trans. on Robotics and Automation*, Vol. 18, pp. 498-510, August, 2002.
- [75] Sun, D., Dong, H.N., and Tso, S.K., "Tracking stabilization of differential mobile robots using adaptive synchronized control", *Proc. 2002 IEEE Int. Conf. Robotics and Automation*, pp. 976-981, 2002.
- [76] Sun, D., "Position synchronization of multiple motion axes with adaptive coupling control." *Automatica*, Vol. 39, No. 6, pp. 997-1005, June, 2003.

-
- [77] Sun, D., Feng, G., Lam, C.M., and Dong, H.N., "Orientation control of a differential mobile robot through wheels' synchronization," *to appear in IEEE/ASME Trans. on Mechatronics*, 2005.
- [78] Tarokh, M., "Combined adaptive and computed torque control of robot manipulators", *ASME Dynamic Systems and Control Division (Publication) DSC*, Vol. 42, pp. 115-122, *Advances in Robotics - 1992*, 1992.
- [79] Tsai, L.W., *Robot Analysis, The Mechanics of Serial and Parallel Manipulators*, John Wiley and Sons Inc., New York, 1999.
- [80] Tsai, L.W., "Solving the inverse dynamics of a Stewart-Gough manipulator by the principle of virtual work", *ASME J. of Mechanical Design*, Vol. 122, No. 1, pp. 3-9, 2000.
- [81] Tomizuha, M., Hu, J.S., and Chiu, T.C., "Synchronization of two motion control axes under adaptive feedforward control", *ASME J. of Dynamic Systems, Measurement, and Control*, Vol. 114, No. 6, pp. 196-203, 1992.
- [82] Wan, Y., Wang, S. and Du, H., "Dynamic neural network control of hydraulic parallel robot", *J. of Xi'an Jiaotong University*, Vol. 38, No. 9, pp. 955-958, September, 2004.
- [83] Wu, H, and Handroos, H., "Hybrid fuzzy self-tuning PID controller for a parallel manipulator", *Proc. of the World Congress on Intelligent Control and Automation (WCICA)*, Vol. 3, WCICA 2004, pp. 2545-2549, 2004.
- [84] Zhu, S., *A PC/DSP-based hybrid control system for a planar parallel robotic manipulator*, Master Thesis, University of Toronto, 2004.

Appendix A

The Inverse Jacobian Matrix

The Jacobian matrix of the P-R-R manipulator, referring to equation (4.7), is as follows:

$$\mathbf{J}_P = \begin{bmatrix} \frac{\bar{b}_{1x}}{\bar{a}_{1x}\bar{b}_{1x} + \bar{a}_{1y}\bar{b}_{1y}} & \frac{\bar{b}_{1y}}{\bar{a}_{1x}\bar{b}_{1x} + \bar{a}_{1y}\bar{b}_{1y}} & \frac{\bar{e}_{1x}\bar{b}_{1y} - \bar{e}_{1y}\bar{b}_{1x}}{\bar{a}_{1x}\bar{b}_{1x} + \bar{a}_{1y}\bar{b}_{1y}} \\ \frac{\bar{b}_{2x}}{\bar{a}_{2x}\bar{b}_{2x} + \bar{a}_{2y}\bar{b}_{2y}} & \frac{\bar{b}_{2y}}{\bar{a}_{2x}\bar{b}_{2x} + \bar{a}_{2y}\bar{b}_{2y}} & \frac{\bar{e}_{2x}\bar{b}_{2y} - \bar{e}_{2y}\bar{b}_{2x}}{\bar{a}_{2x}\bar{b}_{2x} + \bar{a}_{2y}\bar{b}_{2y}} \\ \frac{\bar{b}_{3x}}{\bar{a}_{3x}\bar{b}_{3x} + \bar{a}_{3y}\bar{b}_{3y}} & \frac{\bar{b}_{3y}}{\bar{a}_{3x}\bar{b}_{3x} + \bar{a}_{3y}\bar{b}_{3y}} & \frac{\bar{e}_{3x}\bar{b}_{3y} - \bar{e}_{3y}\bar{b}_{3x}}{\bar{a}_{3x}\bar{b}_{3x} + \bar{a}_{3y}\bar{b}_{3y}} \end{bmatrix} \quad (\text{A.1})$$

Using Maple software, we obtain the symbolic expression of the inverse Jacobian matrix

$$\mathbf{J}_P^{-1} = \frac{1}{\Delta\mathbf{J}_P} \begin{bmatrix} \mathbf{J}_{11}^* & \mathbf{J}_{12}^* & \mathbf{J}_{13}^* \\ \mathbf{J}_{21}^* & \mathbf{J}_{22}^* & \mathbf{J}_{23}^* \\ \mathbf{J}_{31}^* & \mathbf{J}_{32}^* & \mathbf{J}_{33}^* \end{bmatrix} \quad (\text{A.2})$$

where:

$$\begin{aligned} \Delta\mathbf{J}_P = & -\bar{b}_{3x}\bar{b}_{1y}\bar{e}_{2x}\bar{b}_{2y} + \bar{b}_{3x}\bar{b}_{1y}\bar{e}_{2y}\bar{b}_{2x} + \bar{b}_{3x}\bar{b}_{2y}\bar{e}_{1x}\bar{b}_{1y} - \bar{b}_{3x}\bar{b}_{2y}\bar{e}_{1y}\bar{b}_{1x} \\ & + \bar{b}_{2x}\bar{b}_{1y}\bar{e}_{3x}\bar{b}_{3y} - \bar{b}_{2x}\bar{b}_{1y}\bar{e}_{3y}\bar{b}_{3x} - \bar{b}_{2x}\bar{b}_{3y}\bar{e}_{1x}\bar{b}_{1y} + \bar{b}_{2x}\bar{b}_{3y}\bar{e}_{1y}\bar{b}_{1x} \\ & - \bar{b}_{1x}\bar{b}_{2y}\bar{e}_{3x}\bar{b}_{3y} + \bar{b}_{1x}\bar{b}_{2y}\bar{e}_{3y}\bar{b}_{3x} + \bar{b}_{1x}\bar{b}_{3y}\bar{e}_{2x}\bar{b}_{2y} - \bar{b}_{1x}\bar{b}_{3y}\bar{e}_{2y}\bar{b}_{2x} \end{aligned} \quad (\text{A.3})$$

$$\mathbf{J}_{11}^* = -(\bar{b}_{2y}\bar{e}_{3x}\bar{b}_{3y} - \bar{b}_{2y}\bar{e}_{3y}\bar{b}_{3x} - \bar{b}_{3y}\bar{e}_{2x}\bar{b}_{2y} + \bar{b}_{3y}\bar{e}_{2y}\bar{b}_{2x})(\bar{a}_{1x}\bar{b}_{1x} + \bar{a}_{1y}\bar{b}_{1y}) \quad (\text{A.4})$$

$$\mathbf{J}_{12}^* = (\bar{b}_{3y}\bar{e}_{1y}\bar{b}_{1x} + \bar{b}_{1y}\bar{e}_{3x}\bar{b}_{3y} - \bar{b}_{1y}\bar{e}_{3y}\bar{b}_{3x} - \bar{b}_{3y}\bar{e}_{1x}\bar{b}_{1y})(\bar{a}_{2x}\bar{b}_{2x} + \bar{a}_{2y}\bar{b}_{2y}) \quad (\text{A.5})$$

$$\mathbf{J}_{13}^* = -(\bar{b}_{1y}\bar{e}_{2x}\bar{b}_{2y} - \bar{b}_{1y}\bar{e}_{2y}\bar{b}_{2x} - \bar{b}_{2y}\bar{e}_{1x}\bar{b}_{1y} + \bar{b}_{2y}\bar{e}_{1y}\bar{b}_{1x})(\bar{a}_{3x}\bar{b}_{3x} + \bar{a}_{3y}\bar{b}_{3y}) \quad (\text{A.6})$$

$$\mathbf{J}_{21}^* = \left(\bar{b}_{2x} \bar{e}_{3x} \bar{b}_{3y} - \bar{b}_{2x} \bar{e}_{3y} \bar{b}_{3x} - \bar{b}_{3x} \bar{e}_{2x} \bar{b}_{2y} + \bar{b}_{3x} \bar{e}_{2y} \bar{b}_{2x} \right) \left(\bar{a}_{1x} \bar{b}_{1x} + \bar{a}_{1y} \bar{b}_{1y} \right) \quad (\text{A.7})$$

$$\mathbf{J}_{22}^* = - \left(\bar{b}_{1x} \bar{e}_{3x} \bar{b}_{3y} - \bar{b}_{1x} \bar{e}_{3y} \bar{b}_{3x} - \bar{b}_{3x} \bar{e}_{1x} \bar{b}_{1y} + \bar{b}_{3x} \bar{e}_{1y} \bar{b}_{1x} \right) \left(\bar{a}_{2x} \bar{b}_{2x} + \bar{a}_{2y} \bar{b}_{2y} \right) \quad (\text{A.8})$$

$$\mathbf{J}_{23}^* = \left(\bar{b}_{1x} \bar{e}_{2x} \bar{b}_{2y} - \bar{b}_{1x} \bar{e}_{2y} \bar{b}_{2x} - \bar{b}_{2x} \bar{e}_{1x} \bar{b}_{1y} + \bar{b}_{2x} \bar{e}_{1y} \bar{b}_{1x} \right) \left(\bar{a}_{3x} \bar{b}_{3x} + \bar{a}_{3y} \bar{b}_{3y} \right) \quad (\text{A.9})$$

$$\mathbf{J}_{31}^* = - \left(-\bar{b}_{3x} \bar{b}_{2y} + \bar{b}_{2x} \bar{b}_{3y} \right) \left(\bar{a}_{1x} \bar{b}_{1x} + \bar{a}_{1y} \bar{b}_{1y} \right) \quad (\text{A.10})$$

$$\mathbf{J}_{32}^* = \left(-\bar{b}_{3x} \bar{b}_{1y} + \bar{b}_{1x} \bar{b}_{3y} \right) \left(\bar{a}_{2x} \bar{b}_{2x} + \bar{a}_{2y} \bar{b}_{2y} \right) \quad (\text{A.11})$$

$$\mathbf{J}_{31}^* = - \left(\bar{b}_{1x} \bar{b}_{2y} - \bar{b}_{2x} \bar{b}_{1y} \right) \left(\bar{a}_{3x} \bar{b}_{3x} + \bar{a}_{3y} \bar{b}_{3y} \right) \quad (\text{A.12})$$

Appendix B

The Expression of the Convex Combined Closed-loop Transfer Matrix

The closed-loop transfer matrix $\bar{\mathbf{H}}$ of the P-R-R manipulator, referring to equation (6.42), has the following form:

$$\bar{\mathbf{H}} = \frac{\begin{bmatrix} \bar{\mathbf{H}}_{11} & \bar{\mathbf{H}}_{12} & \cdots & \bar{\mathbf{H}}_{19} \\ \bar{\mathbf{H}}_{21} & \bar{\mathbf{H}}_{22} & \cdots & \bar{\mathbf{H}}_{29} \\ \vdots & \vdots & \ddots & \vdots \\ \bar{\mathbf{H}}_{61} & \bar{\mathbf{H}}_{62} & \cdots & \bar{\mathbf{H}}_{69} \end{bmatrix}}{\Delta\bar{\mathbf{H}}} \quad (\text{B.1})$$

where:

$$\begin{aligned} \Delta\bar{\mathbf{H}} = & -s^6 + 3.476s^5K_d - 3.947s^4K_d^2 + 3.476s^4K_p + 1.463s^3K_d^3 - 7.894s^3K_pK_d \\ & - 3.947s^2K_p^2 + 4.390s^2K_pK_d^2 + 4.390sK_p^2K_d + 1.463K_p^3 \end{aligned} \quad (\text{B.2})$$

$$\begin{aligned} \bar{\mathbf{H}}_{11} = & 1.172K_p s^4 - 2.697K_pK_d s^3 + 1.463K_pK_d^2 s^2 + 2.927K_p^2K_d s \\ & - 2.700K_p^2 s^2 - 0.002K_pK_d^2 s + 1.463K_p^3 \end{aligned} \quad (\text{B.3})$$

$$\begin{aligned} \bar{\mathbf{H}}_{21} = & -0.043K_p s^4 + 0.036K_pK_d s^3 + 0.000K_pK_d^2 s^2 + 0.00K_p^2K_d s \\ & + 0.099K_p^2 s^2 + 0.054K_pK_d^2 s + 0.000K_p^3 \end{aligned} \quad (\text{B.4})$$

$$\begin{aligned} \bar{\mathbf{H}}_{31} = & -0.043K_p s^4 + 0.066K_pK_d s^3 + 0.000K_pK_d^2 s^2 + 0.000K_p^2K_d s \\ & + 0.099K_p^2 s^2 + 0.053K_pK_d^2 s + 0.000K_p^3 \end{aligned} \quad (\text{B.5})$$

$$\begin{aligned}\bar{H}_{41} = & 1.172K_p s^5 - 2.697K_p K_d s^4 + 1.463K_p K_d^2 s^3 + 2.927K_p^2 K_d s^2 \\ & - 2.700K_p^2 s^3 - 0.002K_p K_d^2 s^2 + 1.463K_p^3 s\end{aligned}\quad (\text{B.6})$$

$$\begin{aligned}\bar{H}_{51} = & -0.043K_p s^5 + 0.036K_p K_d s^4 + 0.000K_p K_d^2 s^3 + 0.00K_p^2 K_d s^2 \\ & + 0.099K_p^2 s^3 + 0.054K_p K_d^2 s^2 + 0.000K_p^3 s\end{aligned}\quad (\text{B.7})$$

$$\begin{aligned}\bar{H}_{61} = & -0.043K_p s^5 + 0.066K_p K_d s^4 + 0.000K_p K_d^2 s^3 + 0.000K_p^2 K_d s^2 \\ & + 0.099K_p^2 s^3 + 0.053K_p K_d^2 s^2 + 0.000K_p^3 s\end{aligned}\quad (\text{B.8})$$

$$\begin{aligned}\bar{H}_{12} = & -0.109K_p s^4 + 0.091K_p K_d s^3 + 0.039K_p K_d^2 s^2 + 0.079K_p^2 K_d s \\ & + 0.222K_p^2 s^2 + 0.150K_p K_d^2 s + 0.039K_p^3\end{aligned}\quad (\text{B.9})$$

$$\begin{aligned}\bar{H}_{22} = & 1.436K_p s^4 - 2.928K_p K_d s^3 + 1.503K_p K_d^2 s^2 + 3.006K_p^2 K_d s \\ & - 2.929K_p^2 s^2 + 0.040K_p K_d^2 s + 1.503K_p^3\end{aligned}\quad (\text{B.10})$$

$$\begin{aligned}\bar{H}_{32} = & -0.109K_p s^4 - 0.132K_p K_d s^3 + 1.034K_p K_d^2 s^2 + 2.069K_p^2 K_d s \\ & - 0.222K_p^2 s^2 - 1.145K_p K_d^2 s + 1.034K_p^3\end{aligned}\quad (\text{B.11})$$

$$\begin{aligned}\bar{H}_{42} = & -0.109K_p s^5 + 0.091K_p K_d s^4 + 0.039K_p K_d^2 s^3 + 0.079K_p^2 K_d s^2 \\ & + 0.222K_p^2 s^3 + 0.150K_p K_d^2 s^2 + 0.039K_p^3 s\end{aligned}\quad (\text{B.12})$$

$$\begin{aligned}\bar{H}_{52} = & 1.436K_p s^5 - 2.928K_p K_d s^4 + 1.503K_p K_d^2 s^3 + 3.006K_p^2 K_d s^2 \\ & - 2.929K_p^2 s^3 + 0.040K_p K_d^2 s^2 + 1.503K_p^3 s\end{aligned}\quad (\text{B.13})$$

$$\begin{aligned}\bar{H}_{62} = & -0.109K_p s^5 - 0.132K_p K_d s^4 + 1.034K_p K_d^2 s^3 + 2.069K_p^2 K_d s^2 \\ & - 0.222K_p^2 s^3 - 1.145K_p K_d^2 s^2 + 1.034K_p^3 s\end{aligned}\quad (\text{B.14})$$

$$\begin{aligned}\bar{H}_{13} = & 0.033K_p s^4 - 0.036K_p K_d s^3 - 0.006K_p K_d^2 s^2 - 0.025K_p^2 K_d s \\ & + 0.086K_p^2 s^2 - 0.061K_p K_d^2 s - 0.019K_p^3\end{aligned}\quad (\text{B.15})$$

$$\begin{aligned}\bar{H}_{23} = & 0.033K_p s^4 - 0.244K_p K_d s^3 + 0.077K_p K_d^2 s^2 + 0.324K_p^2 K_d s \\ & + 0.086K_p^2 s^2 + 0.021K_p K_d^2 s + 0.247K_p^3\end{aligned}\quad (\text{B.16})$$

$$\begin{aligned}\bar{\mathbf{H}}_{33} = & 0.868K_p s^4 - 2.253K_p K_d s^3 + 1.457K_p K_d^2 s^2 + 2.902K_p^2 K_d s \\ & + 2.264K_p^2 s^2 + 0.001K_p K_d^2 s + 1.444K_p^3\end{aligned}\quad (\text{B.17})$$

$$\begin{aligned}\bar{\mathbf{H}}_{43} = & 0.033K_p s^5 - 0.036K_p K_d s^4 - 0.006K_p K_d^2 s^3 - 0.025K_p^2 K_d s^2 \\ & + 0.086K_p^2 s^3 - 0.061K_p K_d^2 s^2 - 0.019K_p^3 s\end{aligned}\quad (\text{B.18})$$

$$\begin{aligned}\bar{\mathbf{H}}_{53} = & 0.033K_p s^5 - 0.244K_p K_d s^4 + 0.077K_p K_d^2 s^3 + 0.324K_p^2 K_d s^2 \\ & + 0.086K_p^2 s^3 + 0.021K_p K_d^2 s^2 + 0.247K_p^3 s\end{aligned}\quad (\text{B.19})$$

$$\begin{aligned}\bar{\mathbf{H}}_{63} = & 0.868K_p s^5 - 2.253K_p K_d s^4 + 1.457K_p K_d^2 s^3 + 2.902K_p^2 K_d s^2 \\ & + 2.264K_p^2 s^3 + 0.001K_p K_d^2 s^2 + 1.444K_p^3 s\end{aligned}\quad (\text{B.20})$$

$$\begin{aligned}\bar{\mathbf{H}}_{14} = & 1.172K_d s^4 - 1.323K_d^2 s^3 - 1.702K_d^3 s^2 + 2.918K_p K_d^2 s \\ & - 0.006K_p K_d s^2 - 0.061K_d^3 s + 4.620K_p^2 K_d\end{aligned}\quad (\text{B.21})$$

$$\begin{aligned}\bar{\mathbf{H}}_{24} = & -0.043K_d s^4 - 0.015K_d^2 s^3 + 0.158K_d^3 s^2 + 0.084K_p K_d^2 s \\ & + 0.150K_p K_d s^2 + 0.096K_d^3 s - 0.074K_p^2 K_d\end{aligned}\quad (\text{B.22})$$

$$\begin{aligned}\bar{\mathbf{H}}_{34} = & -0.043K_d s^4 + 0.016K_d^2 s^3 + 0.083K_d^3 s^2 - 0.060K_p K_d^2 s \\ & + 0.150K_p K_d s^2 + 0.024K_d^3 s - 0.146K_p^2 K_d\end{aligned}\quad (\text{B.23})$$

$$\begin{aligned}\bar{\mathbf{H}}_{44} = & 1.172K_d s^5 - 1.323K_d^2 s^4 - 1.702K_d^3 s^3 + 2.918K_p K_d^2 s^2 \\ & - 0.006K_p K_d s^3 - 0.061K_d^3 s^2 + 4.620K_p^2 K_d s\end{aligned}\quad (\text{B.24})$$

$$\begin{aligned}\bar{\mathbf{H}}_{54} = & -0.043K_d s^5 - 0.015K_d^2 s^4 + 0.158K_d^3 s^3 + 0.084K_p K_d^2 s^2 \\ & + 0.150K_p K_d s^3 + 0.096K_d^3 s^2 - 0.074K_p^2 K_d s\end{aligned}\quad (\text{B.25})$$

$$\begin{aligned}\bar{\mathbf{H}}_{64} = & -0.043K_d s^5 + 0.016K_d^2 s^4 + 0.083K_d^3 s^3 - 0.060K_p K_d^2 s^2 \\ & + 0.150K_p K_d s^3 + 0.024K_d^3 s^2 - 0.146K_p^2 K_d s\end{aligned}\quad (\text{B.26})$$

$$\begin{aligned}\bar{\mathbf{H}}_{15} = & -0.109K_d s^4 - 0.066K_d^2 s^3 + 0.319K_d^3 s^2 + 0.000K_p K_d^2 s \\ & + 0.379K_p K_d s^2 + 0.111K_d^3 s - 0.319K_p^2 K_d\end{aligned}\quad (\text{B.27})$$

$$\begin{aligned}\bar{H}_{25} = & 1.436K_d s^4 - 0.866K_d^2 s^3 - 2.741K_d^3 s^2 + 2.928K_p K_d^2 s \\ & - 4.991K_p K_d s^2 + 0.000K_d^3 s + 5.668K_p^2 K_d\end{aligned}\quad (\text{B.28})$$

$$\begin{aligned}\bar{H}_{35} = & -0.109K_d s^4 - 0.024K_d^2 s^3 + 0.319K_d^3 s^2 - 0.001K_p K_d^2 s \\ & + 0.379K_p K_d s^2 + 0.111K_d^3 s - 0.320K_p^2 K_d\end{aligned}\quad (\text{B.29})$$

$$\begin{aligned}\bar{H}_{45} = & -0.109K_d s^5 - 0.066K_d^2 s^4 + 0.319K_d^3 s^3 + 0.000K_p K_d^2 s^2 \\ & + 0.379K_p K_d s^3 + 0.111K_d^3 s^2 - 0.319K_p^2 K_d s\end{aligned}\quad (\text{B.30})$$

$$\begin{aligned}\bar{H}_{55} = & 1.436K_d s^5 - 0.866K_d^2 s^4 - 2.741K_d^3 s^3 + 2.928K_p K_d^2 s^2 \\ & - 4.991K_p K_d s^3 + 0.000K_d^3 s^2 + 5.668K_p^2 K_d s\end{aligned}\quad (\text{B.31})$$

$$\begin{aligned}\bar{H}_{65} = & -0.109K_d s^5 - 0.024K_d^2 s^4 + 0.319K_d^3 s^3 - 0.001K_p K_d^2 s^2 \\ & + 0.379K_p K_d s^3 + 0.111K_d^3 s^2 - 0.320K_p^2 K_d s\end{aligned}\quad (\text{B.32})$$

$$\begin{aligned}\bar{H}_{16} = & 0.033K_d s^4 - 0.093K_d^2 s^3 - 0.084K_d^3 s^2 - 0.018K_p K_d^2 s \\ & - 0.115K_p K_d s^2 - 0.064K_d^3 s + 0.066K_p^2 K_d\end{aligned}\quad (\text{B.33})$$

$$\begin{aligned}\bar{H}_{26} = & 0.033K_d s^4 - 0.103K_d^2 s^3 + 0.04K_d^3 s^2 + 0.230K_p K_d^2 s \\ & - 0.115K_p K_d s^2 + 0.060K_d^3 s + 0.190K_p^2 K_d\end{aligned}\quad (\text{B.34})$$

$$\begin{aligned}\bar{H}_{36} = & 0.868K_d s^4 - 1.505K_d^2 s^3 - 0.515K_d^3 s^2 + 2.909K_p K_d^2 s \\ & - 3.017K_p K_d s^2 - 0.002K_d^3 s - 3.424K_p^2 K_d\end{aligned}\quad (\text{B.35})$$

$$\begin{aligned}\bar{H}_{46} = & 0.033K_d s^5 - 0.093K_d^2 s^4 - 0.084K_d^3 s^3 - 0.018K_p K_d^2 s^3 \\ & - 0.115K_p K_d s^3 - 0.064K_d^3 s^2 + 0.066K_p^2 K_d s\end{aligned}\quad (\text{B.36})$$

$$\begin{aligned}\bar{H}_{56} = & 0.033K_d s^5 - 0.103K_d^2 s^4 + 0.04K_d^3 s^3 + 0.230K_p K_d^2 s^2 \\ & - 0.115K_p K_d s^3 + 0.060K_d^2 s^2 + 0.190K_p^2 K_d s\end{aligned}\quad (\text{B.37})$$

$$\begin{aligned}\bar{H}_{66} = & 0.868K_d s^5 - 1.505K_d^2 s^4 - 0.515K_d^3 s^3 + 2.909K_p K_d^2 s^2 \\ & - 3.017K_p K_d s^3 - 0.002K_d^3 s^2 - 3.424K_p^2 K_d s\end{aligned}\quad (\text{B.38})$$

$$\bar{H}_{17} = s^4 - 2.304s^3 K_d + 1.250s^2 K_d^2 - 2.304s^2 K_p - 2.51s K_p K_d + 1.250K_p^2 \quad (\text{B.39})$$

$$\bar{\mathbf{H}}_{27} = -0.043s^3K_d - 0.043s^2K_p + 0.036s^2K_d^2 + 0.072sK_pK_d + 0.036K_p^2 \quad (\text{B.40})$$

$$\bar{\mathbf{H}}_{37} = -0.043s^3K_d - 0.043s^2K_p + 0.066s^2K_d^2 + 0.132sK_pK_d + 0.066K_p^2 \quad (\text{B.41})$$

$$\bar{\mathbf{H}}_{47} = s^5 - 2.304s^4K_d + 1.250s^3K_d^2 - 2.304s^3K_p - 2.51s^2K_pK_d + 1.250sK_p^2 \quad (\text{B.42})$$

$$\bar{\mathbf{H}}_{57} = -0.043s^4K_d - 0.043s^3K_p + 0.036s^3K_d^2 + 0.072s^2K_pK_d + 0.036sK_p^2 \quad (\text{B.43})$$

$$\bar{\mathbf{H}}_{67} = -0.043s^4K_d - 0.043s^3K_p + 0.066s^3K_d^2 + 0.132s^2K_pK_d + 0.066sK_p^2 \quad (\text{B.44})$$

$$\bar{\mathbf{H}}_{18} = -0.109s^3K_d + 0.091s^2K_d^2 - 0.109s^2K_p + 0.182sK_pK_d + 0.091K_p^2 \quad (\text{B.45})$$

$$\bar{\mathbf{H}}_{28} = s^4 - 2.040s^3K_d + 1.020s^3K_d^2 + 2.040s^2K_p - 2.038sK_pK_d + 1.019K_p^2 \quad (\text{B.46})$$

$$\bar{\mathbf{H}}_{38} = -0.109s^3K_d - 0.109s^2K_p + 0.132s^2K_d^2 + 0.264sK_pK_d + 0.132K_p^2 \quad (\text{B.47})$$

$$\bar{\mathbf{H}}_{48} = -0.109s^4K_d + 0.091s^3K_d^2 - 0.109s^3K_p + 0.182s^2K_pK_d + 0.091sK_p^2 \quad (\text{B.48})$$

$$\bar{\mathbf{H}}_{58} = s^5 - 2.040s^4K_d + 1.020s^4K_d^2 + 2.040s^3K_p - 2.038s^2K_pK_d + 1.019sK_p^2 \quad (\text{B.49})$$

$$\bar{\mathbf{H}}_{68} = -0.109s^4K_d - 0.109s^3K_p + 0.132s^3K_d^2 + 0.264s^2K_pK_d + 0.132sK_p^2 \quad (\text{B.50})$$

$$\bar{\mathbf{H}}_{19} = 0.033s^3K_d + 0.033s^2K_p - 0.051s^2K_d^2 - 0.102sK_pK_d - 0.051K_p^2 \quad (\text{B.51})$$

$$\bar{\mathbf{H}}_{29} = 0.033s^3K_d + 0.033s^2K_p - 0.04s^2K_d^2 - 0.08sK_pK_d - 0.04K_p^2 \quad (\text{B.52})$$

$$\bar{\mathbf{H}}_{39} = s^4 - 2.608s^3K_d + 1.678s^2K_d^2 + 2.608s^2K_p + 3.356sK_pK_d + 1.678K_p^2 \quad (\text{B.53})$$

$$\bar{\mathbf{H}}_{49} = 0.033s^4K_d + 0.033s^3K_p - 0.051s^3K_d^2 - 0.102s^2K_pK_d - 0.051sK_p^2 \quad (\text{B.54})$$

$$\bar{\mathbf{H}}_{59} = 0.033s^4K_d + 0.033s^3K_p - 0.04s^3K_d^2 - 0.08s^2K_pK_d - 0.04sK_p^2 \quad (\text{B.55})$$

$$\bar{\mathbf{H}}_{69} = s^5 - 2.608s^4K_d + 1.678s^3K_d^2 + 2.608s^3K_p + 3.356s^2K_pK_d + 1.678sK_p^2 \quad (\text{B.56})$$

Substituting the values of K_p, K_d into (B.2) ~ (B.56), we have the closed-loop transfer matrices of the three sampling system, $\bar{\mathbf{H}}_1, \bar{\mathbf{H}}_2, \bar{\mathbf{H}}_3$. Using the obtained combination

vector, we have the closed-loop transfer matrix of the robotic system $\bar{\mathbf{H}}^*$ that can satisfy the three specifications simultaneously. $\bar{\mathbf{H}}^*$ has the similar expression to (B.1), where

$$\begin{aligned} \Delta \bar{\mathbf{H}}^* = & -s^{18} + 0.139 s^{17} + 24.32 s^{16} - 2.997 s^{15} - 259.3 s^{14} + 231.5 s^{13} + 1571 s^{12} - 3103 s^{11} \\ & - 5957 s^{10} + 1.847 \times 10^4 s^9 + 5214 s^8 - 5.915 \times 10^4 s^7 + 4.238 \times 10^4 s^6 + 1.068 \times 10^5 s^5 \\ & - 1.318 \times 10^5 s^4 + 2.309 \times 10^4 s^3 + 1.116 \times 10^5 s^2 + 4.31 \times 10^4 s + 4787 \end{aligned} \quad (\text{B.57})$$

$$\begin{aligned} \bar{\mathbf{H}}_{11}^* = & 2.593 s^{16} - 0.3189 s^{15} - 55.93 s^{14} + 5.993 s^{13} + 519.6 s^{12} - 397.6 s^{11} \\ & - 2690 s^{10} + 4424 s^9 + 8492 s^8 - 2.089 \times 10^4 s^7 - 8904 s^6 + 4.974 \times 10^4 s^5 \\ & - 1.645 \times 10^4 s^4 - 5.948 \times 10^4 s^3 + 2.773 \times 10^4 s^2 + 2.877 \times 10^4 s + 4783 \end{aligned} \quad (\text{B.58})$$

$$\begin{aligned} \bar{\mathbf{H}}_{21}^* = & -0.09513 s^{16} + 0.009798 s^{15} + 2.052 s^{14} - 0.1813 s^{13} - 18.37 s^{12} + 14.19 s^{11} \\ & + 88.43 s^{10} - 159.9 s^9 - 248.1 s^8 + 683 s^7 + 118.3 s^6 - 1287 s^5 + 988.5 s^4 \\ & + 921.4 s^3 + 153.5 s^2 + 0.008198 s \end{aligned} \quad (\text{B.59})$$

$$\begin{aligned} \bar{\mathbf{H}}_{31}^* = & -0.09513 s^{16} + 0.0107 s^{15} + 2.052 s^{14} - 0.1961 s^{13} - 18.36 s^{12} + 14.29 s^{11} \\ & + 88.3 s^{10} - 160.3 s^9 - 247.2 s^8 + 683.7 s^7 + 116.1 s^6 - 1285 s^5 + 990.4 s^4 \\ & + 921.7 s^3 + 153.5 s^2 + 0.008198 s \end{aligned} \quad (\text{B.60})$$

$$\begin{aligned} \bar{\mathbf{H}}_{41}^* = & 2.593 s^{17} - 0.3189 s^{16} - 55.93 s^{15} + 5.993 s^{14} + 519.6 s^{13} - 397.6 s^{12} \\ & - 2690 s^{11} + 4424 s^{10} + 8492 s^9 - 2.089 \times 10^4 s^8 - 8904 s^7 + 4.974 \times 10^4 s^6 \\ & - 1.645 \times 10^4 s^5 - 5.948 \times 10^4 s^4 + 2.773 \times 10^4 s^3 + 2.877 \times 10^4 s^2 + 4783 s \end{aligned} \quad (\text{B.61})$$

$$\begin{aligned} \bar{\mathbf{H}}_{51}^* = & -0.09513 s^{17} + 0.009798 s^{16} + 2.052 s^{15} - 0.1813 s^{14} - 18.37 s^{13} + 14.19 s^{12} \\ & + 88.43 s^{11} - 159.9 s^{10} - 248.1 s^9 + 683 s^8 + 118.3 s^7 - 1287 s^6 + 988.5 s^5 \\ & + 921.4 s^4 + 153.5 s^3 + 0.008198 s^2 \end{aligned} \quad (\text{B.62})$$

$$\begin{aligned} \bar{\mathbf{H}}_{61}^* = & -0.09513 s^{17} + 0.0107 s^{16} + 2.052 s^{15} - 0.1961 s^{14} - 18.36 s^{13} + 14.29 s^{12} \\ & + 88.3 s^{11} - 160.3 s^{10} - 247.2 s^9 + 683.7 s^8 + 116.1 s^7 - 1285 s^6 + 990.4 s^5 \\ & + 921.7 s^4 + 153.5 s^3 + 0.008198 s^2 \end{aligned} \quad (\text{B.63})$$

$$\begin{aligned} \bar{\mathbf{H}}_{12}^* = & -0.2411 s^{16} + 0.02483 s^{15} + 5.051 s^{14} - 0.4401 s^{13} - 43.7 s^{12} + 35.67 s^{11} \\ & + 201.2 s^{10} - 385.1 s^9 - 529.1 s^8 + 1540 s^7 + 46.03 s^6 - 2550 s^5 \\ & + 2490 s^4 + 1151 s^3 + 1195 s^2 + 767 s + 127.5 \end{aligned} \quad (\text{B.64})$$

$$\begin{aligned}\bar{H}_{22}^* &= 3.177s^{16} - 0.3794s^{15} - 66.56s^{14} + 6.935s^{13} + 602.2s^{12} - 482.6s^{11} \\ &\quad - 3040s^{10} + 5156s^9 + 9379s^8 - 2.341 \times 10^4 s^7 - 8488s^6 + 5.386 \times 10^4 s^5 \\ &\quad - 1.833 \times 10^4 s^4 - 6.256 \times 10^4 s^3 + 2.825 \times 10^4 s^2 + 2.956 \times 10^4 s + 4914\end{aligned}\quad (B.65)$$

$$\begin{aligned}\bar{H}_{32}^* &= -0.2411s^{16} + 0.01809s^{15} + 2.745s^{14} + 0.0212s^{13} + 5.266s^{12} + 28.79s^{11} \\ &\quad - 227.6s^{10} - 58.95s^9 + 1477s^8 - 2006s^7 - 5408s^6 + 1.238 \times 10^4 s^5 \\ &\quad + 5128s^4 - 2.634 \times 10^4 s^3 + 2.221 \times 10^4 s^2 + 2.03 \times 10^4 s + 3381\end{aligned}\quad (B.66)$$

$$\begin{aligned}\bar{H}_{42}^* &= -0.2411s^{17} + 0.02483s^{16} + 5.051s^{15} - 0.4401s^{14} - 43.7s^{13} + 35.67s^{12} \\ &\quad + 201.2s^{11} - 385.1s^{10} - 529.1s^9 + 1540s^8 + 46.03s^7 - 2550s^6 \\ &\quad + 2490s^5 + 1151s^4 + 1195s^3 + 767s^2 + 127.5s\end{aligned}\quad (B.67)$$

$$\begin{aligned}\bar{H}_{52}^* &= 3.177s^{17} - 0.3794s^{16} - 66.56s^{15} + 6.935s^{14} + 602.2s^{13} - 482.6s^{12} \\ &\quad - 3040s^{11} + 5156s^{10} + 9379s^9 - 2.341 \times 10^4 s^8 - 8488s^7 + 5.386 \times 10^4 s^6 \\ &\quad - 1.833 \times 10^4 s^5 - 6.256 \times 10^4 s^4 + 2.825 \times 10^4 s^3 + 2.956 \times 10^4 s^2 + 4914s\end{aligned}\quad (B.68)$$

$$\begin{aligned}\bar{H}_{62}^* &= -0.2411s^{17} + 0.01809s^{16} + 2.745s^{15} + 0.0212s^{14} + 5.266s^{13} + 28.79s^{12} \\ &\quad - 227.6s^{11} - 58.95s^{10} + 1477s^9 - 2006s^8 - 5408s^7 + 1.238 \times 10^4 s^6 \\ &\quad + 5128s^5 - 2.634 \times 10^4 s^4 + 2.221 \times 10^4 s^3 + 2.03 \times 10^4 s^2 + 3381s\end{aligned}\quad (B.69)$$

$$\begin{aligned}\bar{H}_{13}^* &= 0.07301s^{16} - 0.007772s^{15} - 0.7331s^{14} + 0.06374s^{13} + 0.6996s^{12} \\ &\quad - 9.871s^{11} + 21.62s^{10} + 15.03s^9 - 125.9s^8 + 244.1s^7 + 541.9s^6 \\ &\quad - 992.2s^5 + 768.3s^4 + 1247s^3 - 279.5s^2 - 373.4s - 62.12\end{aligned}\quad (B.70)$$

$$\begin{aligned}\bar{H}_{23}^* &= 0.0639s^{16} - 0.01281s^{15} - 0.7357s^{14} + 0.1838s^{13} + 3.719s^{12} - 10.59s^{11} \\ &\quad - 18.05s^{10} + 26.45s^9 + 114.5s^8 - 110.5s^7 - 268s^6 + 1198s^5 \\ &\quad + 2187s^4 - 3895s^3 + 4619s^2 + 4010s + 667.1\end{aligned}\quad (B.71)$$

$$\begin{aligned}\bar{H}_{33}^* &= 1.681s^{16} - 0.2173s^{15} - 19.36s^{14} + 2.547s^{13} + 60.9s^{12} - 256.6s^{11} \\ &\quad + 118.1s^{10} + 566.1s^9 - 987.8s^8 + 2885s^7 + 7105s^6 - 7310s^5 \\ &\quad + 2.966 \times 10^4 s^4 - 7772s^3 + 2.961 \times 10^4 s^2 + 2.346 \times 10^4 s + 3900\end{aligned}\quad (B.72)$$

$$\begin{aligned}\bar{H}_{43}^* &= 0.07301s^{17} - 0.007772s^{16} - 0.7331s^{15} + 0.06374s^{14} + 0.6996s^{13} \\ &\quad - 9.871s^{12} + 21.62s^{11} + 15.03s^{10} - 125.9s^9 + 244.1s^8 + 541.9s^7 \\ &\quad - 992.2s^6 + 768.3s^5 + 1247s^4 - 279.5s^3 - 373.4s^2 - 62.12s\end{aligned}\quad (B.73)$$

$$\begin{aligned}\bar{H}_{53}^* &= 0.0639 s^{17} - 0.01281s^{16} - 0.7357s^{15} + 0.1838s^{14} + 3.719s^{13} - 10.59s^{12} \\ &\quad - 18.05s^{11} + 26.45s^{10} + 114.5s^9 - 110.5s^8 - 268s^7 + 1198s^6 \\ &\quad + 2187s^5 - 3895s^4 + 4619s^3 + 4010s^2 + 667.1s\end{aligned}\quad (B.74)$$

$$\begin{aligned}\bar{H}_{63}^* &= 1.681 s^{17} - 0.2173s^{16} - 19.36s^{15} + 2.547s^{14} + 60.9s^{13} - 256.6s^{12} \\ &\quad + 118.1s^{11} + 566.1s^{10} - 987.8s^9 + 2885s^8 + 7105s^7 - 7310s^6 \\ &\quad + 2.966 \times 10^4 s^5 - 7772s^4 + 2.961 \times 10^4 s^3 + 2.346 \times 10^4 s^2 + 3900s\end{aligned}\quad (B.75)$$

$$\begin{aligned}\bar{H}_{14}^* &= 0.01728 s^{16} - 0.001855s^{15} - 0.2855s^{14} + 0.02483s^{13} + 2.212s^{12} - 2.64s^{11} \\ &\quad - 11.16 s^{10} + 18.52s^9 + 42.51s^8 - 83.24s^7 - 60.39s^6 + 305.8s^5 + 208.5s^4 \\ &\quad - 659.8s^3 + 621.9s^2 + 561.1s + 93.57\end{aligned}\quad (B.76)$$

$$\begin{aligned}\bar{H}_{24}^* &= -0.0006341s^{16} + 6.086 \times 10^{-5} s^{15} + 0.01478s^{14} - 0.001191s^{13} - 0.1467s^{12} \\ &\quad + 0.101s^{11} + 0.8059s^{10} - 1.316s^9 - 2.678s^8 + 6.749s^7 + 3.453s^6 \\ &\quad - 16.7s^5 + 7.004s^4 + 20.06s^3 - 8.352s^2 - 8.981s - 1.499\end{aligned}\quad (B.77)$$

$$\begin{aligned}\bar{H}_{34}^* &= -0.0006341s^{16} + 6.086 \times 10^{-5} s^{15} + 0.01478s^{14} - 0.001254s^{13} - 0.1508s^{12} \\ &\quad + 0.1024s^{11} + 0.8722s^{10} - 1.328s^9 - 3.121s^8 + 7.375s^7 + 4.986s^6 \\ &\quad - 20.94s^5 + 4.042s^4 + 30.14s^3 - 18.22s^2 - 17.75s - 2.957\end{aligned}\quad (B.78)$$

$$\begin{aligned}\bar{H}_{44}^* &= 0.01728 s^{17} - 0.001855s^{16} - 0.2855s^{15} + 0.02483s^{14} + 2.212s^{13} - 2.64s^{12} \\ &\quad - 11.16 s^{11} + 18.52s^{10} + 42.51s^9 - 83.24s^8 - 60.39s^7 + 305.8s^6 + 208.5s^5 \\ &\quad - 659.8s^4 + 621.9s^3 + 561.1s^2 + 93.57s\end{aligned}\quad (B.79)$$

$$\begin{aligned}\bar{H}_{54}^* &= -0.0006341s^{17} + 6.086 \times 10^{-5} s^{16} + 0.01478s^{15} - 0.001191s^{14} - 0.1467s^{13} \\ &\quad + 0.101s^{12} + 0.8059s^{11} - 1.316s^{10} - 2.678s^9 + 6.749s^8 + 3.453s^7 \\ &\quad - 16.7s^6 + 7.004s^5 + 20.06s^4 - 8.352s^3 - 8.981s^2 - 1.499s\end{aligned}\quad (B.80)$$

$$\begin{aligned}\bar{H}_{64}^* &= -0.0006341s^{17} + 6.086 \times 10^{-5} s^{16} + 0.01478s^{15} - 0.001254s^{14} - 0.1508s^{13} \\ &\quad + 0.1024s^{12} + 0.8722s^{11} - 1.328s^{10} - 3.121s^9 + 7.375s^8 + 4.986s^7 \\ &\quad - 20.94s^6 + 4.042s^5 + 30.14s^4 - 18.22s^3 - 17.75s^2 - 2.957s\end{aligned}\quad (B.81)$$

$$\begin{aligned}\bar{H}_{15}^* &= -0.001607s^{16} + 0.0001307s^{15} + 0.03744s^{14} - 0.002723s^{13} - 0.3787s^{12} \\ &\quad + 0.2556 s^{11} + 2.164s^{10} - 3.341s^9 - 7.611s^8 + 18.19s^7 + 11.61s^6 \\ &\quad - 50.02 s^5 + 12.16s^4 + 69.2s^3 - 39.15s^2 - 38.77 s - 6.461\end{aligned}\quad (B.82)$$

$$\begin{aligned}\bar{H}_{25}^* &= 0.02118s^{16} - 0.002106s^{15} - 0.4931s^{14} + 0.04343s^{13} + 5.07s^{12} - 3.438s^{11} \\ &\quad - 29.79s^{10} + 44.4s^9 + 108.9s^8 - 252.6s^7 - 183.1s^6 + 744s^5 - 100.6s^4 \\ &\quad - 1117s^3 + 716.6s^2 + 689.4s + 114.8\end{aligned}\quad (B.83)$$

$$\begin{aligned}\bar{H}_{35}^* &= -0.001607s^{16} + 0.00014s^{15} + 0.03744s^{14} - 0.002875s^{13} - 0.3788s^{12} \\ &\quad + 0.2566s^{11} + 2.163s^{10} - 3.345s^9 - 7.607s^8 + 18.2s^7 + 11.6s^6 \\ &\quad - 50.05s^5 + 12.14s^4 + 69.35s^3 - 39.28s^2 - 38.89s - 6.481\end{aligned}\quad (B.84)$$

$$\begin{aligned}\bar{H}_{45}^* &= -0.001607s^{17} + 0.0001307s^{16} + 0.03744s^{15} - 0.002723s^{14} - 0.3787s^{13} \\ &\quad + 0.2556s^{12} + 2.164s^{11} - 3.341s^{10} - 7.611s^9 + 18.19s^8 + 11.61s^7 \\ &\quad - 50.02s^6 + 12.16s^5 + 69.2s^4 - 39.15s^3 - 38.77s^2 - 6.461s\end{aligned}\quad (B.85)$$

$$\begin{aligned}\bar{H}_{55}^* &= 0.02118s^{17} - 0.002106s^{16} - 0.4931s^{15} + 0.04343s^{14} + 5.07s^{13} - 3.438s^{12} \\ &\quad - 29.79s^{11} + 44.4s^{10} + 108.9s^9 - 252.6s^8 - 183.1s^7 + 744s^6 - 100.6s^5 \\ &\quad - 1117s^4 + 716.6s^3 + 689.4s^2 + 114.8s\end{aligned}\quad (B.86)$$

$$\begin{aligned}\bar{H}_{65}^* &= -0.001607s^{17} + 0.00014s^{16} + 0.03744s^{15} - 0.002875s^{14} - 0.3788s^{13} \\ &\quad + 0.2566s^{12} + 2.163s^{11} - 3.345s^{10} - 7.607s^9 + 18.2s^8 + 11.6s^7 \\ &\quad - 50.05s^6 + 12.14s^5 + 69.35s^4 - 39.28s^3 - 38.89s^2 - 6.481s\end{aligned}\quad (B.87)$$

$$\begin{aligned}\bar{H}_{16}^* &= 0.0004866s^{16} - 6.455 \times 10^{-5}s^{15} - 0.01134s^{14} + 0.001227s^{13} + 0.113s^{12} \\ &\quad - 0.07989s^{11} - 0.6239s^{10} + 1.019s^9 + 2.091s^8 - 5.275s^7 - 2.786s^6 \\ &\quad + 13.32s^5 - 5.056s^4 - 16.65s^3 + 7.698s^2 + 8.019s + 1.337\end{aligned}\quad (B.88)$$

$$\begin{aligned}\bar{H}_{26}^* &= 0.0004866s^{16} - 6.676 \times 10^{-5}s^{15} - 0.01134s^{14} + 0.001371s^{13} + 0.12s^{12} \\ &\quad - 0.08253s^{11} - 0.7378s^{10} + 1.041s^9 + 2.851s^8 - 6.355s^7 \\ &\quad - 5.421s^6 + 20.6s^5 + 0.03931s^4 - 34.01s^3 + 24.69s^2 + 23.13s + 3.848\end{aligned}\quad (B.89)$$

$$\begin{aligned}\bar{H}_{36}^* &= 0.0128s^{16} - 0.00149s^{15} - 0.298s^{14} + 0.0303s^{13} + 2.68s^{12} - 2.076s^{11} \\ &\quad - 11.65s^{10} + 26.51s^9 + 22.51s^8 - 95.76s^7 + 42.33s^6 + 51.36s^5 \\ &\quad - 359s^4 + 299.1s^3 - 491.9s^2 - 415.7s - 69.35\end{aligned}\quad (B.90)$$

$$\begin{aligned}\bar{H}_{46}^* &= 0.0004866s^{17} - 6.455 \times 10^{-5}s^{16} - 0.01134s^{15} + 0.001227s^{14} + 0.113s^{13} \\ &\quad - 0.07989s^{12} - 0.6239s^{11} + 1.019s^{10} + 2.091s^9 - 5.275s^8 - 2.786s^7 \\ &\quad + 13.32s^6 - 5.056s^5 - 16.65s^4 + 7.698s^3 + 8.019s^2 + 1.337s\end{aligned}\quad (B.91)$$

$$\begin{aligned}\bar{H}_{56}^* &= 0.0004866 s^{17} - 6.676 \times 10^{-5} s^{16} - 0.01134 s^{15} + 0.001371 s^{14} + 0.12 s^{13} \\ &\quad - 0.08253 s^{12} - 0.7378 s^{11} + 1.041 s^{10} + 2.851 s^9 - 6.355 s^8 \\ &\quad - 5.421 s^7 + 20.6 s^6 + 0.03931 s^5 - 34.01 s^4 + 24.69 s^3 + 23.13 s^2 + 3.848 s\end{aligned}\quad (B.92)$$

$$\begin{aligned}\bar{H}_{66}^* &= 0.0128 s^{17} - 0.00149 s^{16} - 0.298 s^{15} + 0.0303 s^{14} + 2.68 s^{13} - 2.076 s^{12} \\ &\quad - 11.65 s^{11} + 26.51 s^{10} + 22.51 s^9 - 95.76 s^8 + 42.33 s^7 + 51.36 s^6 \\ &\quad - 359 s^5 + 299.1 s^4 - 491.9 s^3 - 415.7 s^2 - 69.35 s\end{aligned}\quad (B.93)$$

$$\begin{aligned}\bar{H}_{17}^* &= 0.9992 s^{16} - 0.1248 s^{15} - 21.08 s^{14} + 2.142 s^{13} + 193 s^{12} - 162 s^{11} \\ &\quad - 988.7 s^{10} + 1771 s^9 + 3121 s^8 - 8155 s^7 - 2859 s^6 + 1.893 \times 10^4 s^5 \\ &\quad - 7125 s^4 - 2.261 \times 10^4 s^3 + 9912 s^2 + 1.053 \times 10^4 s + 1758\end{aligned}\quad (B.94)$$

$$\begin{aligned}\bar{H}_{27}^* &= -0.0006341 s^{15} - 0.0832 s^{14} + 0.02009 s^{13} + 1.515 s^{12} - 0.2213 s^{11} \\ &\quad - 11.62 s^{10} + 13.35 s^9 + 48.11 s^8 - 110.9 s^7 - 117.1 s^6 + 363.4 s^5 \\ &\quad - 111.3 s^4 - 537.9 s^3 + 311.7 s^2 + 304.7 s + 50.64\end{aligned}\quad (B.95)$$

$$\begin{aligned}\bar{H}_{37}^* &= -0.0006341 s^{15} - 0.08319 s^{14} + 0.02182 s^{13} + 1.628 s^{12} - 0.26 s^{11} - 13.48 s^{10} \\ &\quad + 13.68 s^9 + 60.62 s^8 - 128.7 s^7 - 160.7 s^6 + 484.3 s^5 - 26.54 s^4 - 828 s^3 \\ &\quad + 597.8 s^2 + 558.6 s + 92.85\end{aligned}\quad (B.96)$$

$$\begin{aligned}\bar{H}_{47}^* &= 0.9992 s^{17} - 0.1248 s^{16} - 21.08 s^{15} + 2.142 s^{14} + 193 s^{13} - 162 s^{12} \\ &\quad - 988.7 s^{11} + 1771 s^{10} + 3121 s^9 - 8155 s^8 - 2859 s^7 + 1.893 \times 10^4 s^6 \\ &\quad - 7125 s^5 - 2.261 \times 10^4 s^4 + 9912 s^3 + 1.053 \times 10^4 s^2 + 1758 s\end{aligned}\quad (B.97)$$

$$\begin{aligned}\bar{H}_{57}^* &= -0.0006341 s^{16} - 0.0832 s^{15} + 0.02009 s^{14} + 1.515 s^{13} - 0.2213 s^{12} \\ &\quad - 11.62 s^{11} + 13.35 s^{10} + 48.11 s^9 - 110.9 s^8 - 117.1 s^7 + 363.4 s^6 \\ &\quad - 111.3 s^5 - 537.9 s^4 + 311.7 s^3 + 304.7 s^2 + 50.64 s\end{aligned}\quad (B.98)$$

$$\begin{aligned}\bar{H}_{67}^* &= -0.0006341 s^{16} - 0.08319 s^{15} + 0.02182 s^{14} + 1.628 s^{13} - 0.26 s^{12} - 13.48 s^{11} \\ &\quad + 13.68 s^{10} + 60.62 s^9 - 128.7 s^8 - 160.7 s^7 + 484.3 s^6 - 26.54 s^5 - 828 s^4 \\ &\quad + 597.8 s^3 + 558.6 s^2 + 92.85 s\end{aligned}\quad (B.99)$$

$$\begin{aligned}\bar{H}_{18}^* &= -0.001607 s^{15} - 0.2109 s^{14} + 0.05092 s^{13} + 3.84 s^{12} - 0.5607 s^{11} - 29.43 s^{10} \\ &\quad + 33.83 s^9 + 121.8 s^8 - 281 s^7 - 296.4 s^6 + 920.1 s^5 - 282.7 s^4 \\ &\quad - 1361 s^3 + 787.8 s^2 + 770.2 s + 128\end{aligned}\quad (B.100)$$

$$\begin{aligned}\bar{H}_{28}^* &= 0.9992s^{16} - 0.121s^{15} - 12.67s^{14} + 1.328s^{13} + 52.61s^{12} - 151.3s^{11} \\ &\quad - 17.63s^{10} + 487.8s^9 - 386s^8 + 976.1s^7 + 4202s^6 - 4177s^5 \\ &\quad + 1.353 \times 10^4 s^4 - 1155s^3 + 1.096 \times 10^4 s^2 + 8582s + 1433\end{aligned}\quad (B.101)$$

$$\begin{aligned}\bar{H}_{38}^* &= -0.001607s^{15} + 0.2557s^{14} + 0.01094s^{13} - 3.745s^{12} - 0.03373s^{11} \\ &\quad + 21.13s^{10} - 36.86s^9 - 50.25s^8 + 194.1s^7 + 16.07s^6 - 146.5s^5 \\ &\quad + 1018s^4 - 695s^3 + 1356s^2 + 1117s + 185.7\end{aligned}\quad (B.102)$$

$$\begin{aligned}\bar{H}_{48}^* &= -0.001607s^{16} - 0.2109s^{15} + 0.05092s^{14} + 3.84s^{13} - 0.5607s^{12} - 29.43s^{11} \\ &\quad + 33.83s^{10} + 121.8s^9 - 281s^8 - 296.4s^7 + 920.1s^6 - 282.7s^5 \\ &\quad - 1361s^4 + 787.8s^3 + 770.2s^2 + 128s\end{aligned}\quad (B.103)$$

$$\begin{aligned}\bar{H}_{58}^* &= 0.9992s^{17} - 0.121s^{16} - 12.67s^{15} + 1.328s^{14} + 52.61s^{13} - 151.3s^{12} \\ &\quad - 17.63s^{11} + 487.8s^{10} - 386s^9 + 976.1s^8 + 4202s^7 - 4177s^6 \\ &\quad + 1.353 \times 10^4 s^5 - 1155s^4 + 1.096 \times 10^4 s^3 + 8582s^2 + 1433s\end{aligned}\quad (B.104)$$

$$\begin{aligned}\bar{H}_{68}^* &= -0.001607s^{16} + 0.2557s^{15} + 0.01094s^{14} - 3.745s^{13} - 0.03373s^{12} \\ &\quad + 21.13s^{11} - 36.86s^{10} - 50.25s^9 + 194.1s^8 + 16.07s^7 - 146.5s^6 \\ &\quad + 1018s^5 - 695s^4 + 1356s^3 + 1117s^2 + 185.7s\end{aligned}\quad (B.105)$$

$$\begin{aligned}\bar{H}_{19}^* &= 0.0004866s^{15} - 0.09879s^{14} + 0.003857s^{13} + 1.446s^{12} - 0.09873s^{11} \\ &\quad - 8.135s^{10} + 14.95s^9 + 18.39s^8 - 77.42s^7 + 0.2594s^6 + 60.83s^5 \\ &\quad - 408.7s^4 + 282.8s^3 - 511s^2 - 429.5s - 71.75\end{aligned}\quad (B.106)$$

$$\begin{aligned}\bar{H}_{29}^* &= 0.0004866s^{15} - 0.07749s^{14} - 0.003307s^{13} + 1.135s^{12} + 0.01017s^{11} \\ &\quad - 6.402s^{10} + 11.17s^9 + 15.23s^8 - 58.81s^7 - 4.868s^6 + 44.39s^5 \\ &\quad - 308.6s^4 + 210.6s^3 - 410.8s^2 - 338.5s - 56.27\end{aligned}\quad (B.107)$$

$$\begin{aligned}\bar{H}_{39}^* &= 0.9992s^{16} - 0.1293s^{15} - 11.57s^{14} + 1.522s^{13} + 36.82s^{12} - 153.6s^{11} \\ &\quad + 68.01s^{10} + 343.9s^9 - 583.4s^8 + 1710s^7 + 4265s^6 - 4353s^5 \\ &\quad + 1.787 \times 10^4 s^4 - 4740s^3 + 1.792 \times 10^4 s^2 + 1.42 \times 10^4 s + 2361\end{aligned}\quad (B.108)$$

$$\begin{aligned}\bar{H}_{49}^* &= 0.0004866s^{16} - 0.09879s^{15} + 0.003857s^{14} + 1.446s^{13} - 0.09873s^{12} \\ &\quad - 8.135s^{11} + 14.95s^{10} + 18.39s^9 - 77.42s^8 + 0.2594s^7 + 60.83s^6 \\ &\quad - 408.7s^5 + 282.8s^4 - 511s^3 - 429.5s^2 - 71.75s\end{aligned}\quad (B.109)$$

$$\begin{aligned}\bar{\mathbf{H}}_{59}^* &= 0.0004866 s^{16} - 0.07749s^{15} - 0.003307s^{14} + 1.135s^{13} + 0.01017s^{12} \\ &\quad - 6.402s^{11} + 11.17s^{10} + 15.23s^9 - 58.81s^8 - 4.868s^7 + 44.39s^6 \\ &\quad - 308.6s^5 + 210.6s^4 - 410.8s^3 - 338.5s^2 - 56.27s\end{aligned}\quad (\text{B.110})$$

$$\begin{aligned}\bar{\mathbf{H}}_{69}^* &= 0.9992s^{17} - 0.1293s^{16} - 11.57s^{15} + 1.522s^{14} + 36.82s^{13} - 153.6s^{12} \\ &\quad + 68.01s^{11} + 343.9s^{10} - 583.4s^9 + 1710s^8 + 4265s^7 - 4353s^6 \\ &\quad + 1.787 \times 10^{-4}s^5 - 4740s^4 + 1.792 \times 10^{-4}s^3 + 1.42 \times 10^{-4}s^2 + 2361s\end{aligned}\quad (\text{B.111})$$

In terms of (6.8) and (6.9), from (8.57) ~ (8.111), we derive the C-S controller $\bar{\mathbf{K}}^*(s)$,

which is a 3×6 matrix as follows:

$$\bar{\mathbf{K}}_{11}^* = \frac{35.32s^3 + 21.23s^2 + 4.287 \times 10^7 s + 2.82 \times 10^9}{s^3 + 6400s^2 + 5.4 \times 10^7 s + 9.432 \times 10^9} \quad (\text{B.112})$$

$$\bar{\mathbf{K}}_{21}^* = \frac{3.24s^3 + 1.43s^2 + 4.200 \times 10^6 s + 3.41 \times 10^8}{s^3 + 6400s^2 + 5.4 \times 10^7 s + 9.432 \times 10^9} \quad (\text{B.113})$$

$$\bar{\mathbf{K}}_{31}^* = \frac{3.01s^3 + 1.04s^2 + 4.200 \times 10^6 s + 3.21 \times 10^8}{s^3 + 6400s^2 + 5.4 \times 10^7 s + 9.432 \times 10^9} \quad (\text{B.114})$$

$$\bar{\mathbf{K}}_{21}^* = \frac{2.32s^3 + 1.23s^2 + 4.221 \times 10^6 s + 3.28 \times 10^8}{s^3 + 6400s^2 + 5.4 \times 10^7 s + 9.432 \times 10^9} \quad (\text{B.115})$$

$$\bar{\mathbf{K}}_{22}^* = \frac{56.73s^3 + 39.22s^2 + 8.21 \times 10^7 s + 1.02 \times 10^9}{s^3 + 6400s^2 + 5.4 \times 10^7 s + 9.432 \times 10^9} \quad (\text{B.116})$$

$$\bar{\mathbf{K}}_{23}^* = \frac{3.10s^3 + 1.35s^2 + 2.21 \times 10^6 s + 8.27 \times 10^8}{s^3 + 6400s^2 + 5.4 \times 10^7 s + 9.432 \times 10^9} \quad (\text{B.117})$$

$$\bar{\mathbf{K}}_{31}^* = \frac{3.12s^3 + 1.02s^2 + 4.287 \times 10^6 s + 3.30 \times 10^8}{s^3 + 6400s^2 + 5.4 \times 10^7 s + 9.432 \times 10^9} \quad (\text{B.118})$$

$$\bar{\mathbf{K}}_{32}^* = \frac{3.10s^3 + 1.42s^2 + 2.40 \times 10^6 s + 8.21 \times 10^8}{s^3 + 6400s^2 + 5.4 \times 10^7 s + 9.432 \times 10^9} \quad (\text{B.119})$$

$$\bar{\mathbf{K}}_{33}^* = \frac{35.32s^3 + 21.23s^2 + 4.287 \times 10^7 s + 2.82 \times 10^9}{s^3 + 6400s^2 + 5.4 \times 10^7 s + 9.432 \times 10^9} \quad (\text{B.120})$$

$$\bar{K}_{14}^* = \frac{3.53s^3 + 2.12s^2 + 4.29 \times 10^6 s + 2.82 \times 10^8}{s^3 + 6530s^2 + 5.4 \times 10^7 s + 9.912 \times 10^9} \quad (\text{B.121})$$

$$\bar{K}_{24}^* = \frac{0.324s^3 + 0.143s^2 + 4.200 \times 10^5 s + 3.40 \times 10^7}{s^3 + 6530s^2 + 5.4 \times 10^7 s + 9.912 \times 10^9} \quad (\text{B.122})$$

$$\bar{K}_{34}^* = \frac{0.30s^3 + 0.1s^2 + 4.20 \times 10^5 s + 3.20 \times 10^7}{s^3 + 6530s^2 + 5.4 \times 10^7 s + 9.912 \times 10^9} \quad (\text{B.123})$$

$$\bar{K}_{15}^* = \frac{0.23s^3 + 0.12s^2 + 4.20 \times 10^5 s + 3.22 \times 10^7}{s^3 + 6530s^2 + 5.4 \times 10^7 s + 9.912 \times 10^9} \quad (\text{B.124})$$

$$\bar{K}_{25}^* = \frac{5.62s^3 + 3.92s^2 + 8.21 \times 10^6 s + 1.01 \times 10^8}{s^3 + 6530s^2 + 5.4 \times 10^7 s + 9.912 \times 10^9} \quad (\text{B.125})$$

$$\bar{K}_{35}^* = \frac{0.32s^3 + 0.12s^2 + 2.21 \times 10^5 s + 8.22 \times 10^7}{s^3 + 6530s^2 + 5.4 \times 10^7 s + 9.912 \times 10^9} \quad (\text{B.126})$$

$$\bar{K}_{16}^* = \frac{0.31s^3 + 0.99s^2 + 4.26 \times 10^5 s + 3.28 \times 10^7}{s^3 + 6530s^2 + 5.4 \times 10^7 s + 9.912 \times 10^9} \quad (\text{B.127})$$

$$\bar{K}_{26}^* = \frac{0.29s^3 + 0.12s^2 + 2.40 \times 10^5 s + 8.30 \times 10^7}{s^3 + 6530s^2 + 5.4 \times 10^7 s + 9.912 \times 10^9} \quad (\text{B.128})$$

$$\bar{K}_{36}^* = \frac{3.54s^3 + 2.12s^2 + 4.29 \times 10^6 s + 2.82 \times 10^8}{s^3 + 6530s^2 + 5.4 \times 10^7 s + 9.912 \times 10^9} \quad (\text{B.129})$$